2009

# Seismic Analysis of Rehabilitated Buried Segmented Pipes Using CIPP Trenchless Technology

Sami Jasem
*University of Windsor*

# Seismic Analysis of Rehabilitated Buried Segmented Pipes

# Using CIPP Trenchless Technology

**By**

**Sami Mirri Kadhim Jasem**

**A Dissertation**
**Submitted to the Faculty of Graduate Studies through**
**Civil Engineering in Partial Fulfillment of the**
**Requirements for the Degree of Doctor of Philosophy at the**
**University of Windsor**

**Windsor, Ontario, Canada**

**2009**

Seismic Analysis of Rehabilitated Buried Segmented Pipes Using CIPP Trenchless Technology

By

Sami Mirri Kadhim Jasem

APPROVED BY:

Dr. A. El Damatty, External Examiner
University of Western Ontario

Dr. W. Altenhof
Department of Mechanical, Automotive and Materials Engineering

Dr. S. Cheng
Department of Civil and Environmental Engineering

Dr. B. B. Budkowska
Department of Civil and Environmental Engineering

Dr. F. Ghrib, Principal Advisor
Department of Civil and Environmental Engineering

Dr. N. Hearn, Co-Advisor

Dr. A. Tayebi, Special Member
President and CEO, Novel Technologies Solutions

Dr. A. T. Alpas, Chair of Defense
Department of Mechanical, Automotive and Materials Engineering

June 29, 2009

## Author's Declaration of Originality

I hereby certify that I am the sole author of this thesis and that no part of this thesis has been published or submitted for publication.

I certify that, to the best of my knowledge, my thesis does not infringe upon anyone's copyright nor violate any proprietary rights and that any ideas, techniques, quotations, or any other material from the work of other people included in my thesis, published or otherwise, are fully acknowledged in accordance with the standard referencing practices. Furthermore, to the extent that I have included copyrighted material that surpasses the bounds of fair dealing within the meaning of the Canada Copyright Act, I certify that I have obtained a written permission from the copyright owner(s) to include such material(s) in my thesis and have included copies of such copyright clearances to my appendix.

I declare that this is a true copy of my thesis, including any final revisions, as approved by my thesis committee and the Graduate Studies office, and that this thesis has not been submitted for a higher degree to any other University or Institution.

## ABSTRACT

The recent developments of analytical and experimental tests for underground pipelines rehabilitation are presented. The finite element simulation results appear to give reasonable estimates for encased liner buckling pressure tests. Despite its simplicity, the finite element model outperforms all analytical methods. This work shows that further analytical, field, and/or laboratory studies and finite element analyses are required in order to fully understand the host pipe-liner interaction behaviour and to determine the related applicability of liners design under different conditions of pipe deteriorations, liner geometry, and various pipe materials. The development of better analytical formula does not seem to be possible with the existing tests, which have shown significant variability.

This work also describes the numerical modeling of the axial compression and bending behaviours of segmented pipe joints using the finite element method. The results of published full-scale tests by others (Bouabid, 1993 and Singhal, 1984) of unrestrained joints for typical rigid pipes were used to validate and calibrate the finite element models. The research develops a tool to use numerical simulation results of joint behaviour for seismic analysis of buried segmented pipeline networks subjected to axial and transverse permanent ground deformations. These numerical simulation models are verified using the available analytical and numerical models for longitudinal permanent ground deformation (Selventhiran, 2002) and transverse permanent ground deformation (Liu and O'Rourke, 1997).

Further, the current study develops a tool to use numerical simulation results of joint behaviour for seismic analysis of buried segmented pipeline networks including axial and transverse permanent ground deformation investigations. The developed numerical models are used for the seismic analysis of typical rigid segmented pipelines. Failure analysis of the segmented pipeline is achieved in order to determine the potential of the pipeline joints for damage and failure under seismic effects.

Finally, this work also explores the numerical modeling of delamination of rehabilitated segmented buried pipelines using a cured-in-place technique. Two finite element analyses procedures considering friction effects in the contact boundary between the host pipe and the liner are proposed to predict the axial/flexural behaviour of the unrestrained joint and the delamination in rehabilitated segmented pipeline under external quasi-static loads or seismic effects. It is found that the encased liner is debonded or delaminated at the joint region resulting in a decrease in the rigidity of the joint when the axial and flexural loads are increased. A parametric study is carried out to investigate the influence of the host pipe material, liner material, liner thickness, pipe stiffness, and interface condition on the seismic behaviours of buried rehabilitated segmented pipelines. The results of effects of the liner thickness on the seismic responses of buried rehabilitated segmented pipelines indicate that the liner strain is a decreasing function of the liner.

# DEDICATION

**To the Memory of My Precious Parents**

**To My Beloved Wife Ashwaq**

**To My Sons, Ahmed and Mohammed**

**To My Daughters, Lukaa and Huda**

**For Their Endless Love and Support**

بسم الله الرحمن الرحيم

أقرأ بأسم ربك الذي خلق * خلق الانسان من علق *

أقرأ وربك الاكرم * الذي علم بالقلم *

علم الأنسان ما لم يعلم *

***The above is the Arabic script of the first verses revealed to Prophet Mohammed (pbuh) of the Holly Quran which may be translated as:***

*In the name of Allah (The Lord), Most Gracious, Most Merciful.*

*Read! In the name of thy Lord, Who created,*
*Created man out of a clot of congealed blood.*
*Read! And thy Lord is Most Bountiful,*
*He who taught (writing) by the pen,*
*Taught man that which he knew not.*

## ACKNOWLEDGEMENTS

I would like to express my gratitude to my supervisors Dr. Faouzi Ghrib, Dr. Abedlkader Tayebi, and Dr. Natalyia Hearn. They have always been extremely generous with their time, knowledge, and ideas and allowed me great support, encouragement, and advice throughout the course of this research. Their enthusiastic approach to research, their endless excitement, their cheerful moral support, and their pleasant personalities have made this experience all the more enjoyable and I am greatly appreciative.

I would also like to thank my committee members Dr. Shaohong Cheng, Dr. Barbara Budkowska, and Dr. William Altenhof for their helpful discussions and for their advice.

To Ms. Catherine Wilson, Ms. Anne-Marie Bartlett, and Mr. Pop Lucin, I extend special thanks for all their help during my study period.

To Patrick Seguin and Paul Fraser many thanks, for their help in fixing the server troubleshooting, for downloading, and for installation of the required softwares.

I would like to express my grateful thanks to the faculty members of the Department of Civil and Environmental Engineering, University of Windsor, for their continuous encouragement. I would like to thank the University of Windsor for the tuition scholarship award from 2005 to 2007. The financial support from the Natural Science and Engineering Research Council of Canada (NSERC) is gratefully acknowledged.

I also would like to express my sincere appreciation to my wife Ashwaq, and to my sons Ahmed and Mohammed, and to my daughters Lukaa and Huda; with special thanks for their continuous patience and support in so many ways.

Finally, and above all, this work was possible to come to existence by the will and help of God, Most Gracious, and Most Merciful.

# TABLE OF CONTENTS

**CHAPTER 3**

**CIPP LINERS BUCKLING MODELS FOR REHABILITATION PIPELINE – A COMPARATIVE STUDY**



**CHAPTER 4**

**MODELING OF AXIAL AND BENDING BEHAVIOR OF UNRESTRAINED JOINTS IN SEGMENTED PIPELINES**

## LIST OF TABLES

## LIST OF FIGURES

# CHAPTER 1

# INTRODUCTION

## 1.1 INTRODUCTION

Buried pipeline utilities (e.g., concrete and vitrified clay pipes) represent a critical component within civil engineering infrastructure systems. Over time, many of these systems become defective and suffer from overloading and loss of capacity. Where systems have not been maintained, and in some cases where land subsidence has occurred due to ground shaking, these systems have deteriorated significantly and are in need of rehabilitation because the problems of leaking water, gas distribution pipes and sewage collection pipes can be extensive. Thus, pipeline utilities in areas of seismic activity should require the enhancement of the seismic resistance of their rehabilitated pipes.

The seismic behaviours of buried pipelines are to be distinguished from that of above-ground structures. The seismic responses of conventional structures are governed by inertia forces transmitted from ground motion. For pipelines, the relative movement of the pipes with respect to the surrounding soil is generally neglected and the inertia forces due to the weight of the pipeline and its contents are considered to be relatively unimportant. Further, the buried pipe-soil system is so stiff and it is governed by a quasi-static solution; the subsequent inertia and damping effect are usually neglected (O'Rourke and Liu, 1999).

During an earthquake, ground motion may cause saturated cohesionless soil deposits to lose strength and stiffness, resulting in boiling, in excessive ground deformation (lateral flow), in settlement of buildings, in failure of slopes, earth dams, and lifelines, and in total or partial collapse of retaining walls and other structures (Helgeson, 1997). Pipeline damage may occur as a result of overstressing of the pipe due to traveling waves, liquefaction of cohesionless soils (possibly including landslides), or displacement across

an active fault. Due to a seismic event, buried pipelines can be damaged either by transient seismic wave propagation or by permanent ground deformation. Typically, pipeline damage is due to a combination of these hazards (O'Rourke and Liu, 1999). Extensive research studies have been performed (e.g., Liu, 1996; Liu and O'Rourke, 1997, and Selventhiran, 2002) investigating the effects of seismic motions and ground deformations on buried pipelines, focusing on the extent and causes of failures and on the determination of their structural behaviours under seismic effects.

Deteriorated pipes require either replacement or rehabilitation. Rehabilitation is achieved using either conventional open-trench methods or trenchless construction technologies. Conventional open-trench methods, while effective, can be costly and disruptive in areas where significant infrastructure such as buildings and roads already exists. In many cases, trenchless technology systems can provide an innovative, cost-effective alternative. Trenchless technology systems are often used for the installation, replacement, and renovation/rehabilitation of underground pipes where personnel entry is not possible.

Trenchless technology uses sophisticated equipment to install and rehabilitate water, sewer, and gas pipelines and other infrastructure by no-dig methods. In recent years, rehabilitation of underground pipes by relining the deteriorated host pipe with an inner pipe or lining material has gained acceptance. The most common relining method is the use of cured-in-place pipe (CIPP), which is the main focus of this study.

There have been a number of suggested potential methods in the literature during the past 40 years to determine the structural behaviour of encased liners (e.g., ASTM F1216, 1993, 2007; Guice et al., 1994; Chunduru, 1996; Falter, 1996; McAlpine, 1996; El-Sawy and Moore, 1997; Omara, 1997; Moore, 1998; Boot, 1998; Lu, 1999; Zhu, 2000; Thépot, 2000; Gumbel, 2001; Wang, 2002; and Zhao, 2003). Despite the considerable amount of effort spent over the past four decades to develop liner design procedures, general agreement on a unique practical formula has not yet been achieved.

## 1.2 RESEARCH SIGNIFICANCE

Worldwide, infrastructures are deteriorating in earthquake-prone areas. Damaged buried pipes require either rehabilitation or replacement. In many cases, where replacing deteriorated buried pipelines is either too costly or too disruptive, rehabilitation using trenchless construction technologies is considered.

All previous studies have concentrated on the short-term (elastic behaviour) and long-term (creep behaviour) performance of buried pipelines (i.e., the transverse lateral stability and strength against buckling) due to hydrostatic pressure. However, the predominant failure mechanism during earthquakes is combined axial strain/buckling and/or bending in the longitudinal and transverse directions. Except for the brief work of Moore (1998), there have been limited previous studies addressing either an extensive comparative study of available analytical numerical models or the existing experimental tests for studying the buckling problem of encased liners. No previous studies investigate the effects of delamination propagation on the structural capacity of rehabilitated pipelines subjected to external pressure or seismic effects.

The structural behaviour of restrained and unrestrained joints of pipelines have been explored through many analytical and experimental investigations during the last two decades such as those of Singhal, (1983, and 1984), Bouabid, (1993), Selventhiran, (2002), and Meis, (2003). However, to the best knowledge of the author, no experimental test results are available to determine the axial and bending stiffness of rubber gasket unrestrained joints of small diameters for vitrified clay, non-reinforced concrete, and reinforced concrete pipes. This lack of research regarding the structural behaviour of such type of joint was the impetus for part of the research program reported herein since joint stiffness is an important input for the numerical simulation of segmented pipeline behaviour.

Although several studies have discussed the numerical modeling of a buried pipeline with seismic effect, a literature survey of previous research indicates that limited or no

specified work has been conducted on the earthquake-resistant design of trenchless rehabilitation methods for buried pipelines to assess or improve their seismic performance. Moreover, there have been no previous studies addressing the effects of delamination propagation on the structural capacity of rehabilitated pipelines subjected to external pressure and seismic effects. Therefore, research into the structural behaviours of rehabilitated pipelines must be done in order to understand their seismic performance in order to reduce the damaging results of earthquakes. Hence, the importance of the proposed research is in answering these areas of major concern.

## 1.3 OBJECTIVES AND SCOPE

The first goal of this research is to study and evaluate the technical literature for analytical and experimental tests on buckling of liners currently used for underground pipelines rehabilitation, including any recent developments. The study also aims to develop a finite element model designed to evaluate the critical buckling pressure of liners encased in perfectly circular and/or oval host pipes by simulating the available experimental short-term and long-term tests.

Another purpose of this work is to develop a numerical modeling methodology to predict the axial and rotational stiffness of unrestrained joints for segmented small-diameter pipelines including vitrified clay, non-reinforced concrete, and reinforced concrete pipes. These stiffnesses are key parameters for the seismic analysis of the buried pipelines.

The third objective for this research is to study the seismic performance of rehabilitated segmented rigid buried pipelines subjected to earthquake effects using experimental results and numerical models. A parametric study for the effect of the burial depths, the interactions between the liner and the host pipe, liner geometry, and host pipe material has been achieved. However, in order to look into the response of rehabilitated buried pipes and the influence of each of these parameters under seismic conditions, the proposed research will focus on the analysis and the comparison of available

experimental and numerical models by performing an analysis of variance or reliability analysis and sensitivity analysis to identify the main parameters having the largest influence on the seismic performance of the CIPP lining as a trenchless rehabilitation method.

Finally, the last aim of the current work is to explore the delamination propagation at the joint region of rehabilitated segmented buried pipelines under seismic effects and to establish the general framework and develop universal numerical procedures for qualifying lining rehabilitations systems for earthquakes, a task that has not been yet performed by the research community. In this regard, the research will focus on the seismic behaviours of rehabilitated segmented rigid pipes such as reinforced concrete pipes, non-reinforced concrete pipes, and vitrified clay pipes.

## 1.4 ORGANIZATION OF THE DISSERTATION

This dissertation is organized into seven chapters in an attempt to logically proceed through the reasoning behind the research, the work itself, the results and analysis, comparison of the results, conclusions and recommendations arising from the results. A review of relevant previous research, the description of proposed research, the objectives of this study and outline of the program scope are presented in chapter 1. Chapter 2 reviews the literature relevant to this study and includes two parts: part I provides a review of previous research literature dealing with buried pipelines performance in past earthquakes, seismic hazard fundamentals, response of segmented pipelines, and pipe failure modes due to seismic effects; part II reviews the literature dealing with the current methods of analysis and design of liners for buried pipes rehabilitation. Chapter 3 presents a comparative study of liners buckling models for pipeline rehabilitation. Chapter 4 presents a methodology of finite element modeling of axial and rotational behaviours of unrestrained joints. Chapter 5 describes the numerical modeling procedures for the seismic behaviours of buried segmented pipelines subjected to longitudinal and transverse permanent ground deformation (PGD), a parametric study to explore the most important factors, and failure analysis to predict the potential of the pipeline joints for

damage. Chapter 6 presents an overview of the proposed finite element modeling procedure for the rehabilitated pipeline behaviours. The thesis closes with chapter 7, a summary of the significant findings and conclusions in addition to recommendations for future research. Selected details of pipes dimensions and material properties as well as soil spring stiffnesses calculations are presented in the appendices.

# CHAPTER 2

# LITERATURE REVIEW

# PART I: BURIED PIPES UNDER SEISMIC EFFECTS

## 2.1 INTRODUCTION

Pipelines can be classified as either continuous, such as steel pipelines with welded joints, or segmented, such as cast or ductile iron pipes with rubber gasketed joints, concrete pipes, etc. Segmented pipes usually are connected using different types of pipe joints. Moreover, buried pipes are usually classified according to their structural performances as either rigid (e.g., concrete pipes and vitrified clay pipes), which typically have a high degree of stiffness compared to the soil stiffness; or flexible (e.g., steel pipes and ductile iron pipes), which have comparatively low stiffness (Moser, 2001).

In general, buried pipes derive their ability to support the earth above them from two sources; first, the structural/material strength of the pipe wall to resist the external loads; and second, the lateral pressure of the soil at the sides of the pipes. Lateral pressure of the soil produces stresses in the pipe ring in directions opposite to those produced by the vertical loads. Therefore, this lateral pressure will help slightly to assist the pipe in supporting the vertical loads. However, in rigid pipes the structural/material strength of the pipe wall is the predominant source of supporting strength. Rigid pipes deform very little under the vertical loads so consequently, the sides do not move outward enough to develop any appreciable passive resistance pressure (Moser, 2001).

The pipeline material, whether it is flexible or rigid, as well as the joining systems determine the ability of the pipeline to resist the motion and energy associated with earthquakes. Thus, the pipe must be of sufficient strength and durability to resist earthquake tremors without rupture or cracking (Tucker, 1995). There have been

numerous investigations on the seismic behaviour of buried pipelines reported in the literature. Some closely related research work is reviewed in this chapter.

## 2.2 SEISMIC HAZARDS FUNDAMENTALS

For buried pipelines, seismic hazards can be classified as either transient ground deformation (TGD) or permanent ground deformation (PGD) hazards. This section reviews seismic hazards due to both transient ground deformation and permanent ground deformation effects, the failure modes and corresponding failure criteria for buried pipeline subject to seismic effects, and commonly used techniques to model the soil-pipe interaction in both the longitudinal and transverse directions. Figure 2.1 summarizes the seismic hazards of buried pipes.

### 2.2.1 TRANSIENT GROUND DEFORMATION HAZARD (TGD)

Transient ground deformation, which occurs as a result of seismic wave propagation (i.e., ground shaking) at a particular site, is characterized by the peak ground motion parameters (acceleration and velocity) as well as the appropriate propagation velocity. A good example of where transient ground deformation was responsible for high pipeline repair rates was in the 1985 Michoacan earthquake, which caused widespread damage to the water supply system in Mexico City. Ayala and O'Rourke (1989) reported that there was no soil liquefaction or permanent ground deformation in the Mexico City area, and they attributed the water system disruption primarily to seismic wave propagation effects.

#### A. WAVE PROPAGATION FUNDAMENTALS

A pipeline buried in soil that is subjected to the passage of seismic waves (e.g., compression, shear, and surface waves) will incur longitudinal and bending strains as it conforms to the associated ground strains.

## B. EFFECTIVE PROPAGATION VELOCITY

Since pipelines typically are buried horizontally at a depth of 1 m to 3 m below the ground surface, both body and surface waves are of interest. With regard to body waves, only S-waves are considered herein since S-waves carry more energy and tend to generate larger ground motion than P-waves do. For S-waves, the horizontal propagation velocity (the propagation velocity with respect to the ground surface) is the key parameter. O'Rourke *et al.* (1982) have studied the apparent horizontal propagation velocity, $C_o$, for body waves and they developed an analytical technique for evaluating the angle of incidence of S-waves. The apparent propagation velocity for S-waves is then given by:

$$C_o = \frac{C_s}{\sin \gamma_s} \tag{2.1}$$

where $\gamma_s$ is the incidence angle of S-waves with respect to the vertical axis and $C_s$ is the shear wave velocity of the surface soils.

For surface waves, only R-waves are considered since L-waves generate bending strains in buried pipelines that, particularly for moderate pipe diameters, are significantly less than the axial strain induced by R-wave's. Since R-waves always travel parallel to the ground surface, the phase velocity of the waves $C_{ph}$ (the velocity at which a transient vertical disturbance at a given frequency, originating at the ground surface, propagates across the surface of the medium) is the apparent propagation velocity. However, the phase velocity is a function of the variation of the shear wave velocity with depth and, unlike body waves, is also a function of frequency. For R-waves, the wavelength $\lambda$, frequency $f$, and phase velocity $C_{ph}$ are interrelated by:

$$C_{ph} = \lambda f \tag{2.2}$$

## C. GROUND STRAIN AND CURVATURE

For the analysis and design of buried pipelines, the effects of seismic wave propagation are typically characterized by ground strain and curvature. Newmark (1967) developed a simplified procedure to estimate ground strain. He showed that the maximum ground strain $\varepsilon_g$ (tension and compression) in the direction of wave propagation is given by:

$$\varepsilon_g = \frac{V_m}{C_o} \tag{2.3}$$

where $V_m$ is the maximum horizontal ground velocity in the direction of wave propagation. Similarly, the maximum ground curvature, $\kappa_g$, is given by:

$$\kappa_g = \frac{A_m}{C_o^2} \tag{2.4}$$

These two relations for ground strain and curvature along the direction of wave propagation are relatively straightforward. The ground motion parameter $A_m$ is the maximum particle acceleration that can be obtained from earthquake records or from attenuation relations. However, these relations for ground strain and curvature need to be modified if the direction of interest is not parallel to the direction of wave propagation.

Consider the case of S-waves. If the pipeline is oriented parallel to the direction of propagation, S-waves would induce bending in the pipeline. Equation 2.4 gives the corresponding ground curvature for the $C_o$ given in Equation 2.1. If there is an angle in the horizontal plane between the pipe axes, the resulting ground strain along the pipe axis is a function of this angle in the horizontal plane. Yeh (1974) showed that for an angle of 45° in the horizontal plane, the maximum ground strain is:

$$\varepsilon_g = \frac{V_m}{2C_o} \tag{2.5}$$

### 2.2.2 PERMANENT GROUND DEFORMATION HAZARD (PGD)

Permanent ground deformation occurs as a result of surface faulting, landsliding, seismic settlement, and lateral spreading due to soil liquefaction.

#### A. FAULTING

ASCE (1984) defined faulting as a relative movement between two adjacent portions of the earth crust. The movement is concentrated in relatively narrow fault zones. The fault can move horizontally, vertically, or as a combination of the two. During an earthquake this displacement occurs suddenly, but it can also occur gradually over a period of time due to tectonic activity.

Various empirical relations between fault displacement and moment magnitude have been proposed. They all have a similar logarithmic form. Newmark and Hall (1975) investigated the problem for the first time, and developed the cable model. Wells and Coppersmith (1994) extended the previous studies by including data from recent earthquakes and from new investigations of older earthquakes.

#### B. LANDSLIDE

Landslides are mass movements of the ground, which may be triggered by seismic shaking. Landslides include rockfalls, slumps, shallow slides, deep translation, and rotational movement. A large number of systems have been developed to classify landslides. The most widely used classification system in the United States was devised by Varnes (1978). Varnes identified five principal categories based on soil movements, geometry of the slide, and the types of material involved. Varne's categories are: falls, topples, slides, spreads, and flows.

### C. LATERAL SPREADING

Lateral spreading is considered to be one of the most common mechanisms of ground deformation caused by liquefaction during an earthquake (O'Rourke and Lane, 1989). Lateral spreads develop when loose saturated sandy soil deposits are liquefied due to seismic shaking (O'Rourke and Liu, 2000). Liquefaction causes the saturated cohesionless soil to lose its shear strength and stiffness, which in turn results in boiling, excessive ground deformation (lateral flow or movement), settlement of buildings, failure of slopes and lifelines, and total or partial collapse of other structures (Sun, 2001).

### D. SEISMIC GROUND SETTLEMENT

Earthquake-induced subsidence may be caused by densification of dry sand, consolidation of clay, or consolidation of liquefied soil. Among these three types, liquefaction-induced ground settlement is considered the most important because it can lead to larger ground movement and hence brings higher potential for damage to a buried pipeline system. Ground settlement induced by soil liquefaction was reported in the Marina District during the 1989 Loma Prieta earthquake (O'Rourke, 1991).

## 2.3 PIPE FAILURE MODES AND CRITERION FOR SEGMENTED PIPES

Design limits for buried pipes are the points at which buried pipes fail. Failure (i.e., collapse under service conditions) is directly related to stress, strain, deflection or buckling. Causes of failure of buried pipes are widely varied and dependent upon many factors such as soil stiffness, pipe stiffness, and loading distribution (Moser, 2001).

For segmented pipelines, observed seismic failure is most often due to distress at the pipe joints (Selventhiran, 2002). Axial pull-out, sometimes in combination with relative angular rotation at joints, is a common failure mechanism in areas of tensile ground strain since the shear strength of the joint caulking materials is much less than the tensile strength in the pipe. In areas of compressive ground strain, crushing of bell and spigot

joints is a fairly common failure mechanism in, for example, concrete pipes (O'Rourke and Liu, 1999). Moreover, when surface loading is conveyed to defected segmented rigid pipes, some displacement and rotation will occur at the joint and at the cracks.

O'Rourke and Liu (1999) reported that failure modes for corrosion-free segmented pipelines with bell and spigot type joints are axial pull-out at joints, crushing at the joints, and round flexural cracks in pipe segments away from the joints (see Figure 2.2). For small-diameter segmented pipes, circumferential flexural failures have been observed in areas of ground curvature. Figure 2.3 illustrates the typical patterns of failure mechanisms for segmented pipelines. This section describes the failure modes for segmented buried pipelines subjected to seismic loading.

### 2.3.1 AXIAL PULL-OUT

In terms of failure criterion, information for the various types of segmented pipes is relatively less well developed for continuous pipes. Elhmadi and O'Rourke (1989) summarized the available information on joint pull-out failure. Based on previous laboratory tests, they established a cumulative distribution for leakage as a function of the normalized joint axial displacement (joint opening/joint depth). They suggested that a relative joint displacement corresponding to 50% of the total joint depth as the failure criterion for pull-out of segmented pipelines with rigid joints. Also, Bouabid and O'Rourke (1994) suggested that, at moderate internal pressures, the relative joint displacement leading to significant leakage corresponds to roughly half the total joint depth. Hence, it would appear that a relative axial joint extension of roughly half the total joint depth may be an appropriate failure criterion for many types of segmented pipes.

### 2.3.2 CRUSHING OF BELL AND SPIGOT JOINTS

Ayala and O'Rourke (1989) reported that most of the concrete cylinder pipe failures in Mexico City during the 1985 Michoacan earthquake were due to joint crushing. The corresponding failure criterion, based on laboratory tests for crushing of bell and spigot

joints, is apparently not well established at this time. According to Bouabid and O'Rourke (1994), for the reinforced concrete cylinder pipes with rubber gasket joints, joint failure can start at either the inner concrete lining or the outer concrete lining. That is, a circumferential crack starts to form in the ends of the concrete lining when the applied load nears the ultimate value. After the concrete lining cracks, the critical section then becomes the welded interface between the steel joint ring and the steel pipe cylinder. The eccentricity existing between these two elements causes some denting (or even local buckling) near this weld region. Such damage eventually would result in a leakage path and/or cause the section to burst.

Both Bouabid and O'Rourke (1994) as well as Krathy and Salvadori (1978) proposed that the crushing failure criterion for concrete pipes can be taken as the ultimate compression force of the concrete core at joints, $F_u$, that is:

$$F_u = \sigma_{comp} \cdot A_{core} \tag{2.6}$$

where $\sigma_{comp}$ is the compressive strength of the concrete and $A_{core}$ is the cross-section of the concrete core for plain concrete pipes, while for reinforced concrete pipes, the transformed area of the steel bars needs to be added.

### 2.3.3 CIRCUMFERENTIAL FLEXURAL FAILURE AND JOINT ROTATION

When a rigid segmented pipeline system such as cast iron pipe with cement/lead joints is subjected to bending induced by lateral permanent ground movement or seismic shaking, the ground curvature is accommodated by some combination of rotation at the joints and flexure in the pipe segments. The relative distribution of these mechanisms depends on the joint rotation and pipe segment flexural stiffness. O'Rourke and Liu (1999) provided a listing of such manufacturers' recommendations of allowable angular offset as shown in Table 2.1. On the other hand, for vitrified clay or concrete pipes subject to ground curvature, the failure mode is one in which cracks typically occur at the bell and spigot ends due in part to the joint ring eccentricity. For round flexural cracks, it seems

reasonable to use the pipe curvature corresponding to the smaller of the ultimate tensile or compressive strains for the material (O'Rourke and Liu, 1999).

## 2.4 SOIL-PIPE INTERACTION

Many problems in geotechnical engineering involve interactions between two materials. Soil-structure interaction takes place in a thin layer of soil, called the interface. An example of a system that involves interface is underground pipelines. When such systems are subjected to loads, the interface may deform following different modes such as slippage and debonding. It is important to model the soil-pipe interface accurately in order to obtain a realistic solution to the interaction problem. Constitutive models for the characterization of the behaviour of interfaces include factors such as adhesion, friction, roughness, irreversible deformations, hardening, and softening (Missacotte, 2000).

The response of structures to the earthquake excitation is influenced by the behaviour of supporting soil deposits. Buried pipes are damaged in earthquakes due to forces and deformation imposed on them through interactions at the pipe-soil interface. That is, the ground moves and thereby causes the pipe to deform. For the purpose of analysis, any arbitrary ground deformation can be decomposed into a longitudinal component (soil movement parallel to the pipe axis) and a transverse component (soil movement perpendicular to the pipe axis). Both of the two types of pipe-soil interactions are discussed in the following section. In the transverse direction, interactions involve relative deformation and loading in both the horizontal and vertical planes. For relative ground movements in the vertical direction, one must distinguish between upward and downward pipe movements, since the interaction forces are different for these two cases.

Soil interaction forces for a pipeline surrounded by non-liquefied soil are well established. They are based upon laboratory tests. For example, Trautmann and O'Rourke (1983) established a force-deformation relation for horizontal lateral movement. Also, the ASCE Committee on Gas and Liquid Fuel Lifelines (ASCE, 1984) has suggested, for the purpose of analysis, idealized elasto-plastic models as shown in Figure 2.4. Note that the

elasto-plastic model is fully characterized by two parameters: the maximum soil resistances $t_u$, $p_u$, and $q_u$ in the horizontal axial, horizontal transverse, and vertical transverse directions respectively; and the maximum elastic deformations $x_u$, $y_u$, and $z_u$. The equivalent elastic soil spring coefficients are simply the ratio of the maximum resistance divided by the maximum elastic deformation, for example ($t_u/x_u$) for the axial (longitudinal) case. Note that this spring coefficient is effective only for relative displacements less than the maximum values of $x_u$, $y_u$, and $z_u$, after which the resistance is constant.

The soil spring stiffness increases as a function of the effective soil stress and is a decreasing function of excess water pressures. The equivalent spring stiffness coefficients for axial/lateral or vertical soil movement can be estimated from the ASCE guideline (1984) as described in the following sections. Table 2.2 summarizes the idealized load-deformation relations for soil springs at the pipe-soil interface as proposed by the ASCE guideline (1984).

### 2.4.1 LONGITUDINAL MOVEMENT

Relative movement parallel to the pipe axis results in longitudinal (horizontal axial) forces at the pipe-soil interface. For the elasto-plastic model, the 1984 ASCE guideline provides the following relations for clay and sand:

For sand,

$$t_u = 0.5\ \pi D\ \bar{\gamma}\ H\ (1+k_o)\ \tan(k\ \varphi) \tag{2.8}$$

$$x_u = (0.1\sim0.2)\ in. = (2.54\sim5.08)\ 10^{-3}\ m \tag{2.9}$$

For clay,

$$t_u = \pi D\, \alpha_o\, S_u \tag{2.10}$$

$$x_u = (0.1\sim0.2)\ in. = (2.54\sim5.08)\ 10^{-3}\ m \tag{2.11}$$

where $D$ is the pipe diameter, $S_u$ is the undrained shear strength of the surrounding soil, $\alpha_o$ is an empirical adhesion coefficient varying with $S_u$, $\gamma^-$ is the effective unit weight of the soil, $H$ is the depth to the springline of the pipeline, $\varphi$ is the angle of shear resistance of the sand, and ($k_o$) is the coefficient of lateral soil pressure at rest. The magnitude of ($k_o$) for normally consolidated cohesionless soil has been reported to range from 0.35 to 0.47 (Perloff and Baron, 1976). However, one expects ($k_o$) to be somewhat larger because of backfilling and compaction of the soil around pipelines. O'Rourke *et al.* (1985) recommend ($k_o$ = 1.0) as a conservative estimate under most conditions of pipeline burial. Finally, $k$ is the reduction factor depending on the outer-surface characteristics and hardness of the pipe. For concrete pipe or for steel or cast iron pipe with cement coating, $k$= 1.0; for cast iron or rough steel, $k$ ranges from 0.7 to 1.0; while for smooth steel or for a pipe with smooth and relatively hard coating, $k$ ranges from 0.5 to 0.7.

### 2.4.2 HORIZONTAL TRANSVERSE MOVEMENT

Relative movement perpendicular to the pipe axis in the horizontal plane results in horizontal transverse forces at the pipe-soil interface. For the elasto-plastic model, the ASCE guideline (1984) provides the following relations for sand and clay:

For sand,

$$p_u = D\, \gamma^-\, H\, N_{qh} \tag{2.12}$$

$$y_u = \{(0.07\sim0.10)\ (H+\frac{D}{2})\}in. = \{(1.78\sim2.54)\ (H+\frac{D}{2})\ 10^{-3}\}m \quad \text{loose sand} \tag{2.13}$$

$$y_u = \{(0.03\sim0.05)\ (H+\frac{D}{2})\}in. = \{(0.76\sim1.27)\ (H+\frac{D}{2})\ 10^{-3}\}m \quad \text{medium sand} \qquad (2.14)$$

$$y_u = \{(0.02\sim0.03)\ (H+\frac{D}{2})\}in. = \{(0.50\sim0.76)\ (H+\frac{D}{2})\ 10^{-3}\}m \quad \text{dense sand} \qquad (2.15)$$

For clay,

$$p_u = D\ N_{ch}\ S_u \qquad (2.16)$$

$$y_u = (0.03\sim0.05)(H+\frac{D}{2})\ in. = (0.76\sim1.27)(H+\frac{D}{2})10^{-3}\ m \qquad (2.17)$$

where $N_{qh}$ $N_{ch}$ are the horizontal bearing capacity factors for sand and clay respectively.

### 2.4.3 VERTICAL TRANSVERSE MOVEMENT

Relative upward movement perpendicular to the pipe axis results in lateral forces at the pipe-soil interface. For the elasto-plastic model, the ASCE guideline (1984) provides the following relations for sand and clay:

For sand,

$$q_u = \gamma^{-}\ H\ N_{qv}\ D \qquad (2.18)$$

$$z_u = (0.01\sim 0.02)\ H\ (in.) = (2.54\sim5.08)\ 10^{-3}\ \ H\ (m) \qquad (2.19)$$

For clay,

$$q_u = S_u\ N_{cv}\ D \qquad (2.20)$$

$$z_u = (0.1\sim0.2)\ H\ \ (in.) = (2.54\sim5.08)\ 10^{-3}\ \ H\ (m) \qquad (2.21)$$

where $N_{qv}$ is the vertical uplift factor for sand and $N_{cv}$ is the vertical uplift factor for clay. Relative downward movement perpendicular to the pipe axis in the vertical plane results in lateral forces at the pipe-soil interface. For the elasto-plastic model, the ASCE guideline (1984) provides the following relations for sand and clay:

For sand,

$$q_u = \gamma^{-} H N_q D + 0.5 \gamma D^2 N_\gamma \tag{2.22}$$

$$z_u = (0.10\sim0.15)\, H \ (in.) = (2.54\sim5.08)\, 10^{-3} \ H \ (m) \tag{2.23}$$

For clay,

$$q_u = C N_c D \tag{2.24}$$

$$z_u = (0.10\sim0.15)\, H \ (in.) = (2.54\sim5.08)\, 10^{-3} \ H \ (m) \tag{2.25}$$

where $\gamma$ is the total unit weight of sand, $N_q$ and $N_\gamma$ are the bearing capacity factors for horizontal strip footings on sand loaded in the vertical downward direction, and $N_c$, is the bearing capacity factor for horizontal strip footings on clay loaded in the vertical downward direction.

## 2.5 RESPONSE OF SEGMENTED PIPELINES SUBJECTED TO PGD

Segmented pipes typically have bell and spigot joints and can be made of cast iron, ductile iron, steel, concrete, or vitrified clay. As mentioned previously, there are three main failure modes for segmented pipes: axial pull-out at joints, crushing of the bell and spigot joints, and round flexural cracks in the pipe segment away from the joints. Similar to the response of continuous pipelines, the behaviour of a given buried segmented pipeline is a function of the type of the permanent ground deformation (e.g., longitudinal

or transverse), the amount of ground movement $\delta$, the width of the permanent ground deformation zone $W$, and the pattern of ground movement within the zone (see Figure 2.5). In reference to the type of permanent ground deformation, Suzuki (1988) concluded that damage due to longitudinal permanent ground deformation was more common than damage due to transverse permanent ground deformation based on the observed damage to segmented gas pipelines during the 1964 Niigata earthquake. In those cases, the joints were pulled out in the tension region and buckled in the compression region.

### 2.5.1 RESPONSE OF SEGMENTED PIPELINES SUBJECTED TO LONGITUDINAL PGD

As with the continuous pipelines, longitudinal PGD induces axial strains in the pipe segments and relative axial displacements at the joints since the strength of the joints is generally less than the strength of the pipe itself (O'Rourke and Liu, 1999). The joints' failure depends on the strength and deformation capacity of the joints as well as the pattern of the PGD.

The study of Hamada *et al.* (1986) of liquefaction in the 1964 Niigata earthquake and 1983 Nihonkai-Chubu earthquake provide a wealth of information on observed longitudinal PGD patterns. In terms of the PGD pattern, Figure 2.6 shows longitudinal PGD observed along five of 27 lines in Noshiro City resulting from the 1983 Nihonkai-Chubu earthquake. In this Figure the height of the vertical line is proportional to the observed horizontal PGD at the point. Note that about 20% of the observed patterns (6 out of 27) have the same general shape as shown in Figure 2.6a and they show relatively uniform PGD movement over the whole length of the lateral spread zone. Information on transverse PGD is more limited (Liu 1996). For the purpose of analysis, O'Rourke and Nordberg (1992) have idealized five patterns as shown in Figure 2.7. That is, the block pattern in Figure 2.7a is an idealization of the relatively uniform longitudinal pattern in Figure 2.6a, while the Ramp, Ramp-Block, Symmetric Ridge and Asymmetric Ridge patterns are idealization of the observed patterns in Figure 2.6b, c, d, and e, respectively.

Herein, two types of PGD patterns are considered in detail. For the distributed deformation case (e.g., the idealized Ridge pattern in Figure 2.7c) ground strain exists over a significant portion of the PGD zone. For the abrupt deformation case, such as the idealized block pattern in Figure 2.7a, relative movement exists only at the margins of the PGD zone and the ground strain between the margins is zero.

## A. DISTRIBUTED DEFORMATION

The response of segmented pipelines subjected to a distributed deformation of longitudinal PGD is similar to that for segmented pipelines subject to wave propagation in that the spatially distributed PGD results in a region of ground strain (O'Rourke and Liu, 1999). That is, the Ridge, Asymmetric Ridge, and Ramp patterns in Figure 2.7 result in ground strain over the whole length of the PGD zone, while the Ramp-Block pattern results in uniform ground strain over a portion of the zone. For example, the ground strain $\varepsilon_g$ for the Ridge pattern is:

$$\varepsilon_g = \frac{2\delta}{W} \tag{2.26}$$

where $\delta$ is the permanent horizontal displacement of ground (i.e., PGD). By assuming that pipe segments are rigid and all of the longitudinal PGD is accommodated by the extension or contraction of the joints, the average relative displacement $\Delta u_{avg}$ at the joints is given by the ground strain $2\delta/W$ times the pipe segment length $L_o$ as:

$$\Delta u_{avg} = \frac{2\delta L_o}{W} \tag{2.27}$$

Although Equation 2.27 represents the average behaviour, the joint displacements for uniform ground strain varied somewhat from joint to joint due to variation in joint stiffness. A relatively flexible joint is expected to experience larger joint displacements than adjacent stiffer joints. To gauge the effects of a distributed deformation pattern of longitudinal PGD on segmented pipe, expected joint openings are calculated. If the

corresponding joint opening is larger than the joint capacity of typical segmented pipelines (segmented joints typically leak for relative displacement on the order of half the total joint depth), then the typical segmented pipelines are vulnerable and consideration should be given to replacement by continuous pipelines or segmented pipelines with special joints (having large contraction/expansion capacity and/or anti-pull-out restraints) when crossing a potential longitudinal PGD zone. However, the potential for damage due to something other than joint pull-out of simple bell and spigot joints is more difficult to evaluate. For example, tensile, failure of various types of restrained joints or crushing of simple bell and spigot joints typically involves some slippage in the joint before significant load is transferred across the joint.

### B. ABRUPT DEFORMATION

Abrupt longitudinal PGD refers to ground movements with large relative offsets at localized points. The block pattern in Figure 2.7a provides an example. In this case, the ground strain is zero away from the margins of the PGD zone; there is a tensile opening or gap at the head of the zone and a localized compressive mound at the toe. The ramp and ramp-block patterns in Figure 2.7b and d also have an abrupt offset, but for these patterns this offset is at only one end of the PGD zone. At the head of the zone (i.e., the tension gap), pipeline failure for typical bell and spigot joints is probable. In the simplest model, one expects joint leakage or pull-out if the relative joint displacement corresponding to leakage or pull-out respectively is less than the ground offset (which is $\delta$ in Figure 2.7).

## 2.5.2 RESPONSE OF SEGMENTED PIPELINES SUBJECTED TO TRANSVERSE PGD

In considering the response of segmented pipelines subjected to transverse PGD, one must differentiate between spatially distributed transverse PGD and localized abrupt transverse PGD, the later being a special case of fault offset (intersection angle of 90°).

## A. SPATIALLY DISTRIBUTED PGD

For segmented pipelines subjected to spatially distributed transverse PGD, the failure modes include: (1) round cracks in the pipe segments and crushing of bell and spigot joints due to bending; and (2) pull-out at the joint due to axial elongation (i.e., arc-length effects). O'Rourke and Nordberg (1991) studied the maximum joint opening due to both joint rotation and axial extension of segmented pipes (i.e., arc-length effects), which results when pipe segments move to follow the specified displacement pattern.

Assuming that the pipe segments are rigid (i.e., $EA = \infty$, $EI = \infty$) and that the lateral displacement at the midpoint of the rigid pipe segment exactly matches the spatially distributed PGD at that point, O'Rourke and Nordberg developed the expression defining the arc-length effects by computing the relative axial displacement at a joint $\Delta x_t$ due to axial extension as:

$$\Delta x_t = \frac{L_o}{2}\left(\frac{\pi\delta}{W}\sin\frac{2\pi x}{W}\right)^2 \tag{2.28}$$

where $x$ is the distance from the margin of the PGD zone and $W$ is the width of the PGD zone.

The axial displacements are largest for joints near $x = 0.25W$ and $x = 0.75W$. Hence, a pure joint pull-out failure mode is most likely to occur at the locations $0.25W$ away from the center of the PGD zone. The peak relative axial displacement due to arc-length effect is given by:

$$\Delta x_t = \frac{L_o}{2}\left(\frac{\pi\delta}{W}\right)^2 \tag{2.29}$$

The peak axial strain due to arc-length effect is given by:

$$\varepsilon_a = \left(\frac{\pi\delta}{2W}\right)^2 \tag{2.30}$$

If the small strain theory is applied, the expected displacement of the ground will be small and subsequently the arc-length effect estimated by Equation 2.30 will be too small and could be neglected. If the large strain theory is applied, the joint openings due to arc-length effects should be calculated separately using Equation 2.30 and added to the computed finite element model results.

Assuming the slope of the rigid pipe segment exactly matches the ground slope at the segment midpoint, the joint opening due to the joint rotation $\Delta x_t$ is as follows:

$$\Delta x_t = \begin{cases} \frac{\pi^2 \delta D L_o}{W^2} \cos\frac{2\pi x}{W} & \text{for } \Delta x_t > \Delta\theta \frac{D}{2} \end{cases} \tag{2.31}$$

$$\Delta x_t = \begin{cases} \frac{2\pi^2 \delta D L_o}{W^2} \cos\frac{2\pi x}{W} & \text{for } \Delta x_t < \Delta\theta \frac{D}{2} \end{cases} \tag{2.32}$$

where $D$ is the pipe diameter and $\Delta\theta$ is the relative joint rotation between adjacent segments.

The functions developed in Equations 2.31 and 2.32 are at a maximum at $x = 0,\ 0.5W$, and $W$. Hence, a pure joint rotation failure and/or flexural round cracks are more likely to occur at the margins and middle point of the PGD zone. The total maximum opening at one side of a joint $\Delta x$ due to the transverse PGD is simply the sum of axial extension and rotation effects. However, the axial and rotational components are largest at different points, as discussed previously. Combining these effects, the resulting maximum joint opening is:

$$\Delta x = \begin{cases} \frac{\pi^2 \delta L_o}{W^2}\left(\frac{2D}{\delta}\right) & \text{for} \quad 0.268 \le \frac{D}{\delta} > 3.73 \end{cases} \tag{2.33}$$

$$\Delta x = \begin{cases} \frac{\pi^2 \delta L_o}{2W^2}(1+(\frac{D}{\delta})^2) & \text{for} \quad \text{other} \end{cases} \qquad (2.34)$$

Note that the maximum joint opening in these relationships is an increasing function of the $\delta/W$ and $D/\delta$ ratios. The response of segmented buried pipes to seismic excitation is shown in Figure 2.8.

## 2.6 RESPONSE OF SEGMENTED PIPELINE TO WAVE PROPAGATION

The seismic loads on buried pipelines imposed by wave propagation are typically characterized by ground strains.

### 2.6.1 SEGMENTED PIPELINE SUBJECTED TO TENSILE GROUND STRAIN

Wang (1979) determined the pipe strain and joint deformation for rigid segmented pipe using the analytical model shown in Figure 2.9, in which the joint is modeled as a linear spring with axial stiffness. Wang's model correctly captures the trend of decreasing joint opening as concurrent with increasing joint stiffness. However, it assumes an equivalent linear joint stiffness while laboratory tests suggest that joint axial behaviour is non-linear. Furthermore, for a given stiffness, the relative displacement at each joint in the model is the same. That is, Wang's model does not capture the variation in displacement from joint to joint.

For a long straight run of segmented pipe, the ground strain is accommodated by a combination of pipe strain and relative axial displacement (expansion/contraction) at pipe joints. As noted by Iwamoto *et al.* (1984), since the overall axial stiffness for the pipe segments is typically much larger than that for the joints, the ground strain results primarily in relative displacement of the joints.

Elhmadi and O'Rourke (1990) considered a model somewhat similar to that shown in Figure 2.9, specifically a cast iron pipe with lead caulked joints subjected to tensile ground strain, in which the joint properties varied from joint to joint and the soil properties varied from one pipe segment to another. They reported that the variability of joint displacement was a decreasing function of pipe diameter. As a first approximation, assuming that the pipe segment axial strain can be neglected (i.e., rigid segment) and that all joints experience the same movement, the maximum joint movement $\Delta u$ is:

$$\Delta u = \varepsilon_{max} \, . \, L_o \tag{2.35}$$

where $\varepsilon_{max}$ is the maximum ground strain parallel to the pipeline axis, as given by Equation 2.3.

For ground motion perpendicular to the pipe axis, the bending strain is small and can be neglected and all joints experience the same relative rotation (O'Rourke and Liu, 1999). The maximum relative rotation at pipe joint $\Delta\theta$ can be estimated by:

$$\Delta\theta = \kappa_g \, . \, L_o \tag{2.36}$$

where $\kappa_g$ is the maximum ground curvature, as given by Equation 2.4.

### 2.6.2 SEGMENTED PIPELINE SUBJECTED TO COMPRESSIVE GROUND STRAIN

Extensive damage to concrete pipelines has occurred when these elements are subjected to compressive ground strain. For wave propagation resulting in compressive ground strain, the failure mode of interest is crushing, (i.e., telescoping) at pipe joints. Bouabid (1993) conducted a series of laboratory tests on reinforced concrete cylinder pipelines with rubber gasketed joints. He presented a force–displacement relationship, based upon the thickness of the pipe wall, the diameter pipe, and the concrete strength, in order to establish the joint crushing force.

## 2.7 SUMMARY AND CONCLUSIONS

In summary, most frequent and severe damage resulting from seismic effects usually occurs at or near a pipeline joint. Most of the failures result from ground strains, which develop axial or shear forces in the pipeline and at the joints. Based on past analytical solutions, numerical simulations, and field and laboratory studies on buried pipelines under seismic effect, the following conclusions can be stated:

1. Pipelines are mainly affected by seismic wave and by the influence of fluctuant deformation of the surrounding soil.

2. Pipelines buried in soft soil experience more damage than do those in firm soil.

3. Pipe strains are highly sensitive to phase differences in the wave propagation through the soil along the pipe axis. However, damage to pipelines is most frequent where the pipes are parallel to the direction of propagation of the seismic wave and less frequent when the pipeline is normal to the direction of wave propagation. Thus, axial strain is significant in buried pipelines.

4. The seismic performance of large-diameter pipes is better than that of small diameter pipes, indicating that the stiffness of the pipeline may restrain the deformation of the surrounding soil. However, axial strains usually dominate in pipes of small diameter while bending strains appear to become important in larger pipes.

5. Pipes generally move with surrounding soils. The locations of tee joints and elbows will concentrate stress; therefore, most pipeline damage occurs at or near joints. However, the pipeline displacements are less than those of surrounding soils.

6. Rigid joints (lead or caulked) and mechanical joints are more vulnerable to seismic damage than are flexible rubber gasket joints, because the latter absorb more strain.

7. Active and passive pressures in the soil and soil friction angles are some of the major parameters that influence pipeline damage due to fault movement.

8. In general, the increase in the depth of the embedment seems to reduce the damage in a buried pipeline.

9. Natural frequencies of pipes are too high to cause the state of resonance that occurs under earthquake acceleration.

10. Pipeline failures due to buckling phenomena appear to be particularly dominant in pipelines crossing a fault. Pipes made of lower grades of steel show more resistance to large-fault displacement due to their larger ductility. Thus, it appears that ductility is the most important factor for the seismic resistant design of buried pipes.

Table 2.1 Typical Manufacturers' Recommendations of Allowable Angular Offset for Pipes Laying Purposes (After O'Rourke and Liu, 1999)

| *D* mm (in) | Cast Iron | Ductile Iron | | Prestressed Concrete | Concrete |
|---|---|---|---|---|---|
| | | Push on Joint | Mechanical Joint | | |
| 100 (4) | 4° 00′ | 5° | 8° 18′ | | |
| 150 (6) | 3° 30′ | 5° | 7° 07′ | | |
| 200 (8) | 3° 14′ | 4° | 5° 21′ | | |
| 250 (10) | | 4° | 5° 21′ | | |
| 300 (12) | 3° 00′ | 4° | 5° 21′ | | |
| 350 (14) | | 3° | 3° 35′ | | |
| 400 (16) | 2° 41′ | 3° | 3° 35′ | | 2° 19′ |
| 450 (18) | | 3° | 3° 00′ | | 2° 04′ |
| 500 (20) | 2° 09′ | 3° | 3° 30′ | | 1° 52′ |
| 600 (24) | 1° 47′ | 2° | 2° 23′ | | 1° 34′ |
| 675 (27) | | 2° | 2° 23′ | | 1° 24′ |
| 750 (30) | 1° 26′ | 2° | 2° 23′ | 1° 44′ | 1° 15′ |
| 825 (33) | | 1° 30′ | | 1° 35′ | 1° 09′ |
| 950 (36) | | 1° 30′ | 2° 05′ | 1° 28′ | 1° 03′ |
| 1050 (42) | | 1° 30′ | 2° 00′ | 1° 16′ | 1° 03′ |
| 1200 (48) | | 1° 30′ | 2° 00′ | 1° 06′ | 1° 03′ |
| 1500 (60) | | 1° 30′ | | 0° 56′ | |
| 1800 (72) | | 1° 30′ | | 0° 56′ | |

Table 2.2 Summary of Idealized Load-Deformation Relations for Soil Springs at Pipe-Soil Interface (ASCE, 1984)

| Movement Direction | | Soil Type | Maximum Soil Resistance Force lb (N) | Maximum Elastic Deformation mm (in) |
|---|---|---|---|---|
| Longitudinal | Longitudinal | Sand | $t_u = 0.5\ \pi D\ \gamma^{-} H\ (1+k_o)\ tan(k\varphi)$ | $x_u = (0.1\sim0.2)$ |
| | | Clay | $t_u = \pi D\ \alpha S_u$ | $x_u = (0.1\sim0.2)$ |
| Transverse | Horizontal | Sand | $P_u = D\ \gamma^{-} H\ N_{qh}$ | For loose sand $y_u = \{(0.07\sim0.10)(H+\frac{D}{2})\}$ |
| | | | | For medium sand $y_u = \{(0.03\sim0.05)(H+\frac{D}{2})\}$ |
| | | | | For dense sand $y_u = \{(0.02\sim0.03)(H+\frac{D}{2})\}$ |
| | | Clay | $P_u = D\ N_{ch} S_u$ | $y_u = \{(0.03\sim0.05)(H+\frac{D}{2})\}$ |
| | Vertical upward | Sand | $q_u = \gamma^{-} H\ N_{qv} D$ | $z_u = (0.01\sim 0.02)\ H$ |
| | | Clay | $q_u = S_u N_{cv} D$ | $z_u = (0.1\sim0.2)\ H$ |
| | Vertical downward | Sand | $q_u = \gamma^{-} H\ N_q\ D + 0.5\ \gamma\ D^{'}\ N_r$ | $z_u = (0.10\sim0.15)\ H$ |
| | | Clay | $q_u = C\ N_c\ D$ | $z_u = (0.10\sim0.15)\ H$ |

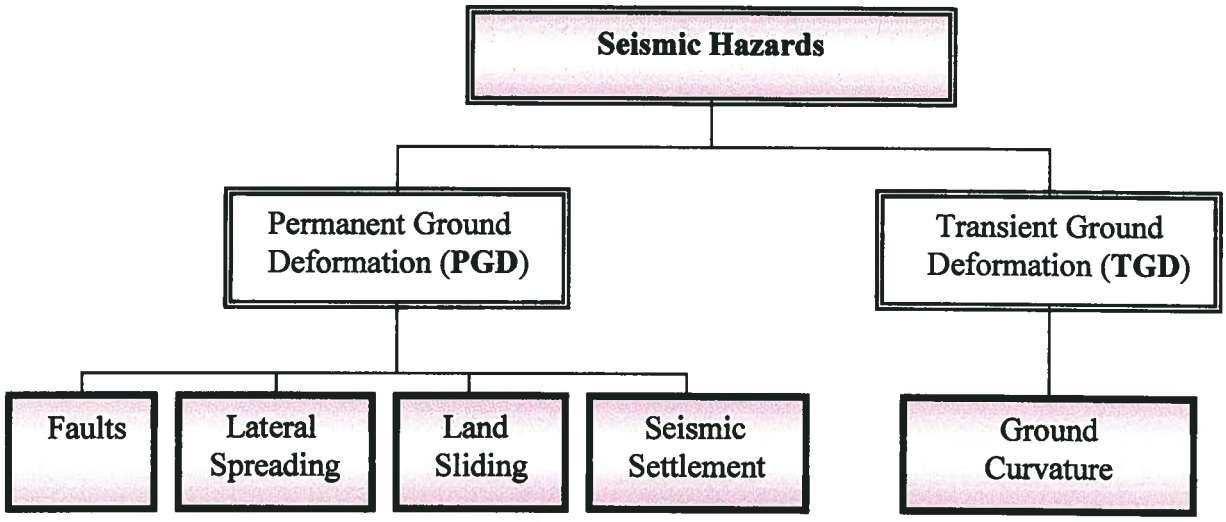


Figure 2.1 Common Types of Seismic Hazards of Buried Pipes

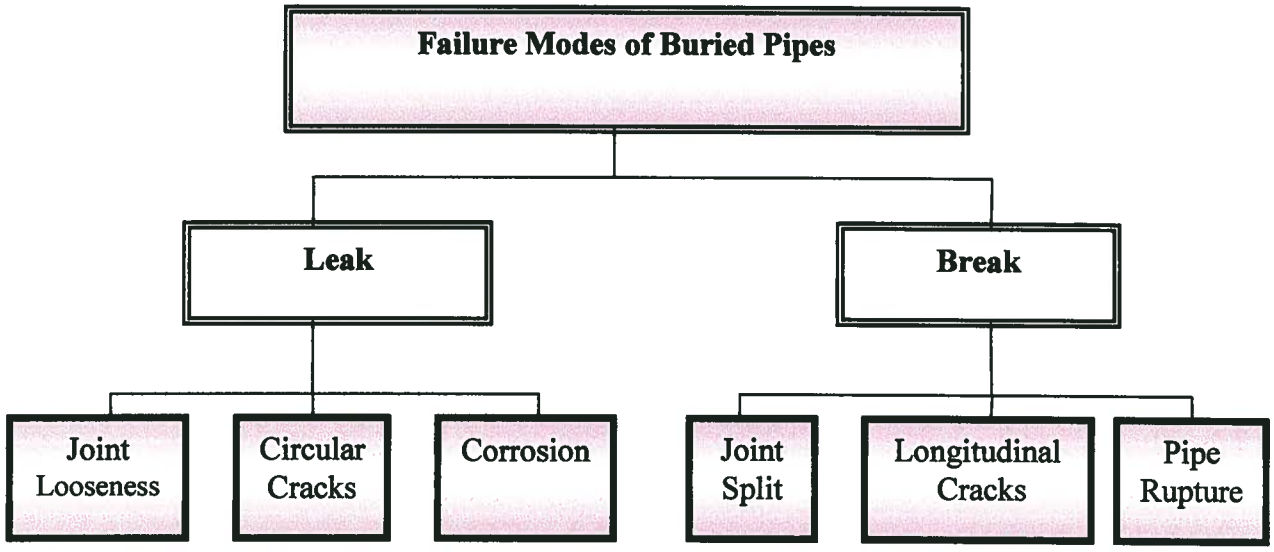


Figure 2.2 Buried Pipes Modes for Different Damage Causes

(a) Pipe Segment Break

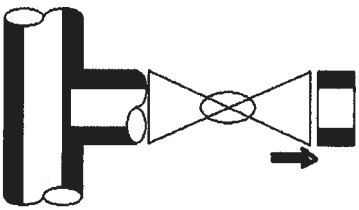

(d) Disconnection at Tee

(b) Break in Union Piece

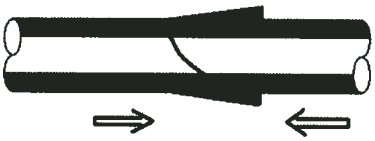

(e) Compressive Telescoping

(c) Blowout at Tee

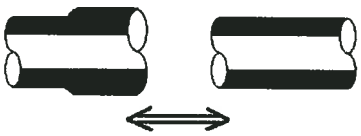

(f) Tensile Pull-out at Joint

Figure 2.3 Patterns of Failure Mechanisms for Segmented Pipelines
(After O'Rourke and Ballantyne, 1992)

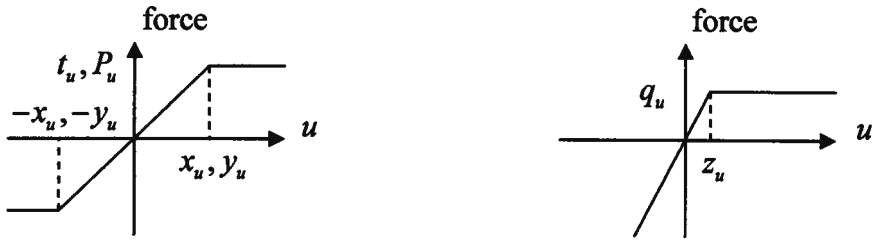


(a) Horizontal Spring (Axial/Transverse) (b) Vertical Spring (Transverse)

Figure 2.4 Idealized Load-Deformation Relations for Soil Springs at Pipe-Soil Interface (After ASCE guidline, 1984)

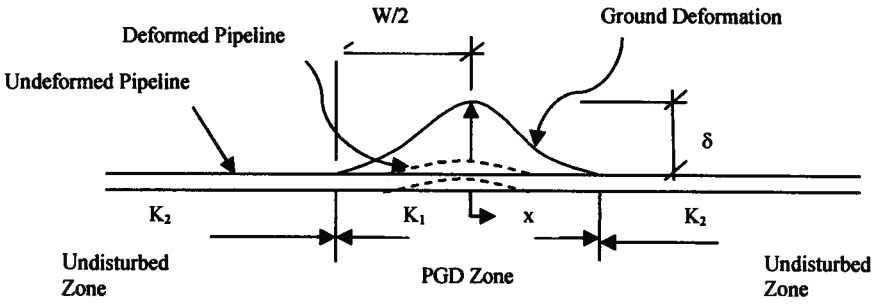


Figure 2.5 Schematic Illustration of PGD Pattern for a Continuous Pipe Subjected to Seismic Effect (After Miyajima and Kitaura, 1989)

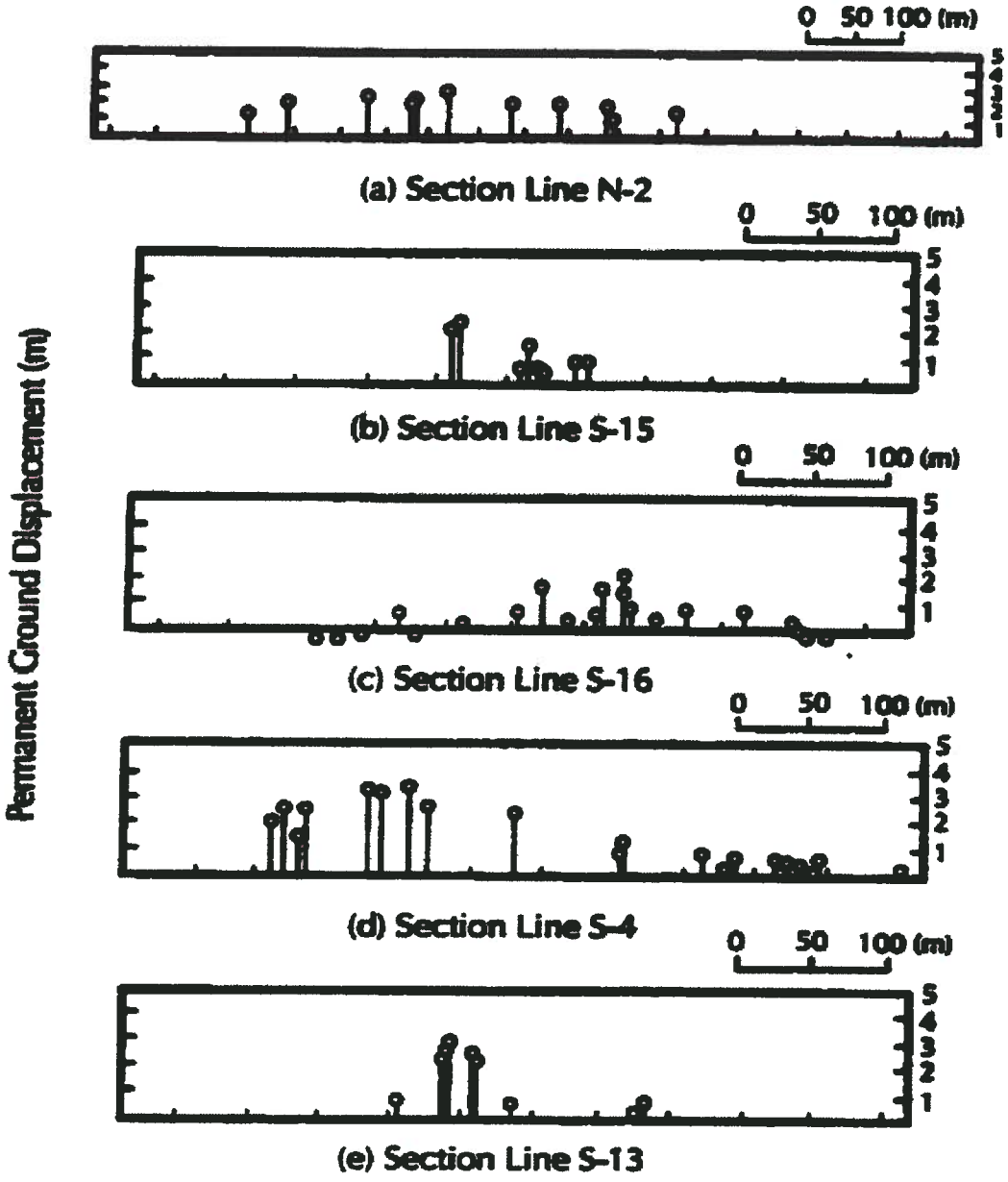


Figure 2.6 Observed Axial Ground Deformation (Hamada *et al.*, 1986)

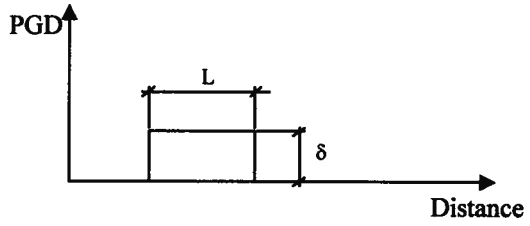


(a) Block Pattern

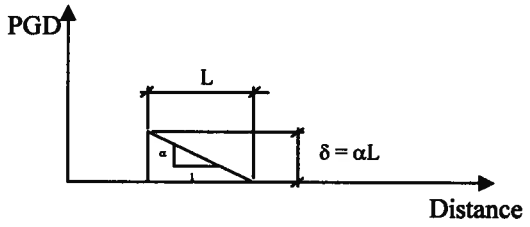


(b) Ramp Pattern

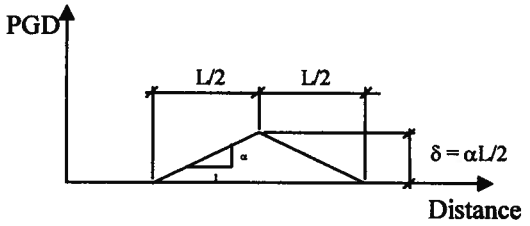


(c) Ridge Pattern

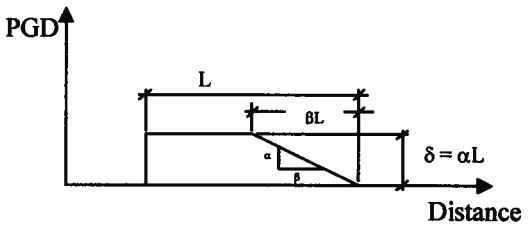


(d) Ramp-Block Pattern

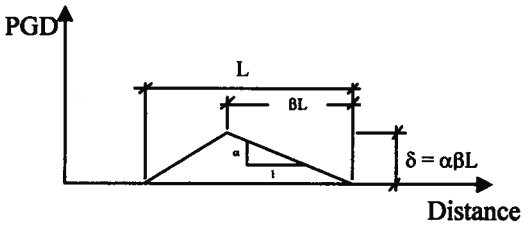


(e) Asymmetric Ridge Pattern

Figure 2.7 PGD Patterns for a Buried Pipeline Subjected to Seismic Effect (After O'Rourke and Nordberg, 1992)

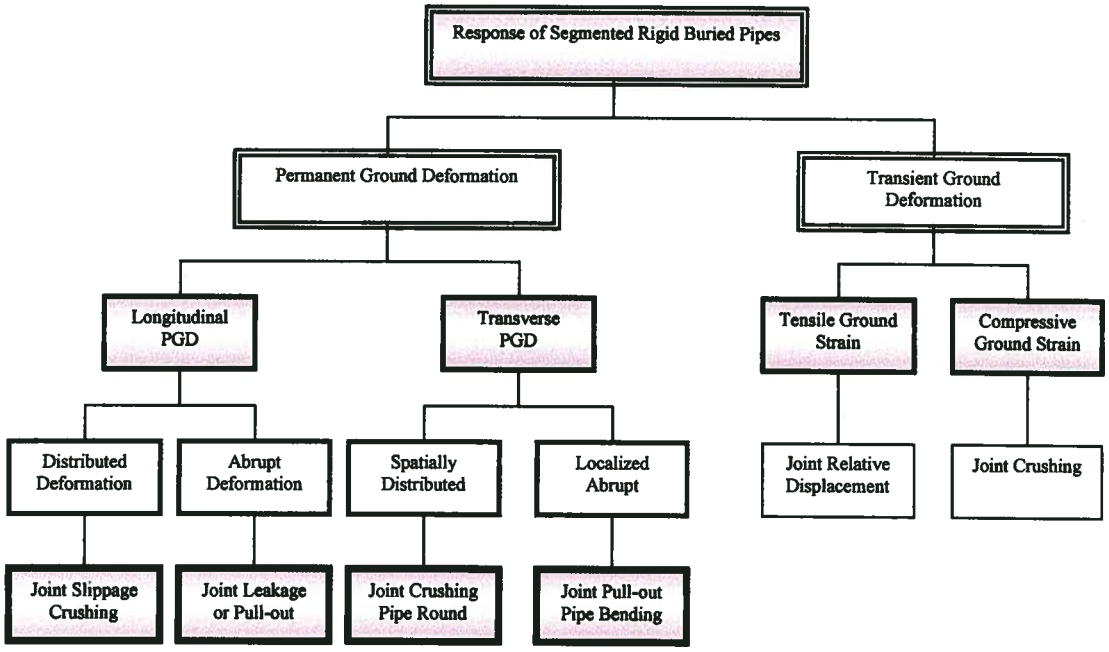


Figure 2.8 Segmented Buried Pipe Responses to Seismic Excitation

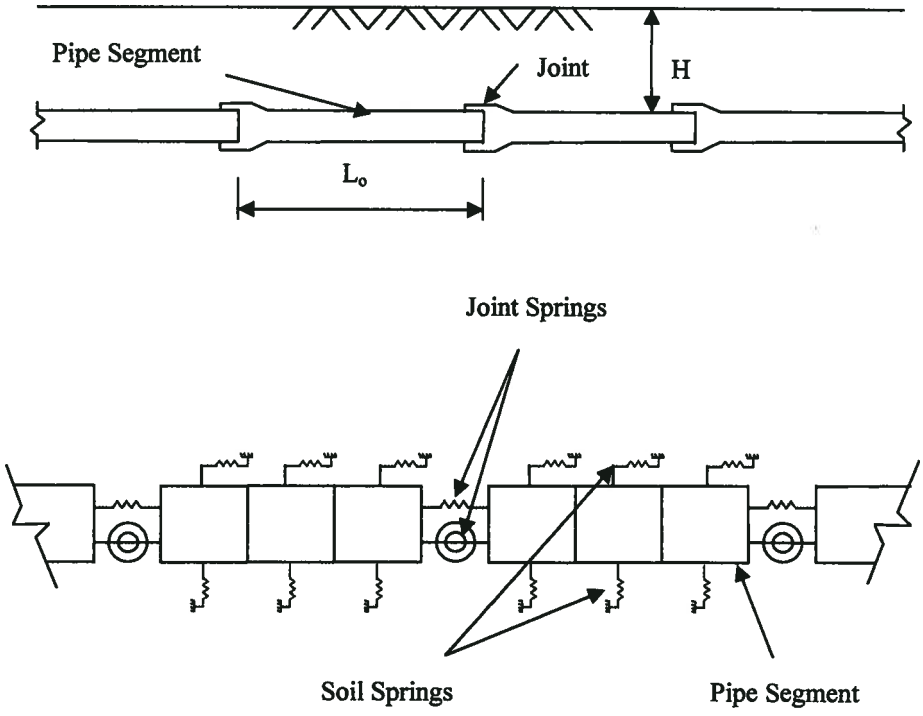


Figure 2.9 Model of Buried Segmented Pipe (After Wang, 1979)

# PART II: BURIED PIPES REHABILITATION

## 2.8 INTRODUCTION

Traditionally, the installation, inspection, repair, and replacement of underground utilities are carried out using open-cut construction methods. Such operations may prove to be costly as additional costs typically are incurred both by the need to restore landscape features (i.e., sidewalks, pavement, and brick paving) and also to implement extensive temporary traffic control measures. Aside from the associated high agency costs, open-cut trenching operations often result in high user ("social") costs due to the disruption of traffic and its subsequent adverse impact on nearby businesses (Allouche and Ariaratnam, 2002).

Through trenchless technology techniques, new pipelines can be installed or pipelines can be rehabilitated without the need for cut-and-fill excavation. The use of such techniques can offer numerous benefits, including:

- Minimize overall cost and provide economic alternatives to traditional open-cut methods of installation, renewal, and/or repair.
- Reduce environmental impact.
- Reduce public disruptions to pedestrians and vehicular traffic.
- Reduce construction time.
- Restore pipeline integrity.
- Retain existing landscaping.

The rapid growth in popularity of trenchless construction has encouraged the development of a large number of new technologies and variations of existing methods, each of these with its own advantages and limitations. Since the mid-1980s, a number of commercially available repair processes offering "trenchless" or "no-dig" solutions have emerged to dominate the pipeline industry. From the successful use of closed-circuit television monitoring (CCTV) to state-of-the-art robotics, continuing technological developments have made trenchless solutions increasingly practical, economic, and

effective. It is anticipated that utilization of trenchless technology techniques will increase as municipalities and utilities companies search for cost reduction and less disruption in providing services to their customers (Lueke, 2003). Zhao and Rajani (2002) compiled and plotted a total of 174 data records for different methods of trenchless techniques in terms of overall average cost (at year 2001 value and in $ CDN) as shown in Figure 2.10. It is clear from this cost comparison that all such renovation/rehabilitation techniques cost less than the open-cut method. However, costs of all trenchless rehabilitation methods increase with increase in pipe diameter.

Where buried old pipeline systems have not been maintained, and in some cases where land subsidence has occurred due to ground shaking, the problems of breaking and leaking can be extensive. Today, many alternatives are available for installation, replacement, and renovation/rehabilitation of deteriorating buried pipeline systems. Rehabilitation of defective pipelines with some residual structural and physical life is one of the trenchless technology applications. Alternative rehabilitation techniques are shown in Figure 2.11. Pipe lining methods include close-fit lining, sliplining, and spray lining, and cured–in-place lining (CIPP).

The close-fit lining method temporarily reduces the cross-sectional area of the new pipe before it is installed, and then expands it to its original size and shape after placement to provide a close-fit with the existing pipe.

The slip lining process is also known as insertion method. This method consists of sliding a new pipeline of smaller diameter into the existing pipeline and usually the annulus space between the existing and new pipe is grouted. The main advantages of this method are the minimal excavation required and the little interference with the underground structures. However, there can be a significant loss of hydraulic capacity.

The spray lining is a method of lining pipes with a thin lining of quick setting epoxy resin or polyurethane material (typically 1 mm thick), which is sprayed onto a cleaned surface of host pipe. The aim of this technique is to isolate the host pipe from the conveyed

medium. There may be some potential for this technique to be used to reinforce the structural capabilities of the host pipe.

CIPP lining is the main focus of this research and involves the insertion of a flexible fiber tube coated with a thermosetting resin into an existing pipe barrel by hydrostatic or air inversion. Once installed, the resin is cured under ambient conditions or through applied heat provided by circulating steam or hot water throughout the tube. The liner is expanded and bonded to the host pipe to form a tight fitting liner within the host pipe upon the hardening of the resin. The CIPP process is classified as renovation because it incorporates the liner fabric to produce improved performance of the original pipeline.

CIPP liners have many applications from sewer mainlines and lateral, industrial and special waste pipelines to pressure pipe. The key design consideration in CIPP liner installation is the ability of the cured-in-place pipe to withstand buckling. The resin and the lining tube type combine to determine the design thickness of the liner necessary to avoid potential buckling. For typical installations, the resin is the primary structural component of the system. Resins are categorized into three generic types namely; unsaturated polyester, vinyl ester, and epoxy. Unsaturated polyester resins are the most widely used resins in cured-in-place lining for municipal sewerage systems due to their chemical resistance, excellent workability during installation, and economic feasibility. For industrial and pressure pipeline rehabilitations that require special corrosion resistance and higher temperature performance needs, vinyl ester and epoxy resins are used.

These liners are often installed in structurally sound host pipes that lie below the water table and are consequently subjected to external hydrostatic pressure. This external pressure will induce deflections of the liner within the host pipe. To prevent liner collapse, the thickness of a liner system must be chosen that will resist this external pressure over the lifetime of the liner system. One solution is to apply an internal polymer liner to the pipeline. In that case, any loads due to the soil surrounding the pipeline are carried by the existing rigid pipeline while the liner carries only the pressure from any

fluid within the groundwater transmitted through the cracked pipeline. The liner should be designed to carry the external groundwater pressure with an adequate factor of safety.

## 2.9 PARAMETER DEFINITIONS

There are many parameters related to the trenchless technology techniques. Those parameters are presented in the following sections:

### 2.9.1 STANDARD DIMENSION RATIO (SDR)

Standard Dimension Ratio , *SDR,* is defined as the average outer diameter, $D_o$, for the circular liners (or the average of the mean minor and major diameters for oval liners) to the minimum thickness of the liner, *t,* and is given as:

$$SDR = \frac{D_o}{t} \tag{2.37}$$

Notice that in some studies, the Dimensional Ratio *DR* is used instead of *SDR*, where DR is expressed as:

$$DR = \frac{D_i}{t} = \frac{D_o - t}{t} = \frac{D_o}{t} - 1 = SDR - 1 \tag{2.38}$$

where $D_i$ is defined as the average inner diameter for the host pipe.

### 2.9.2 IMPERFECTIONS

Another aspect of the liner problem is the existence of any material or geometrical imperfections. Material imperfections are very hard to measure and this issue has received little attention. On the other hand, many studies had been conducted to evaluate the effect of geometrical imperfections (e.g., Chicurel, 1968; Li and Guice, 1995). The

types of imperfections used in these studies can be categorized as either global or local. Global imperfections are related to the whole arrangement of the pipe and the rigid cavity, and those reported in the literature are due to either ovality in the liner or eccentric alignment of the liner with respect to the host pipe due to lack of perfect fit. Local imperfections are those caused by local deviation from the original pipe or rigid cavity shapes, and have taken the form of a section assumed to be detached from the cavity confining it. The previous research showed that both types of imperfections are important and must be considered, in order to assess their effects on liner stability (El-Sawy, 1996).

Many factors reduce the buckling pressure of encased liners. Local liner imperfections, host pipe ovality, and any gap between the liner and the host pipe (i.e., lack of perfect fit) are major factors reducing buckling pressure. The issues of local liner imperfections and ovality have been discussed in other studies on tightly fitted liners (e.g., Moore and El-Sawy, 1996; El-Sawy and Moore, 1997). Calculation of stresses due to the effect of external hydrostatic pressure, particularly the flexure stress; is very sensitive to imperfections. It cannot be assumed that with certain combinations of imperfections, the limit state for material rupture could be reached before the limit state for stability of shape.

Most of the current design models give some importance to oval imperfections of the host pipe and annular gap imperfections due to shrinkage, as well as to a horizontal deflection of limited angular extension. A consensus emerged concerning three imperfections: an ovality imperfection, an annular gap imperfection, and a local imperfection (intrusion). These three imperfections are not always measurable, and default values were defined based on experimental results and numerical evaluations. Figure 2.12 presents the above three types of liners imperfections.

## A. OVAL IMPERFECTIONS

Oval imperfections occur due to the shape of longitudinally broken host pipe and are viewed as the elliptical deformation of a rigid pipe with longitudinal cracks. Ovality is defined as follows (Moore, 1998):

$$q = \frac{D_h - D_v}{D_h + D_v} x100 \tag{2.39}$$

where $q$ is the percentage of ovality of original host pipe expressed as %, $D_h$ is the horizontal (major) inside diameter, and $D_v$ is the vertical (minor) inside diameter.

In the present study, the initial ovality of the liner is always assumed to be the same as that of its host pipe. Most deteriorated pipes have various degrees of ovality (they are not perfectly circular). The estimation of oval imperfection is fairly variable. Some models do not hesitate to measure ovality directly using visual estimation from a photograph of the pipe or from video print. Elliptical ovality is encountered only with flexible pipes, since it implies a capacity of deformation that rigid pipes does not have.

## B. ANNULAR GAP

Any gap between the liner and its host pipe will allow the liner to deform more freely than would a tightly fitted liner, leading to lower elastic or an inelastic critical pressure. The annular gap is caused due to shrinkage during the cooling phase of the CIPP inversion process; a small radial gap usually develops between the liner and the host pipe. The gap can define in either even distributed mode or uneven distributed mode, and it is assumed to be uniform and is characterized simply by its thickness or amplitude $Wg$ (see Figure 2.12). However, with regard to ovality, a percentage of the radius or of the diameter tends to be used. Note that the models use different definitions. One practice is to divide the amplitude by the average radius $R$ of the liner or the host pipe:

$$g = \frac{W_g}{R} x100 \tag{2.40}$$

where $g$ is the percentage of annual gap expressed as %. However, some models (e.g., Hall and Zhu, 2001) use the host pipe diameter $D$ instead of the radius $R$ in the previous equation. On the other hand, in the unevenly distributed case, the gap is assumed to have the maximum magnitude $Wg$ on one side and no gap on the opposite side. However, the first definition is the most common and the easiest to extend to non-circular situations.

### C. LOCAL INTRUSIONS (IMPERFECTIONS)

Local or longitudinal intrusion is characterized by its angular extension and its maximum amplitude. Longitudinal intrusion in a liner (which is not applied by most of the models) is defined by the following equation (Thepot, 2000):

$$w(\varphi) = w_v.\cos^2(\frac{\Pi}{2}.\frac{\varphi}{\varphi_v}) \qquad \text{Valid for } -\varphi_v \le \varphi \le +\varphi_v \tag{2.41}$$

where $w_v$ is the maximum deflection of the liner expressed as % and $\varphi_v$ is the total critical angle for longitudinal intrusion in the liner (see Figure 2.12).

## 2.10 LINER BUCKLING MODELS

In addition to the extensive analytical and experimental studies that have been undertaken during the past 40 years to investigate the buckling phenomenon in liners, many liner buckling formulas are published in national regulations (e.g., the ASTM F1216, 1993, in North America and the WRc SRM, 1994 in the United Kingdom). Previous and current liner design practices and research are presented in more details in the next chapter through an extensive comparative study among analytical models, experimental tests, and numerical simulations for critical buckling in encased liners.

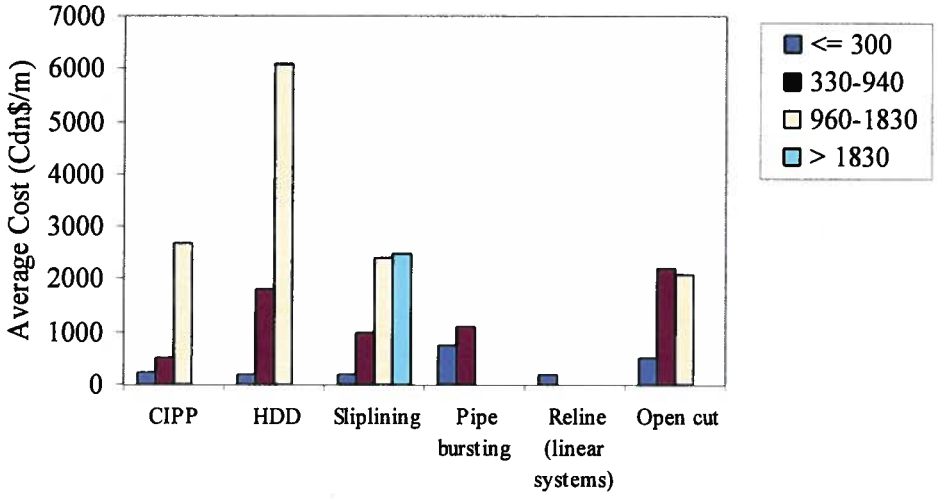


Figure 2.10 Average Costs of Trenchless Methods for Four Diameter Ranges (After Zhao and Rajani, 2002)

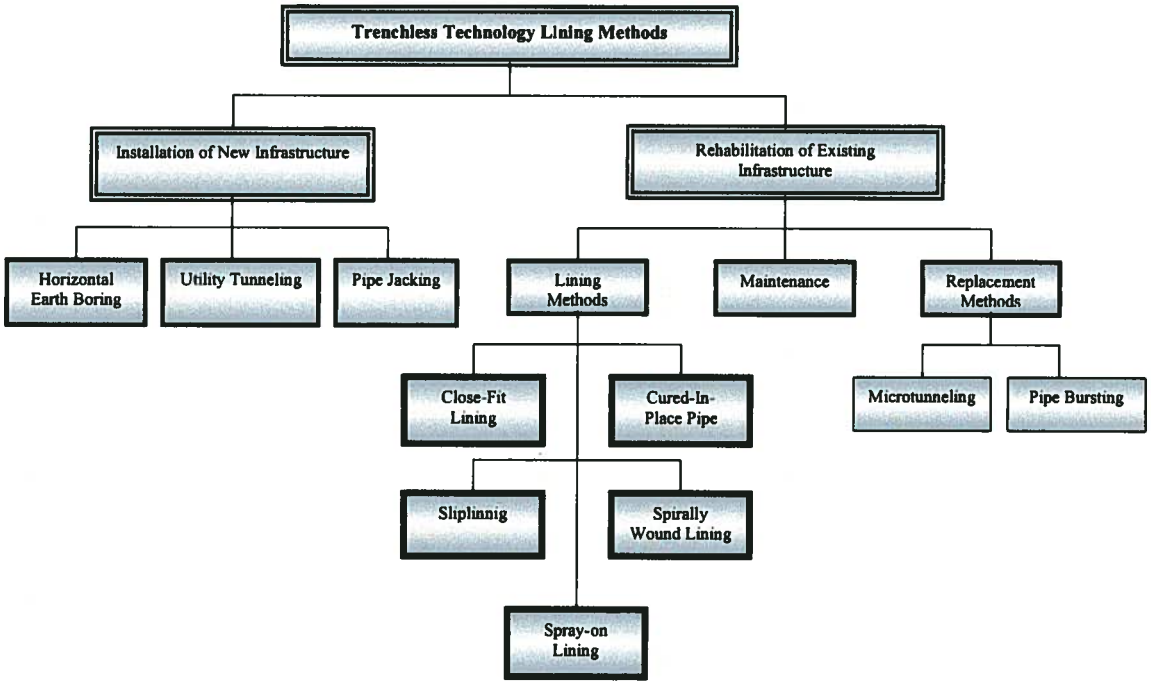


Figure 2.11 Alternative Rehabilitation Techniques of Pipeline (After Schrock, 1994)

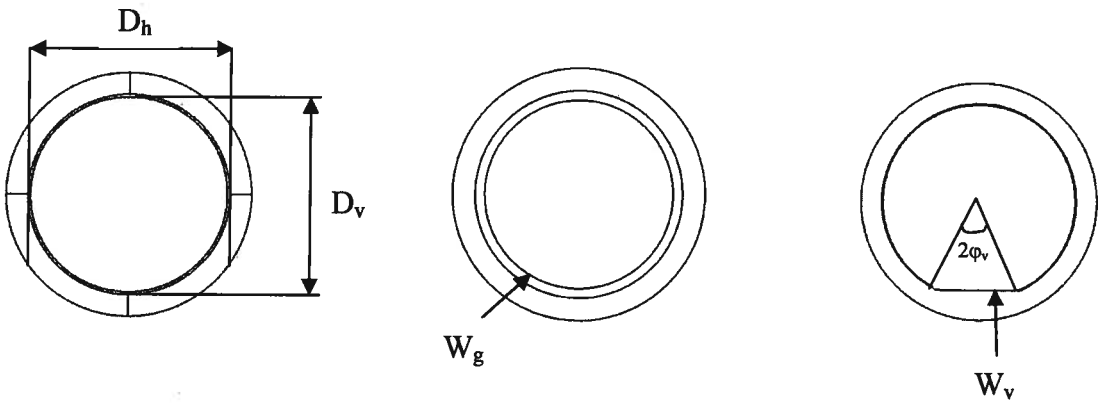


(a) Oval Imperfections (b) Annular Gap (c) Local Intrusions

Figure 2.12 Types of Imperfections (After Thépot, 2004)

# CHAPTER 3

# CIPP LINERS BUCKLING MODELS FOR REHABILITATED PIPELINE A COMPARATIVE STUDY

## 3.1 INTRODUCTION

The CIPP lining is used with growing importance to infrastructure systems for trenchless rehabilitation of sewers or other pipelines. CIPP lining is fabricated of a felt continuous liner impregnated with a thermosetting resin. Using water pressure, this liner is inverted through the damaged pipeline and pressed against its walls. Once in place, it is cured by circulating hot water inside the liner. The CIPP does not require annulus grouting and can be designed to exactly fit the shape of the existing pipes. The flexibility of the resin tube allows it to navigate through defective pipe, realigning offset joints, filling missing sections, and resealing cracked pipes. In this case, any loads due to the soil surrounding the pipeline are carried by the existing rigid pipeline while the liner carries only the pressure from the groundwater transmitted through the cracked pipeline. All installation techniques depend primarily on the visco-elastic and thermoplastic natures of the liner material. If the installation procedure is not carefully controlled, the final liner may end up being loose relative to the damaged host pipeline and eccentric alignment of the liner with respect to the host pipeline may occur. Most existing lining technologies fail to produce tightly fitted liners even in controlled lab environments, resulting in significantly affected liner stability (El-Sawy, 1996). Buckling of encased liners is one of the most important phenomena to be considered in the design of rehabilitated pipelines and it subsequently attracts a great deal of research work.

This chapter presents an extensive comparative study for the major work of the analytical, numerical models, and the experimental tests for investigating the buckling problem of encased liners. In total thirteen analytical formulas besides the ASTM F1216 standard (1993 and 2007) are reviewed and discussed. Most of the existing analytical solutions are derived from either Timoshenko or Gere's (1961) or Glock's

(1977) formulations. The characteristics of each of the reviewed models are presented and a general formula is proposed for buckling pressure of encased liner. Available experimental work dealing with encased liner buckling in pipeline rehabilitation is also reviewed and discussed. A statistical analysis of variance (ANOVA) and capability analyses of the experimental results are developed to study the consistency of published test results.

As an alternative to analytical models, this work presents a finite element analysis including geometric non-linearity and large-strain formulations to simulate the short-term buckling behaviour of encased circular and oval liners as well as the long-term buckling behaviours of encased circular liners. The performances of the reviewed analytical models and the proposed finite element analysis are studied by predicting the critical buckling pressure of the available experimental results. From the numerical simulation predictions, it is clear that the developed finite element models took into account the ovality, gap, and geometric non-linearity effects, and thus captured the buckling phenomena successfully.

The chapter is organized into three main sections. The first section commences with a brief review and analysis of the available buckling theories of liners and the critique of the existing analytical models. The second part of the chapter presents up-to-date buckling experimental studies and a statistical analysis of the results. Finally, the finite element models developed for predicting the buckling behaviour of encased liners are presented in the last section. The performances of these models are proven by simulating the existing experimental tests results of critical buckling pressure for encased liners.

## 3.2 BUCKLING THEORIES OF LINERS

Buckling of the liner is one of the major structural problems that need to be addressed when analyzing the structural behaviours of rehabilitated pipelines. Because the original pipe can be extensively damaged, external water pressure becomes the governing design load. For modeling purposes, the liner is usually considered as being a thin cylindrical

shell encased in a rigid pipe. Buckling behaviour of thin-walled cylindrical shells subject to external pressure is a classical structural stability problem and was first studied in the late nineteenth century. Liner longitudinal dimension is generally considered very large compared to the cross-section; it is therefore legitimate to consider the shell as a ring.

The purpose of this section is to review the major analytical models for calculating the buckling load of a liner. The behaviour of the liner encased in a rigid host pipe is complex by nature and it is difficult to solve the associated buckling problem analytically. Different simplifications are needed in order to address the problem. It is usually assumed that due to its rigidity, the host pipe carries the soil loads while the liner carries the ground water pressure, the grouting pressure during installation, and the internal fluid pressure (El-Sawy, 1996).

Most of the existing analytical solutions for the buckling load of liners use Timoshenko and Gere's (1961) formula for a free ring subjected to uniform external pressure. However, it is worth mentioning that Levy (1884) was probably the first to propose an analytical solution to the problem of buckling pressure in thin rings. In his solution, Levy used small deformation hypothesis to develop the critical buckling pressure in terms of the elastic modulus of ring material, the ring's cross-section moment of inertia, and its radius. The derivation of Levy equation which is widely used as a basis for the design of underground pipes was based on the buckling phenomenon of a free (without outside constraint) thin curved bar with a circular axis under a uniform external pressure as illustrated in Figure 3.1. It is assumed that there exists a small deflection to make the ring slightly deflected from the circular form. With the geometrical relation shown in Figure 3.1, the bending moment at any cross-section of the ring can be expressed as:

$$M = M_o - pr(w_o - w) \tag{3.1}$$

where $M$ is the bending moment, $M_o$ is the bending moment at springline points ( points A and B), $p$ is the external uniform pressure, $w$ is the deflection of the ring in the radial

direction and $w_o$ is the deflection of the ring in the radial direction at springline points A and B ( see Figure 3.1).

It is assumed that AB (horizontal axis) and OD (vertical axis) are axes of symmetry for the buckled ring. Then the action of the removed lower portion can be represented by bending moment $M_o$ acting on each of the cross sections A and B. The deflection of the ring in radial direction $w$ can be expressed by the following differential equation:

$$\frac{\partial^2 w}{\partial^2 \theta} + w = -\frac{Mr^2}{EI} \tag{3.2}$$

where $I$ is the moment of inertia and $r$ denoted the ring radius.

Defining $k$ as:

$$k^2 = 1 + \frac{pr^3}{EI} \tag{3.3}$$

Then, substituting the expression for $M$ from Equation 3.1, the differential equation for ring buckling becomes:

$$\frac{\partial^2 w}{\partial^2 \theta} + kw = \frac{-M_o r^2 + pr^3 w_o}{EI} \tag{3.4}$$

The solution of this differential equation is expressed in the following general form:

$$W = A_1 \sin k\theta + A_2 \cos k\theta + \frac{-M_o r^2 + pr^3 w_o}{EI} \tag{3.5}$$

Apply boundary conditions at cross sections AB & OD of the buckling ring.

From symmetry: $\left( \frac{dw}{d\theta} \right)_{\theta=\pi/2} = 0$ this leads to $A_1 = 0$

$$\left(\frac{dw}{d\theta}\right)_{\theta=0} = 0 \qquad \text{this leads to} \quad \frac{\sin k\pi}{2} = 0$$

The smallest non-zero root of this equation is $\frac{k\pi}{2} = \pi$ and therefore $k_{cr}$ = 2. Buckling will always follow the lowest mode without additional constraints. It should be noted that the first mode $k$ = 2 corresponds to rigid body motion and odd modes correspond to conditions wherein there is only one axis of symmetry. Figure 3.2 shows the expected buckling modes of an encased ring.

Substituting this into Equation 3.3 produces:

$$2^2 = 1 + \frac{Pr^3}{EI} \tag{3.6}$$

So, the minimum value of the critical pressure as follows:

$$P_{cr} = \frac{3EI}{r^3} \tag{3.7}$$

Assuming plane strain condition of infinitely long ring by using the effective modulus $\frac{E}{1-\nu^2}$ instead of $E$ where ν is the Poisson's ratio for the ring material. The moment of inertia $I$ is expressed as $I = \frac{t^3}{12}$ where $t$ is the thickness of the ring. Timoshenko and Gere (1961) generalized Levy's model and gave the critical buckling pressure $P_{cr}$ of a free ring or an arch with pinned or fixed ends subject to uniform external pressure (see Figure 3.1). Defining $r = \frac{D_i}{2}$; the resulting expression for the critical pressure equation for unsupported or free pipe may be written as:

$$P_{cr} = \frac{4E}{1-\nu^2}\left(\frac{t}{r}\right)^3 = \frac{2E}{1-\nu^2}\left(\frac{t}{D_i}\right)^3 \tag{3.7}$$

Recall that $DR = \frac{D_i}{t}$ = *SDR-1* (see section 2.9), Equation 3.7 can be rewritten as follows):

$$P_{cr}^{o} = \frac{2E}{1-\nu^2}\frac{1}{(DR)^3} = \frac{2E}{1-\nu^2}\frac{1}{(SDR-1)^3} \tag{3.8}$$

Timoshenko and Gere model for the free pipe (i.e., Equations 3.7 and 3.8) neglects the existence of the host pipe as a rigid constraint confining the liner. Following the work of Timoshenko and Gere, many researchers proposed modifications to this expression; it is therefore referred to as the base formula.

Extensive literature addressing the stability of a liner is available. Most of the existing models consider the liner to be a ring encased in a rigid cavity. The stability problem appears in the literature in different forms according to the engineering application under consideration. Among the first attempts to solve the buckling problem of a liner was that of Chicurel (1968), who studied the "shrink buckling" of a thin elastic circular ring, compressed during insertion into a circular ring of smaller diameter. The shrink buckling phenomenon is different than the buckling of cast-in place pipe (CIPP) because shrinking is caused by hoop compression while buckling is due to an external uniform pressure. Thereafter, Cheney's (1971) used small deformation linear theory in considering the buckling of rigidly encased rings or shells under an external uniform pressure. Glock (1977) analyzed rings subjected to external uniform pressure and to thermal loading. Glock's model assumes that there is no friction between the ring and the rigid cavity, but unlike Cheney's and Chicurel's models, Glock's model does not require the cavity wall to move inward with the ring. The author derived an analytical expression for the buckling load by assuming a buckling mode shape to express the potential energy of the ring. He solved the buckling problem by minimizing the potential energy expressed in terms of the deflection amplitude and the curvilinear coordinate of the ring. The simplified form of the buckling pressure for encased liner is given by:

$$P_{cr} = \frac{E}{1-\nu^2}\left(\frac{t}{D}\right)^{2.2} = \frac{E}{1-\nu^2}\frac{1}{(SDR-1)^{2.2}} \tag{3.9}$$

where $D$ is the mean diameter to the center line of the wall of the liner $D = D_0 - t$ (see Omara 1997 for more details about the buckling mode shape and full derivation of Glock's formula).

For practical application of any analytical model, it is crucial to consider the damage state of the rehabilitated pipe. The current ASTM standard F1216 (1993 and 2007) for designing rehabilitated pipe liners considers two conditions for the structural performance of the deteriorated host pipe: "partially deteriorated" pipe, and "fully deteriorated" pipe. In the case of partially deteriorated condition, the CIPP liner is designed to support the hydraulic load due to groundwater pressure only, while the liner is designed to withstand all possible loadings in the case of fully deteriorated host pipe. The ASTM approach to the design load is to consider the full soil load from the pipe to the surface, essentially ignoring the fact that the liner will be installed within a pipe that is still stable and the arching capability of a soil that has been in place for many years.

Buckling experiments of Aggarwal and Cooper (1984) as well as Lo and Zhang (1994) clearly demonstrate a significant buckling enhancement gained by the support of the liner from the constraining effects of the host pipe. An enhancement factor $K$ was defined by Aggarwal and Cooper (1984) as the ratio of $P_{\text{cr-test}}$ to $P_{cr\text{-theory}}$. This enhancement factor reflected the difference between the results by experiment and results by Timoshenko and Gere's solution (i.e., Equation 3.8). The main conclusion of Aggarwal and Cooper was that an enhancement factor $K \geq 7$ is obtained for most of the specimens (46 out of 49), and they recommended $K=7$ for design.

The ASTM standard F1216 used the concept of enhancement factor $K$ (minimum value of 7 is recommended where there is full support of the existing pipe), and added another factor $C$ to account for the ovality of the liner (See Table 3.1).

The current ASTM F1216 for partially deteriorated gravity pipe condition defined the buckling pressure for encased liner by the following equation:

$$P = \frac{2KE}{1-\upsilon^2}\frac{1}{(SDR-1)^3}\frac{C}{N} \tag{3.10}$$

where:

$K$ = enhancement factor

$C$ = ovality reduction factor

$N$ = factor of safety

The ASTM recommended that the long-term modulus of elasticity of the liner (over 50 years of service life) to set at 50% of the initial value of the modulus of elasticity of the liner material.

The ASTM design practice employs a single stability value for all liners, which is not conservative for thick liners. Although, ovality factor as well as the enhancement factor is included in the ASTM formula, the main shortcomings of ASTM approach can be summarized as follows:

1. Annular gap is not included.
2. Other types of imperfections cannot be considered (such as longitudinal intrusions).
3. Uncertainty in extending a short-term model to predict long-term model.

Recognizing the major effects of initial deformation and initial annular gap, Falter (1996) introduced two multiplicative factors associated to each of these initial imperfections in Glock's equation. Falter (1996) provided a liner buckling formula as:

$$P_{cr} = k_{v,s} \cdot \alpha_D \cdot S_L \tag{3.11}$$

where $k_{v,s}$ is the reduction factor for the simultaneous existence of initial deflections and gaps, (assuming that $k_{v,s} \approx K_v x\, K_s$), $K_v$ is the reduction factor for initial deformation (local intrusion), and $K_s$ is the reduction factor for initial annular gap. While $\alpha_D$ is the snap

through factor of the rigidly bedded pipe without initial deflections and without gaps. It can be expressed as:

$$\alpha_D = 2.62\left(\frac{r_L}{S_L}\right)^{0.8} \tag{3.12}$$

where $r_L$ is the average liners radius and $S_L$ is the stiffness of liner, which can be expressed as:

$$S_L = \frac{(EI)_L}{r_L^3} = \frac{E}{12}\left(\frac{t_L}{r_L}\right)^3 \tag{3.13}$$

where $t_L$ is the liner wall thickness. If Equation (3.13) is modified to include the standard dimension ratio *SDR*, which is defined as the outside diameter over the liner thickness, this equation can be changed to the following form:

$$P_{cr} = k_{v,s} E \frac{1}{(SDR-1)^{2.2}} \tag{3.14}$$

with $\frac{r_L}{t_L} = \frac{SDR-1}{2}$, Equation (3.14) is identical to Glock's model with gap effects and initial deformations added. Thus the long-term buckling model can be expressed as:

$$P_{cr} = k_{v,s}.\alpha_D.S_L = K_v.K_s.E\frac{1}{(SDR-1)^{2.2}} \tag{3.15}$$

Chunduru (1996) investigated the performance of High Density Polyethylene (HDPE) deformed/reformed liners. He modified the ASTM F1216 equation and instead of the enhancement factor *K*, added two new constants to account for the lining and the stress concentration factors. Based on the results of several laboratory experiments, Chunduru modified the classical buckling equation to estimate the critical buckling resistance of a deformed/reformed HDPE liner under short-term external loads. He expressed the modified form of the classical buckling equation for HDPE liner system as follows:

$$P_{cr} = \frac{2EC\alpha\beta}{(1-\upsilon^2)(SDR)^3 N} \tag{3.16}$$

where:

$C$ is the reduction factor to account for liner ovality.

$\alpha$ is the lining factor (1 to 6) depending on the size of the gap between the liner and the existing host pipe, $\alpha \approx 1$ for a pipe that is totally unrestrained and, $\alpha \approx 6$ for a pipe that is totally constrained.

$\beta$ is the stress concentration factor

$\beta$ = (*ODavg* of the liner / *ODavg* of the common pipe)$^{1.11}$

where ODavg is the outside average diameter.

Chunduru concluded that the stress concentrations resulting from manufacturing and installation significantly influence the buckling resistance of a deformed/reformed HDPE liner system and the long-term critical buckling resistance of the liner material was found one-forth of that of the critical buckling resistance measured during short-term tests.

Similarly, Omara (1997) modified Glock's model to include an ovality reduction factor (see Tables 3.1 and 3.2). Omara's model is given as:

$$P_{cr} = \frac{CE}{1-\upsilon^2}\left(\frac{1}{SDR-1}\right)^m \tag{3.17}$$

Omara used the best-fitting regression analysis of Aggarwal and Cooper's experimental data to verify his model (C = 1.07 and m = 2.17). The test results were compared with his mathematical model and the current design practice (ASTM F1216). The analysis showed that ASTM F1216 underestimated the buckling pressure for all degrees of ovality under study. His mathematical model showed good agreement with the experimental results but still overestimated the critical pressure for all degrees of ovality.

The concept of comparing the buckling pressures of free and encased liners has been used by both researchers and developers of CIPP liners design codes (El-Sawy and Moore 1997). The idea is to quantify the enhancement factor, $K$, which is used to define the

relationship between buckling pressure for free liner $P_{cr}^{0}$ as described by Timoshenko and Gere (Equation 3.7 and 3.8), and the critical pressure for encased liner $P_{cr}$ developed by Glock and given in Equation (3.9); can be expressed as $P_{cr} = K \times P_{cr}^{0}$ where $K$, is a enhancement factor given by $K = 0.5\left(\frac{\mathrm{D}}{\mathrm{t}}\right)^{0.8}$ and $P_{cr}^{0}$ is the critical pressure for free pipe obtained by Equation 3.8.

Due to the difficulties associated with the solution of the analytical buckling problem of liners, some researchers turned to finite element methods as an approximation technique. El-Sawy and Moore (1997) used non-linear finite element analysis to investigate the stability of a tightly fitted liner used in the rehabilitation of a partially deteriorated rigid pipe subjected to external fluid pressure. This model includes geometrical non-linearities (i.e., large deformations), material non-linearities, and interaction between the liner and the rigid cavity. A parametric study was undertaken to determine the effect of the initial liner geometry. The results of the parametric study are used to develop a new design method to overcome the shortcomings of the current ASTM F1216 design specifications. The critical buckling pressure of a tightly fitted liner used for rigid pipe rehabilitation (i.e. partially deteriorated pipe) can be written as:

$$P_{cr} = \frac{2E}{1-\upsilon^2}\left(\frac{t}{2R_o}\right)^3 KC\alpha \tag{3.18}$$

where $P_{cr}$ is the critical buckling pressure, $\alpha$ is the factor accounts for the reduction in the critical pressure due to a single local imperfection, and $R_o$ is the radius of circular liner. The first part in this expression represents the critical pressure for the unsupported circular liner (Levy, 1984). El-Sawy and Moore define the enhancement factor "$K$" which quantifies the increase in critical pressure for the circular liner due to encasement by:

$$K = \frac{1}{2}\left(\frac{2R_o}{t}\right)^{0.8} \tag{3.19}$$

The ovality factor "$C$", is defined by the exponential form $C = e^{-q/18}$ .

El-Sawy and Moore considered three types of imperfections (ovality, gaps and local intrusion). These imperfections were found to be additive, i.e., the critical buckling pressure could be rewritten in following form in terms of Glock's solution:

$$P_{cr} = P_{Glock}\, C\, R_{\Delta} \tag{3.20}$$

where $R_{\Delta}$ is the correction factor for effect of longitudinal imperfection.

Moore (1998) examined the buckling of a ring encased in a rigid cavity by using one-lobe model. He presented a modified version of El-Sawy and Moore's model to account for local imperfections and elliptical geometry. The critical pressure value is given as:

$$P_{cr} = 2.275\left(\frac{t}{D}\right)^{2.2} E \tag{3.21}$$

Equation (3.19) also can be expressed as:

$$P_{cr} = \frac{2.275E}{1-\upsilon^2}\left(\frac{1}{SDR-1}\right)^{2.2} \tag{3.22}$$

Boot (1998) modified Glock's model and developed an analytical solution for the elastic buckling pressure of loosely fitted liners that encompassed single-lobe, classical Glock's hypothesis, and a two-lobe buckling modes. Boot extended Glock's closed-form theory to take into account the initial gap imperfections and also to reflect the observed two-lobe buckling mode. The generalized buckling equation he derived, when converted to plane strain conditions for long pipe, can be expressed in convenient dimensionless form simply as:

$$\frac{P_{cr}}{E^*} = C\left(\frac{t}{D}\right)^{-m} \tag{3.23}$$

where $E^*$ is the plane strain modulus of elasticity and the coefficients $C$ and m depend on the ovality and the annular gap (i.e., $C$ and $m$ are functions of imperfections in the system) and are obtained by interpolating the results from FE analysis or by directly solving the Glock's equation appropriately modified for imperfect behaviour. For zero imperfections $m$ = -2.2, and the coefficient $C$ has value of (1.003) for one-lobe buckling and (1.323) for two-lobe buckling. It is important to mention that for the case of no gap (i.e., for the case of tightly fitted liner) Boot's solution reduces to Glock's solution.

Lu (1999) used Omara's work and introduced a modified Glock's model; he included a new reduction factor associated with the percentage of annular gap. Lu studied Omara's model and concluded that Omara's model was incomplete because it neglected the reduction effect of gap on the prediction of critical buckling pressure. Furthermore, he noted that Omara's model neglected the gap effect on the determination of $\frac{S_o}{L_o}$ ratio. Based on his study, he constructed a modified model given as:

$$P_{cr} = C_{oval} C_{gap} \frac{E}{1-\upsilon^2}\left(\frac{1}{SDR-1}\right)^{2.2} \tag{3.24}$$

where $C_{oval}=e^{\frac{-q}{20}}$ is the ovality reduction factor and $C_{gap}$ is the gap reduction factor, which is defined as:

$$C_{gap} = \frac{1}{1+R_g(1.3SDR-7.7)} \tag{3.25}$$

where $R_g$ is the gap ratio $=\frac{W_g}{R_o}$ , $W_g$ is the maximum gap size between liner and host pipe and $R_o$ is the mean radius of inside pipe. Lu also verified his model using the testing data obtained from short-term buckling tests conducted in Louisiana Tech University (Seemann, 2000). The comparison showed that the critical pressures calculated from the proposed equation were close but higher than the actual critical pressures.

Thépot (2000) generalized Glock's analysis to study non-circular liner with annular gap and one-lobe or two-lobe. Denoting $k$ the number of the lobe (i.e., 1 or 2), $P$ the mean perimeter of the liner, and $A$ its cross-section area, the author developed a solution for the buckling pressure of a non-circular lining (egg-shaped) subject to external water pressure as follows:

$$P_{cr} = 2.02k^{0.4}\frac{EI^{0.6}EA^{0.4}}{P^{0.4}r^{1.8}} \tag{3.26}$$

Equation (3.26) which is applicable for the 3x2 egg-shaped lining; is equivalent to the Glock's formula for the circular lining. Comparison between the Glock's formula (Equation 3. 9) and Thépot's formula shows that the buckling pressure of a 3x2 egg-shaped lining of height H is equal to that of a circular lining with a diameter of (1.71 H). For a circular lining using $r = D/2$ and $P = \pi D$, Equation (3.26) can be simplified as follows:

$$P_{cr} = \frac{1.204E}{1-\upsilon^2}\left(\frac{1}{SDR-1}\right)^{2.2} \tag{3.27}$$

Gumbel (2001) developed a model based on the prediction of buckling behaviour of close-fitting liners for use in gravity sewer pipes under hydrostatic loading caused by external groundwater pressure. Gumbel addresses the major issues with the ASTM F 1216 approach. The improvements suggested in the Gumbel approach by separating the imperfection effects into those that related to the host pipe (system imperfections) and those that related to the particular renovation technique (characteristic imperfections) were a useful concept in addressing the issue of imperfections in liner design (see Figure 3.3). Gumbel in his solution showed how this theory could be developed into design charts or a spreadsheet based calculation approach that provides a better design prediction of liner behaviour than the current ASTM F1216 formula (see Figure 3.4).

This literature survey shows the extensive work that has addressed the buckling problem of liners and the different enhancements that have been introduced during the past thirty years. However, the fundamental hypothesis has not changed considerably. While analytical solutions always appeal often to engineers because such solutions allow fast design process, the quality of the predictions often remains questionable. Table 3.1 summarizes the presented major analytical models and lists their main features.

## 3.3 CRITIQUE OF EXISTING ANALYTICAL MODELS

Fundamentally, all above-discussed analytical models have been derived from either Timoshenko and Gere's equation or Glock's formula (i.e., Equation 3.8 or 3.9). It is generally admitted that Glock's formula is superior to Timoshenko and Gere's equation mainly because the former is based on better and sounder physical assumptions. Glock's model also takes into consideration the pipe-liner interaction. Recent design models take into account two imperfections (ovality and annular gap), with the one-lobe mode generally associated with the lowest critical buckling pressure (e.g., El-Sawy and Moore, 1997). Most design models previously discussed focus mainly on the stability problem and do not consider material capacity. For certain combinations of imperfections, it is possible that the limit state associated with the material behaviour may be reached before the stability limit state (Thépot, 2000). Therefore, a rehabilitated pipe structural response must be verified for all expected failure modes, not only for that of the stability of the liner.

It is possible to express all previously discussed analytical models in the following form:

$$P_{cr} = \frac{aE}{1-\upsilon^2}\frac{1}{(SDR-1)^b} \tag{3.28}$$

The coefficient $a$ may be related to the parameters $K$ and $C$ (which include the effect of the enhancement factor, the ovality, and other imperfections) is full of uncertainty. The coefficient $b$ may be related to the parameter $SDR$ (which includes the effect of liner

stiffness) is well defined. Coefficients *a* and *b* will vary with the analytical model of the buckling phenomena and they are summarized in Table 3.2. The physical meanings of each of these coefficients differ from one analytical model to another. It is also interesting to compare existing analytical models with Timoshenko and Gere's equation by using the concept of the enhancement factor as defined earlier. Table 3.2 shows the imperfection factors for each of the discussed analytical models. All those with an exponent of 0.8 are related to Glock's equation.

## 3.4 EXPERIMETAL STUDIES OF LINER BUCKLING

Along with analytical models, there were extensive experimental studies that addressed the buckling of encased liner subjected to external uniform pressure, e.g., Water Research Center (WRc) tests (1982, 1983), Aggarwal and Cooper (1984), Utah State University (Watkins, 1988 and 1993), Welch (1989), Lo and Zhang (1994), Trenchless Technology Center (TTC) at Louisiana Tech. University (Guice *et al.*, 1994; Straughan *et al.*, 1995; 1998a, b ; Omara, 1997; Seemann, 2000), and Tulane University (Bakeer and Barber, 1996; Bakeer *et al.*, 1999 and 2001). These particular tests investigated the influence of different parameters including the diameter, the thickness, and the length of the liner. Besides these geometric parameters, most of the experimental tests included the effect of the material properties of the liner. In general, the experimental investigations dealt with CIPP liners. Usually, the liner inserted in the host pipe and the specimens were sealed at both ends. Some research studies distinguished between the short-term and long-term behaviours of the liner because of the variability of its creep properties over time. In this section, fourteen selected sets of experimental work tests will be used to study the performance of the presented analytical models for predicting the buckling pressure of liners (see Table 3.8). Those selected tests are the main buckling tests available for the last three decades which are commonly used by buckling models researchers and codes developers. Furthermore, those tests cover the short-term tests for circular and oval host pipes and the long-term experiments as well.

The first series of tests is due to Aggarwal and Cooper (1984), who conducted external pressure tests on 49 specimens of encased liners with a relatively large range of standard dimension ratio *SDR* from 29.86 to 90.25 and a variety of liner material properties (modulus of elasticity varying from 960 MPa to 2570 MPa). The host pipe was made of steel. Aggarwal and Cooper reported the size of the gap between the liner and steel host pipe, but made no mention of how it was measured or calculated. The concept of "enhancement factor" discussed earlier originated from this research work. Aggarwal and Cooper indicated that the values of the enhancement factor varied from 6.5 to 25.8. It is worth mentioning that the ASTM F1216 standard selected a conservative enhancement factor of 7 based on this study.

Welch (1989) conducted short-term uniform external pressure tests on 9 specimens of encased slip liners tightly fit into a 450 mm inner diameter fractured clay host pipe with constant standard dimension ratio *SDR* of 45. A relatively short length of 1 meter was chosen. A system of jacks was used to deform the linings to the required shape (ovalities of 0%, 5%, and 10%). Contrary to the common practice for all other buckling tests, the specimens were oriented and tested in a vertical rather than a horizontal position.

Guice *et al.* (1994) and Straughan *et al.* (1995) at the Trenchless Technology Center TTC at Louisiana Tech. University completed the first extensive set of experiments of approximately 200 short-term and long-term buckling tests for five manufacturers and seven pipeline rehabilitation products, specifically cured-in-place pipe. This testing program is known as CPAR (Construction Productivity Advancement Research) tests.

Bakeer and Barber (1996) at Tulane University conducted 90 short-term buckling tests on 80 specimens of HDPE liners reformed inside either 150 mm or 200 mm inner diameter circular steel casing pipe, and 10 specimens of HDPE liners encased into a 200 mm oval steel casing pipe with two standard dimension ratios *SDR*s of 26 and 32.5. The degree of ovality was about 7.4%. Bakeer *et al.* (1999 and 2001) extended the previous tests and conducted long-term buckling tests on about 200 specimens of encased liners tightly fit

into 150 mm and 200 mm inner diameter circular steel host pipe with the same two standard dimension ratios.

A Omara (1997), at the Trenchless Technology Center TTC of Louisiana Tech. University, conducted short-term buckling tests on 18 specimens of encased CIPP liners tightly fit into 300 mm inner diameter oval steel host pipe, with a relatively narrow range of standard dimension ratios from 49.587 to 54.054 and with three different degrees of ovalities (5%, 10%, and 20%). Six pipes were tested for each degree of ovality.

The test program at Louisiana Tech. University continued in 1998, when short-term and long-term buckling tests were carried out. This program is known as the BORSF (Board of Regents Support Fund) tests. Straughan *et al.* (1998a, b) reported the results of short-term buckling tests conducted on 45 specimens of encased liners tightly fit into 200 mm or 300 mm inner diameter circular and oval steel host pipe with a range of *SDR*s from 37.27 to 59.17. In the BORSF tests performed for oval liners, which was also reported by Seemann (2000) and Seemann *et al.* (2001), the liners were allowed to carry the external pressure for a maximum of 10,000 hours (long-term buckling test limit); most of the liners buckled long before the 10,000 hour limit was reached. Short-term tests were performed on two sets of oval liners with ovalities of 3% and 5%, which were much smaller than the ovalities in Omara's tests (5%, 10%, and 20%).

Seemann (2000), at the Trenchless Technology Center TTC of the Louisiana Tech. University conducted short-term buckling tests on 15 specimens of CIPP liners encased into 300 mm inner diameter circular and oval steel host pipe with a relatively narrow range of *SDR*s from 41.987 to 42.117 and with three different degrees of ovalities (0%, 2%, and 5%). Each pipe specimen was 1.82 m long. Prior to lining, five host pipes were hydraulically pressed to an ovality of 2%, and another five were pressed to an ovality of 5%. The remaining five host pipes were not pressed (i.e., ovality of 0%). The 15 pipes/liners were arranged in a 42.7 m run-in sequence, in a straight line from 0% to 5%, with removable clamshells between the pipes.

The main features of the seven sets of experimental programs for buckling of liners are summarized in Table 3.3. Figure 3.5 shows a typical buckling test frame setup.

## 3.5 STATISTICAL ANALYSIS OF BUCKLING EXPERIMENTS

Statistical analysis of the experimental tests results described earlier was carried out using the statistical analysis software SPSS (2006) and is summarized in Table 3.4. Both the analysis of variance (ANOVA) and capability analysis are reported in this table. The descriptive statistics for most of the tests data (except Welch,1989 and Omara, 1997) indicates that both the standard deviation and the coefficient of variation of the measured critical buckling pressure are too high, and fluctuated from 16% for the CPAR tests (1994) to 59% for Aggarwal and Cooper (1984), the latter representing the upper bond for this fluctuation. This reflects a severe variability of the tests results and confirms the deviation from the normal distribution curve significantly. Moreover, the dispersion factor ($\delta$) of all the experimental tests results ranges from 1.657 to 2.509. This shows that all the tests data are over-dispersed ($\delta$ is greater than 1) and widely scattered (Crawley, 1993). The higher dispersion factor is consistent with the high fluctuation and variability shown in the ANOVA analysis parameters (i.e., the standard deviation and the coefficient of variation).

A fundamental task in many statistical analyses is to characterize the variability of a data set. A further characterization of the data includes skewness and kurtosis. Skewness is a measure of symmetry, or more precisely, the lack of symmetry. A distribution, or data set, is symmetric if it looks the same to the left and right of the center point. Kurtosis is a measure of whether the data are peaked or flat relative to a normal distribution. That is, data sets with high kurtosis tend to have a distinct peak near the mean, decline rather rapidly, and have heavy tails. Data sets with low kurtosis tend to have a flat top near the mean rather than a sharp peak. A uniform distribution would be the extreme case. Usually, a normally distributed data should have skewness and kurtosis near 0 and 3, respectively (NIST/SEMATECH, 2006). If skewness is greater than 0, the data distribution is skewed to the right, having more observations on the left; this is the case

for the Aggarwal and Cooper tests (1984), Welch (1989) circular host pipe (short-term tests), CPAR tests (1994), Bakeer *et al.* tests (1996), and BORSF (1998) oval host pipe (short-term and long-term tests). On the other hand, if skewness is smaller than 0, the data distribution is skewed to the left, having more observations on the right; the case for the BORSF (1998) circular host pipe/short-term tests, Seemann tests (2000), and Welch (1989) oval host pipe (short-term tests). Moreover, if the kurtosis of the data is less than 3, distribution has a thicker tail and a lower peak compared to a normal distribution, which is the case for all the experimental tests results. Further, kurtosis larger than 3 indicates a higher peak and a thinner tail. The ANOVA results showed that none of the tests had skewness close to 0 or kurtosis close to 3.

The normality tests (Kolmogorov-Smirnov and Shapiro-Wilk) of the ANOVA analysis depend on the assumption that data were sampled from a normal distribution (i.e., Gaussian distribution). Thus, the tests compared the cumulative distribution of the data within the expected cumulative Gaussian distribution. The normality tests of the experimental tests results show that Aggarwal and Cooper (1984) and CPAR (1994), with significance levels of 0.003 and 0.001, respectively, had the best consistency among all test results for circular host pipe. While normality tests of the ANOVA analysis indicate that some of the individual tests have better α-value (i.e., significance level); which means that they are considered normally distributed, when the statistical analysis is performed on all experimental results as a set of data (i.e., mixed tests), the consistency drops significantly. This indicates a lack of coherence between different test results because of the absence of consistent procedure for conducting those tests.

An important technique used to determine how well a process meets a set of specification limits is called a process capability analysis. Traditionally, process capability analysis has been based on the assumption that each variable that characterizes a product or test behaves independently. In such cases, it is sufficient to make separate capability statements about each. It is worth mentioning that there are two critical assumptions to consider when performing process capability analyses with continuous data, namely: (i) the process is in statistical control, and (ii) the distribution of the process is considered

normal. If these assumptions are not met, the resulting statistics may be highly unreliable. The capability index $C_{pk}$ compares the distance between the mean and the nearer standard limits to 3 times the standard deviation. In either case, the index must be greater than 1 for the process to be capable of keeping virtually the entire product within standard, although most industrial companies prefer this value to be more than 1.33 (Montgomery, 1996). As shown in Table 3.4, almost all experimental models show the natural variability of these tests and confirm that none of them is normally distributed or capable (since $C_{pk} < 1$ for all tests). To improve the performance of the tests in order to be capable, it is recommended that future buckling tests be more controlled and robust to minimize the considerable variation in each test result.

However, it is important to mention that test results with low numbers of specimens ( less than 30) may reduce the quality of the statistic of all the test data as a set (Mendenhall *et al.*, 2003). Moreover, the specimen length can have a significant effect on the measured buckling pressures if the ends of the liner are clamped to the host pipe (Moore, 1998). Welch (1989) and Aggarwal and Cooper (1984) used unconstrained short cylinder buckling specimens with length-to-diameter ratios *L/D* of approximately 4, while others (e.g., Guice *et al.*, 1994; Bakeer and Barber, 1996; Straughan *et al.*, 1998; Bakeer *et al.*, 1999, 2001) used length-to-diameter ratios of 6 to 12 in order to eliminate the effect of the restrained ends of the liner on its buckling resistance.

Nevertheless, no experimental test took into account that encased liner in real conditions is subjected to non-uniform groundwater pressure since only uniform pressure was applied in the experimental tests. However, the Aggarwal and Cooper (1984) show the lowest scattering and the most consistent test measurements with a reasonable number of specimens in comparison with other tests. Furthermore, this test also indicate the higher correlation coefficient ($R^2$ = 0.78) when it is used to evaluate the Glock's analytical model using the best-fitting regression technique (see Table 3.8).

## 3.6 THE PERFORMANCE OF ANALYTICAL MODELS

The performance of analytical models is studied through the prediction of the buckling pressure measured from seven experimental programs. Both short-term (i.e., buckling) and long-term (i.e., creep) behaviours' are considered. For the short-term, the predictions of the models are studied for a total of 126 circular and 32 oval host-pipe specimens. A total number of 205 circular host-pipe specimens under long-term conditions are used for the evaluation of the analytical models. Tables 3.5 to 3.7, as well as Figures 3.8 to 3.10, show a comparison between the critical buckling pressure for the discussed analytical models and the available experimental data for encased liners. The three models of Timoshenko and Gere, Chicurel, and Cheney are excluded from the performance analysis (even they are shown in Tables 3.5 to 3.7) because they are primitive and do not represent the physics of the real pipe-liners system.

The ASTM F1216 underestimates the measured buckling pressure up to 39% for short-term circular host pipe but overestimates the tests results reported by Bakeer by 143%. For the oval host pipe cases, the standard ASTM equation underestimates the measured buckling pressure by up to 53% but the overestimation of Bakeer and BORSF tests is 26% and 12%, respectively. For the long-term tests, the ASTM F1216 underestimates the CPAR and BORSEF tests by 44% and 42% respectively, and overestimates the Bakeer tests by 157%. This performance may be due to the fact that the ASTM F1216 approach neglects the effect of annular gap, the number of lobes, local intrusion, and other imperfections. It is important to note that the ASTM F1216 is conservative for both the short-term and the long-term predictions of critical buckling pressure.

Falter's and Chunduru's models performance is close to that of the ASTM F1216. Both models underestimate all the experimental tests (except the Bakeer tests) by averages of 39%, 38%, and 53% for the short-term (circular and oval case) and long-term tests, respectively, because both Falter and Chunduru inappropriately combine imperfections by multiplying the reduction factors associated with the individual imperfections and initial gap.

Table 3.5 and Figure 3.8 show that the El-Sawy/Moore and Moore's models underestimate only the Aggarwal and Cooper tests result, and overestimate all other tests results. This overestimation is due to the fact that their model cannot be used when ovality and gap are present at the same time. All theoretical models of Glock, El-Sawy/Moore, Lu, Moore, Omara, Boot, Thépot, and Gumbel have approximately fluctuated buckling performance and they overestimate or underestimate the experimental results. The relatively consistent performance of the later described group of models is perhaps due to the fact that all those models are based on Glock's formula.

The experimental results of Bakeer and Barber (1996) are overestimated by all theoretical models. The reason for this discrepancy may be the fact that among all the tests, the Bakeer tests used reformed HDPE liner with the lower modulus of elasticity for the liner material and also the lowest *SDR*, which is very sensitive to imperfections so that stresses will be concentrated at the stretched or compressed sections of the U-liner and thus causing buckling to occur at a significantly lower pressure.

As shown in Tables 3.5, 3.6, and 3.7, the performance factor denoted, $P_f$, is introduced. It is defined as the ratio of the critical buckling pressure of the test to that estimated by the analytical model. As shown in these tables, the mean value of $P_f$ for the different models for all tests ranged from 0.15 to 2.86, while the ASTM F1216 model gives mean values of 1.29, 1.51, and 1.32 for circular host pipe, and oval host pipe short-term tests and long-term tests, respectively.

From Figure 3.9, it is obvious that for oval host pipe, for the majority of the analytical models, the critical buckling resistance of its liner is considerably lower than that of a perfectly circular liner. The variability depends on the degree of ovality. For the same liner thickness, the increase in elliptical diameter increases the standard dimension ratio *SDR*, which subsequently reduces the critical buckling pressure.

For the long-term tests, it is obvious from Table 3.7 and Figure 3.10 that the long-term critical buckling pressures are lower than the short-term pressures by about 36% to 53%.

This is due to the fact that as the liner becomes thinner and compressed because its stiffness decreases with time due to the creep effect. Moreover, the long-term test results showed larger variability in comparison to the short-term test results. For example, the BORSEF long-term tests showed a performance factor was varying from 0.4 to 2.27 while the performance factor for the BORSEF short-term tests was varying from 0.2 to 1.26.

Omara (1997) evaluated the Timoshenko and Glock's analytical models along with the Aggarwal and Cooper tests data using the best-fitting regression approach. In the present study this evaluation is extended for all existing experimental tests data, with the Timoshenko model replaced by the ASTM F1216 model. The results of the best-fitting regression analyses for these tests are presented in Table 3.8. From these results, the performance factor $P_f$ fluctuated from 0.776 to 1.295, which is close to the range of finite element prediction for $P_f$ from 1.058 to 1.253.

As illustrated in Table 3.8, some of the tests have a value of the exponent $b$ (which includes the effect of the liner stiffness) of approximately 2 with high correlation coefficients ($R^2$ more that 0.70) (e.g., Aggarwal and Cooper, Bakeer *et al.*, BORSF). This reflects that these tests are too close to Glock's model exponent and they captured the physics of the buckling phenomena. The other parameter, $a$, which includes the effect of other factors such as the enhancement, the ovality, and other imperfections indicate a wide variation. This means that this coefficient is full of uncertainty for all existing tests except those of Aggarwal and Cooper test ($a$ equal 1.121) which is too close to Glock's model. (see Table 3.2). On the other hand, when the major phenomena are approximated within the finite element simulation, the performance factors are generally consistent and close to 1. This shows clearly why there is a need for developing a common protocol for conducting statistically significant buckling tests with the intent of identifying the effect of the enhancement factor $K$, the ovality $C$, and other imperfections on the critical buckling pressure for encased liners. Attempts were made to combine all tests data within a given group; however, as shown in Table 3.8, the best-fit-regression analysis for the mixed tests leads to no physical response and gives very low correlation coefficients or

negative values for the exponent *b* (e.g., Omara, all short-term tests with oval host pipe, all long-term tests).

By analyzing the performance of the available analytical models, it is found that there is no particular model that is superior to the rest. A given analytical model can vary from one test to another and can shift from being good to poor predictor. It is worth mentioning that many researchers report large variability in the magnitude and the shape of the liner deformation for identical specimens. This can be attributed to imperfections and stresses induced in the liner during fabrication. Moreover, no analytical model considers the real condition for encased liner that is subjected to non-uniform groundwater pressure, rather than to the uniform pressure assumed in all analytical models. However, Glock's formula seems to be the closest analytical model for which can predict the critical buckling pressure for encased liners because it gives the best-fitting in comparison to the Aggarwal and Cooper (1984) test data (see Table 3.8).

In summary, the dispersion of the results of all analytical and experimental models is very wide and reflects considerable fluctuation among the current liner buckling models. Each of the models has its limitations and does not provide evidence for consistent prediction from one test to another. The present analytical models remain incapable of taking into account some of the major important parameters such as visco-elastic behaviour for long-term response, the host-pipe ovality, and the gap between the liner and the host-pipe. The need for a numerical simulation tool is, therefore, obvious. On the other hand, it is relatively easy to develop a simple finite element model to simulate the behaviour of a liner-pipe structural response with a good level of accuracy. The development of such model is discussed in the following section.

## 3.7 NUMERICAL SIMULATIONS FOR LINERS BUCKLING

The purpose of this section is to develop a finite element model for the analysis of buckling of liner subjected to uniform external pressure. The model is developed using the commercial software ABAQUS (Hibbitt *et al.*, 2005) but could be easily adapted for

other packages. The features of ABAQUS which are employed are described where necessary. Assumptions made in constructing the numerical analysis are presented first and are followed by a description of the implantation of the finite element model.

### 3.7.1 MODEL ASSUMPTIONS

The assumptions used in setting up the finite element models of the encased liner are addressed as follow:

#### A. LOADING CONDITION

According to current ASTM F1216, the encased liner is designed to withstand only the hydrostatic pressure caused by the underground water which infiltrates through the cracks in the host pipe. The original pipe-soil system is assumed to be strong enough to resist all the loads transferred from the surrounding soils. The liner is assumed to interact only with the host pipe. Therefore the only loads acting on the encased liner are the external ground water pressure and the contact forces from the host pipe.

#### B. MATERIAL PROPERTIES

There are a variety of liner materials for pipelines available in the market corresponding to a wide range of mechanical properties. The liner material is assumed to be elastic and perfectly plastic with no strain hardening for the short-term buckling tests. Moreover, it is assumed that the liner materials are homogeneous and isotropic. This assumption is typical for unreinforced thermoplastic products such as Polyethylene and HDPE (Wang, 2002). For long-term models the liner material is assumed to have visco-elastic properties to capture the creep behavior of the liner.

Two common laws are provided in ABAQUS to describe the creep behavior of materials namely; the power law and the hyperbolic-sine law models. The power-law creep model is attractive for its simplicity. The power-law model can be used in its "time hardening"

form or in the corresponding "strain hardening" form. The time-hardening version of the power-law creep model is most suitable when the stress state remains essentially constant. The time-hardening form can be expressed as follow:

$$\varepsilon^{cr} = Aq^n t^m \tag{3.29}$$

where $\varepsilon^{cr}$ is the uniaxial equivalent creep strain rate, q is the uniaxial equivalent deviatoric stress, t is the total time, A, n and m are material properties defined by the user as functions of the temperature. For physically reasonable behavior; A and n must be positive and $-1 < m \leq 0$. Since total time is used in the expression, such reasonable behavior also typically requires that small step times compared to the creep time be used for any steps for which creep is not active in an analysis; this is necessary to avoid changes in the hardening behavior in subsequent steps.

The strain-hardening version of power-law creep should be used when the stress state varies during an analysis. The strain-hardening form can be expressed as follow:

$$\varepsilon^{cr} = \left( Aq^n \left[ (m+1)\varepsilon \right]^m \right)^{\frac{1}{m+1}} \tag{3.30}$$

where $\varepsilon$ is the uniaxial equivalent creep strain.

Creep behaviour is defined through the CREEP option, where a strain-hardening form of the constitutive relation is employed to model the creep behavior of the encased liner in this study. The creep law coefficients used for the finite modeling are $A = 1.00788x10^{-8}$, $n = 1.14585$, $m = -0.76$ respectively, based on the experimental data of Zhu (2000). The liner material properties used in the numerical models of the short-term and long-term tests are based on the tests data described in Table 3.3. The plastic stress is assumed to have an average value of 55 MPa (8000 psi) for the CIPP liner (Zhu, 2000).

### C. 2D CONFIGURATION

Compared with the diameter of the liner, the liner thickness is very small and the liner system can be simplified as a thin-walled circular cylinder. Along the longitudinal direction, the contact conditions between the encased liner and the host pipe are assumed to unchanging. To simplify the solution procedures, the original problem can be viewed as a ring configuration with the plane strain assumption, and the assumption of a single cross-section of the liner (with a length of unity) can be used to represent the entire encased liner. A bi-linear, four-noded, plane- strain continuum element (denoted as CPE4 in ABAQUS) is used to model the liner wall.

## 3.7.2 FEA MODEL

### A. DEFINITION OF GEOMETRIC PARAMETERS

The geometry of the pipe-liner system can be characterized by the liner dimension ratio *SDR*, the annular gap between the liner and the host pipe, and the ovality of the host pipe. These parameters are defined earlier and described in Table 3.3 based on the tests data.

### B. CONSTRAINT FROM THE HOST PIPE

ABAQUS offers an approach to defining the contact interaction based on defining pairs of surfaces that may interact with each other. The surfaces of the contact area for the liner and the host pipe are defined by the SURFACE command and the potential for contact is set up using CONTACT PAIR command. In order to be conservative, the contact interaction between the liner and the host pipe is considered to be smooth; no shear force can be transmitted through the liner-pipe interface. However, it is always possible to revise this assumption and generate a more realistic interface model. The friction is usually defined as zero for the current study by assuming both surfaces are smooth. In this finite element simulation, the host pipe is assumed to be rigid and modeled as rigid element (denoted as R2D2). The set is defined as fixed without any transition or rotation

relative to a reference node. It is therefore assumed implicitly that the host pipe acts only as a boundary to the liner and does not interfere in the deformation of the system. All degrees of freedom of the reference node are inhibited to full constrain the host pipe against any motion.

## C. MODEL SETUPS

Previous investigations (Zhao, 1999) showed that the one-lobe and two-lobe buckling modes are referred to as the lower and the upper bound critical pressures. Single -lobe buckling occurs at lower buckling pressures than does double-lobe buckling. Moreover, El-Sawy (1996) reported that the one-lobe buckling is the more likely in practice. Thus, in this study one-lobe model is used for the numerical simulations. The gap is assumed to be unevenly distributed as shown in Figure 3.6. For simplicity, encased liners assumed to buckle along the vertical axis. Due to symmetry of the one-lobe case, only one half of the liner and the host pipe are modeled as shown in Figure 3.6. To represent the one-lobe configuration, the bottom nodes where the liner touches the host were constrained while the top end of the liner is free.

## D. SOLUTION PROCEDURES

Short-term buckling will be modeled assuming rate-independent elasto-plastic material behaviour. Long-term buckling is modeled assuming rate-independent elasto-plastic material behavior (i.e., creep behaviour). However, for long-term creep, time-dependent model is used with visco-elastic material behaviour based on available long-term experimental data for the encased liner. In the short-term buckling the pressure is assumed to increase monotonically from zero to the buckling pressure while for long-term buckling the pressure is assumed to be constant until buckling is reached. Two different solution processes in ABAQUS can be used to simulate the short-term and long-term buckling: STATIC for time-independent loading and VISCO for time-dependent creeping behavior (i.e., quasi-static analysis). Both procedures can deal with the material and geometric non-linearity resulting from finite displacements of the encased liner

during buckling process. ABAQUS allows the user to step through the loading or time history to be analyzed by dividing the problem into steps. For short-term analyses, a step is static analysis where the pressure changes from one magnitude to another. The effect of the previous step is always updated and is included in the response of the new step. In the creep-induced liner buckling model (the long-term model), the liner will deform elastically under applied external pressure. In long-term buckling analyses, an additional VISCO step applied to a STATIC step which applies a pressure which is less than the critical pressure (i.e., groundwater pressure). The VISCO step is included to incorporate the effects of creep deformation. Automatic time-stepping is governed by accuracy tolerance parameters which are specified by the user. The four parameters defined the accuracy of the automatic time increment during creep response; used for the finite modeling in this study are the maximum difference in the creep strain increment = $1x10^{-4}$, the initial time increment = $1x10^{-7}$, the time period of the step = $5.2561x10^{7}$, the maximum time increment allowed = $1x10^{-3}$, based on the work of Zhu (2000). The solution will stop when the liner collapses. At that point, any attempted time increment is less than or equal to the minimum time step.

### E. MESH SENSITIVITY

Since the stress distribution is very sensitive to the size of the elements in both directions a mesh refinement analysis is performed to optimize the minimum number of layers of elements. It was found that a minimum of four layers consists of 1280 continuum elements are necessary to capture the buckling behaviour of the liner and obtain a better matching with the experimental results within acceptable computation time. Each element has a relatively an aspect ratio that is near one.

## 3.7.3 MODEL VERIFICATION

The developed finite element model has been verified with previous studies (Seemann tests 2000 and Zhu, 2000) as shown in Figure 3.7. Tables 3.5, 3.6, and 3.7 as well as

Figures 3.8, 3.9, and 3.10 show the finite element model prediction and comparison with the analytical and experimental results. From these tables and figures, it is clear that the finite element model results represent a lower bound for all the experimental results. Moreover, the performance factor for the finite element simulation showed the best consistency in predicting the results of all the available experimental tests when compared with analytical models (see Figures 3.8, 3.9 and 3.10). Nevertheless, the errors between the finite element prediction and the short-term and long-term tests were less than 10% and 11%, respectively. The finite element results are slightly on the conservative side because both the gap and the ovality were included. The non-friction interface also contributed toward these conservative results.

## 3.8 SUMMARY AND CONCLUSIONS

A review of major existing analytical models for the prediction of buckling pressure on encased liners is presented. The study of the experimental tests programs of buckling of encased liners under short and long-term conditions showed that there was poor consistency of most of the test programs. However, when the data set includes all available short-term or long-term results, the statistics of these results indicate no consistency, suggesting a lack of uniform protocol in conducting buckling tests on liners. Moreover, it is worthwhile mentioning that neither the analytical models nor the experimental tests take into account that encased liner in real conditions is subjected to non-uniform groundwater pressure and not uniform pressure as assumed in the analytical models or as applied in the existing experimental tests.

The comparison between the analytical models and the existing tests showed that no model has clear superiority over the others. This is related to the fact that all the analytical models use the same methodology and assumptions (with some improvements and modifications) and therefore they inherit the same characteristics. However, Glock's formula has less fluctuation in comparison to the other analytical models. Thus, the Glock's equation seems the closest analytical formula for predicting the critical buckling

pressure on encased liners. Further, the lowest scattering and the most consistent test measurements with a reasonable number of specimens is those of the Aggarwal and Cooper (1984). The development of a better analytical formula does not seem to be possible with the existing tests that have shown significant variability. Thus, it is recommended that more controlled, robust, and statistically significant tests must be carried out in a highly controlled environment in order to minimize the scattering and variability observed in this study and to properly validate any new analytical model.

From the comparison of the Bakeer *et al.* tests (1996, 1999, and 2001) on reformed HDPE liner with the critical buckling predictions of other analytical models, it is clear that liner stability is significantly influenced by liner and host pipe geometry as well as by the method of installation of the encased liner. All analytical models show overestimated the Bakeer *et al.* tests results. Thus, a new design method is needed for the reformed HDPE encased liner. The ASTM F1216 standard predictions are too conservative and if it is used in practical design, the liner thickness and thus the cost of the rehabilitation will increase. The interaction effects for the most common defects (gap, ovality, and longitudinal imperfections) need to be considered in pipe rehabilitation design standards. Thus, the design approaches presented by El-Sawy and Moore, (1997), Moore, (1998), and Gumbel, (2001) offer improvements over the ASTM F1216.

Numerical simulation of buckling of encased liners is an alternative that addresses the main problems in an effective way. The models proposed in this chapter are purposely made simple and their performance is superior to that of any of the analytical models. Both short-term and long-term finite element models can effectively predict the liner buckling resistance for a given pressure when based on appropriate material properties and liner configurations. Despite the simplicity of the finite element model the results appear to be slightly on the conservative side, but most importantly they are consistent from one test to another. Finite element models have the advantage of being extendable to include ovality, gap, and geometric non-linearity effects, and they capture the buckling phenomena successfully.

Table 3.1 Summary of Main Features of Analytical Liner Buckling Models

| Buckling Model | | Model Formula | Model Main Features |
|---|---|---|---|
| Free Ring | Levy (1884) | $P_{cr} = \frac{3EI}{r^3}$ | • Free thin circular ring with pinned or fixed ends subjected to uniform external pressure.<br>• Appropriate for short pipes only.<br>• Derivation based on small deflection linear theory/plane stress condition. |
| | Timoshenko and Gere (1961) | $P_{cr}^{o} = \frac{2E}{1-\upsilon^2}\frac{1}{(SDR-1)^3}$ | • Free thin circular ring with fixed ends subjected to external uniform hydrostatic pressure.<br>• Assume infinitely long pipes.<br>• Derivation based on small deflection linear theory/plane stress condition. |
| Encased Ring | Chicurel (1968) | $P_{cr} = \frac{2.76E}{1-\upsilon^2}\frac{1}{(SDR-1)^{2.2}}$ | • Encased thin circular ring subjected to hoop compression.<br>• Assume no friction between the ring and the outside constraint.<br>• Assume the cavity and ring walls buckle inward radially.<br>• Assume infinitely long pipes.<br>• Derivation based on minimum potential energy/ shrink buckling. |
| | Cheney (1971) | $P_{cr} = \frac{2.55E}{1-\upsilon^2}\frac{1}{(SDR-1)^{2.2}}$ | • Encased thin circular ring subjected to external uniform pressure.<br>• Assume the cavity and ring walls buckle inward radially.<br>• Assume infinitely long pipes.<br>• Derivation based on small deflection linear theory/ minimum potential energy. |

Table 3.1 Summary of Main Features of Analytical Liner Buckling Models (cont.)

| Buckling Model | | Model Formula | Model Main Features |
|---|---|---|---|
| Encased Ring | Glock (1977) | $P_{cr} = \frac{E}{1-\nu^2}\left(\frac{t}{D}\right)^{2.2}$ or $P_{cr} = \frac{E}{1-\upsilon^2}\frac{1}{(SDR-1)^{2.2}}$ | • Encased thin circular ring subjected to external uniform pressure.<br>• Assume no friction between the ring and the outside constraint.<br>• Assume one-lobe buckling mode.<br>• Assume that the flexural and tensile modulus of the ring are approximately equal.<br>• Derivation based on small deflection nonlinear theory/ minimum potential energy/ plane strain condition. |
| | ASTM (1993) | $P = \frac{2KE}{1-\upsilon^2}\frac{1}{(SDR-1)^3}\frac{C}{N}$ | • Encased thin circular ring subjected to external uniform hydrostatic pressure.<br>• Modify Timoshenko model by introducing the enhancement factor $K$, ovality reduction factor $C$, and safety factor $N$.<br>• Assume infinitely long partially deteriorated pipes. |
| | Falter (1996) | $P_{cr} = K_v K_s \frac{E}{1-\nu^2}\frac{1}{(SDR-1)^{2.2}}$ | • Encased thin circular ring subjected to external uniform pressure.<br>• Modify Glock's formula by introducing two types of imperfections namely ; the reduction factor for initial deformation $K_v$, and the reduction factor for initial gap $K_s$. |

Table 3.1 Summary of Main Features of Analytical Liner Buckling Models (cont.)

| Buckling Model | | Model Formula | Model Main Features |
|---|---|---|---|
| Encased Ring | Chunduru (1996) | $P_{cr} = \frac{2C\alpha\beta E}{1-\upsilon^2}\frac{1}{(SDR-1)^3}$ | • Encased thin circular ring subjected to external uniform pressure.<br>• Modify Timoshenko model by introducing three reduction factors; the ovality reduction factor $C$, lining factor $\alpha$, and the stress concentration factor $\beta$. |
| | Omara (1997) | $P_{cr} = \frac{CE}{1-\upsilon^2}\left(\frac{1}{SDR-1}\right)^m$ | • Encased thin circular ring subjected to external uniform hydrostatic pressure.<br>• Use the best –fitting regression to analyze Aggarwal and Cooper (1984) experimental data.<br>• Modify Glock's formula by introducing a coefficient $C = 1.07$ and an exponent $m = 2.17$. |
| | El-Sawy and Moore (1997) | $P_{cr} = \frac{E}{1-\upsilon^2}\left(\frac{1}{SDR-1}\right)^{2.2} e^{-q/18}$ | • Encased thin circular ring subjected to external uniform hydrostatic pressure.<br>• Use the finite element solution to account for the impact of initial ovality.<br>• Modify Glock's formula by introducing a reduction factor ($e^{-q/18}$) for the initial ovality ($q$). |

Table 3.1 Summary of Main Features of Analytical Liner Buckling Models (cont.)

| Buckling Model | | Model Formula | Model Main Features |
|---|---|---|---|
| Encased Ring | Moore (1998) | $P_{cr} = \frac{E}{1-\upsilon^2}\left(\frac{1}{SDR-1}\right)^{2.2} e^{-q/18} e^{-0.56\Delta/t}$ | • Encased thin circular ring subjected to external uniform hydrostatic pressure.<br>• Modify El-Sawy and Moore formula by introducing another reduction factor for the initial local imperfections and elliptical geometry ( $e^{-0.56\Delta/t}$ ), where $\Delta$ is the initial amplitude of a small imperfection in the initial liner geometry. |
| | Boot (1998) | $P_{cr} = C\frac{E}{1-\nu^2}\left(\frac{D}{t}\right)^m$ | • Encased thin circular ring subjected to external uniform pressure.<br>• Extend Glock's formula to take into account the initial gap imperfections and also to reflect the 2-lobe buckling mode. |
| | Lu (1999) | $P_{cr} = \frac{C_{oval}C_{gap}E}{1-\upsilon^2}\left(\frac{1}{SDR-1}\right)^{2.2}$ | • Encased thin circular ring subjected to external uniform pressure.<br>• Modify Glock's formula by introducing two types of imperfections namely ; the reduction factor for ovality ( $C_{oval}$ ), and for initial gap ( $C_{gap}$ ). |
| | Thépot (2000) | $P_{cr} = 2.02k^{0.4}\frac{EI^{0.6}EA^{0.4}}{P^{0.4}r^{1.8}}$ | • Extended Glock's formula to include circular and non-circular (egg-shaped and horseshoe-shaped) host pipes.<br>• Account for the effect of gap and ovality.<br>• Account for 1-lobe and 2-lobe buckling modes. |

Table 3.1 Summary of Main Features of Analytical Liner Buckling Models (cont.)

| Buckling Model | | Model Formula | Model Main Features |
|---|---|---|---|
| Encased Ring | Gumbel (2001) | $P_{cr} = k_i . c_o \frac{E}{1-\nu^2}\left(\frac{D}{t}\right)^{-2.2}$ | • Modify Glock's model by introducing an overall reduction factor ($k_i$) and an ovality coefficient ($c_o$).<br>• Separated the imperfection effects into system imperfections related to the host pipe and characteristic imperfections related to the renovation technique. |

Table 3.2 Parameters of Analytical Liner Buckling Models

| Liner Buckling Model | Coefficients | | Imperfection Factors |
|---|---|---|---|
| | $a$ | $b$ | |
| ASTM F1216 (1993) | $2KC$ | 3.0 | $KC$ |
| Timoshenko (1961) | 2.00 | 3.0 | 1 |
| Chicurel (1968) | 2.76 | 2.2 | $1.38(D/t)^{0.8}$ |
| Cheney (1971) | 2.55 | 2.2 | $1.275(D/t)^{0.8}$ |
| Glock (1977) | 1.00 | 2.2 | $0.5(D/t)^{0.8}$ |
| Falter (1996) | $K_vK_s$ | 2.2 | $0.5K_vK_s(D/t)^{0.8}$ |
| Chunduru (1996) | $2C\alpha\beta$ | 3.0 | $C\alpha\beta$ |
| Omara (1997) | 1.07 | 2.17 | $0.535(D/t)^{0.83}$ |
| El-Sawy and Moore (1997) | $e^{-q/18}$ | 2.2 | $0.5\,e^{-q/18}\,(D/t)^{0.8}$ |
| Moore (1998) | $e^{-q/18}e^{-0.56\Delta/t}$ | 2.2 | $0.5\,e^{-q/18}e^{-0.56\Delta/t}\,(D/t)^{0.8}$ |
| Boot (1998) | 1.003 | 2.2 | $0.5(D/t)^{0.8}$ |
| Lu (1999) | $C_{oval}C_{gap}$ | 2.2 | $0.5C_{oval}C_{gap}(D/t)^{0.8}$ |
| Thèpot (2000) | 1.204 | 2.2 | $0.602(D/t)^{0.8}$ |
| Gumbel (2001) | $c_o.\ k_i$ | 2.2 | $0.5\ c_o.k_i\ (D/t)^{0.8}$ |

Table 3.3 Summary of Main Features of Experimental Liner Buckling Tests

| Buckling Tests | No. of Tests | *D* (mm) | *t* (mm) | *SDR* | *L/D* | *E* (MPa) | Liner /Resin | Other features |
|---|---|---|---|---|---|---|---|---|
| Aggarwal and Cooper (1984) | 49 | 250 | 2.8-8.4 | 30-90 | 3.5-4.5* | 960 - 2570 | CIPP** | • Gap measurement or calculation is not reported.<br>• Pressurized water used to apply external pressure. |
| Welch (1989) | 9 | 450 | 10 | 45 | 0.45 | 1100 | Slip liner | • Compressed air used to apply external pressure.<br>• Ovality of 0%, 5%, and 10%. |
| CPAR (1994)*** | 200 | 300 | 4.8-9.8 | 30-70 | 6 | 1950 - 12300 | CIPP | • Standard and enhanced resin.<br>• Volumetric gap measurement.<br>• Pressurized water used to apply external pressure. |
| Bakeer *et al.*** (1996, 1999, 2001) | 90 | 150 & 200 | 4.6-7.6 | 26 and 32.5 | 10 | 1050 | HDPE | • Compressed air used to apply external pressure.<br>• Ovality of 0% and 7%. |

* Scaled values estimated from the pictures in their report because they did not report L/D values (El-Sawy, 1996).
** Different types of resin used in their tests.
*CPAR and Bakeer *et al.* (1999, 2001) experimental data are used for long-term buckling behaviour.

Table 3.3 Summary of Main Features of Experimental Liner Buckling Tests - (cont.)

| Buckling Tests | No. of Tests | *D* (mm) | *t* (mm) | *SDR* | *L/D* | *E* (MPa) | Liner /Resin | Other features |
|---|---|---|---|---|---|---|---|---|
| Omara (1997) | 18 | 300 | 5.6-6.1 | 50-54 | 10 | 2695 | CIPP | • Ovality of 5%, 10%, and 20%.<br>• Pressurized water used to apply external pressure. |
| BORSF (1998)*** | 195 | 200 & 300 | 3.7-7.9 | 37-59 | 10 | 3086 | CIPP | • Volumetric gap measurement.<br>• Pressurized water used to apply external pressure. |
| Seemann (2000) | 15 | 300 | 7.1-7.9 | 41.98-42.12 | 10 | 3137 | CIPP | • Ovality of 0%, 2%, and 5%.<br>• Pressurized water used to apply external pressure.<br>• Volumetric gap measurement. |

*BORSF experimental data are used for long-term buckling behaviour.

Table 3.4 Summary of Statistical Analysis Parameters of Liner Critical Buckling Pressure Tests

| Buckling Tests | | | No. of Tests | Analysis of Variance (ANOVA) | | | | | Dispersion Factor | Capability Analysis | Normality Tests | |
|---|---|---|---|---|---|---|---|---|---|---|---|---|
| | | | | Mean (kPa) | Standard Deviation (kPa) | Coeff. of Variation | Kurtosis | Skewness | | Capability Index | Kolmogorov-Smirnov** | Shapiro-Wilk |
| | | | | | | | | | | *Cpk* | α -value | α -value |
| Short – Term Tests | Circular Host Pipe | Aggarwal and Cooper (1984) | 49 | 565.6 | 334.6 | 0.5916 | 1.341 | 1.167 | 2.456 | 0.10 | 0.003 | 0.001 |
| | | Welch (1989) | 3 | 335.7 | - | - | 0 | 0.560 | 1.705 | - | 0 | 0.790 |
| | | CPAR (1994) | 26 | 642.7 | 353.9 | 0.5507 | 1.605 | 1.401 | 2.466 | 0.13 | 0.001 | 0.001 |
| | | Bakeer and Barber (1996) | 8 | 342.2 | 100.2 | 0.2930 | -1.481 | 0.261 | 2.234 | 0.28 | 0.200 | 0.309 |
| | | BORSF (1998) | 35 | 688.5 | 180.5 | 0.2622 | -0.188 | -0.606 | 2.509 | 0.11 | 0.200 | 0.148 |
| | | Seemann (2000) | 5 | 847.8 | 71.3 | 0.0841 | -1.283 | -0.502 | 2.246 | 0.41 | 0.200 | 0.798 |
| | Oval Host Pipe | Welch (1989) | 3 | 251.7 | 26.2 | 0.1039 | 0 | -0.560 | 1.657 | 0.83 | 0 | 0.790 |
| | | Bakeer and Barber (1996) | 8 | 342.2 | 100.2 | 0.2930 | -1.481 | 0.261 | 2.234 | 0.28 | 0.200 | 0.309 |
| | | Omara (1997) | 6 | 380.7 | 30.6 | 0.0803 | 0.669 | 0.760 | 2.181 | 0.35 | 0.200 | 0.797 |
| | | BORSF (1998) | 10 | 601.2 | 96.2 | 0.1600 | -1.680 | 0.420 | 2.383 | 0.24 | 0.200 | 0.292 |
| | | Seemann (2000) | 5 | 847.8 | 71.3 | 0.0841 | -1.283 | -0.502 | 2.246 | 0.41 | 0.200 | 0.768 |
| Long – Term Tests | Circular Host Pipe | Bakeer *et al.* (1999, 2001) | 20 | 162.0 | 43.9 | 0.2708 | -1.171 | 0.150 | 2.185 | 0.16 | 0.199 | 0.150 |
| | | CPAR (1994) | 35 | 411.5 | 68.2 | 0.1657 | -1.189 | 0.157 | 2.414 | 0.11 | 0.083 | 0.160 |
| | | BORSF (1998) | 150 | 378.8 | 105.3 | 0.2781 | -0.810 | 0.442 | 2.419 | 0.12 | 0.005 | 0 |
| Mixed Tests | All Short-Term Tests - Circular | | 126 | 607.2 | 298.3 | 0.4913 | 0.970 | 0.970 | 2.496 | 0.50 | 0.097 | 0 |
| | All Short-Term Tests - Oval | | 32 | 500.9 | 209.2 | 0.4177 | 0.531 | 0.531 | 2.436 | 0.23 | 0.200 | 0.070 |
| | All Long-Term Tests- Circular | | 158 | 585.6 | 285.2 | 0.4870 | -0.807 | -0.807 | 2.492 | 0.30 | 0 | |

Table 3.5 Analytical Critical Buckling Pressure and Performance Factor for Different Models (Short-Term Tests, Circular Host Pipe)

| Liner Buckling Model | Aggarwal and Cooper (1984) | | Welch (1989) | | CPAR Tests (1994) | | Bakeer and Barber (1996) | | BORSF Tests (1998) | | Seemann (2000) | |
|---|---|---|---|---|---|---|---|---|---|---|---|---|
| | $P_{cr}$ (kPa) | $P_f$ | $P_{cr}$ (kPa) | $P_f$ | $P_{cr}$ (kPa) | $P_f$ | $P_{cr}$ (kPa) | $P_f$ | $P_{cr}$ (kPa) | $P_f$ | $P_{cr}$ (kPa) | $P_f$ |
| Tests (mean) | 566 | - | 252 | - | 643 | - | 342 | - | 689 | - | 848 | - |
| Finite Element Model | 531 | 1.07 | 216 | 1.17 | 586 | 1.10 | 305 | 1.12 | 602 | 1.15 | 677 | 1.25 |
| ASTM F1216 (1993) | 348 | 2.04 | 186 | 1.37 | 624 | 1.28 | 832 | 0.43 | 521 | 1.39 | 703 | 1.20 |
| Timoshenko (1961) | 50 | 14.25 | 26 | 9.47 | 89 | 8.95 | 119 | 2.99 | 75 | 9.67 | 101 | 8.46 |
| Chicurel (1968) | 1328 | 0.45 | 770 | 0.33 | 2531 | 0.28 | 2300 | 0.18 | 2153 | 0.32 | 2700 | 0.30 |
| Cheney (1971) | 1227 | 0.49 | 711 | 0.37 | 2338 | 0.32 | 2125 | 0.18 | 1989 | 0.35 | 2495 | 0.34 |
| Glock (1977) | 481 | 1.25 | 279 | 0.90 | 917 | 0.82 | 834 | 0.40 | 780 | 0.88 | 978 | 0.86 |
| Falter (1996) | 232 | 2.59 | 134 | 1.87 | 443 | 1.68 | 403 | 0.86 | 377 | 1.84 | 473 | 1.80 |
| Chunduru (1996) | 298 | 2.38 | 159 | 1.57 | 535 | 1.49 | 713 | 0.50 | 447 | 1.61 | 603 | 1.40 |
| Omara (1997) | 576 | 1.04 | 334 | 0.77 | 1100 | 0.68 | 985 | 0.38 | 936 | 0.75 | 1170 | 0.72 |
| El-Sawy/Moore (1997) | 481 | 1.25 | 279 | 0.90 | 917 | 0.82 | 834 | 0.40 | 780 | 0.88 | 978 | 0.86 |
| Moore (1998) | 304 | 2.58 | 279 | 0.90 | 917 | 0.82 | 834 | 0.40 | 780 | 0.88 | 967 | 0.90 |
| Boot (1998) | 577 | 1.04 | 335 | 0.77 | 1103 | 0.68 | 988 | 0.38 | 938 | 0.75 | 1174 | 0.72 |
| Lu (1999) | 284 | 1.99 | 279 | 0.90 | 917 | 0.82 | 834 | 0.40 | 780 | 0.88 | 935 | 0.92 |
| Thépot (2000) | 579 | 1.05 | 336 | 0.77 | 1104 | 0.68 | 1003 | 0.38 | 939 | 0.74 | 1178 | 0.72 |
| Gumble (2001) | 296 | 2.37 | 184 | 1.39 | 655 | 1.14 | 477 | 0.97 | 535 | 1.26 | 629 | 1.35 |

Note: Grey cells represent best estimation.

Table 3.6 Analytical Critical Buckling Pressure and Performance Factor for Different Models
(Short-Term Tests, Oval Host Pipe)

| Liner Buckling Model | Welch (1989) Ovality = 5% | | Bakeer and Barber (1996) Ovality = 7% | | Omara (1997) Ovality = 5% | | BORSF Tests (1998) Ovality = 3% | | Seemann (2000) Ovality = 5% | |
|---|---|---|---|---|---|---|---|---|---|---|
| | $P_{cr}$ (kPa) | $P_f$ | $P_{cr}$ (kPa) | $P_f$ | $P_{cr}$ (kPa) | $P_f$ | $P_{cr}$ (kPa) | $P_f$ | $P_{cr}$ (kPa) | $P_f$ |
| Tests (mean) | 252 | - | 342 | - | 381 | - | 601 | - | 517 | - |
| Finite Element Model | 228 | 1.11 | 295 | 1.16 | 306 | 1.25 | 546 | 1.10 | 481 | 1.08 |
| ASTM F1216 (1993) | 119 | 2.10 | 431 | 0.84 | 214 | 1.80 | 675 | 0.90 | 450 | 1.15 |
| Timoshenko (1961) | 26 | 9.47 | 119 | 2.99 | 48 | 8.02 | 126 | 4.80 | 101 | 5.12 |
| Chicurel (1968) | 770 | 0.33 | 2300 | 0.18 | 1501 | 0.27 | 3208 | 0.20 | 2700 | 0.19 |
| Cheney (1971) | 711 | 0.37 | 2125 | 0.18 | 1386 | 0.28 | 2964 | 0.22 | 2495 | 0.21 |
| Glock (1977) | 279 | 0.90 | 834 | 0.40 | 544 | 0.68 | 1163 | 0.51 | 978 | 0.53 |
| Falter (1996) | 134 | 1.87 | 403 | 0.86 | 263 | 1.45 | 562 | 1.07 | 473 | 1.10 |
| Chunduru (1996) | 102 | 2.47 | 369 | 0.95 | 183 | 2.10 | 579 | 1.06 | 386 | 1.34 |
| Omara (1997) | 334 | 0.77 | 985 | 0.38 | 654 | 0.58 | 1388 | 0.45 | 1170 | 0.44 |
| El-Sawy/Moore (1997) | 211 | 1.20 | 553 | 0.63 | 412 | 0.93 | 982 | 0.61 | 741 | 0.70 |
| Moore (1998) | 211 | 1.20 | 553 | 0.63 | 354 | 1.07 | 982 | 0.61 | 732 | 0.71 |
| Boot (1998) | 335 | 0.77 | 988 | 0.38 | 656 | 0.58 | 1392 | 0.45 | 1174 | 0.44 |
| Lu (1999) | 217 | 1.17 | 576 | 0.59 | 226 | 1.47 | 998 | 0.60 | 728 | 0.71 |
| Thèpot (2000) | 336 | 0.77 | 1003 | 0.38 | 655 | 0.58 | 1400 | 0.44 | 1178 | 0.44 |
| Gumble (2001) | 184 | 1.39 | 477 | 0.97 | 360 | 1.05 | 535 | 1.26 | 600 | 1.45 |

Note: Grey cells represent best estimation.

Table 3.7 Analytical Critical Buckling Pressure and Performance Factor for Different Models (Long-Term Tests, Circular Host Pipe)

| Liner Buckling Model | Bakeer *et al.* (1999, 2001) | | CPAR Tests (1994) | | BORSF Tests (1998) | |
|---|---|---|---|---|---|---|
| | $P_{cr}$ (kPa) | $P_f$ | $P_{cr}$ (kPa) | $P_f$ | $P_{cr}$ (kPa) | $P_f$ |
| Tests (mean) | 162 | - | 412 | - | 379 | - |
| Finite Element Model | 134 | 1.21 | 388 | 1.06 | 346 | 1.10 |
| ASTM F1216 (1993) | 416 | 0.41 | 230 | 1.79 | 221 | 1.76 |
| Timoshenko (1961) | 59 | 2.86 | 33 | 12.51 | 32 | 12.35 |
| Chicurel (1968) | 1150 | 0.15 | 1089 | 0.38 | 956 | 0.40 |
| Cheney (1971) | 1063 | 0.15 | 1006 | 0.40 | 883 | 0.43 |
| Glock (1977) | 417 | 0.38 | 394 | 1.04 | 346 | 1.09 |
| Falter (1996) | 201 | 0.83 | 191 | 2.15 | 167 | 2.27 |
| Chunduru (1996) | 357 | 0.48 | 197 | 2.08 | 189 | 2.05 |
| Omara (1997) | 492 | 0.36 | 475 | 0.87 | 416 | 0.91 |
| El-Sawy/Moore (1997) | 417 | 0.38 | 394 | 1.04 | 346 | 1.09 |
| Moore (1998) | 417 | 0.38 | 366 | 1.13 | 346 | 1.09 |
| Boot (1998) | 494 | 0.36 | 477 | 0.87 | 417 | 0.91 |
| Lu (1999) | 417 | 0.38 | 303 | 1.36 | 346 | 1.09 |
| Thépot (2000) | 502 | 0.36 | 475 | 0.87 | 417 | 0.91 |
| Gumble (2001) | 239 | 0.72 | 327 | 1.35 | 268 | 1.89 |

Note: Grey cells represent best estimation.

Table 3.8 Summary of Best-Fitting Regression Evaluation of Theoretical Models with Experimental Data

| Buckling Test Type | Test Model | ASTM F1216 | | Glock | | Best-Fitting Regression | | | | | FEA |
|---|---|---|---|---|---|---|---|---|---|---|---|
| | | $\text{Log}(P_f)$ | $P_f$ | $\text{Log}(P_f)$ | $P_f$ | $a$ | $b$ | $R^2$ | $\text{Log}(P_f)$ | $P_f$ | $P_f$ |
| Short-Term (Circular) | Aggarwal and Cooper (1984) | 0.272 | 2.036 | 0.077 | 1.255 | 1.121 | 2.19 | 0.78 | 0.011 | 1.077 | 1.073 |
| | Welch (1989) | 0.130 | 1.355 | -0.046 | 0.903 | - | - | - | -0.112 | 0.776 | 1.171 |
| | CPAR (1994) | 0.078 | 1.279 | -0.115 | 0.811 | 0.138 | 1.8066 | 0.44 | 0.088 | 1.295 | 1.101 |
| | Bakeer and Barber (1996) | -0.377 | 0.427 | -0.389 | 0.412 | 0.236 | 2.0353 | 0.71 | -0.001 | 1.008 | 1.122 |
| | BORSF (1998) | 0.160 | 1.472 | -0.036 | 0.933 | 0.567 | 2.0889 | 0.70 | 0.023 | 1.068 | 1.154 |
| | Seemann (2000) | 0.081 | 1.210 | -0.063 | 0.868 | 0.003 | 0.6463 | 0.04 | 0.000 | 1.002 | 1.072 |
| Short-Term (Oval) | Welch (1989) | 0.324 | 2.118 | -0.046 | 0.903 | - | - | - | -0.112 | 0.776 | 1.113 |
| | Bakeer and Barber (1996) | -0.091 | 0.825 | -0.389 | 0.412 | 0.236 | 2.0353 | 0.71 | -0.001 | 1.008 | 1.108 |
| | Omara (1997) | 0.251 | 1.789 | -0.156 | 0.701 | 2E-8 | -2.324 | 0.15 | -0.000 | 1.002 | 1.253 |
| | BORSF (1998) | 0.277 | 1.926 | -0.036 | 0.933 | 0.001 | 0.0306 | 4E-5 | 0.049 | 1.166 | 1.102 |
| | Seemann (2000) | 0.275 | 1.891 | -0.063 | 0.868 | 0.003 | 0.6463 | 0.04 | -0.000 | 1.002 | 1.084 |
| Long-Term (Circular) | CPAR (1994) | 0.248 | 1.786 | 0.013 | 1.042 | 81.22 | 3.2951 | 0.24 | -0.007 | 0.994 | 1.058 |
| | BORSF (1998) | 0.238 | 1.764 | 0.032 | 1.095 | 4E-6 | -0.980 | 0.24 | 0.023 | 1.131 | 1.086 |
| | Bakeer *et al.* (1999,2001) | -0.400 | 0.407 | -0.412 | 0.393 | 0.160 | 1.9355 | 0.65 | 0.001 | 1.017 | 1.209 |
| Mixed | All-short-term-tests-(Circular) | - | - | - | - | 0.021 | 1.2193 | 0.27 | - | - | - |
| | All-short-term-tests-(Oval) | - | - | - | - | 1e-4 | -0.154 | 0.01 | - | - | - |
| | All-long-term-tests (Circular) | - | - | - | - | 2e-6 | -1.231 | 0.72 | - | - | - |

Note: Grey cells represent best estimation.

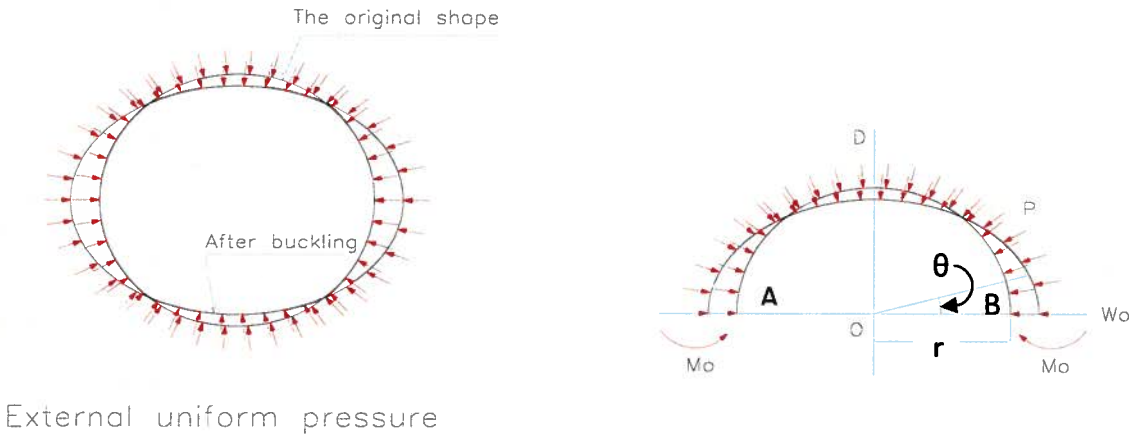


Figure 3.1 Buckling Model of a Free Ring (After Timoshenko and Gere, 1961)

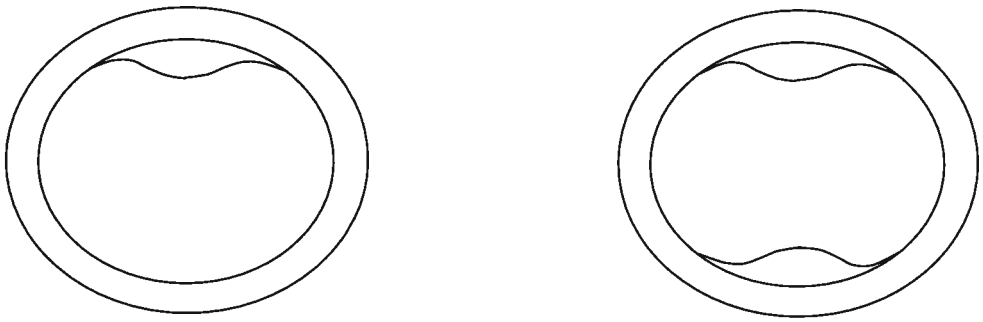

One-lobe
(a)

Two-lobe
(b)

Figure 3.2 Buckling Modes of Encased Thin Ring (After Seemann, 2000)

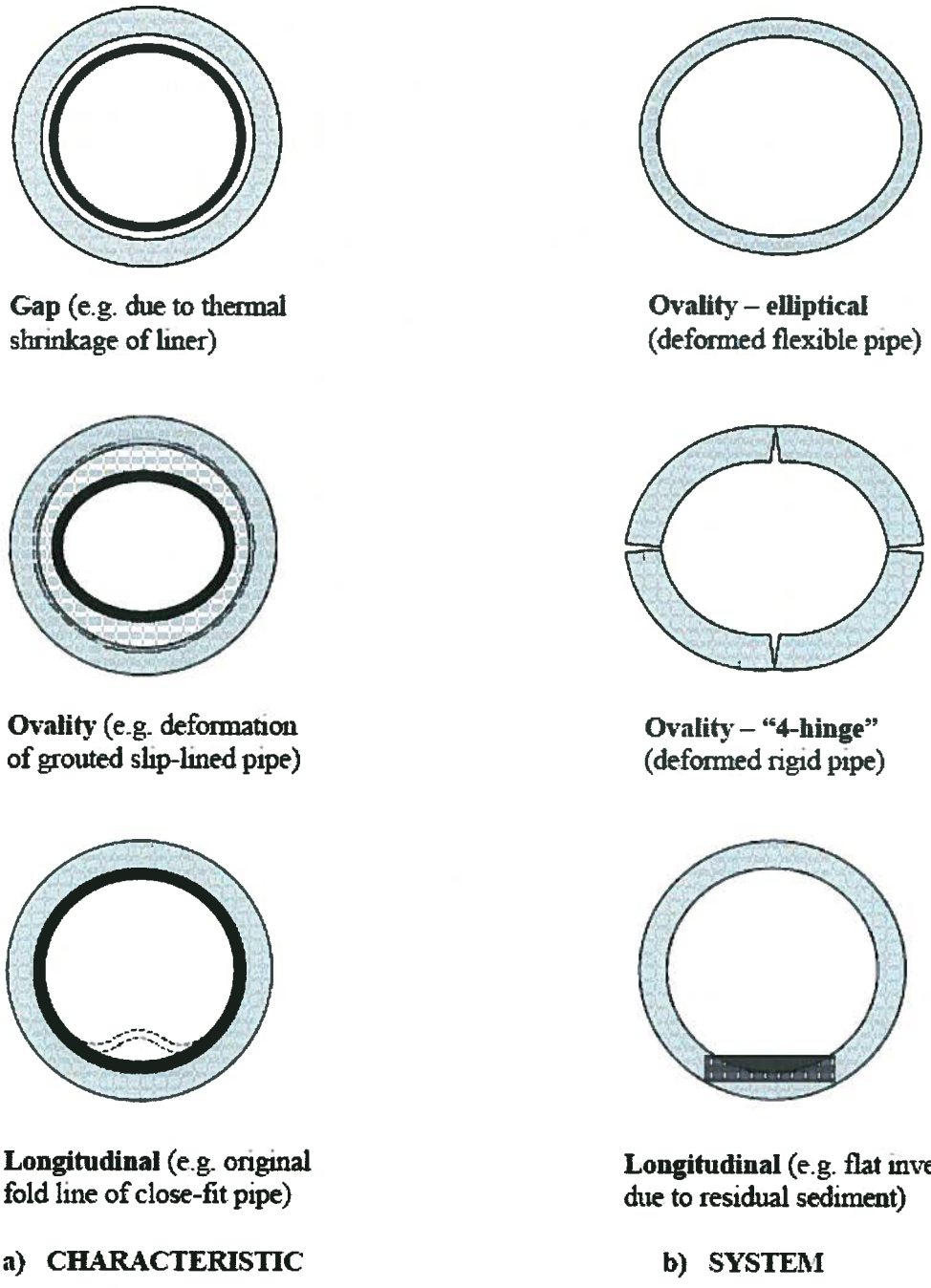


Figure 3.3 Examples of Characteristics (Renovation Techniques) and System (Host Pipe) Imperfections Affecting Liner-Buckling Resistance (After Gumbel, 2001)

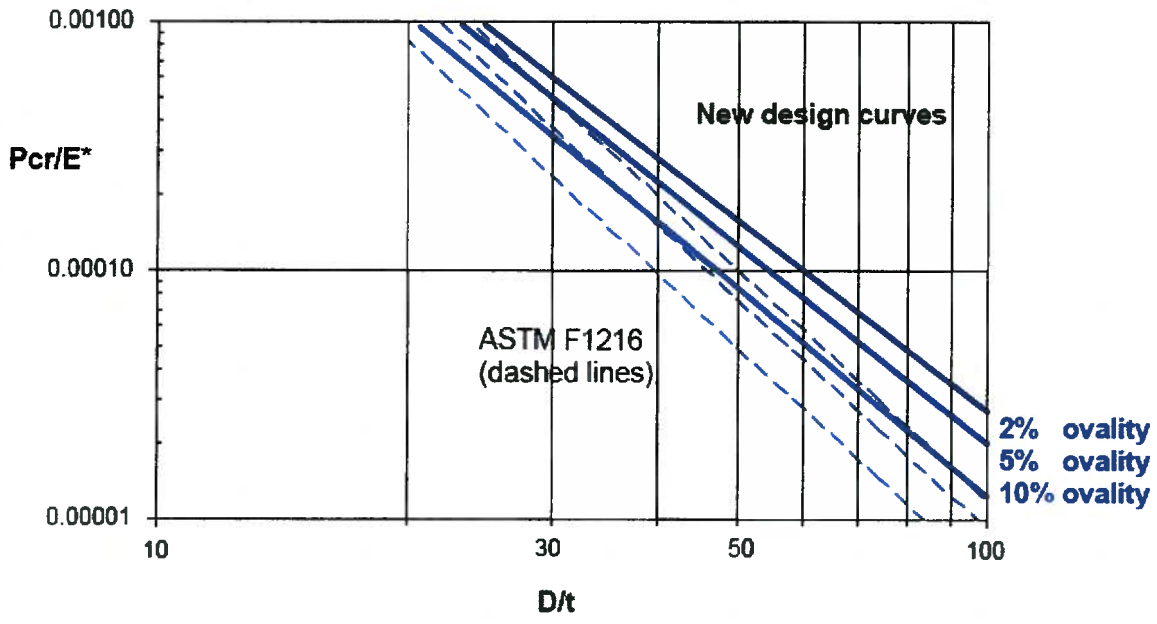


Figure 3.4 Typical Form of New Design Chart for CIPP Incorporating a Characteristic Gap Imperfection (here 0.5%) (After Gumbel, 2001)

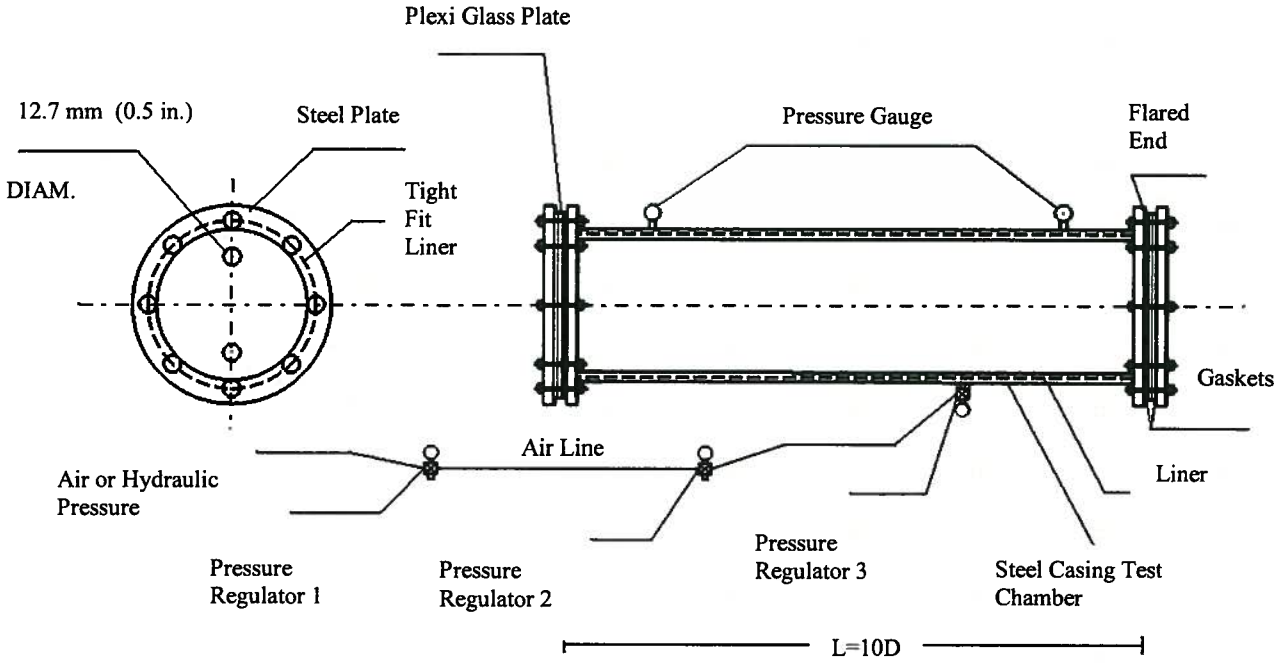


Figure 3.5 Test Frame for Conducting Buckling Tests (After Bakeer *et al.*, 1996)

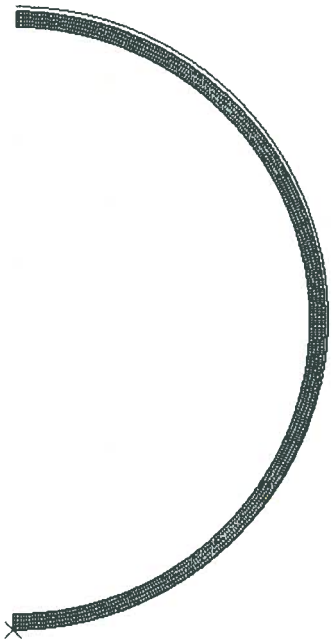

Figure 3.6 Schematic of a Numerical Model Mesh for One-Lobe Liner Buckling

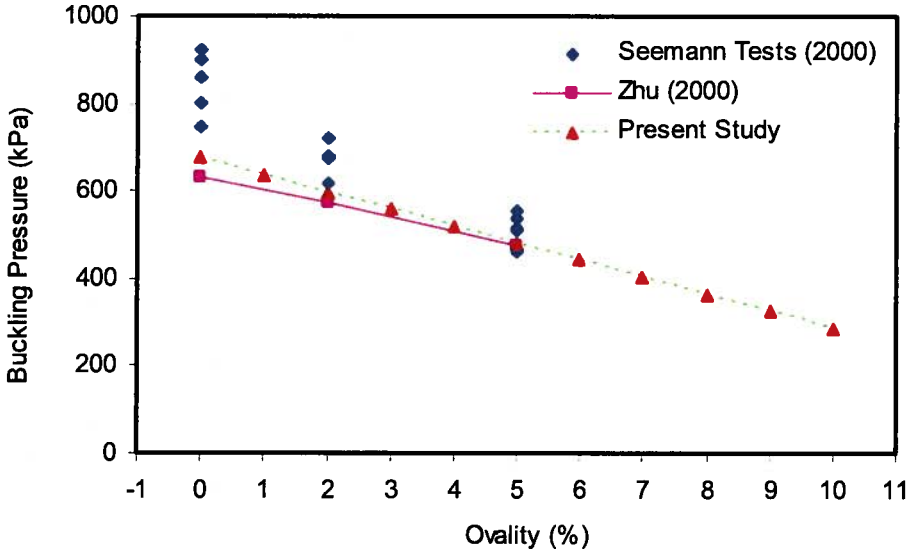


Figure 3.7 Comparison of Seemann Tests (2000) with Numerical Models of Zhu (2000) and Present Study

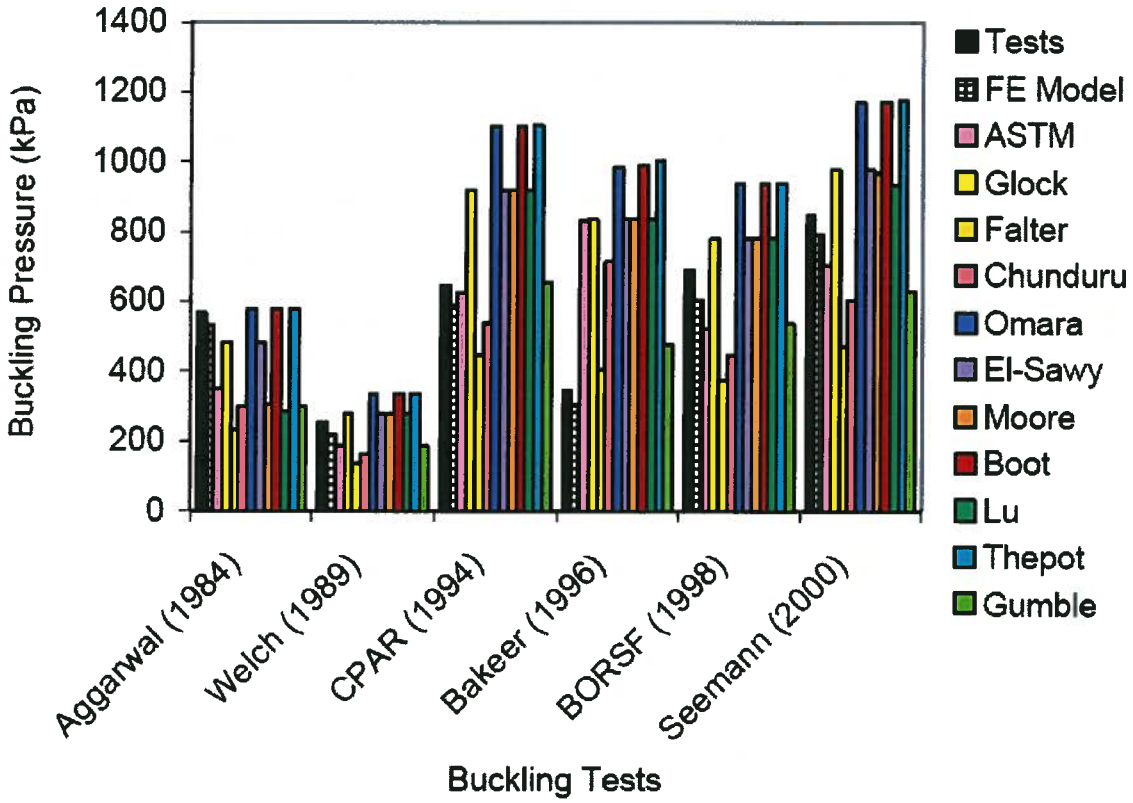


Figure 3.8 Comparison of Analytical Buckling Pressure for Different Buckling Models with Experimental Tests (Short-Term, Circular Host Pipe)

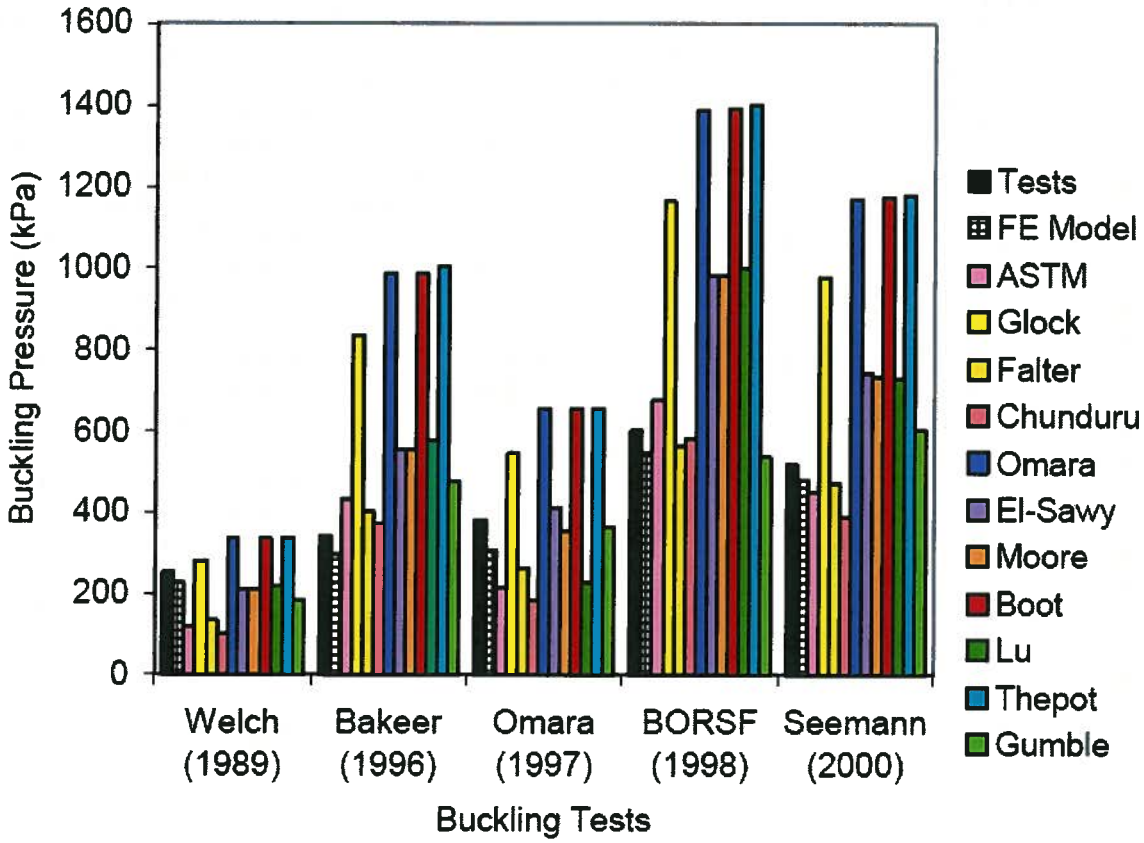


Figure 3.9 Comparison of Analytical Buckling Pressure for Different Buckling Models with Experimental Tests (Short-Term, Oval Host Pipe)

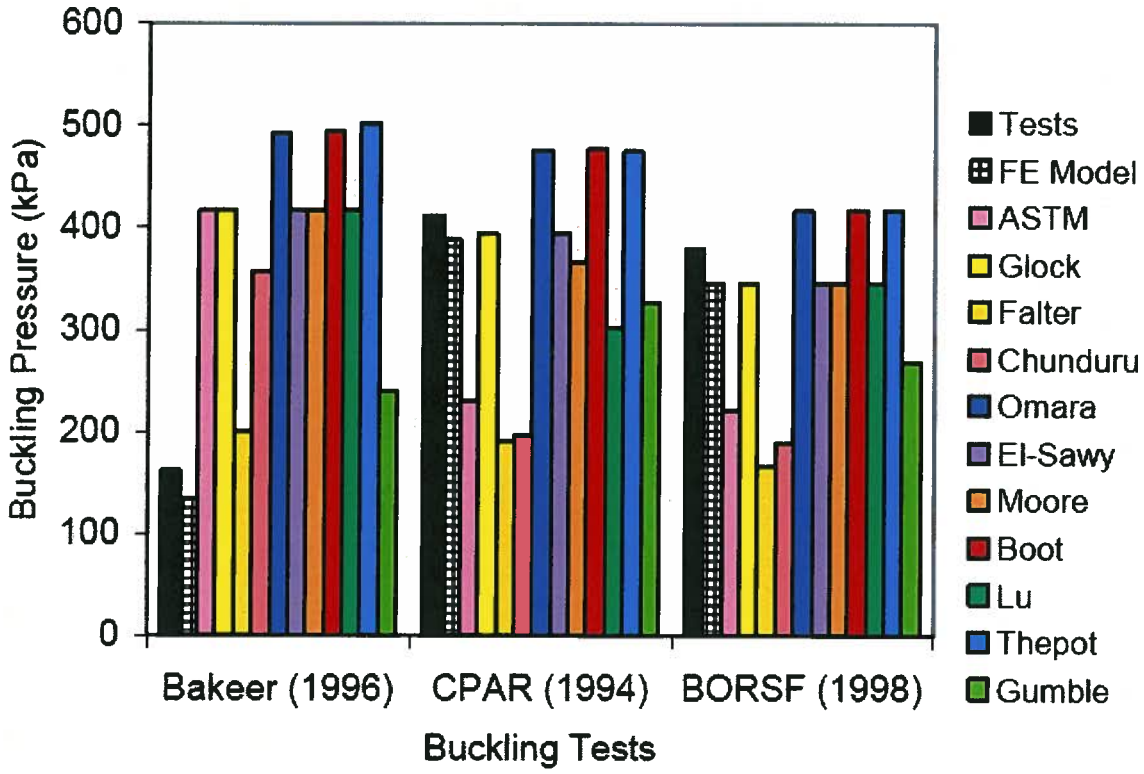


Figure 3.10 Comparison of Analytical Buckling Pressure for Different Buckling Models with Experimental Tests (Long-Term, Circular Host Pipe)

# CHAPTER 4

# MODELING OF AXIAL AND BENDING BEHAVIOUR OF UNRESTRAINED JOINTS IN SEGMENTED PIPELINES

## 4.1 INTRODUCTION

Buried pipeline systems are commonly used to transport a wide variety of substances and materials including water, sewage, oil, natural gas, electric power, and telecommunication cables. Pipelines represent a critical component within infrastructure systems. These pipelines carry materials essential to the support of life; in fact they actually are often referred to as "lifelines" (O'Rourke and Liu, 1999). Utilities pipelines in particular, vitrified clay and concrete pipes have been in service where for more than 100 years. Over time, many of these systems become defective and suffer from overloading and loss of capacity. Further, it has been shown that pipelines are vulnerable to seismic motions and ground movements that cause joint damage and system failure (Meis, 2003).

The most common joint type used for water mains and sewer pipes is the "push-on" joint, comprising of a plain pipe or "spigot" end that is inserted into an enlarged or "bell" end. Pipe joints are usually classified as either restrained or unrestrained. Unrestrained joints have a high restraint capacity in the compressive direction since the two ends butt up against each other, but essentially zero restraint capacity in the tensile direction. In addition to a high compression capacity, restrained joints have a restraint capacity in the tensile direction provided either by a device that supplies the restraint or by a continuity of the material through the joint (Meis, 2003). Bell-spigot rigid joints are either filled with oakum and asbestos cement or caulked with cement, while the structure of unrestrained joints consist rubber ring of different shapes. The rubber ring gasket, which is compressed during the insertion of the spigot end, provides a watertight seal at the joint and provides a continuity of the material through the joint.

Joint stiffness is an important input for the numerical simulation of segmented pipeline behaviour. To the best knowledge of the author, no experimental test results are available that determine the axial and bending stiffness of rubber gasket unrestrained joints of small diameters for vitrified clay pipes, non-reinforced pipes, and reinforced concrete pipes. This lack of data about the structural behaviour of such joints was the impetus for the work presented in this chapter. Thus, a finite element simulation is developed to simulate the joint structural behaviour. The objective of the finite element modeling is to determine the axial and rotational stiffness and other characteristics of some common rigid pipe unrestrained joints thought to be most strongly influence by the seismic behaviours. These characteristics are the force-displacement behaviour of the joint subject to axial compression as well as the moment-rotation behaviour of the joint subject to bending moment. No axial tensile behaviour is studied, as the unrestrained joint has zero resistance in tension. A finite element analysis with geometric non-linearity and large strain formulation is used to develop such relationships.

Elhmadi and O'Rourke (1990) summarized the available data on joint pull-out failure based on previous laboratory tests. They suggested a relative joint displacement corresponding to 50% of the total joint depth as the failure criterion for pull-out of segmented pipelines with rigid joints. Bouabid and O'Rourke (1994) suggested that, for unrestrained joints at moderate internal pressures, the relative joint tensile displacement leading to significant leakage corresponds to roughly half the total joint depth. They reported that a relative axial joint extension of roughly half the total joint depth may be an appropriate failure criterion for many types of segmented pipes. The numerical modeling presented in this chapter focuses on simulation of the axial compression and bending behaviours of unrestrained joints for three different rigid pipe materials, namely reinforced concrete, non-reinforced concrete, and vitrified clay. Three different nominal pipe diameters of 200 mm, 250 mm, and 300 mm were included to cover the sizes most frequently encountered in practice. Test results obtained from two different laboratory full-scale tests (Bouabid, 1993; Singhal, 1984a, b) are used to validate and calibrate finite element models for compression and bending tests, respectively.

This work explores numerical simulation of the structural behaviours of unrestrained gasket joints, as well as influence of seismic behaviours on buried segmented pipelines of different materials. It begins with a brief review of the experimental tests for the axial/bending behaviours of joints. Then, two finite element models have been developed, verified with tests results, and extended to simulate joints behaviour. The final sections of the chapter report on the numerical modeling of the static axial compression and bending behaviours of joints as well as of segmented pipes, using the finite element method.

## 4.2 AXIAL BEHAVIOURS OF RUBBER GASKET JOINTS

In this section, we attempt to develop a finite element model to characterize the axial behaviours of rubber gasket joints in reinforced concrete, non-reinforced concrete, and vitrified clay pipes. The methodology is based on the development of a finite element model capable of reproducing experimental results presented by Bouabid (1993). The finite element model is then used to propose a simplified rheological constitutive model of the joint consisting of a bi-linear elastic spring.

### 4.2.1 EXPERIMENTAL OBSERVATIONS

The work of Bouabid (1993) on the axial behaviours of rubber gasket joints of reinforced concrete pipes is selected as a reference to develop a finite element model for this system. A series of compression and tension tests were performed by Bouabid (1993) for rubber gasket joints of reinforced concrete cylinder pipes to obtain the force-deformation relationship of the joints. Table 4.1 summarizes the pipe and joint properties for the tested joints.

The test setup consisted of two pipes of 1168.4 mm length (46 in) and one short pipe of 406.4 mm length (16 in). A cross-section view of the experimental setup configuration displaying the upper half of the pipe segments is shown in Figure 4.1. Both ends of the system were bulkheaded, thus resulting in a total of four joints. Joints 1, 3, and 4 in this configuration were sealed with an exterior wrapping of fiberglass. Only joint 2 remained active. Axial compression or tension loads were applied at the left bulkhead while the

right bulkhead was pinned to the test frame. As a result, the left bulkhead and long pipe segment between joints 1 and 2 essentially moved as one unit, while the right bulkhead and the long and short segments between joints 2 and 4 moved as a separate unit. Further details of experimental descriptions and tests results are presented by Bouabid (1993).

These experimental results are compiled with physical and mechanical properties of reinforced concrete pipes in order to calibrate and validate the finite element model for investigating the axial behaviours of unrestrained joints.

### 4.2.2 SIMULATION OF AXIAL BEHAVIOURS OF RUBBER GASKET JOINTS

The purpose of this section is to develop a finite element model for the analysis of axial behavior of rubber gasket joints subjected to compressive or tensile. Assumptions used in setting up the finite element models of the axial behavior of the unstrained rubber gasket joint are addressed in this section.

#### A. LOADING CONDITION

The segmented pipeline system is assumed to be strong enough to resist all compressive, tensile, and bending loads. The joint usually represents the weak portion of the segmented pipeline system where the bell and spigot (female and male) are in contact with the rubber gasket in this region. To study the axial behavior of the joint only compressive and tensile loads acting on the joint region and the contact forces from the rubber gasket are considered.

#### B. MATERIAL PROPERTIES

In the case of the reinforced concrete material, the concept of an equivalent section is used to take into account the presence of the steel rebars. A transformed section is obtained by replacing the steel area by the ratio of the modulus of elasticity of steel to that of concrete (Bouabid, 1993). The reinforced concrete material is simplified in the

finite element analyses by using elastic material, because the compressive stresses in these typical small-diameters pipes are calculated and shown to be relatively low (5 MPa under the ultimate compressive load) so that no significant cracking effects are anticipated. Thus, it is assumed that the pipe material behaviour can be simplified to be linear and most of the expected non-linear behaviour will be concentrated in the joint behaviour. The elastic behaviour of the concrete material is defined through the ELASTIC option used in ABAQUS. The modulus of elasticity and Poisson's ratio for concrete; are assumed to be 28000 MPa and 0.2 respectively, based on the experimental data of Bouabid (1993). Based on the result of a test on rubber gasket carried out and reported by Singhal (1984b), it was found that the engineering stress-strain relationship for the rubber gasket is almost linear. However, the true stress-strain relationship of the rubber gasket follows the typical non-linear curve of the rubber material (i.e., visco-elastic). The initial linear part of the equivalent Young's modulus for the main body of the rubber gasket was found to be 2.55 MPa with a Poisson's ratio of 0.50 (a value of 0.49 is used in model simulation to avoid numerical instabilities). Therefore, the gasket rubber material behaviour simplified and assumed to be elastic. Both concrete pipe and rubber gasket material were assumed to be homogeneous and isotropic. The same material properties used by Bouabid (1993) were used for the simulations (see Table 4.1).

## C. 2D CONFIGURATION

Along the longitudinal direction, the contact conditions between the rubber gasket and the spigot and bell of the pipe joint are assumed to be changing. To simplify the solution procedures, the joint region of a segmented pipeline could be assumed as an axisymmetric problem. A bi-linear, four-noded, axisymmetric solid element (denoted as CAX4 in ABAQUS) is used to model the pipe wall and the rubber gasket.

## D. DEFINITION OF GEOMETRIC PARAMETERS

The geometry of the joint system can be characterized by the total length of tested specimen, the gap between the bell and spigot, and the wall thickness of the concrete

pipe. These parameters are defined earlier and described in Table 4.1 based on the tests data.

## E. CONTACT INTERACTION

Many engineering problems involve contact between two or more components. In these problems a force normal to the contacting surfaces acts on the two bodies when they touch each other. If there is friction between the surfaces, shear forces may be created that resist the tangential motion (sliding) of the bodies. The general aim of contact simulations is to identify the areas on the surfaces that are in contact and to calculate the contact pressures generated. In a finite element analysis contact conditions are a special class of discontinuous constraint, allowing forces to be transmitted from one part of the model to another. The constraint is discontinuous because it is applied only when the two surfaces are in contact. When the two surfaces separate, no constraint is applied.

There are two methods for modeling contact interactions in ABAQUS namely; using (i) contact surfaces or (ii) contact elements. Most contact problems between rigid and/or deformable bodies (which can undergo either small or finite sliding) are modeled by using surface-based contact. ABAQUS has three classifications of contact surfaces; element-based contact surfaces; node-based surfaces; and analytical rigid surfaces. However, the surface-based contact method in ABAQUS cannot be used for certain classes of problems and the contact elements are used in such cases (e.g., contact interaction between two pipelines or tubes where one pipe lies inside the other). The surface-based type of contact uses a strict master-slave weighting when enforcing contact constrains; the nodes of the slave surface are constrained so as not to penetrate into the master surface. The nodes of the master surface can, in principle, penetrate into the slave surface. Thus, the interface between the pipe and the rubber gasket is simulated using element-based contact surfaces of either full-slip or smooth interaction condition. The surfaces of the contact area for the liner and the host pipe are defined by the SURFACE command and the potential for contact is set up using CONTACT PAIR command.

## F. BOUNDARY CONDITIONS

Due to the symmetry of the problem, only the upper longitudinal half of the pipeline and the joint configuration were modeled (see Figure 4.1). The boundary conditions and sequence of load application described in the testing procedure were carefully modeled. The right end of the model was fixed while the left end was subjected to incremental axial static loading simulating the compression or tension tests.

## G. MESH SENSITIVITY

To find a reasonable mesh size, a parametric study was performed using 6, 8, 10, and 12 layers of elements through the bell's thickness to capture the structural behaviour of the joint throughout its wall thickness. The convergence study shows that the average relative error of the joint displacement for the 6, 8, 10, and 12 layers, calculated as the joint displacement difference between the test and the simulation, was 18.4%, 9.5%, 3.7%, and 1.1%, respectively. Further mesh refinements did not yield any results significantly different from those of the best mesh selected. Consequently, using 10 layers of continuum elements (stacked in the wall thickness direction) was assumed to have a relatively small error. Figure 4.2 shows the finite element mesh used for the joint compression/tension tests simulation model.

## H. SOLUTION PROCEDURES

Static solution will be implemented using the STATIC command. ABAQUS allows the user to step through the loading to be analyzed by dividing the problem into steps. The effect of the previous step is always updated and is included in the response of the new step. Because of the contact conditions, the problem to be solved is non-linear.

## I. MODEL VERIFICATION

The finite element model is validated by using measured data from compression and tension experiments (at zero internal pressure) on rubber gasket joints of reinforced

concrete cylinder pipes. The model performance is illustrated by comparing the numerical analysis predicted force-displacement curves with the experimental results. Figure 4.3 shows a comparison of the finite element model predictions with the results obtained from static compression tests. From this figure, it is clear that the finite element model was successful in capturing the non-linear behaviour of the joint under compression. The slippage that occurs under small compressive forces is reproduced with good accuracy. It was not necessary to pursue the analysis up to the locking stage of the joint because this phenomenon will appear only at very large forces and displacement that are out of the design domain regions. Figure 4.4 illustrates a comparison between the tension test results and finite element analysis model predictions. The finite element model simulates successfully the non-linear behaviour of the joint under tension. The difference between the experimental and predicted ultimate displacement is 2.2 and 4.5 % for the compression and tension cases, respectively.

The peak force and the ultimate joint displacement are well estimated by the finite element modeling for both compression and tension cases. The experimental data as shown in Figures 4.3 and 4.4 are fluctuated and scattering around the mean value curves of these tests. Nevertheless, the test mean and the numerical simulation curves are significantly close regardless the variation in the test results. Therefore, the numerical model results are in good agreement with the mean values of the experimental measured response. Thus, the simulation indicates that a good agreement is achieved between the force-displacement curves of Bouabid (1993). Thus, this approximation can be considered adequate for practical purposes. After gaining confidence for the developed finite element model, the analysis will be generalized for typical rubber gasket unrestrained joints where experimental results currently are not available.

### 4.2.3 PREDICTION OF AXIAL BEHAVIOURS OF RUBBER GASKET JOINTS

Experimental data studying the structural behaviours of rubber gasket unrestrained joints for concrete pipes and vitrified clay pipes are very limited and sometimes not available. A validated finite element model can be used as an alternative to study the behaviour of

such a system. In this section, the rubber gasket unrestrained joints in three types of pipes are investigated. Reinforced concrete, non-reinforced concrete, and vitrified clay materials are considered. Three typical diameters for each material are investigated to predict the axial behaviours of unrestrained joints. Table 4.2 summarizes the material properties and the dimensions of the rigid pipes to be used for the numerical analysis prediction of the axial behaviours of the joints (see ASTM C443, ASTM C14, ASTM C700).

The previously validated finite element model is used for the parametric study to predict the structural behaviours of the rubber gasket joints for the rigid pipes listed in Table 4.2. The same contact conditions, boundary conditions, and loading conditions used for the validation will be assumed in the parametric study.

Figures 4.5a, b, and c show the predicted force-displacement relationships obtained by the finite element models for the rubber gasket joints of reinforced concrete pipes, non-reinforced concrete pipes, and vitrified clay pipes, respectively. The simulated global behaviour is similar to the results reported by the Bouabid (1993) compression tests. The slippage starts with small values at low levels of loadings and increases as loadings increase. When the bell-spigot of a segmented pipe becomes in contact, no axial displacement will occur (see Figure 4.3). However, the focus for this study to investigate the stiffness of the joint just before contact can take place. The ultimate axial compression displacements are approximately 5.92 mm, 5.68 mm, and 6.42 mm for the reinforced concrete, non-reinforced, and vitrified clay joints, respectively.

Table 4.3 shows that all the predicted compression capacities of the unrestrained joints for the three types of rigid pipes are less than the maximum allowable displacements for laying purposes as specified by: (1) the ASTM C443 for reinforced concrete pipe, which specifies a maximum displacement of 12 mm difference across opposite sides of the pipe at the rubber gasket joint, and (2) the ASTM C425 standard for vitrified clay pipe, which specifies a range of maximum displacement of 42 mm per meter of the pipe length at the rubber gasket joint for diameters of 76 mm to 300 mm.

On the other hand, Table 4.4 summarizes the predicted axial stiffnesses of the unrestrained joints for the three types of rigid pipes. As shown in Table 4.4, the ultimate displacement and the axial stiffness of the joint in reinforced concrete pipe are significantly larger than those of other rigid pipe types due to its larger wall thickness. Additionally, the results show that the ultimate displacement and the axial stiffness of the joint in vitrified clay pipe are slightly larger than that of other rigid pipe types due to its smaller groove for its rubber gasket, concrete reinforcement, and its larger wall thickness. Finally, the results show that the ultimate displacement and the axial stiffness of the joint in vitrified clay pipe are slightly larger than those for the non-reinforced concrete pipe. This finding is due to the fact that the small sizes of the vitrified clay pipes have larger wall thickness than the non-reinforced concrete pipes and the axial stiffness of the joint increases by increasing the wall thickness (see Table 4.2). For the pipe sizes under study, this behaviour is consistent with the requirements of the ASTM C700 where the minimum strength of the vitrified clay pipes (Class 160) exceeds the ASTM C14 requirement for minimum strength of the non-reinforced concrete pipes (Class II). It was found that both the axial stiffness and the maximum axial compression load of the joint increase slightly with the pipe diameter.

For modeling purposes, it is proposed to simplify the joint behaviour by adopting a bi-linear constitutive law. The experimental as well as the simulation results indicate that joint behaviour has two clear stages: the first stage comprises very small slippage and is dominated by elastic response, whereas the second stage is characterized by higher values of slippage and lower overall system stiffness. The static axial behaviour of the unrestrained gasket joint will be modeled as a bi-linear spring with two stiffnesses characterizing by two global regimes and referred to as elastic and post-elastic stiffness. Both the elastic and the post-elastic axial stiffness are calculated directly from the numerical simulations by determining the slopes of the corresponding elastic and post-elastic responses.

## 4.3 BENDING BEHAVIOURS OF RUBBER GASKET UNRESTRAINED JOINTS

The work of Singhal and Benavides (1983) as well as that of Singhal (1984a, b) are used as references to validate the finite element model. Once the simulation tool is validated, it will be used for a parametric study to investigate the behaviours of a combination of three pipe materials with three diameters. A bi-linear rotational spring is proposed as a simplified constitutive law for gasket unrestrained joints in bending.

### 4.3.1 EXPERIMENTAL OBSERVATIONS

Singhal (1983, 1984a, b) tested rubber gasket joints of ductile iron pipes with various diameters (100 mm, 150 mm, 200 mm, and 250 mm). The primary purpose of the present tests is to determine the structural behaviours, including joint stiffness in bending, of rubber gasket joints in ductile iron pipe. Two segments of ductile iron pipe with lengths of 2546 mm (100.25 in) and 1844 mm (72.6 in) were hung horizontally from wire ropes and simply supported at the ends. Pure bending moment at the joint was imposed by loading the pipe at two points in the joint region using a hydraulic jack.

The load was applied until the joint had rotated to a maximum of 4° to avoid metal-on-metal contact. Singhal reported that during bending tests, a joint rotation exceeding 4° caused metal-on-metal contact leading to very high stresses at the joint. This phenomenon increased significantly the probability of joint failure. The most important conclusion of these tests is that the bending behaviour of the joint is highly dependent on the clearances set up during the design geometry of the joint. A schematic layout of the experimental setup for the bending tests is shown in Figure 4.6.

### 4.3.2 NUMERICAL MODELING OF BENDING BEHAVIOURS OF RUBBER GASKET JOINTS

The purpose of this section is to develop a finite element model for the analysis of bending behavior of rubber gasket joints subjected to bending. Assumptions used in

setting up the finite element models of the rotational behavior of the unstrained rubber gasket joint are addressed in this section.

The same strategy followed previously in section 4.2.2 will be used to develop a structural model for the bending behaviours of rubber gasket unrestrained joints. The bending tests of rubber gasket joints for ductile iron pipes carried out by Singhal (1984a, b) were used as a baseline to verify the finite element model for predicting the moment-rotation response of the joints.

## A. LOADING CONDITION

To study the rotational behavior of the joint only bending loads acting on the joint region and the contact forces from the rubber gasket are considered.

## B. MATERIAL PROPERTIES

Both ductile iron pipe and rubber gasket material were assumed to be homogeneous and isotropic. The rubber gasket will be assumed to have elastic behaviour with the same properties used for simulating the axial behaviour of the joint (see section 4.2.2). The ductile iron pipe material was assumed to have elasto-plastic behaviour. The material parameters reported by Singhal (1984a, b) were used in the simulations (see Table 4.1). However, some of the required data for ductile iron were taken from other typical data (Meis, 2003), because they were not available for the pipes used in Singhal's experiments (e.g., yield stress of 310 MPa, ultimate stress of 492 MPa, and plastic strain at failure of 0.177).

## C. 2D CONFIGURATION

The finite element models consisted of generalized axisymmetric elements (denoted as CAX4I) for the pipe. These elements include incompatible modes that improve the bending response. The primary effect of these modes is to eliminate the parasitic shear

stresses that cause the response of the regular first-order displacement elements to be too stiff in bending. In addition, these modes eliminate the artificial stiffening that occurs due to Poisson's effect in bending, which is manifested in regular displacement elements by a linear variation of the stress perpendicular to the bending direction (Hibbitt *et al.*, 2005).

## D. DEFINITION OF GEOMETRIC PARAMETERS

The geometry of the joint system can be characterized by the total length of tested specimen, the gap between the bell and spigot, and the wall thickness of the cast iron pipe. These parameters are defined earlier and described in Table 4.1 based on the tests data.

## E. CONTACT INTERACTION

As for the axial case, the problem to be solved was non-linear due to the contact conditions. The interface between the pipe and the rubber gasket was simulated using element-based contact surfaces with either full-slip or smooth interaction condition (see section 4.2.2).

## F. BOUNDARY CONDITIONS

Both ends of the model were fixed while the joint was subjected to incremental vertical static load.

## G. MESH SENSITIVITY

To find a reasonable mesh size, a parametric study was performed using 3, 4, 5, and 6 layers of elements through the bell's thickness to capture the flexural behaviour of the joint throughout its wall thickness. The convergence study showed that the average relative error of the joint displacement for the 3, 4, 5, and 6 layers is 16.2%, 7.7%, 2.4% and 0.9%, respectively. Further mesh refinements did not yield any significantly different results. Consequently, using 5 layers of axisymmetric elements (stacked in the wall

thickness direction) is assumed to provide a sufficient accuracy and a reasonable computation time. Figure 4.7 shows the finite element mesh used for the joint bending tests simulation model.

## H. SOLUTION PROCEDURE

Static solution will be implemented using the STATIC command. ABAQUS allows the user to step through the bending loading to be analyzed by dividing the problem into steps. The effect of the previous step is always updated and is included in the response of the new step. Because of the contact conditions, the problem to be solved is non-linear.

## I. MODEL VERIFICATION

Figures 4.8a, b, and c compare the finite element model predictions with the results obtained from static bending tests for three different pipe sizes of 150 mm, 200 mm, and 250 mm. After a rotation of approximately 4°, the bell and spigot come into metal-on-metal contact and the behaviour of the joint becomes independent of the properties of the rubber gasket. As the bell and spigot come into metal-on-metal contact, the joint will fail as a small increment in the rotation of the joint causes a large increase in the bending moment transmitted to the joint.

Several bending tests on pipe joints performed by Singhal (1984a, b) resulted in various curves representing the moment-rotation relationships of the repeated tests for each pipe size. The finite element model results for the bending moment-rotation relationships were between the lower and upper bounds of these test curves. Furthermore, these results indicate that the developed finite element model has enough precision for estimation of the mean peak moment and rotation for rubber gasket unrestrained joints (see Figure 4.8). Thus, the present numerical study results are in good correlation with the range of the experimental results within an ultimate joint rotation error of 3.1% to 4.9%, which is considered adequate for practical purposes. After gaining confidence of the developed finite element model for bending tests for ductile iron joints, the analysis will be

generalized for typical unrestrained pipe rubber gasket joints where experimental results were not available.

### 4.3.3 PREDICTION OF BENDING BEHAVIOURS OF RUBBER GASKET JOINTS

To the best knowledge of the author, no experimental tests are available for the bending behaviours of rubber gasket unrestrained joints for small-diameter rigid pipes (such as vitrified clay, non-reinforced concrete, and reinforced concrete). Thus, a finite element model is used to predict the bending behaviours of these common types of rigid pipe with unrestrained joints. The validated finite element model used for the simulation of the available bending tests is employed to predict the structural behaviours of the rubber gasket unrestrained joints for the rigid pipes. The characteristics of the systems analyzed are summarized in Table 4.2. The contact conditions, boundary conditions, and loading conditions reported by Singhal (1984a, b) are maintained in the analyses.

Figures 4.9a, b, and c show the results of the bending moment and the rotation obtained for rubber gasket joints of reinforced concrete pipes, non-reinforced concrete pipes, and vitrified clay pipes. The ultimate joint rotations occur at relative rotations of approximately 5.5° (0.096 rad), 2.5° (0.044 rad), and 2.0° (0.035 rad) for reinforced concrete, non-reinforced concrete, and vitrified clay joints, respectively.

Observing the global structural behaviours of gasket unrestrained joints in bending, one can distinguish two stages: in the first stage the response is clearly linear, whereas in the second stage the rotational stiffness is reduced but the response remains very close to linear. Therefore, it is legitimate to approximate the bending behaviours of gasket joints by a bi-linear rotational spring element where each of the two stages is characterized by a rotational stiffness. Table 4.5 shows the predicted bending capacities of the unrestrained joints for three types of rigid pipes. As expected, the ultimate rotation and the rotational stiffness of the joint in reinforced concrete pipe are significantly larger than that of other rigid pipes due to its larger wall thickness. Further, the numerical modeling results show

that the ultimate rotation and the rotational stiffness of the joint in non-reinforced concrete pipe are slightly larger than those for the vitrified clay pipe. It is also found that both the rotational stiffness and the maximum bending moment of the joint increase with the diameter of the pipe. This finding is due to the fact that the stiffness of the joint increases with increasing wall thickness. Standards usually permit slight curvatures for installation purposes; e.g., the ASTM C12 standard normally permits maximum angular deflection per joint of 2.4° for installing clay pipelines of 75 mm to 300 mm nominal diameter, while the ASTM C505 standard normally permits maximum angular deflection per joint of 3.5° for installing concrete pipelines of 150 mm to 600 mm nominal diameter. However, typical manufacturer's recommended allowable curvatures for various pipe joints as reported by O'Rourke and Liu (1999).

Table 4.6 summarizes the predicted bending stiffnesses of the rigid pipes with unrestrained joints for reinforced concrete, non-reinforced concrete, and vitrified clay pipes with diameters of 200 mm, 250 mm, and 300 mm. The static bending behaviour of the unrestrained gasket joint will be modeled as a bi-linear spring with two stiffness parameters characterizing the two global regimes and referred to as elastic and post-elastic stiffness, respectively. Both the elastic and the post-elastic rotational stiffness are calculated directly by determining the slope of the corresponding structural response.

## 4.4 SUMMARY AND CONCLUSIONS

This chapter describes the numerical modeling of the axial compression and bending behaviours of segmented pipe joints using the finite element method. The results of published full-scale tests by others (Bouabid, 1993 and Singhal, 1984a, b) of unrestrained joints for typical rigid pipes were used to validate and calibrate the finite element models. This chapter presents the finite element models setup, the results of the numerical models, and the calibration process for these experimental tests. The close agreement between the numerical and experimental results show that the modeling procedures result in simulated joint displacements or rotations that are remarkably consistent with the experimental measurements. The finite element models were extended and used to

predict the axial and rotational stiffnesses of rubber gasket joints for typical rigid pipes. The non-linear behaviour of the joint material was modeled using a bi-linear constitutive law. It was found that the axial/rotational stiffness and the maximum compression load/bending moment is an increasing function of the pipe diameter.

The literature review and the results of the study of the axial and rotational behaviours of typical rigid pipes with unrestrained joints led to the following conclusions:

1. Despite the simplicity of the finite element models used in this work, their performance can be considered adequate for practical design. The proposed models have been validated using available experimental data. Both the axial and rotational capacities of the joint as they influence the overall behaviour the pipeline system are taken into account.

2. Parametric study shows that the axial/rotational stiffness and the ultimate load/bending moment are an increasing function of the pipe diameter as well as of the pipe wall thickness.

3. Due to the lack of acceptable guidelines for the dimensions, tolerances, properties, and capacities of unrestrained rubber gasketed joints, presently, the design of such joints is left up to the pipe manufacturers. Thus, there is an urgent need for research to address the longitudinal discontinuity at unrestrained gasket rubber joints. The methodology presented in this work is the first step toward understanding the structural behaviour of segmented pipelines.

Table 4.1 Experimental Joint Tests Data for Bouabid (1993) and Singhal (1984)

| Test Data | Bouabid (1993) | Singhal (1984a, b) |
|---|---|---|
| Pipe Material | Reinforced Concrete | Ductile Iron |
| Modulus of Elasticity of Pipe Material (E), (MPa) | 28000 | 179000 |
| Poisson's Ratio of Pipe Material | 0.20 | 0.30 |
| Yield Stress, (MPa) | - | 310 |
| Plastic Strain at Failure | - | 0.177 |
| Pipe Outer Diameter ($D_o$), (mm) | 850 | 100-250 |
| Pipe Wall Thickness (t), (mm) | 100 | 12-15 |
| Joint Type | Rubber Gasket | Rubber Gasket |
| Modulus of Elasticity of Gasket Material (E), (MPa) | 2.55 | 2.55 |
| Poisson's Ratio of Rubber Gasket Material | 0.50* | 0.50* |
| Nominal Thickness of Gap between Bell & Spigot, (mm) | 6.35 | 6.35 |
| Total Length of Test Specimen, (mm) | 2743 | 4390 |

* A value of 0.49 is used in model simulations to avoid numerical instabilities

Table 4.2 Properties and Dimensions of Rigid Pipes Used in Numerical Modeling

| Pipe Type | Modulus of Elasticity E (MPa) | Possion's Ratio ν | Inner Diameter (mm) | Wall Thickness (mm) |
|---|---|---|---|---|
| Reinforced Concrete (Wall B) | 28000 | 0.20 | 200 | 51 |
| | | | 250 | 51 |
| | | | 300 | 51 |
| Non-Reinforced Concrete (Class II) | 28000 | 0.20 | 200 | 22 |
| | | | 250 | 25 |
| | | | 300 | 35 |
| Vitrified Clay (Class 160) | 40000 | 0.22 | 200 | 25 |
| | | | 250 | 26 |
| | | | 300 | 28 |

Table 4.3 Ultimate Displacement/ Force of Unrestrained Joints for Rigid Pipes Predicted from FE Models for Compression Tests

| Pipe Material | Ultimate Joint Displacement (mm) | | | Ultimate Compressive Force (N) | | |
|---|---|---|---|---|---|---|
| | 200 mm | 250 mm | 300 mm | 200 mm | 250 mm | 300 mm |
| Reinforced Concrete (Wall B) | 5.916 | 6.148 | 6.237 | 20123 | 21834 | 22950 |
| Non-Reinforced Concrete (Class II) | 4.618 | 5.034 | 5.679 | 5671 | 6695 | 8051 |
| Vitrified Clay (Class 160) | 6.106 | 6.337 | 6.416 | 6695 | 7629 | 8429 |

Table 4.4 Axial Stiffness of Unrestrained Joints for Rigid Pipes Predicted from FE Models of Compression Tests

| Pipe Material | Joint Elastic Stiffness (N/mm) | | | Joint Post-Elastic Stiffness (N/mm) | | |
|---|---|---|---|---|---|---|
| | 200 mm | 250 mm | 300 mm | 200 mm | 250 mm | 300 mm |
| Reinforced Concrete (Wall B) | 12461 | 12807 | 13455 | 2484 | 2567 | 2615 |
| Non-Reinforced Concrete (Class II) | 5156 | 5678 | 6313 | 751 | 832 | 840 |
| Vitrified Clay (Class 160) | 5607 | 5679 | 5775 | 846 | 909 | 977 |

Table 4.5 Ultimate Rotation/Bending Moment of Unrestrained Joints for Rigid Pipes Predicted from FE Models for Bending Tests

| Pipe Material | Ultimate Joint Rotation Radian (degree) | | | Ultimate Joint Bending Moment (N-mm) | | |
|---|---|---|---|---|---|---|
| | 200 mm | 250 mm | 300 mm | 200 mm | 250 mm | 300 mm |
| Reinforced Concrete (Wall B) | 0.096 (5.5°) | 0.096 (5.5°) | 0.096 (5.5°) | 169766 | 205463 | 243184 |
| Non-Reinforced Concrete (Class II) | 0.044 (2.5°) | 0.044 (2.5°) | 0.044 (2.5°) | 31364 | 38104 | 45092 |
| Vitrified Clay (Class 160) | 0.035 (2.0°) | 0.035 (2.0°) | 0.035 (2.0°) | 31285 | 32958 | 39047 |

Table 4.6 Rotational Stiffness of Unrestrained Joints for Rigid Pipes Predicted from FE Models of Bending Tests

| Pipe Material | Joint Elastic Stiffness (N-mm/deg) | | | Joint Post-Elastic Stiffness (N-mm/deg) | | |
|---|---|---|---|---|---|---|
| | 200 mm | 250 mm | 300 mm | 200 mm | 250 mm | 300 mm |
| Reinforced Concrete (Wall B) | 141420 | 146788 | 164333 | 5544 | 7884 | 9615 |
| Non-Reinforced Concrete (Class II) | 40650 | 42565 | 46132 | 3960 | 5642 | 6893 |
| Vitrified Clay (Class 160) | 65644 | 67904 | 78185 | 2147 | 2599 | 4858 |

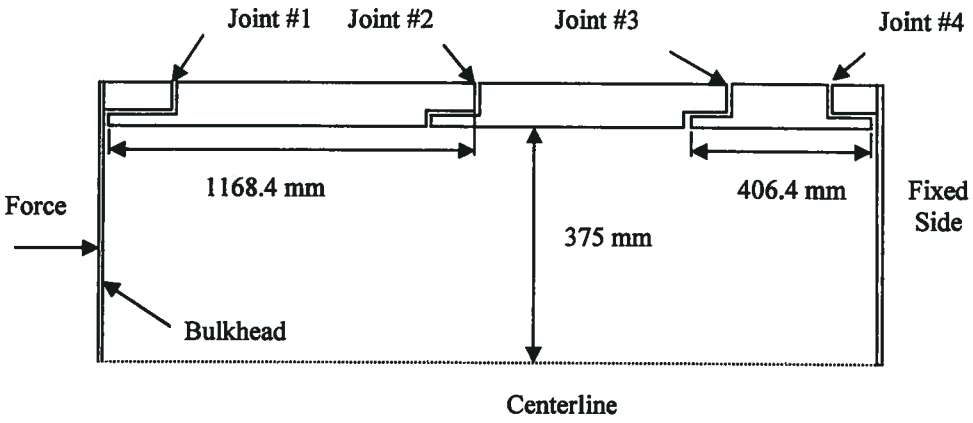


Figure 4.1 Cross-Section View of Compression/Tension Tests Setup
(After Bouabid, 1993)

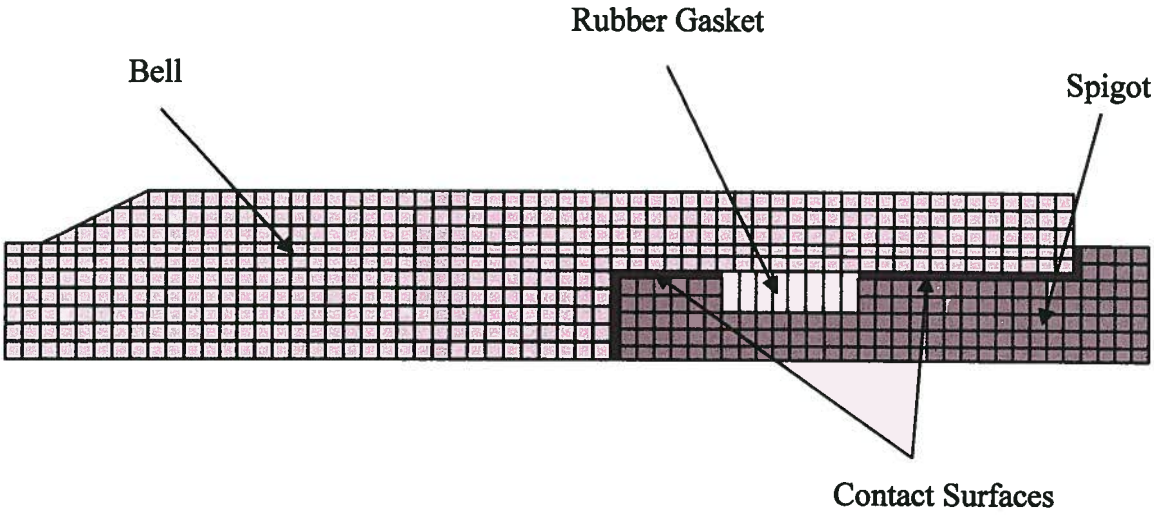


Figure 4.2 Finite Element Mesh Used for the Joint Compression/Tension Tests Models

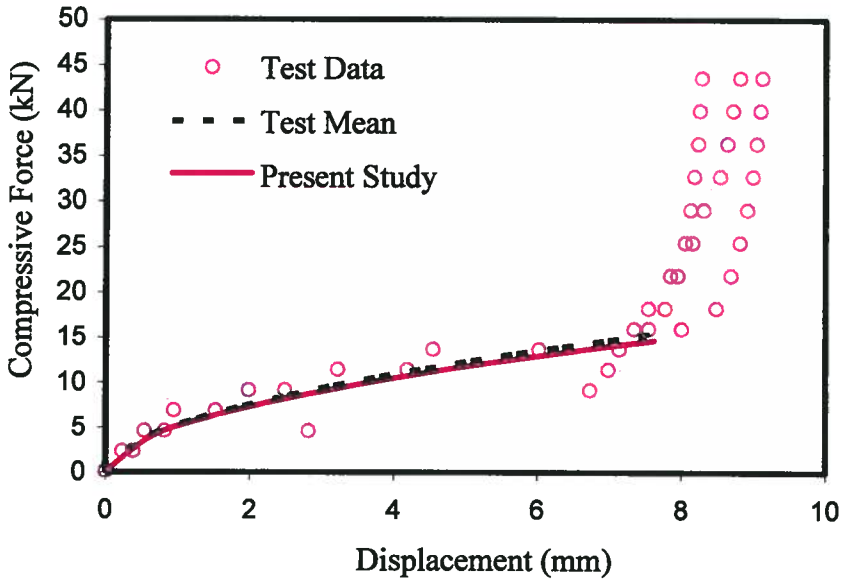


Figure 4.3 Comparison between Finite Element Model Predictions and Compression Tests Measurements (Bouabid, 1993)

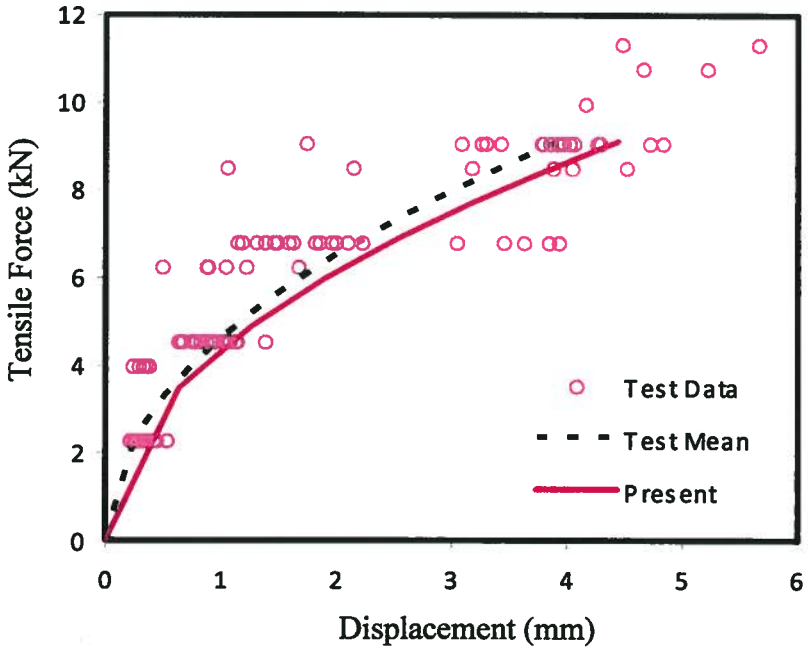


Figure 4.4 Comparison between Finite Element Model Predictions and Tension Tests Measurements (Bouabid, 1993)

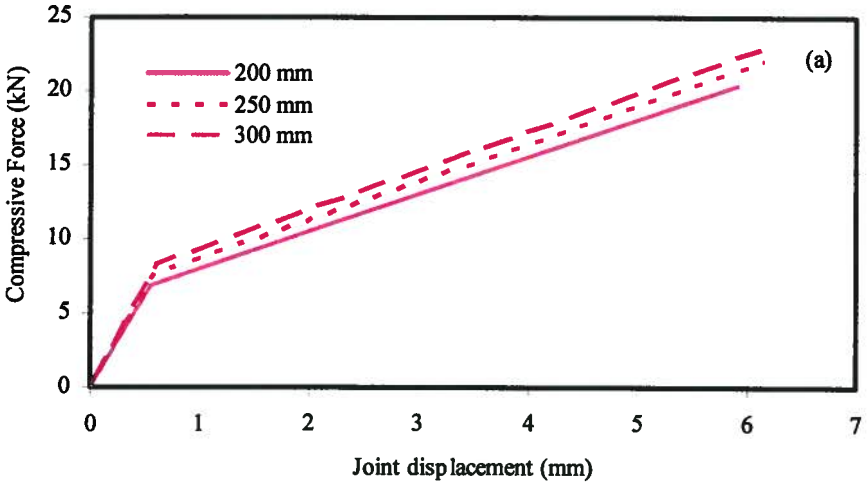


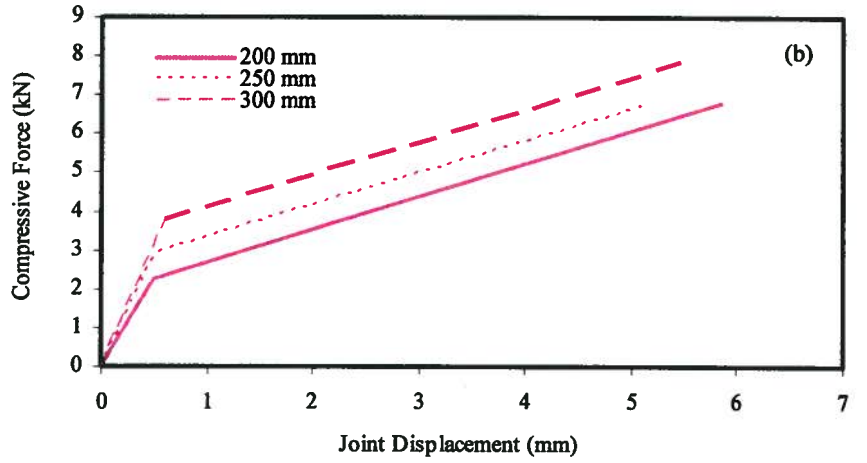


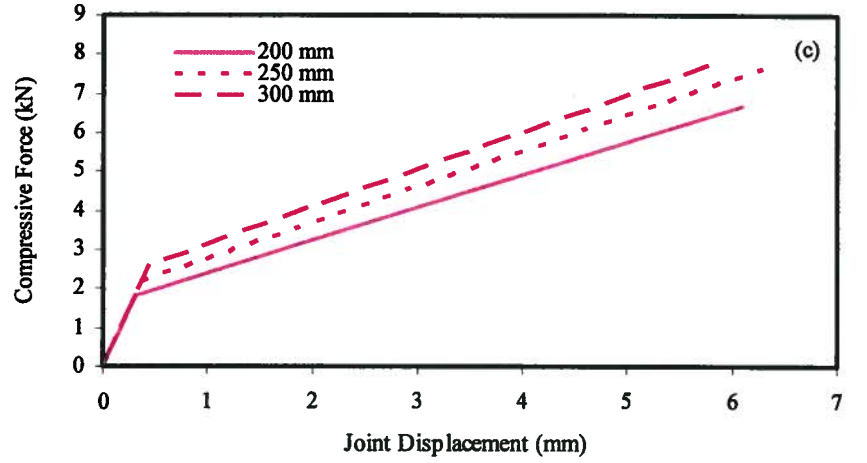


Figure 4.5 Axial Behaviour of Rubber Gasket Unrestrained Joint (Compression Tests Modeling Prediction), (a) Reinforced Concrete (b) Non-Reinforced Concrete, and (c) Vitrified Clay Pipe

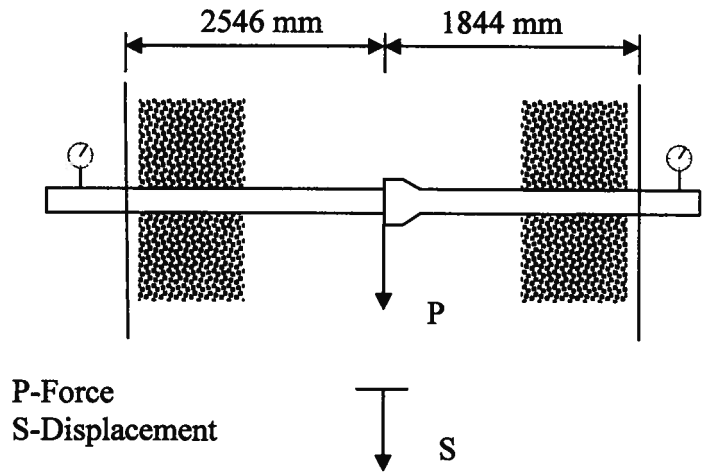


Figure 4.6 Bending Tests Layout (After Singhal, 1984a, b)

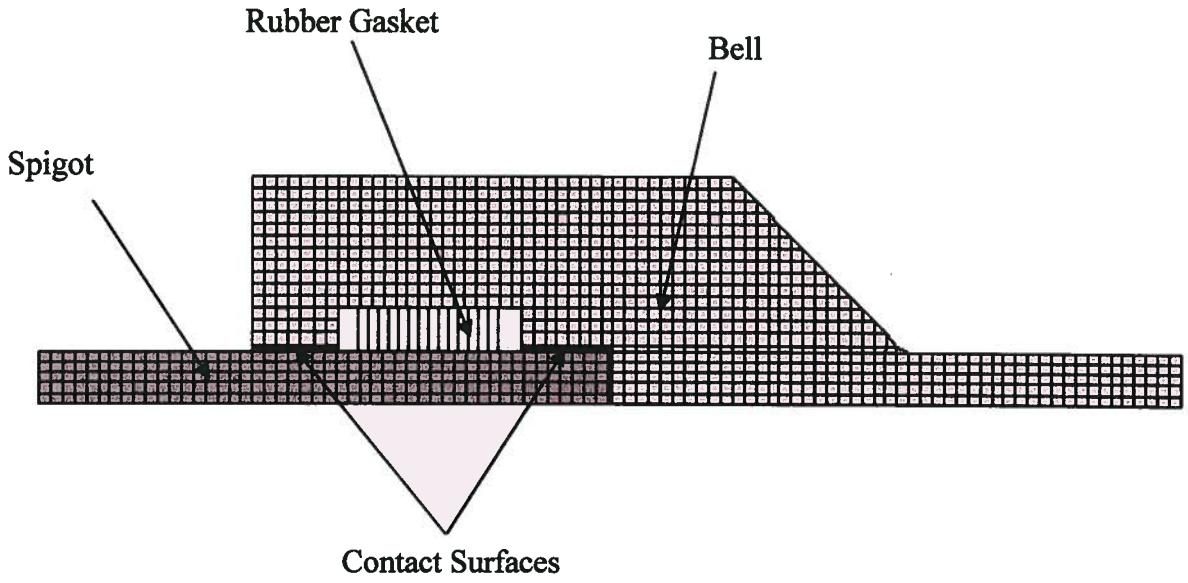


Figure 4.7 Finite Element Mesh Used for Joint Bending Tests Models

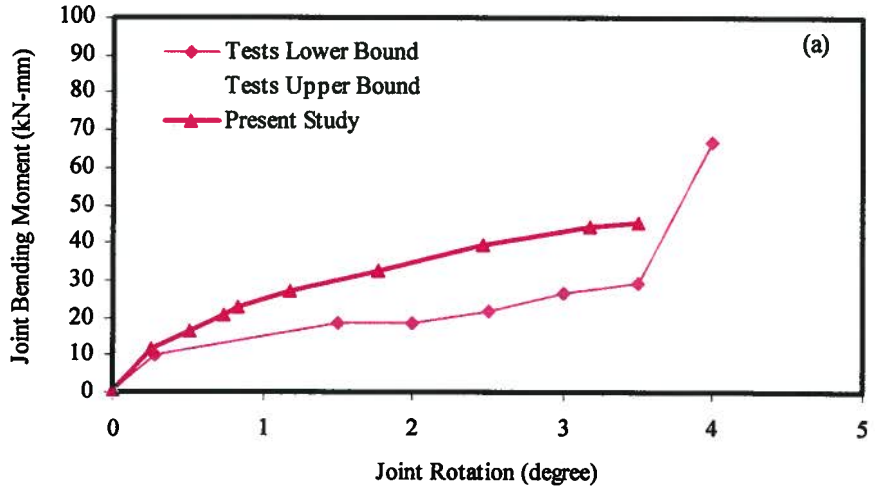


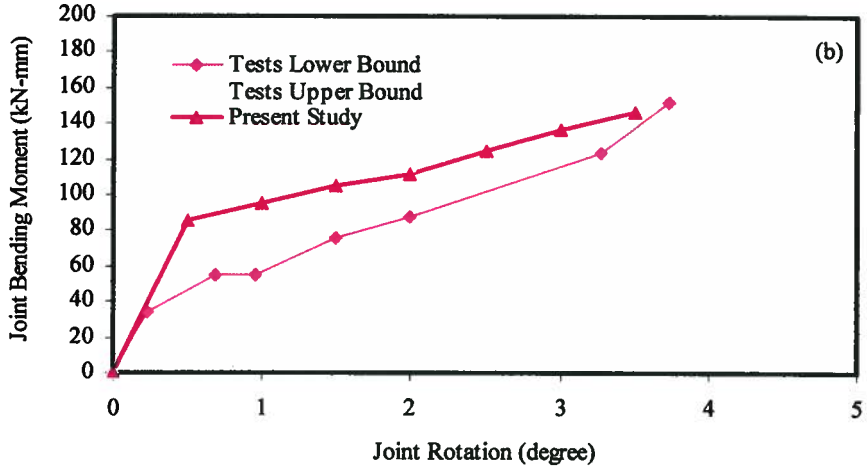


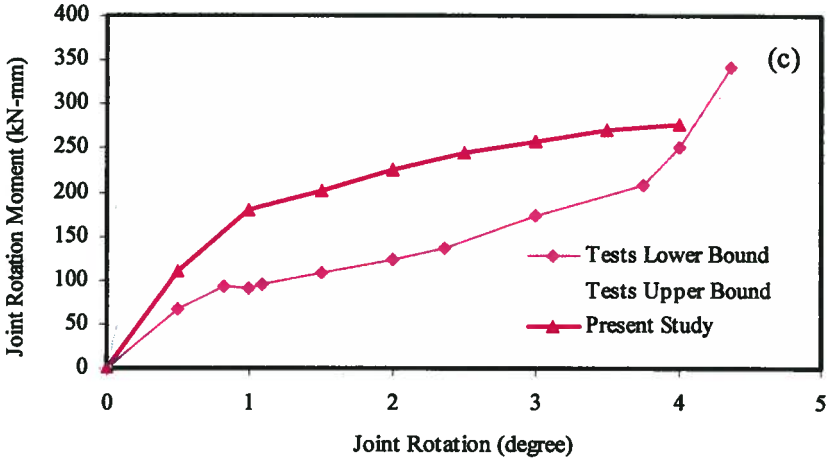


Figure 4.8 Comparison between Finite Element Model Predictions and Bending Tests Results for Ductile Iron Pipe (Singhal, 1984a, b), (a) 150 mm, (b) 200 mm, and (c) 250 mm

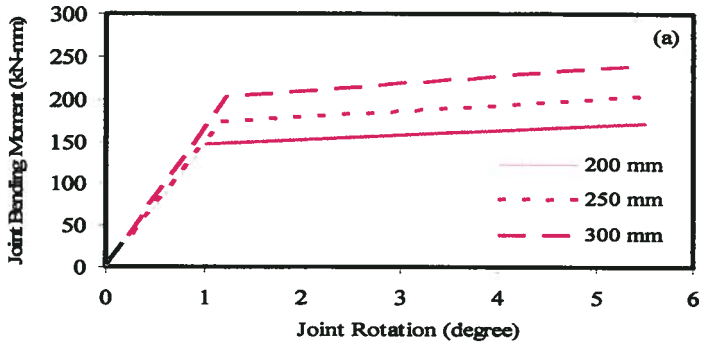


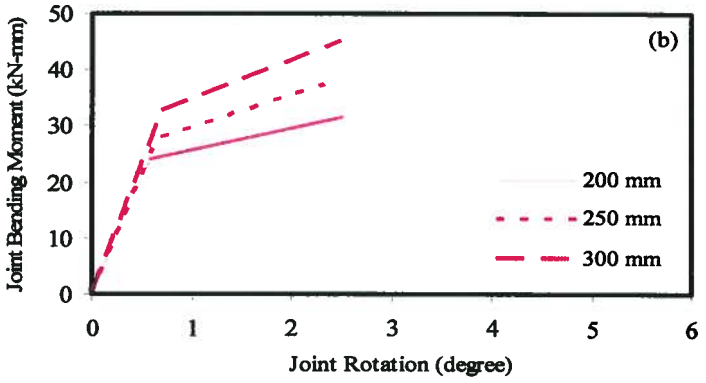


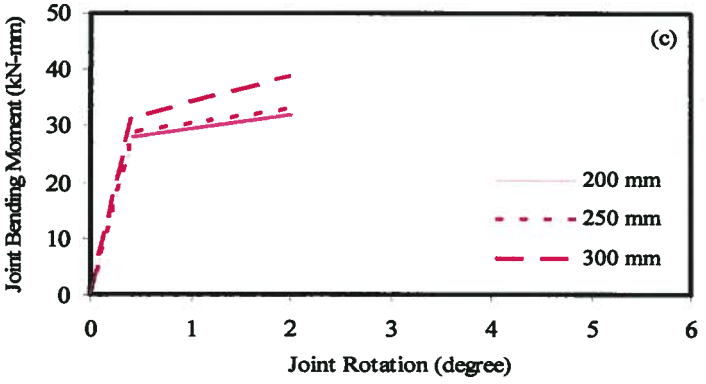


Figure 4.9 Bending Behaviour for Rubber Gasket Unrestrained Joint

(Bending Tests Modeling Prediction)

(a) Reinforced Concrete, (b) Non-Reinforced Concrete, and (c) Vitrified Clay Pipe

# CHAPTER 5

# SEISMIC ANALYSIS OF SEGMENTED PIPELINE SUBJECTED TO LONGITUDINAL AND TRANSVERSE PGD

## 5.1 INTRODUCTION

Pipelines generally transverse large areas and may cross-areas of seismic hazard. Observations from seismic events of segmented pipelines indicate that failure is most often related to distress at the pipe joints (Selventhiran, 2002). Furthermore, O'Rourke and Liu (1999) reported that more than 80% of the breaks in cast iron pipes with small diameters are associated with joints. Axial pull-out, sometimes in combination with relative angular rotation at joints, is a common failure mechanism in areas of tensile ground strain since the shear strength of the joint caulking materials is much less than the tensile strength in the pipe. In areas of compressive ground strain, crushing of bell and spigot joints is a fairly common failure mechanism in, for example, concrete pipes (O'Rourke and Liu, 1999). Moreover, when surface loading is conveyed to defected segmented rigid pipes, some displacement and rotation will occur at the joint and at the cracks.

As mentioned earlier in chapter 2, PGD comprises two components, namely longitudinal PGD and transverse PGD. Similar to the response of continuous pipelines, the behaviour of a given buried segmented pipeline is a function of the type of PGD (e.g., longitudinal or transverse), the amount of ground movement $\delta$, the width of the PGD zone W, and the pattern of ground movement within the zone (O'Rourke and Liu, 1999). In reference to the type of PGD, Suzuki (1988) concluded that, based on the observed damage to segmented gas pipelines during the 1964 Niigata earthquake, damage due to longitudinal PGD was more common than damage due to transverse PGD. In theses cases, the joints were pulled out in the tension regions and buckled in the compression regions. As with continuous pipelines, longitudinal PGD induces axial effects in segmented pipeline,

specifically axial strains in the pipe segments and relative axial displacements at the joints. However, in contrast to the response of continuous pipelines, damage to segmented pipelines subject to longitudinal PGD typically occurs at pipe joints since the strength of the joints is generally less then the strength of the pipe itself. Whether the joints fail depends on the strength and deformation capacity of the joints as well as on the characteristics of the PGD. One particularly important characteristic is the pattern of longitudinal PGD (O'Rourke and Liu, 1999).

Under transverse PGD, a continuous pipeline will stretch and bend as it attempts to accommodate the transverse ground movement. The failure mode for the pipe depends then upon the relative amounts of axial tension (stretching due to arc-length effects) and flexural (bending) strain. That is, if the axial tension strain is low, the pipe wall may buckle in compression due to excessive bending. On the other hand, if the axial tension strain is significant, the pipe may rupture in tension due to the combined effects of axial tension and flexure (Selventhiran, 2002). Further, it is usually recognized that unrestrained joints permit pipe systems to absorb some transient displacements and permanent ground deformation where the pipe sections act as rigid bodies and all movement occurs at the joints (Rucker and Dowding, 2000).

Seismic hazards that could affect buried pipelines are generally described in chapter 2. This chapter explores the seismic analyses of buried segmented pipes subjected to longitudinal and transverse PGD using the finite element method. A parametric study to investigate the effects of the important parameters on the maximum pipe strains for both longitudinal and transverse PGD effects is presented in the following section. A failure analysis of the segmented pipeline under study is carried out in order to predict accurately the potential of the pipeline joints for damage and failure under the seismic influence for both longitudinal and transverse PGD.

## 5.2 NUMERICAL MODELING OF SEGMENTED PIPELINE SUBJECTED TO LONGITUDINAL PGD

Before investigating the response of segmented pipeline subjected to longitudinal PGD, it is imperative to understand the response of continuous pipeline subjected to longitudinal PGD because analytical and numerical solutions exist. Thus, the developed numerical model in this chapter is first verified with published analytical and/or numerical model results of continuous pipeline then is used to predict the seismic behaviours of buried segmented pipelines.

The main objective of the model verification is to predict reality of results estimated with analytical solution or investigated in published research using finite element method. This numerical model simulation is performed via three steps. The following sections will present the procedures for model verification.

### 5.2.1 ANALYTICAL SOLUTIONS FOR CONTINUOUS BURIED PIPELINE SUBJECTED TO LONGITUDINAL PGD

Two separate analytical models of buried pipe response to longitudinal PGD must first be distinguished. In the first model, the pipeline is assumed to be linear elastic. This model is often appropriate for segmented buried pipe with slip joints since slip joints typically fail at load levels for which the rest of the pipe is linear elastic. In the second model, the pipeline is assumed to follow a Ramberg-Osgood-type stress-strain relation. This inelastic model is often appropriate for continuous buried pipe with arc-welded butt joints, since the local buckling or tensile rupture failure modes typically occur when the pipe is beyond the linear elastic range. Because the current study deals with segmented pipelines, the latter model is not included in this study.

For the purpose of analysis of the elastic model, O'Rourke and Nordberg (1992) have idealized five patterns as shown in Figure 2.7. Assuming elastic pipe material and using soil-pipe interface with elasto-plastic or rigid-plastic properties for the force-deformation

relations at the soil-pipe interface, O'Rourke and Nordberg (1992) analyzed the responses of buried continuous pipeline to three idealized patterns of longitudinal PGD (i.e., ramp, block, and symmetric ridge). They reported that the block pattern resulted in the largest seismic pipe strain, $\varepsilon_s$, in an elastic pipe. Thus, the block pattern appears to be the most appropriate model for elastic pipes.

For block pattern of PGD, the seismic pipe axial strain, $\varepsilon_p$, in an elastic pipe is then given by:

$$\varepsilon_p = \begin{cases} \dfrac{\varepsilon_g W}{2L_{em}} & \text{for } W < 4L_{em} \end{cases} \tag{5.1}$$

$$\varepsilon_p = \begin{cases} \dfrac{\varepsilon_g W}{\sqrt{WL_{em}}} & \text{for } W > 4L_{em} \end{cases} \tag{5.2}$$

where $\varepsilon_g$ is the maximum ground strain and $W$ is the PGD zone width and the length f the PGD zone is normalized by the embedment length $L_{em}$ which is defined as the length over which the constant slippage force, $t_u$ , must act to induce a pipe strain equal to the equivalent ground strain. The embedment length is given in the following form:

$$\mathrm{L_{em}} = \frac{\varepsilon_g EA}{t_u} \tag{5.3}$$

Flores-Berrones and O'Rourke (1992) extended the model for a linear elastic pipe with a rigid-plastic soil spring and found that the analytical solution of an idealized Block pattern given in Equations 5.1 and 5.2 gave a reasonable estimate of pipe response for all the observed cases. Some of the pipeline damage resulting from the 1994 Northridge earthquake provides case histories for comparison with the elastic pipe model. Note that the failure criterion for elastic continuous pipe model is when the seismic pipe strain $\varepsilon_p$ (as estimated from Equations 5.1 and 5.2) exceeds the critical pipe strain $\varepsilon_y$ (i.e, yield strain), where $\varepsilon_y = \sigma_{yield}/E_{pipe}$ (Liu 1996). Figure 5.2 shows the analytical solution

prediction of the maximum pipeline strains estimated by Equations 5.1 and 5.2 for continuous buried pipeline. The analytical solution results show an upper limit to the predicted strains in the pipeline in comparison to the numerical modeling. As indicted in Figure 5.2 the pipeline strains predicted by O'Rourke and Nordberg (1992) analytical solution overestimate the predicted strains for the continuous and the segmented pipeline within 3% to 8%, respectively. Thus, this analytical formula represents the upper bond for the predicted stains in continuous buried pipelines.

### 5.2.2 NUMERICAL MODEL VERIFICATION OF SEGMENTED BURIED PIPELINE SUBJECTED TO LONGITUDINAL PGD

The purpose of this section is to develop a finite element model for the analysis of segmented buried pipelines subjected to axial PGD. The assumptions used in setting up the finite element models are addressed in this section.

Wang (1979) developed a numerical model for buried segmented pipeline as shown in Figure 2.9. In Wang model, the pipeline system is modeled using beam elements for the pipe segments and the joints are modeled as linear springs with axial and bending stiffness. Wang's model captures correctly the trend of decreasing joint opening with increased joint stiffness. This oversimplified model assumes an equivalent linear joint stiffness, while laboratory tests suggest that joint behaviour depends on the imposed displacements.

To build an appropriate and satisfactory model for segmented pipeline subjected to longitudinal PGD, reproduction of continuous pipeline model was selected to be the first step for numerical model verification. Selventhiran (2002) verified the behaviour of 1000-meter-long continuous straight pipe (i.e., no joints) subjected to a block-type PGD in the axial direction using the software ADINA. The finite element analysis results were verified against the existing analytical solution of O'Rourke and Nordberg (1992), given in the previous section. Equations 5.1 and 5.2 give the maximum strain in an elastic

continuous pipe. The analysis was limited to one-dimensional and only the axial direction of the pipe was considered for the analysis.

## A. LOADING CONDITION

To study the seismic behavior of the segmented buried pipeline subjected to longitudinal PGD only axial ground permanent deformation acting on the soil springs will be considered. Longitudinal PGD induces axial strains in the pipe segments and relative axial displacements at the joints since the strength of the joints is generally less than the strength of the pipe itself (O'Rourke and Liu, 1999). In these cases, the joints were pulled-out in the tension region and buckled in the compression zone (Selventhiran, 2002). The soil ends of the springs within the loading PGD zone were displaced by the amount of the peak ground displacement $\delta = 0.2$ m while the PGD zone width is varying from 20 m to 550 m. Selventhiran used a uniform block-type PGD in the axial direction (see Table 5.1).

## B. MATERIAL PROPERTIES

Both ductile iron pipe and soil material were assumed to be homogeneous and isotropic. The ductile iron pipe material was assumed to have elasto-plastic behaviour. The material parameters as reported by Selventhiran (2002) were used in the simulations (see Table 5.1). The modulus of elasticity is assumed to be 200 GPa and Poisson's ratio is assumed to be 0.3. The yield stress of 310 MPa, ultimate stress of 492 MPa, and plastic strain at failure of 0.177 (adopted from Meis, 2003). In the present study, the same approach presented by Wang will be used for the soil springs but the surrounding soil spring behavior will be modeled by equivalent non-linear springs as illustrated in Figure 5.1. The soil type used is the medium-dense sand (see Table 5.2). The soil equivalent spring stiffnesses are calculated according to the TCLEE guideline (ASCE, 1984) for the soil properties given in Table 5.2 and is shown in Table 5.1 (see Appendix B).

## C. 2D CONFIGURATION

A pipeline is a continuous structure consisting of pipe segments and connecting joints. The behaviours of individual components of the pipeline do not offer sufficient data for prediction of the overall pipeline behaviour. The components of the pipeline system, consisting of pipe body, joints, soil springs, etc., have to be integrated appropriately in order to evaluate the seismic response of segmented pipes. For numerical simulation studies of pipeline network systems, the stiffness properties of all pipe segments, including joints and the surrounding soil media, must be known. For very long pipelines, the contact conditions between the pipeline and the surrounding soil are assumed to be unchanging. To simplify the solution procedures, the segmented buried pipeline system could be assumed as a plane-strain problem. The pipeline system is modeled using quadratic, three-noded beam elements for the pipeline segments element (denoted as B22 in ABAQUS).

## D. DEFINITION OF GEOMETRIC PARAMETERS

The geometry of the segmented pipeline system can be characterized by the total length of pipeline, the burial depth, and diameter and the wall thickness of the pipe. These parameters are defined earlier and described in Table 5.1 based on Selventhiran data.

## E. CONTACT INTERACTION

ABAQUS offers two types of elements to simulate the pipe-soil interface behavior between a buried pipeline and the surrounding soil namely; (i) PIPE-SOIL INTERACTION element and (ii) the flexible joint element JOINT C. In this study, the pipe-soil interaction is modeled by using the flexible joint element JOINT C. The soil equivalent spring stiffnesses are used to describe soil springs properties for the buried pipeline system (see Table 5.1).

## F. BOUNDARY CONDITIONS

The pipe ends were free to move. One end of each soil spring was connected to the pipeline and the other end to the surrounding soil. The soil ends of the springs outside the PGD zone were fixed, whereas the soil ends of the springs within the loading PGD zone were displaced by a uniform block-type distribution for the ground displacement $\delta$ where the value of the peak ground displacement 0.2 m as shown in Table 5.1

## G. SOLUTION PROCEDURES

Because of the contact conditions, the problem to be solved is non-linear. Static solution will be implemented using the STATIC command. ABAQUS allows the user to step through the displacement loading to be analyzed by dividing the problem into steps. The effect of the previous step is always updated and is included in the response of the new step.

## H. MODEL VERFICATION

Figure 5.2 shows the continuous pipeline model verification. Comparison of theoretical maximum pipeline strains estimated by Equations 5.1 and 5.2, Selventhiran's ADINA model, and ABAQUS model is shown in Figure 5.2. The analytical and the numerical results of Selventhiran and this study showed very close agreement, which indicates that the modeling procedures are consistent with the expected behaviour within a relative error of maximum pipe strain of an average 3.1%.

The following section will discuss the prediction of seismic behaviours for typical buried rigid pipelines in detail, using these numerical modeling procedures.

## 5.3 PREDICTION OF SEISMIC BEHAVIOUR OF SEGMENTED BURIED PIPELINE SUBJECTED TO LONGITUDINAL PGD

The second step to build an appropriate and satisfactory numerical model for segmented pipeline subjected to longitudinal PGD was performed using the same previous model setup, input data, and assumptions for a 100-meter-long continuous pipeline after dividing this total length into 6-meter segments (typical length of ductile iron pipes). The same input data as those for the previous analysis are used (see Table 5.1). The pipeline ends were fixed (assuming that pipeline ends represent manholes). To simulate continuous pipe, very large axial and bending stiffnesses (i.e., penalty coefficients) of $2\times10^{30}$ N/mm and $2\times10^{30}$ N-mm/deg, respectively, were used at joint locations. These large stiffnesses ensured continuity of the displacement and rotation between the two interfaces of the joint. Figure 5.1 shows the segmented pipeline model. A uniform PGD distribution (i.e., block-type PGD (see Figure 2.7a) in the axial direction was used in this model because it results in the largest strain. The soil ends of the springs within the loading zone (i.e., PGD zone) were displaced by the amount of the peak ground displacement $\delta$. The value of the peak ground displacement $\delta$ was set to be 0.2 m and nine span lengths of the loading PGD zone $W$ varying between 2 m and 90 m were considered. Figure 5.2 also shows a comparison between the maximum strain of 100-meter-long continuous and segmented pipeline. The close agreement between the two numerical results shows that the modeling procedures are consistent with the expected behaviour within a relative error of the maximum pipe strain of average of 2.7% to 7.9%.

The reasonable accuracy of the developed finite element model for segmented buried unrestrained pipelines under seismic effects gives confidence that the analysis can be generalized for predicting the seismic behaviour of typical rigid segmented buried pipelines under seismic effects where experimental results and numerical analysis are not available. The dimensions and material properties dimensions of these pipes are listed in Table 4.2. The results of the numerical modeling of joint behaviours (see Tables 4.3, 4.4, 4.5, and 4.6) discussed in the previous chapter are used directly for the development of the segmented pipeline model.

Figures 5.6 to 5.11 show the maximum pipe strains for segmented reinforced concrete pipe of diameter of 200 mm subjected to longitudinal PGD. From these figures, it is obvious that the maximum pipe strain increases as the magnitude of the burial depth of the pipeline increases. This is due to the fact that the increase in the burial depth will increase the interaction force between the pipeline and the surrounding soil. From the same figure, it is clear that the response of the pipeline increases with the PGD zone width until W = 20 m, then decreases thereafter. These phenomena may be caused by the dominant influence of the axial strain until W = 20 m, which may be considered the limit between the cable behaviour and beam behaviour of the buried pipeline (see section 5.4 for more details about the beam behaviour and the cable behaviour). Furthermore, those results will be discussed in more details in the parametric studies (see section 5.5).

Moreover, the developed finite element model for the axial compression and bending behaviours of segmented pipe joints in chapter four can be used to predict the behaviour of buried segmented pipelines subjected to longitudinal PGD.

## 5.4 NUMERICAL MODELING OF SEGMENTED PIPELINE SUBJECTED TO TRANSVERSE PGD

The purpose of these analyses is to validate the numerical modeling first with the published analytical solution and then with published finite element model results for a continuous pipeline subjected to transverse PGD. This numerical model simulation is carried out through three steps. The following sections will present the assumptions and the procedures for model verification.

### 5.4.1 ANALYTICAL SOLUTIONS FOR CONTINUOUS BURIED PIPELINE SUBJECTED TO TRANSVERSE PGD

#### A. LIU AND O'ROURKE ANALYTICAL MODEL (1997)

One of the important parameters required to evaluate the buried pipeline response to spatially distributed transverse PGD is the pattern of the ground deformation, i.e., the variation of the ground displacement across the PGD width. Many researchers have developed different PGD patterns, e.g., O'Rourke (1988), Suzuki *et al.* (1988), Kobayashi *et al.* (1989), and O'Rourke (1989).

Suzuki *et al.* (1988) and Kobayashi *et al.* (1989) approximate the transverse ground deformation by a cosine function raised to the power n, which can be expressed as:

$$y(x) = \delta.\left(\cos\frac{\pi x}{W}\right)^n \tag{5.4}$$

where $y(x)$ is the transverse soil deformation and $x$ is the distance from the margin of the PGD zone (see Figure 5.3). Figure 5.3 also shows the Suzuki *et al.* and Kobayashi *et al.* model for n = 0.2, 1.0, 2.0, and 5.0.

O'Rourke (1989) assumed the following analytical form for spatially distributed transverse PGD:

$$y(x) = \frac{\delta}{2}\left(1-\cos\frac{2\pi x}{W}\right) \tag{5.5}$$

As shown in Figure 5.3, O'Rourke form gives the same shape as both the Suzuki and Kobayashi *et al.'s* with n = 2.0. This figure also shows that all patterns are similar in that the maximum ground deformation occurs at the center of the PGD zone and the ground

deformation at the margins is zero. The patterns differ in the variation of ground deformation between the center of the PGD zone and the margins.

Liu and O'Rourke (1997), based on the O'Rourke (1989) pattern of ground deformation (i.e., Equation 5.5), developed an analytical solution and finite element model utilizing large deformation theory, non-linear pipe-soil interaction forces (i.e., soil springs), and Ramberg-Osgood stress-strain relations for the pipe material. The X-52 grade steel pipe is modeled as a beam coupled by both axial and lateral soil springs. The bases of the soil springs outside of the PGD zone are fixed, while the bases of the soil springs inside the PGD zone move with the soil. The anchor length of the pipe is long enough (up to 400 m) such that both the flexural and axial pipe strain is essentially zero at the two anchor points. The pipe is assumed to be surrounded by loose to moderately dense sand. The data used for Liu and O'Rourke model verification are listed in Table 5.1. The elasto-plastic (i.e., bi-linear) soil springs modeling and the pipe-soil interaction are based on the TCLEE guideline (ASCE, 1984).

Based on the results of a finite element model, Liu and O'Rourke (1997) developed a simplified analytical approach. They suggested that pipe strain is an increasing function of ground displacement for ground displacement less than a certain value, critical ground deformation $\delta_{cr}$, and that pipe strain does not change appreciably thereafter. For larger values of $\delta$, the maximum tensile strain remains constant. The pipe resistance to transverse PGD is due to a combination of flexural stiffness and axial stiffness. Liu and O'Rourke then developed the following analytical relations for an elastic pipe (Equations 5.6 to 5.11). For small widths of the PGD zone, critical ground deformation $\delta_{cr}$ and pipe behaviour are controlled by bending (i.e., beam-like behaviour). The mechanism is the same as that for the stiff pipe case (i.e., two-end fixed beam with constant distributed load) that is given by the beam theory, the critical ground bending deformation is given by:

$$\delta_{cr-bending} = \frac{P_u W^4}{384EI} \tag{5.6}$$

where $P_u$ is the maximum lateral force per unit length at the pipe-soil interface (see section 2.4.2 in chapter 2), $E$ is the modulus of elasticity of the pipe material, and I is the moment of inertia of the pipe cross-sectional area.

For very large widths of the PGD zone, critical ground deformation and pipe behaviour are controlled primarily by the axial force (i.e., cable-like behaviour). The mechanism is the same as that for the flexible cable case (i.e., negligible flexural stiffness). For parabolic cable, the relation between the axial force, $T$, at the ends and the maximum lateral deformation "or sag", $\delta$ is given by:

$$T = \frac{P_u W^2}{8\delta} \tag{5.7}$$

For $\delta_{cr} = 0.5\delta$ Liu and O'Rourke observe that the pipe strain matches fairly well with the ground deformation over the whole width of the PGD zone. Therefore, they assumed that the sag over the middle region of the PGD zone to be $(0.5\delta)$, the interrelationship between the tensile force, $T$, and the ground displacement, $\delta$, is then given by:

$$T = \pi Dt\sigma = \frac{P_u (W/2)^2}{8(\delta/2)} = \frac{P_u W^2}{16\delta} \tag{5.8}$$

where $\sigma$ is the axial stress in the pipe (assumed to be constant within the PGD zone).

Liu and O'Rourke assume that (i) the inward movement of the pipe occurs at the margin of the PGD zone due to the axial force, (ii) a constant longitudinal friction force $t_u$ (see section 2.4.1 in chapter 2), beyond the margins, then suggest that the pipe inward movement at each margin is given by:

$$\Delta_{inward} = \frac{\pi Dt\sigma^2}{2Et_u} \tag{5.9}$$

The total axial elongation of the pipe within the PGD zone is approximated by the average strain given by Equation 2.30 (i.e., arc-length effect) times the width, $W$. This elongation is due to stretching within the zone ($\sigma W/E$) and inward movement at the margins, then from Equation 5.8:

$$\frac{\pi^2\delta^2}{4W} = \frac{\sigma W}{E} + \frac{2\pi Dt\sigma^2}{2Et_u} \tag{5.10}$$

The critical ground deformation, $\delta_{cr\text{-}axial}$, for "cable-like" behaviour and the corresponding axial pipe stress can be calculated by simultaneous solution of Equations 5.8 and 5.9. For any arbitrary width of the PGD zone, anywhere between small and very large, resistance is provided by both flexural (beam) and axial (cable) effects. Liu and O'Rourke consider these elements acting together in parallel, and they suggest the critical ground deformation could be predicted by:

$$\delta_{cr} = \frac{1}{\frac{1}{\delta_{cr-bending}} + \frac{1}{\delta_{cr-axial}}} \tag{5.11}$$

Thus, the maximum strains in an elastic pipe are due to the combined effects of axial tension (cable behaviour) and flexure (beam behaviour) and can be expressed by:

$$\varepsilon_{elastic} = \left\{ \frac{\sigma}{E} \pm \frac{\pi^2\delta D}{W^2} \right. \qquad \text{for} \qquad \delta \le \delta_{cr} \tag{5.12}$$

$$\varepsilon_{elastic} = \left\{ \frac{\sigma}{E} \pm \frac{\pi^2\delta_{cr} D}{W^2} \right. \qquad \text{for} \qquad \delta \ge \delta_{cr} \tag{5.13}$$

where $A$ is the pipe cross-sectional area.

### 5.4.2 NUMERICAL MODEL VERIFICATION OF CONTINUOUS BURIED PIPELINE SUBJECTED TO TRANSVERSE PGD

To validate the numerical model for buried segmented pipeline subjected to transverse PGD, the work of Liu and O'Rourke's model (1997) is used as a reference. The geometry of the system as well as the material properties for the Liu and O'Rourke model are used as given in Table 5.1.

To build an appropriate and satisfactory numerical model for segmented pipeline subjected to transverse PGD the same previous model for a 1000-meter-long continuous pipeline subjected to longitudinal PGD (Selventhiran, 2002) was used. The model assumptions, material properties, contact interface, boundary conditions, and solution are the same (see section 5.2). However, the soil ends of the springs within the loading PGD zone were displaced by a cosine wave-type distribution for the ground displacement $\delta$ where the value of the peak ground displacement varied from 0.5 m to 3 m as shown in Table 5.1.

Figure 5.3 shows the maximum pipe strain estimated by analytical solution, by the Liu and O'Rourke model, and by the present study model for a continuous pipe versus the ground displacement $\delta$ for three different PGD zone widths of $W$ = 10 m, 30 m, and 50 m, respectively. As shown in Figure 5.3, the behaviours of the two numerical models (the present study and that of Liu and O'Rourke) are in good agreement, although there are some differences in magnitude within approximately 4.9% to 8.7% relative error for the maximum pipe strain predictions.

### 5.4.3 NUMERICAL MODEL VERIFICATION OF SEGMENTED BURIED PIPELINE SUBJECTED TO TRANSVERSE PGD

Proceeding to the next step for validation of the present study, a numerical model was then performed using the same previous model setup (i.e., the Liu and O'Rourke model) but for a 100-meter-long continuous pipeline, this total length divided into 6-meter segments (typical length of steel pipe). Once again, nine span-lengths of the loading PGD

zone W varying between 10 m and 90 m were considered. The boundary conditions and input data remained the same as given in the Liu and O'Rourke model (see Table 5.1). The pipeline ends were fixed (assuming that pipeline ends represented manholes). To simulate continuous pipe, very large axial and bending stiffnesses (i.e., penalty coefficient) of $2x10^{30}$ N/mm and $2x10^{30}$ N-mm/deg, respectively, were used. These large stiffnesses ensured continuity of the displacement and rotation between the two interfaces of the joint. Figure 5.3 shows a comparison between the maximum strain of 100-meter-long continuous and segmented pipelines subjected to transverse PGD. The close agreements between the two numerical results show that the modeling procedures are remarkably consistent with the expected behaviour within a relative error of an average of 4.5% to 8.5% for the maximum pipe strain predictions. Typical deformation patterns of the pipe system are shown in Figure 5.5a and b for PGD width of 10 m and 20 m, respectively.

### 5.4.4 PREDICTION OF SEISMIC BEHAVIOUR OF SEGMENTED BURIED PIPELINE

The reasonable accuracy of the developed finite element model for segmented buried unrestrained pipelines under seismic effects gives the necessary confidence that the analysis can be generalized for typical rigid segmented buried pipelines under seismic effects where experimental results and numerical analysis are not available. Therefore, it can be said that the developed finite element model for the axial compression and bending behaviours of segmented pipe joints is rationally applicable for segmented buried unrestrained pipelines subjected to transverse PGD.

## 5.5 PARAMETRIC STUDIES OF SEISMIC ANALYSIS OF BURIED SEGMENTED PIPELINE

This section describes the results of a numerical parametric study for these seismic analyses. The pipe response parameters of interest for each type of pipe material include burial depth $H$, PGD zone width, $W$, PGD magnitude, $\delta$, and pipe diameter $D$. The

present study aims to gain an understanding of the important parameters that affect the seismic behaviours of buried segmented pipelines with unrestrained rubber gasketed joints.

After validating the capability of finite element models for predicting the seismic behaviour of 100-meter-long buried segmented pipeline, the same numerical models are used to conduct the seismic analyses for three types of pipe materials and for three different nominal diameters. Reinforced concrete pipes, non-reinforced concrete pipes, and vitrified clay pipes were considered. The reinforced and non-reinforced concrete pipe segments were 2.44 m (8 ft) long, while the vitrified clay pipe segments were 1.52 m (5 ft) long. Table 4.2 summarizes the material properties and the dimensions of the rigid pipes used for the seismic analysis prediction of the buried segmented pipelines. Based on 27 observed patterns, Flores-Berrones and O'Rourke (1992) showed that the idealized Block pattern gave a reasonable estimate of continuous pipe response subject to longitudinal PGD. As described in section 5.2 O'Rourke and Nordberg (1992) reported that the Block pattern resulted in the largest seismic pipe strain in an elastic pipe among other patterns. Thus, for segmented pipes, one expects that a Block pattern is the most severe pattern. Thus, this loading pattern is used in the present study. For the transverse direction, the cosine function pattern proposed by O'Rourke (1989) was selected among the possibilities. The same boundary conditions and PGD pattern types used for the validation were assumed in the parametric study. However, different PGD amount and width were used.

The pipeline was modeled by beam elements, while the soil-pipe interaction was modeled with equivalent bi-linear springs. The characteristics at the soil-pipe interface were estimated using the formulas given in the TCLEE guideline (ASCE, 1984), based upon the mean soil properties given in Table 5.2. Hence, no variability of soil properties along the numerical models is considered. The results of the simulations of joint axial and bending behaviours for these three types of rigid pipes discussed previously were used to simulate the seismic behaviour of buried segmented pipelines subjected to longitudinal and transverse PGD. The flexible gasket joints, axial and bending behaviours were

modeled as bi-linear springs (developed with the procedures presented in sections 5.2 and 5.3 of this chapter).

Three different nominal pipe diameters of 200 mm, 250 mm, and 300 mm were included in this parametric study in order to cover the sizes most frequently encountered in practice for water distribution and sewers. Tables 5.3 and 5.4 for the longitudinal PGD case and the transverse PGD case, respectively, show that the maximum pipe strain is a decreasing function of the pipe diameter. This behaviour can be explained because as the pipe diameter increases, the pipe wall stiffness and the soil-pipeline interaction force increase accordingly. However, for non-reinforced concrete and vitrified clay pipes with relatively small wall thicknesses, it can be said that the increase in pipe strain is caused by the increase in the soil-pipeline interaction force, rather than by the increase in pipe wall stiffness. It is to be noted that for all cases, the maximum pipe strain due to transverse effects is larger than that due to longitudinal effects. Hence, for the range of nominal diameters considered in this study, transverse PGD appears likely to be the cause of crushing/telescoping damage to segmented pipes, rather than pull-out damage caused by longitudinal PGD. It should be mentioned that all pipes used in this work are rigid pipes. Thus, the expected failure mode is due to joint displacement and/or rotation rather than to yield strain or to rupture of the pipe material.

In both the longitudinal and the transverse PGD, the maximum relative joint displacements and the maximum relative joint rotations occur at the joints within the center of the PGD zone (see Figure 5.5). This is due to the fact that when the margins of the PGD zone are close to the joint of a pipe segment, the corresponding joint displacements and rotations are related to the axial and bending deformations of the joints themselves.

From Tables 5.3 and 5.4, it was found that maximum pipe strains for reinforced concrete pipes are significantly small in comparison to those for non-reinforced concrete and vitrified clay pipes. This finding is due to the fact that the reinforced concrete pipes have the largest wall thickness among the other pipes under study, and the stiffness of the pipe

increases by increasing its wall thickness. On the other hand, although non-reinforced concrete and vitrified clay pipes have approximately the same wall thickness as shown in Table 4.2, vitrified clay pipes have slightly smaller strains than those of non-reinforced concrete pipes. Once again, for the pipe sizes under study, this behaviour is consistent with the requirements of the ASTM C700 where the minimum strength of the vitrified clay pipes (Class 160) exceeds the ASTM C14 requirement for minimum strength of the non-reinforced concrete pipes (Class II).

### 5.5.1 EFFECT OF PGD ZONE WIDTH

To investigate the effect of the PGD zone width $W$, width magnitudes varying between 10 m and 90 m were used. Since, the results indicated that a critical condition in the pipeline was reached at the PGD zone width of 40 m; large PGD zone widths (i.e., $W >$ 40 m) were not investigated. Similarly, for small PGD zone widths (i.e., $W < 10$ m), the transverse loading effects were not significant, and were therefore ignored.

For all types of pipes under study, Figures 5.6, 5.8, 5.10, 5.12, 5.14, and 5.16 show that the maximum pipe strain increases as the width of the PGD zone increases (except for the case of $W = 10$ m, which gives a constant response). In the cases of $W = 20$ m, 30 m, and 40 m, the pipeline response approached a constant value above a critical value of the permanent ground deformation; this means that above the critical PGD, the slip of pipeline begins between soil and pipeline. This slippage can be considered advantageous because it limits the force at the soil-pipe interface and helps to prevent the failure of pipeline. However, it is possible that the pipe failure occurs before slippage. It should be noted that this tendency is reconfirmed for all cases of PGD zone width higher than 20 m.

Figures 5.18, 5.20, and 5.22 for the longitudinal PGD case, as well as Figures 5.25, 5.27, and 5.29 for the transverse PGD case, demonstrate that both joint displacement and rotation are decreasing functions of the PGD zone width and increasing functions of the PGD amount. Moreover, these figures indicate that the increment of the PGD amount has a stronger effect on joint displacement and rotation for the same PGD zone width. The

results show that a critical joint displacement and rotation in the pipeline was reached at a PGD zone width of lower than 40 m.

### 5.5.2 EFFECT OF BURIAL DEPTH

Burial depths of 0.91m (3 ft) to 2.14 m (7 ft) which cover the usual average depths for the investigated rigid pipes, were considered for the both the longitudinal and transverse PGD cases in order to study the effect of burial depth on the seismic responses of buried segmented pipelines. From Figures 5.7, 5.9, and 5.11 for the longitudinal PGD, as well as Figures 5.13, 5.15, and 5.17 for the transverse PGD, it is obvious that the maximum pipe strain increases with the burial depth. This increase is due to the fact that high burial depth will induce a greater interaction force between the pipeline and the surrounding soil. From the same figures, it was found that the response of the pipeline increased with the PGD zone width until $W = 20$ m, then decreased thereafter. This phenomenon may have been caused by the dominant influence of the axial strain until $W = 20$ m, which is considered the limit between the cable behaviour and the beam behaviour of the buried pipeline as reported by Liu and O'Rourke (1997).

Figures 5.19, 5.21, and 5.23 illustrate that the joint displacement decreased slightly as the burial depth increased. This is due to the fact that both the backfill load and the soil-pipe interaction of the buried pipeline will increase as the burial depth increases. These figures show also that the variability of the PGD zone width has larger influence on the joint displacement and rotation than other investigated parameters for the same burial depth. The largest PGD zone width led to less joint displacement and rotation because the PGD magnitude was distributed over more pipe joints.

### 5.5.3 EFFECT OF PGD MAGNITUDE

To explore the effect of the PGD ground displacement, $\delta$, on the seismic responses of buried segmented pipelines, values varying between 0.1 m to 0.8 m were used for the longitudinal PGD case. For the transverse PGD case, ground displacement values varying

between 0.5 m to 3.5 m were selected. These ranges include the recorded longitudinal and transverse PGD from previous seismic events (O'Rourke and Liu, 1999).

As shown in Figures 5.6, 5.8, and 5.10 for the longitudinal PGD case, as well as Figures 5.13, 5.15, and 5.17 for the transverse PGD case, the results indicate that the largest magnitudes of PGD led to the largest strains in the pipelines. Figures 5.18, 5.20, and 5.22 for the longitudinal PGD case confirm the fact that the larger magnitude of PGD led to larger strain in the pipeline. Figures 5.13, 5.15, and 5.17 also show that the maximum pipe tensile strain is somewhat larger than the maximum pipe compressive strain. The largest strains occur at the joints within the center of the PGD zone. Figures 5.24, 5.26, and 5.28 for the transverse PGD also show that the larger amount of PGD led to the larger strain in the pipeline. This is significant, as the resistance of the soil against the pipeline is fully mobilized at relatively small permanent ground displacements.

## 5.6 FAILURE ANALYSIS

For practical analysis of pipeline systems, accurate prediction of the potential damage and failure of the pipeline is vital for safe pipeline design. By identifying the extent and the location of potential problems, strategies to address the problem may then be proposed and evaluated.

For segmented pipelines, observed seismic failure is most often related to distress at the pipe joints (Selventhiran, 2002). Axial pull-out, sometimes in combination with relative angular rotation at joints, is a common failure mechanism in areas of tensile ground strain since the shear strength of the joint caulking materials is much less than the tensile strength in the pipe. In areas of compressive ground strain, when the stress in the joint exceeds the yield stress of the pipe material after bell-to-spigot contact, crushing of bell and spigot joints is a fairly common failure mechanism in segmented rigid pipes (O'Rourke and Liu, 1999). Moreover, when surface loading is conveyed to defected segmented rigid pipes, some displacement and rotation will occur at the joints.

For installation and laying purposes, standards prescribe maximum allowable deflections for several types of low-pressure pipes over which rubber gasket joints must maintain integrity. For example, the standard ASTM C443 specifies a maximum movement of 12 mm difference across opposite sides at the rubber gasket joints of reinforced concrete pipes. The ASTM C425, dealing with vitrified clay pipe, specifies a range of maximum allowable displacement from 42 mm per meter of pipe length for diameter of 76 mm to 300 mm, to 16 mm per meter of pipe length for diameter of 990 mm to 1065 mm. These deflections are typically considered to be the maximum allowable deflections from the true axial direction for installation of such pipes. Standards also permit slight curvatures for installation purposes; e.g., the ASTM C12 standard normally permits maximum angular deflection per joint of 2.4° for installing clay pipelines of 75 mm to 300 mm nominal diameter. Further, the ASTM C505 standard normally permits maximum angular deflection per joint of 3.5° for installing concrete pipelines of 150 mm to 600 mm nominal diameter.

To the best knowledge of the author, there are no specified limit states for seismic design of segmented pipes in water and wastewater application in North America. An alternative approach used by researchers as well as by industry involves relating the manufacturer's recommended allowable angular offsets for laying a segmented pipe on a curve to the allowable joint displacement (i.e., joint opening) for pipes in tension, to the allowable crushing strength after bell-to-spigot contact for pipes in compression, and to the allowable joint rotation for pipes in bending.

For joint pull-out failure, Elhmadi and O'Rourke (1990), based on laboratory tests on cast iron pipes, suggested that lead caulked joints begin to leak when the relative joint displacement is about half the total joint embedment distance. Bouabid and O'Rourke (1994), based on laboratory tests on reinforced cylinder concrete pipes, suggested that the relative joint tensile displacement leading to significant leakage corresponds to roughly 50% of the total joint depth. They also reported that a relative axial joint extension of roughly half the total joint depth may be an appropriate failure criterion for many types of segmented pipes.

Tables 5.6 and 5.7 present the maximum joint displacements and maximum joint rotations for both longitudinal and transverse PGD, respectively. The allowable joint displacements and rotations according to the pipe manufacturer recommendations are also reported. Both axial joint extension and joint rotation contribute to the total joint opening. Thus, failure is assumed to occur when the maximum joint displacement and/or rotation due to PGD effect exceeds the allowable tolerances recommended by the pipe manufacturers.

From Table 5.6, it is clear that all types of pipes will become damaged when the PGD amount exceeds 0.3 m under longitudinal PGD loading. On the other hand, as shown from Table 5.7, it is clear that all types of pipes will become damaged when the PGD amount exceeds 2.5 m under transverse PGD loading. It was thus verified that rigid pipes with rubber gaskets could not resist the PGD generated during an earthquake if the transverse PGD amount exceeds 2.5 m.

## 5.7 SUMMARY AND CONCLUSIONS

This chapter develops a tool to use numerical simulation results of seismic analysis of buried segmented pipeline networks including axial permanent ground deformation investigations. The developed numerical models used for the seismic analysis of buried segmented pipes have been successfully verified with the results of previous studies (Selventhiran, 2002; Liu and O'Rourke, 1997).

A review of the major effects of longitudinal and transverse PGD on the seismic behaviour of buried segmented pipelines led to the following conclusions:

1. The application of these models for the seismic analysis of buried segmented pipelines allows extending existing methodologies developed for continuous pipeline. Thus, the developed finite element models for seismic behaviour of buried segmented pipelines generalize the work of the Selventhiran (2002) and Liu and O'Rourke (1997) models. If

there is a need to refine the modeling of the joints, a multi-linear constitutive law is possible. However, the modeling approach remains the same.

2. Both developed simulation models are considered relatively adequate tools for predicting the unrestrained joints, behaviour for working conditions and for ultimate failure predictions, as well as for the seismic analysis of buried segmented pipelines networks whenever experimental data is not available.

3. The parametric study of the seismic behaviours of buried segmented pipes under axial and transverse PGD showed that the pipe strain increases as the burial depth, the PGD amount, and the PGD zone width increases, while the pipe strain is a decreasing function of the pipe diameter. In all cases, the similarity in the trend of the maximum pipe strain prediction results from the assumed material homogeneity throughout the pipe wall thicknesses.

4. Failure analysis indicates that all types of rigid pipes under longitudinal PGD loading will be subject to pull-out damage when the PGD amount exceeds 0.3 m. Further, all types of rigid pipes under transverse PGD loading will experience crushing/telescoping damage at joints when the PGD amount exceeds 2.5 m. Thus, there is an urgent need for research to develop new techniques to modify the structural behavior of the joint to have more resistance to seismic effect.

5. Parametric study results under transverse PGD loading show smaller joint rotation when compared with the results of longitudinal PGD loading. Thus, it has been shown that in general, longitudinal PGD causes more damage (e.g., joint separation) than does transverse PGD. The damage increases with increasing PGD width and magnitude.

Table 5.1 Data used for Continuous Pipe Models Verification of Selventhiran (2002) and Liu and O'Rourke (1997)

| Model Input Data | Selventhiran (2002) | Liu and O'Rourke (1997) |
|---|---|---|
| Modulus of Elasticity of Pipe Material ($E$), (MPa) | 200000 | 200000 |
| Plastic Strain at Failure | 0.177 | 0.177 |
| Pipe Outer Diameter ($D_o$), (mm) | 203 | 610 |
| Pipe Wall Thickness ($t$), (mm) | 6.5 | 9.5 |
| Pipeline Length ($L$), (m) | 1000 | 400 |
| Burial Depth ($H$), (m) | 1.94 | 1.2 |
| Soil Density ($\gamma$), (N/m$^3$) | 19600 | 18700 |
| Coefficient of Soil Pressure at Rest ($k_o$) | 1.0 | 1.0 |
| Soil Angle of Internal Friction ($\varphi$) | 37° | 35° |
| Yield Axial Displacement of Soil-Pipe Interaction ($x_u$), (mm) | 3.8 | 3.8 |
| Maximum Axial Soil-Pipe Interaction Force ($t_u$), (N/m) | 18240 | 24000 |
| Yield transverse Displacement of Soil-Pipe Interaction ($z_u$), (mm) | - | 60 |
| Maximum Transverse Soil-Pipe Interaction Force ($q_u$), (N/m) | - | 100000 |
| Maximum Ground Axial Displacement ($\delta$), (m) | 0.2 | 0.5-3 |
| PGD Zone Span ($W$), (m) | 20-550 | 400 |
| PGD Pattern Type | Uniform Block | Cosine Function |

Table 5.2 Soil Properties Used for Calculating Equivalent Springs Stiffness for Pipe-Soil Interaction

| Material | Modulus of Elasticity ($E$) (Short-term) MPa (psi) | Poisson's Ratio ($\nu$) | Density ($\gamma$) kg/m$^3$ (pcf) |
|---|---|---|---|
| Soil | 22.4 (3250) | 0.33 | 1920 (120) |
| Soil other properties:<br>Type: Medium-dense sand (coarse grained soil-no fines)<br>Internal angle of friction = $\varphi = 35°$<br>Cohesion = $C = 0$ Pa<br>Modulus of soil reaction = $E' = 2500$ psi = 17.24 MPa | | | |

Table 5.3 Comparison between Seismic Maximum Pipe Strains Due to Longitudinal PGD for Typical Rigid Pipes

| Pipe Type | Inner Diameter (mm) | Seismic Maximum Pipe Strain (x 0.00001) | | | | | | | |
|---|---|---|---|---|---|---|---|---|---|
| | | Longitudinal PGD amount δ (m) | | | | | | | |
| | | 0.1 | 0.2 | 0.3 | 0.4 | 0.5 | 0.6 | 0.7 | 0.8 |
| Reinforced Concrete (Wall B) | 200 | 0.863 | 2.739 | 3.479 | 4.069 | 4.296 | 4.876 | 4.900 | 4.900 |
| | 250 | 0.770 | 2.300 | 3.066 | 3.634 | 4.082 | 4.407 | 4.588 | 4.588 |
| | 300 | 0.652 | 1.840 | 2.660 | 3.168 | 3.705 | 4.036 | 4.206 | 4.114 |
| Non-Reinforced Concrete (Class II) | 200 | 1.588 | 3.572 | 5.281 | 6.883 | 7.826 | 8.305 | 8.685 | 8.685 |
| | 250 | 1.225 | 2.977 | 4.377 | 5.545 | 6.641 | 7.343 | 7.567 | 7.567 |
| | 300 | 0.884 | 2.285 | 3.453 | 4.387 | 5.320 | 5.787 | 6.096 | 6.096 |
| Vitrified Clay (Class 160) | 200 | 2.465 | 4.294 | 5.454 | 6.380 | 7.169 | 7.435 | 7.683 | 7.683 |
| | 250 | 2.054 | 3.723 | 4.940 | 5.698 | 6.400 | 6.798 | 7.067 | 7.067 |
| | 300 | 1.765 | 3.107 | 4.170 | 4.966 | 5.809 | 6.328 | 6.641 | 6.641 |

Table 5.4 Comparison between Seismic Maximum Pipe Strains Due to Transverse PGD for Typical Rigid Pipes

| Pipe Type | Inner Diameter (mm) | Seismic Maximum Pipe Strain (x 0.001) | | | | | | |
|---|---|---|---|---|---|---|---|---|
| | | Transverse PGD amount δ (m) | | | | | | |
| | | 0.5 | 1 | 1.5 | 2 | 2.5 | 3 | 3.5 |
| Reinforced Concrete (Wall B) | 200 | 1.483 | 1.863 | 2.238 | 2.599 | 2.904 | 3.167 | 3.167 |
| | 250 | 1.279 | 1.623 | 1.924 | 2.221 | 2.532 | 2.672 | 2.672 |
| | 300 | 1.019 | 1.402 | 1.652 | 1.840 | 1.984 | 2.117 | 2.117 |
| Non-Reinforced Concrete (Class II) | 200 | 4.640 | 5.830 | 6.680 | 7.287 | 7.652 | 7.849 | 7.849 |
| | 250 | 2.915 | 3.643 | 4.154 | 4.493 | 4.810 | 5.077 | 5.077 |
| | 300 | 1.700 | 2.186 | 2.454 | 2.623 | 2.672 | 2.853 | 2.853 |
| Vitrified Clay (Class 160) | 200 | 3.415 | 4.288 | 5.152 | 5.983 | 6.687 | 7.290 | 7.290 |
| | 250 | 2.943 | 3.737 | 4.429 | 5.112 | 5.829 | 6.151 | 6.151 |
| | 300 | 2.347 | 3.226 | 3.802 | 4.238 | 4.569 | 4.874 | 4.874 |

Table 5.5 Comparison between Allowable Joint Displacement and Seismic Maximum Joint Displacement Due to Longitudinal PGD

| Pipe Type | Inner Diameter (mm) | Allowable* Joint Displacement (mm) | Seismic Maximum Joint Displacement (mm) | | | | | | | |
|---|---|---|---|---|---|---|---|---|---|---|
| | | | Longitudinal PGD amount δ (m) | | | | | | | |
| | | | 0.1 | 0.2 | 0.3 | 0.4 | 0.5 | 0.6 | 0.7 | 0.8 |
| Reinforced Concrete (Wall B) | 200 | 16 | 7.9 | 13.1 | 18.4 | 23.7 | 29.1 | 34.3 | 39.7 | 44.9 |
| | 250 | 16 | 7.3 | 12.6 | 17.8 | 23.4 | 28.6 | 33.1 | 38.8 | 43.3 |
| | 300 | 16 | 7.2 | 12.2 | 17.2 | 22.2 | 27.2 | 32.3 | 37.3 | 42.2 |
| Non-Reinforced Concrete (Class II) | 200 | 14 | 6.6 | 11.0 | 15.4 | 19.9 | 24.4 | 28.7 | 33.2 | 37.7 |
| | 250 | 14 | 6.0 | 10.3 | 14.5 | 19.2 | 23.4 | 27.1 | 31.7 | 35.4 |
| | 300 | 14 | 6.0 | 10.1 | 14.3 | 18.5 | 22.7 | 26.9 | 31.1 | 35.2 |
| Vitrified Clay (Class 160) | 200 | 12 | 6.9 | 11.4 | 16.1 | 20.7 | 25.4 | 29.9 | 34.6 | 39.2 |
| | 250 | 12 | 6.5 | 11.2 | 15.8 | 20.7 | 25.5 | 29.4 | 34.4 | 38.5 |
| | 300 | 12 | 6.5 | 11.0 | 15.4 | 20.0 | 24.6 | 29.1 | 33.6 | 38.0 |

* Pipe manufacturer recommendations.

Table 5.6 Comparison between Allowable Joint Rotation and Seismic Maximum Joint Rotation Due to Transverse PGD

| Pipe Type | Inner Diameter (mm) | Allowable* Joint Rotation (degree) | Seismic Maximum Joint Rotation (degree) | | | | | | |
|---|---|---|---|---|---|---|---|---|---|
| | | | Transverse PGD amount δ (m) | | | | | | |
| | | | 0.5 | 1 | 1.5 | 2 | 2.5 | 3 | 3.5 |
| Reinforced Concrete (Wall B) | 200 | 2.5° | 1.12° | 1.51° | 1.77° | 2.06° | 2.43° | 2.78° | 3.25° |
| | 250 | 2.5° | 1.29° | 1.73° | 2.04° | 2.34° | 2.66° | 2.99° | 3.41° |
| | 300 | 2.5° | 1.50° | 1.88° | 2.26° | 2.62° | 2.94° | 3.21° | 3.52° |
| Non-Reinforced Concrete (Class II) | 200 | 2.2° | 0.90° | 1.16° | 1.47° | 1.77° | 2.09° | 2.40° | 2.62° |
| | 250 | 2.2° | 0.94° | 1.26° | 1.56° | 1.88° | 2.17° | 2.49° | 2.73° |
| | 300 | 2.2° | 1.17° | 1.53° | 1.87° | 2.15° | 2.49° | 2.75° | 2.93° |
| Vitrified Clay (Class 160) | 200 | 2.4° | 0.82° | 1.04° | 1.32° | 1.59° | 1.88° | 2.16° | 2.46° |
| | 250 | 2.4° | 0.85° | 1.14° | 1.41° | 1.69° | 1.95° | 2.25° | 2.59° |
| | 300 | 2.4° | 1.06° | 1.38° | 1.68° | 1.93° | 2.25° | 2.50° | 2.69° |

* Pipe manufacturer recommendations.

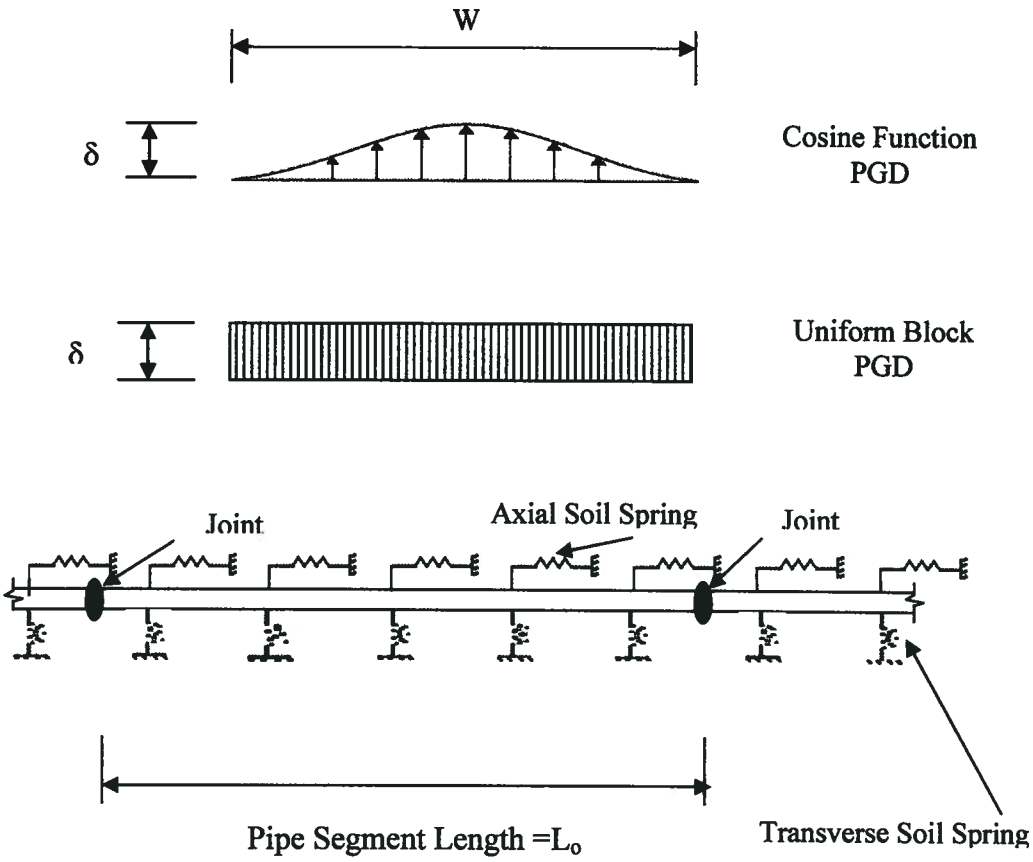


Figure 5.1 Continuous Pipe Subjected to Longitudinal or Transverse PGD
(After O'Rourke and Liu, 1999)

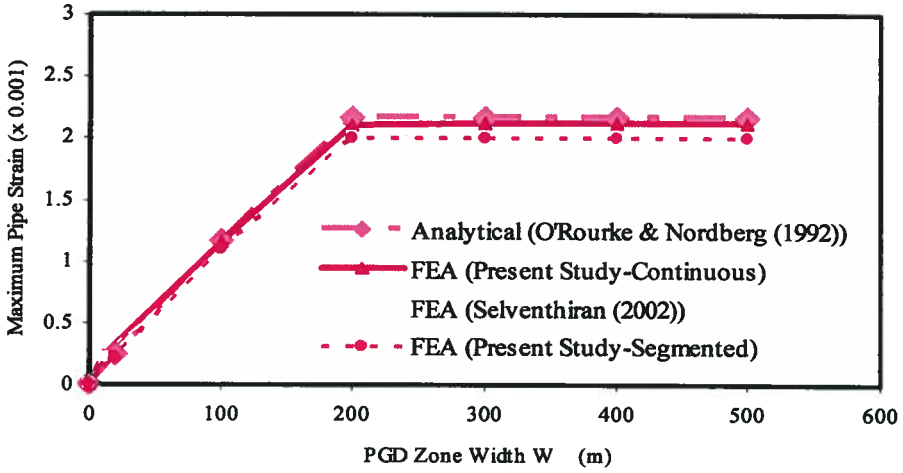


Figure 5.2 Comparison between the Analytical, Finite Element Model Predictions for Continuous Pipe Subjected to Longitudinal PGD

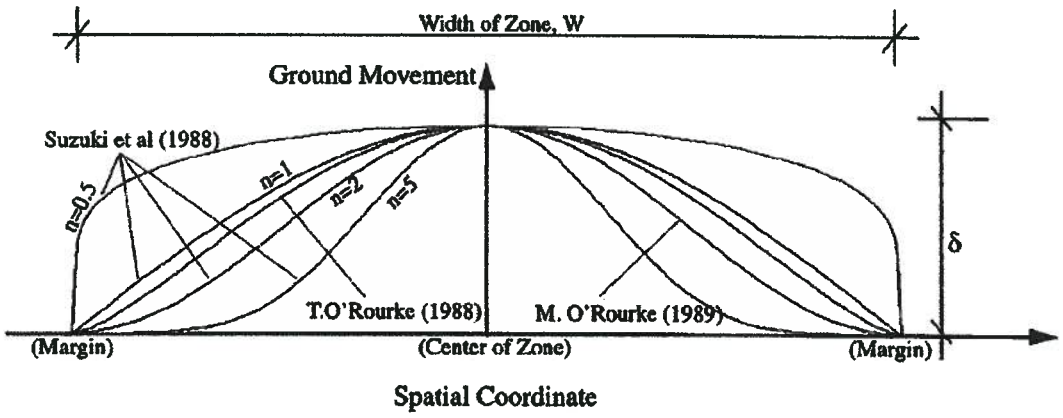


Figure 5.3 Assumed Patterns for Spatially Distributed PGD (After Liu and O'Rourke, 1997)

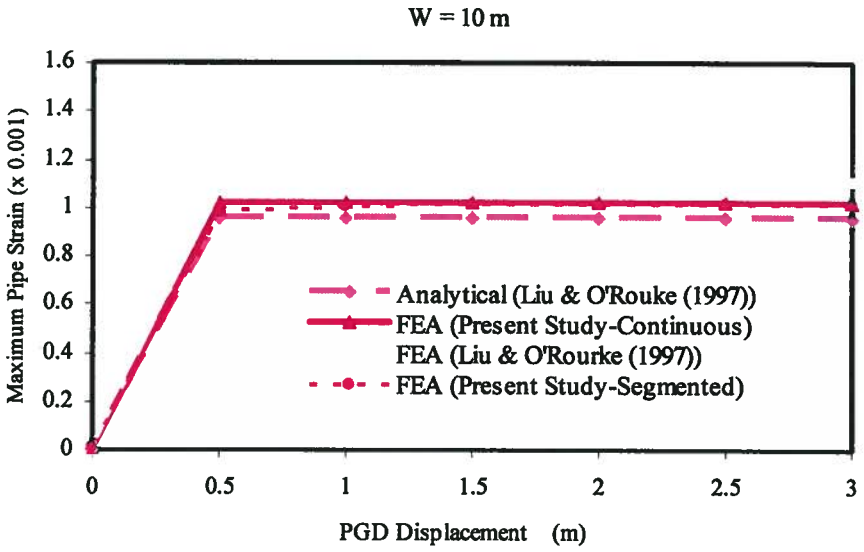


Figure 5.4 Comparison between the Analytical, Finite Element Model Predictions for Continuous Pipe Subjected to Transverse PGD

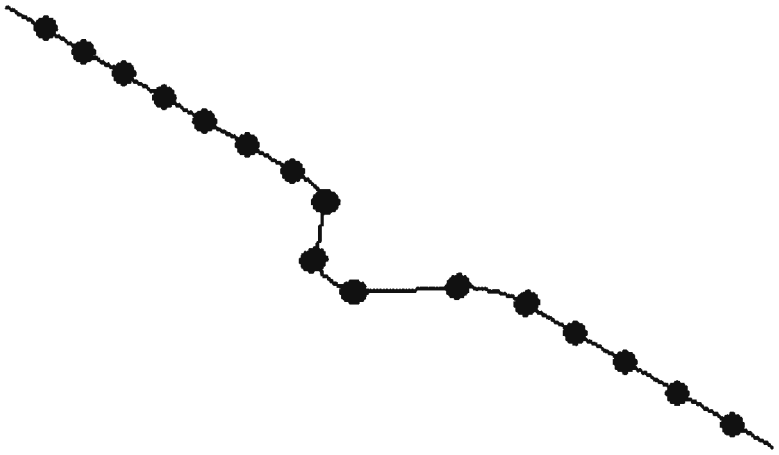

(a) Max. Joint Displacement = 12.2 mm, Max. Joint Rotation = 2.41°
($W$ = 10 m)

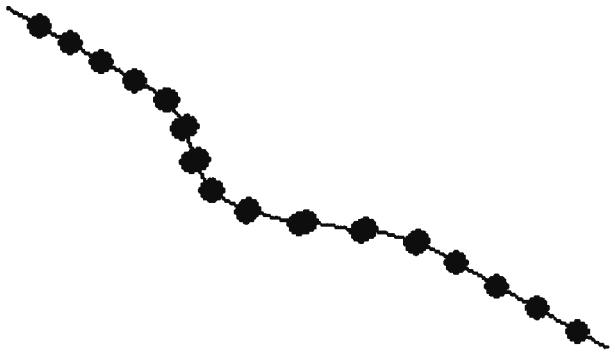

(b) Max. Joint Displacement = 7.2 mm, Max. Joint Rotation = 1.17°
($W$ = 20 m)

Figure 5.5 Longitudinal View for Deformed Shape of Buried Segmented Pipeline Subjected to Transverse PGD

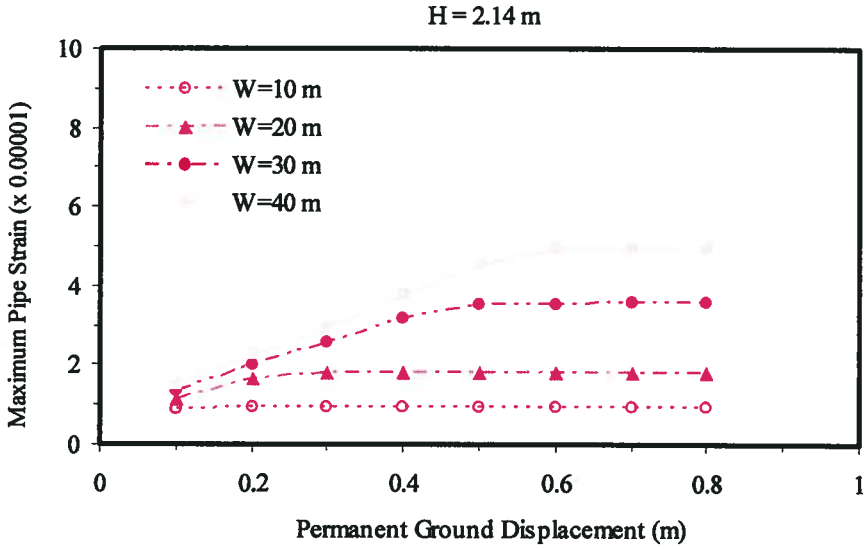


Figure 5.6 Effect of PGD Zone Width in the Response of Segmented Reinforced Concrete Pipe Subjected to Longitudinal PGD

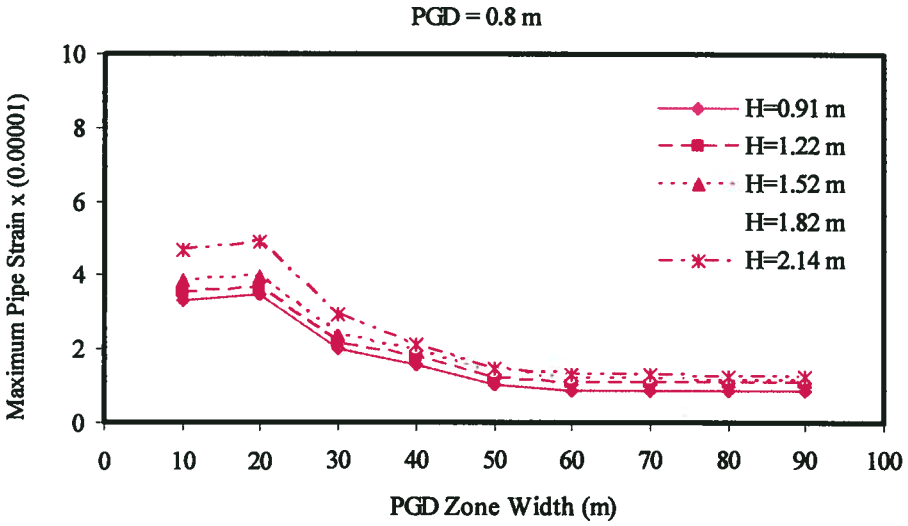


Figure 5.7 Effect of Burial Depth in the Response of Segmented Reinforced Concrete Pipe Subjected to Longitudinal PGD

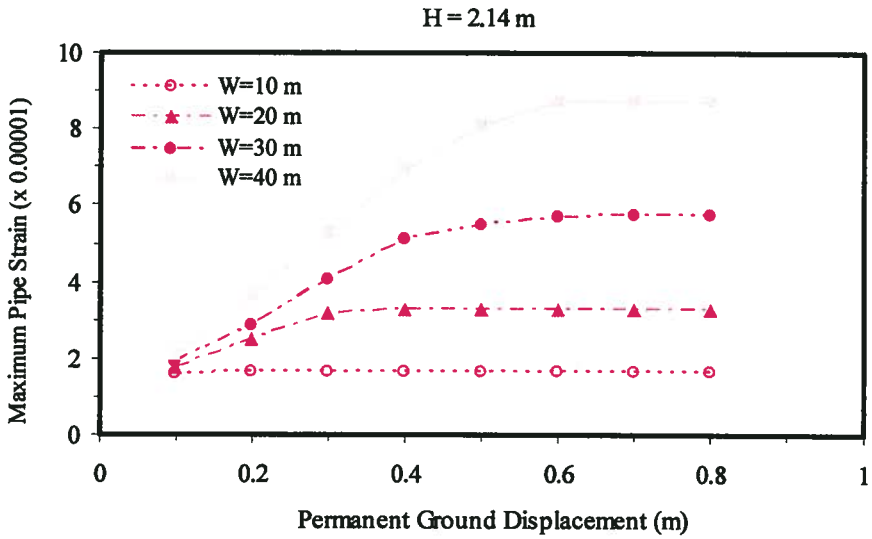


Figure 5.8 Effect of PGD Zone Width in the Response of Segmented Non-Reinforced Concrete Pipe Subjected to Longitudinal PGD

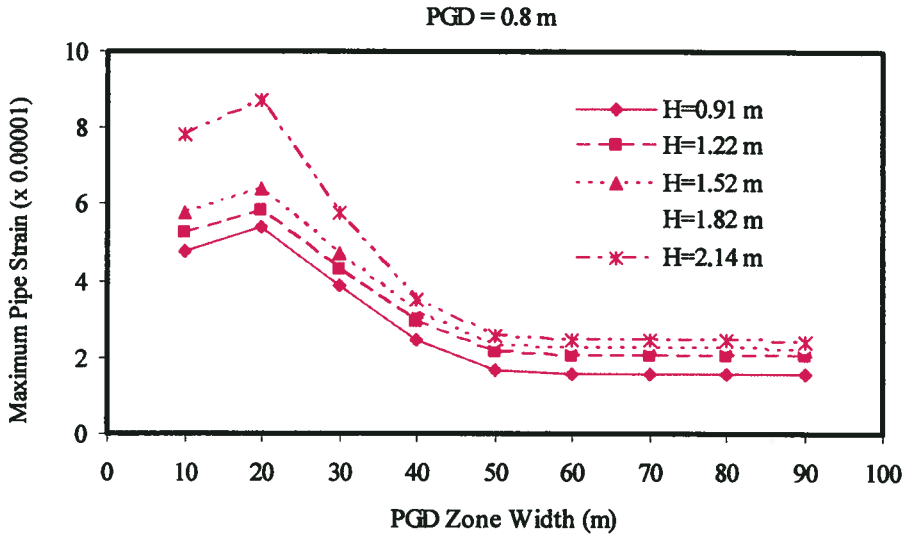


Figure 5.9 Effect of Burial Depth in the Response of Segmented Non-Reinforced Concrete Pipe Subjected to Longitudinal PGD

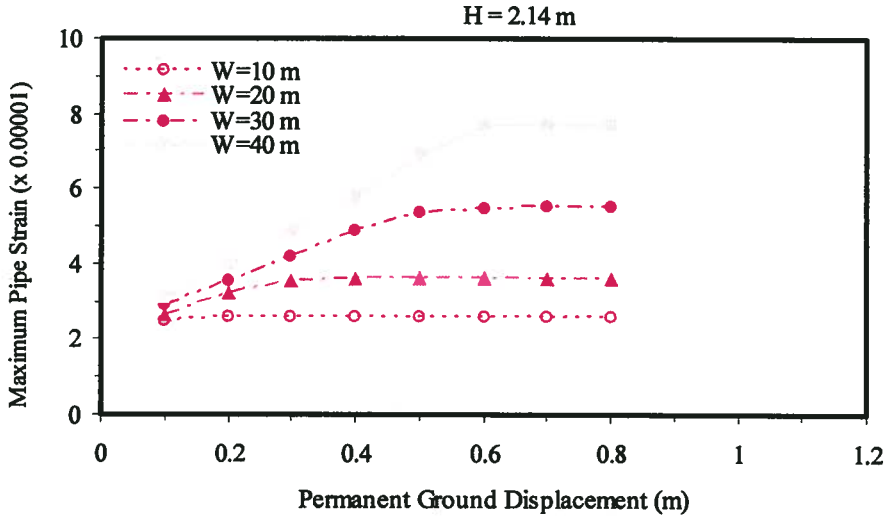


Figure 5.10 Effect of PGD Zone Width in the Response of Segmented Vitrified Clay Pipe Subjected to Longitudinal PGD

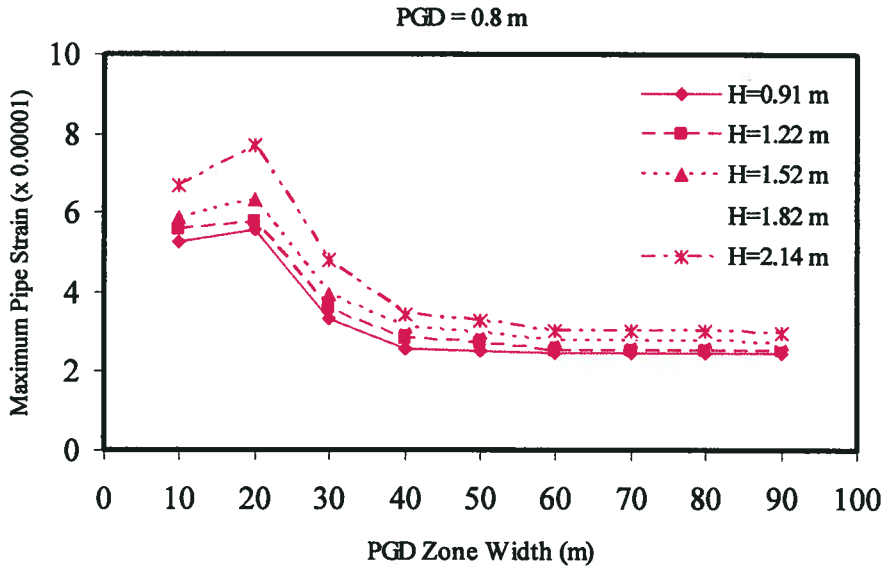


Figure 5.11 Effect of Burial Depth in the Response of Segmented Vitrified Clay Pipe Subjected to Longitudinal PGD

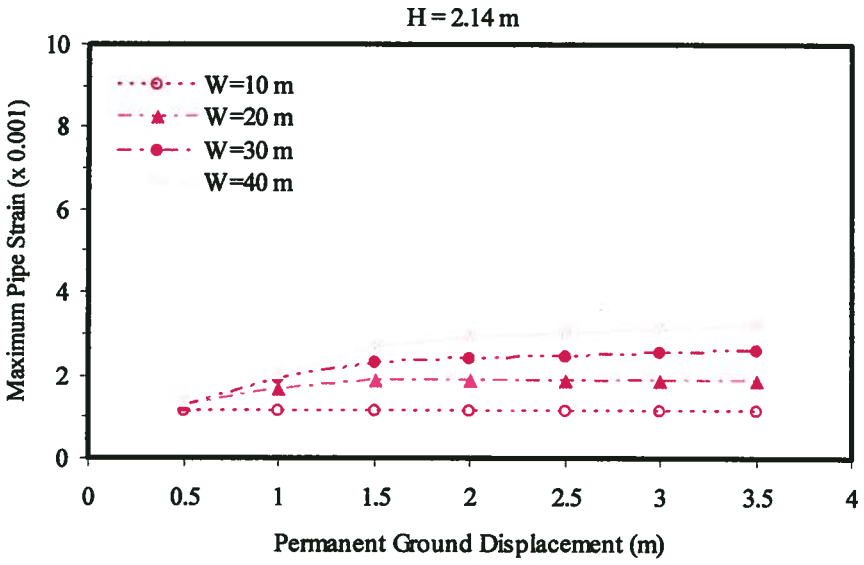


Figure 5.12 Effect of PGD Zone Width in the Response of Segmented Reinforced Concrete Pipe Subjected to Transverse PGD

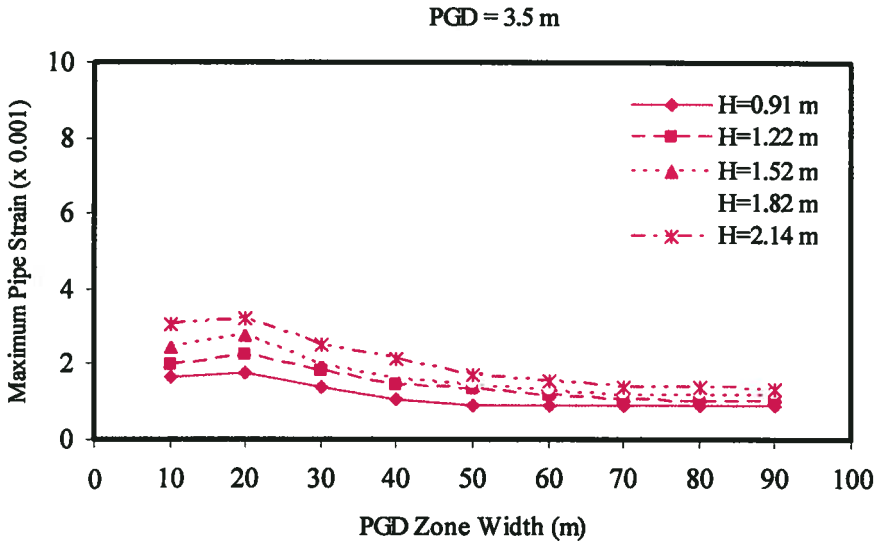


Figure 5.13 Effect of Burial Depth in the Response of Segmented Reinforced Concrete Pipe Subjected to Transverse PGD

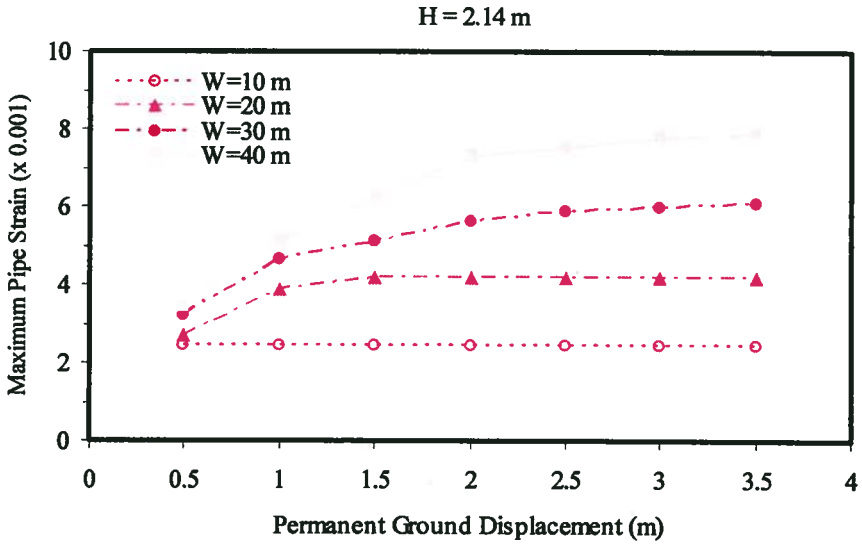


Figure 5.14 Effect of PGD Zone Width in the Response of Segmented Non-Reinforced Concrete Pipe Subjected to Transverse PGD

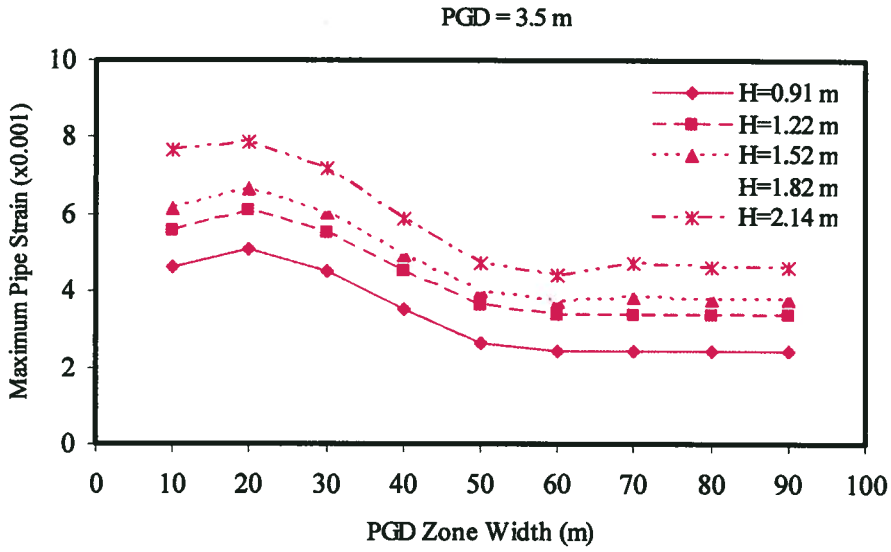


Figure 5.15 Effect of Burial Depth in the Response of Segmented Non-Reinforced Concrete Pipe Subjected to Transverse PGD

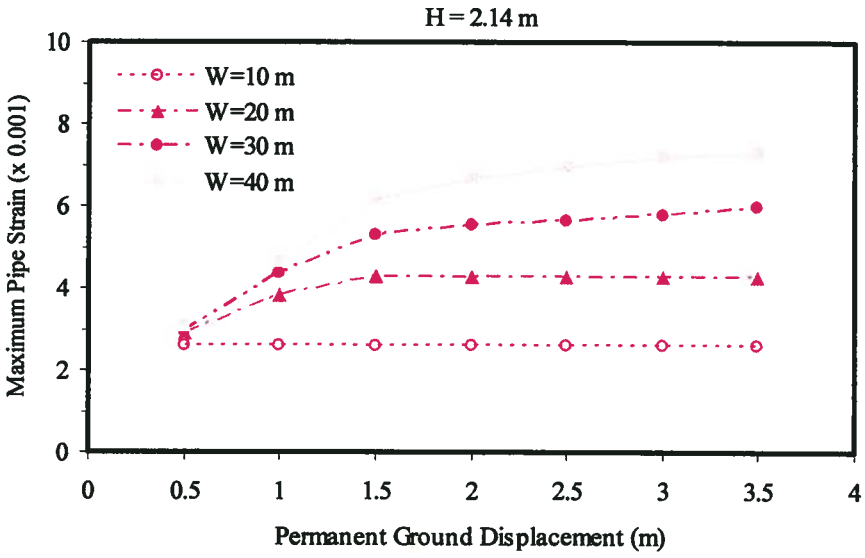


Figure 5.16 Effect of PGD Zone Width in the Response of Segmented Vitrified Clay Pipe Subjected to Transverse PGD

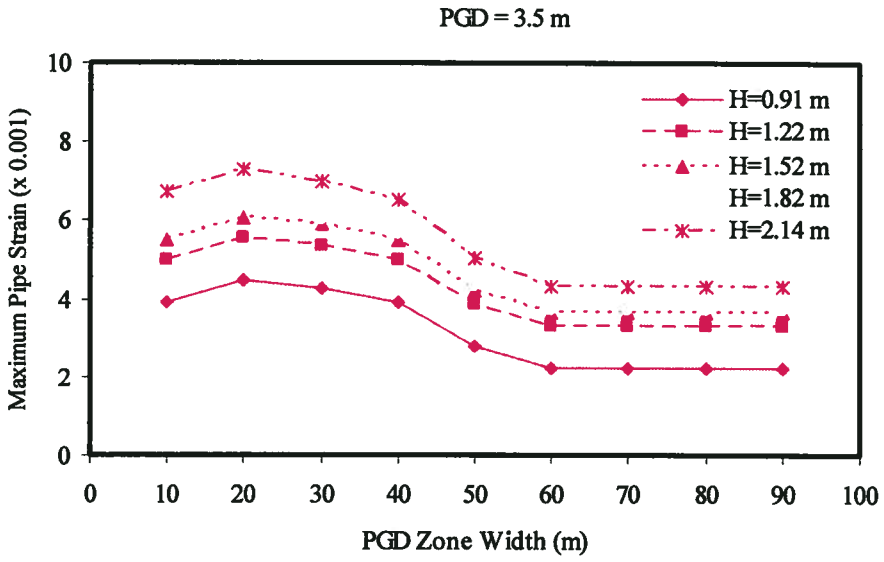


Figure 5.17 Effect of Burial Depth in the Response of Segmented Vitrified Clay Pipe Subjected to Transverse PGD

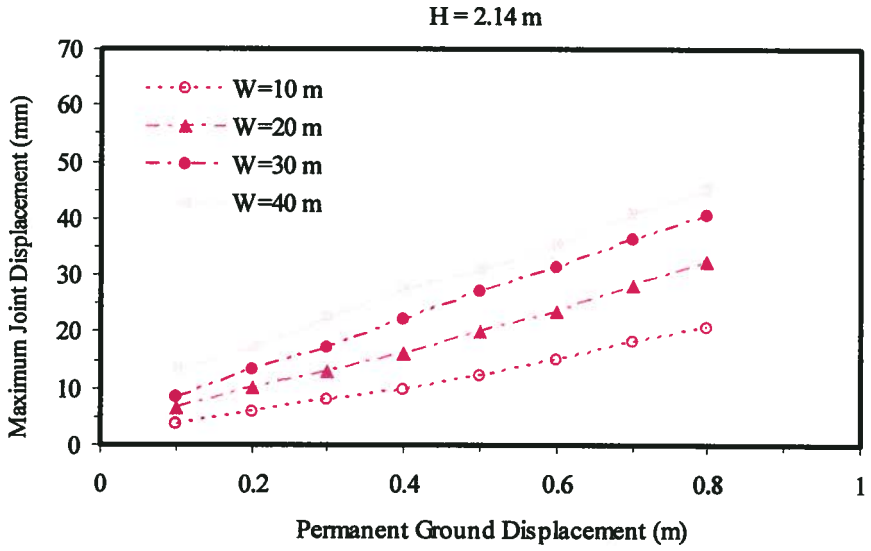


Figure 5.18 Effect of PGD Zone Width on the Joint Displacement of Segmented Reinforced Concrete Pipe Subjected to Longitudinal PGD

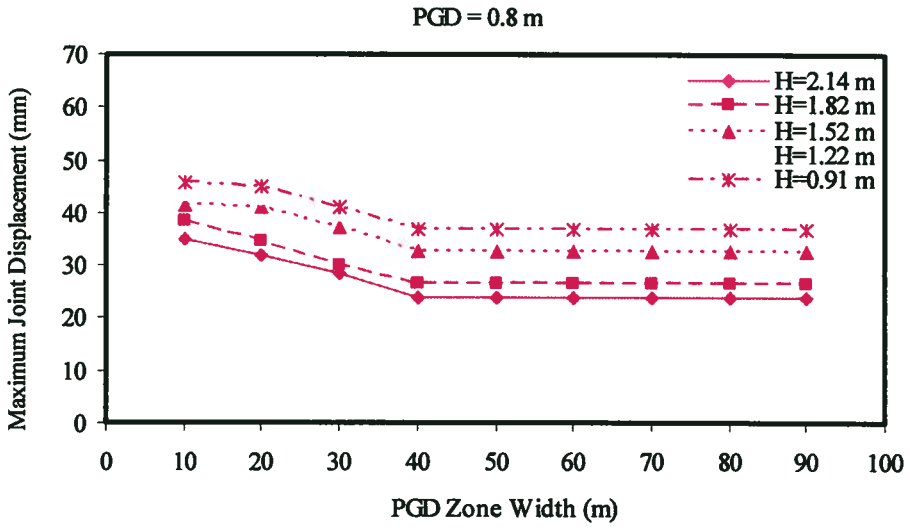


Figure 5.19 Effect of Burial Depth on the Joint Displacement of Segmented Reinforced Concrete Pipe Subjected to Longitudinal PGD

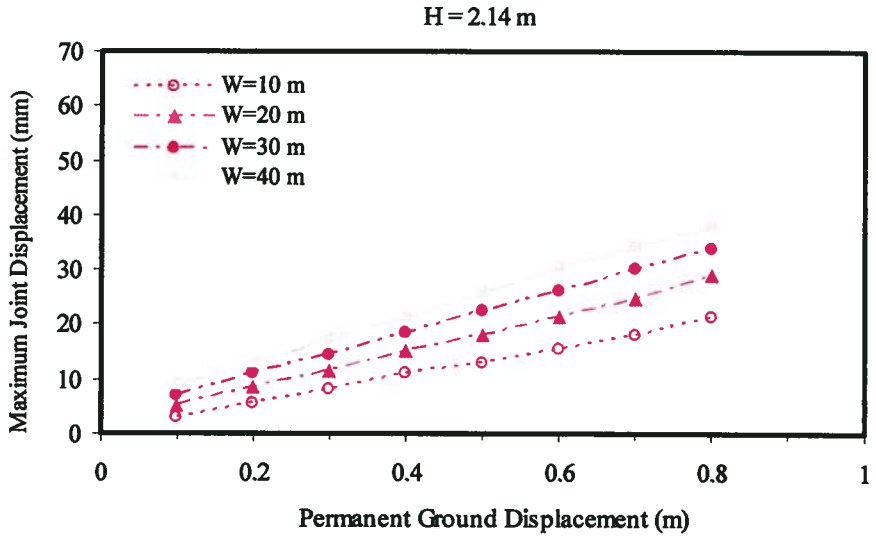


Figure 5.20 Effect of PGD Zone Width on the Joint Displacement of Segmented Non-Reinforced Concrete Pipe Subjected to Longitudinal PGD

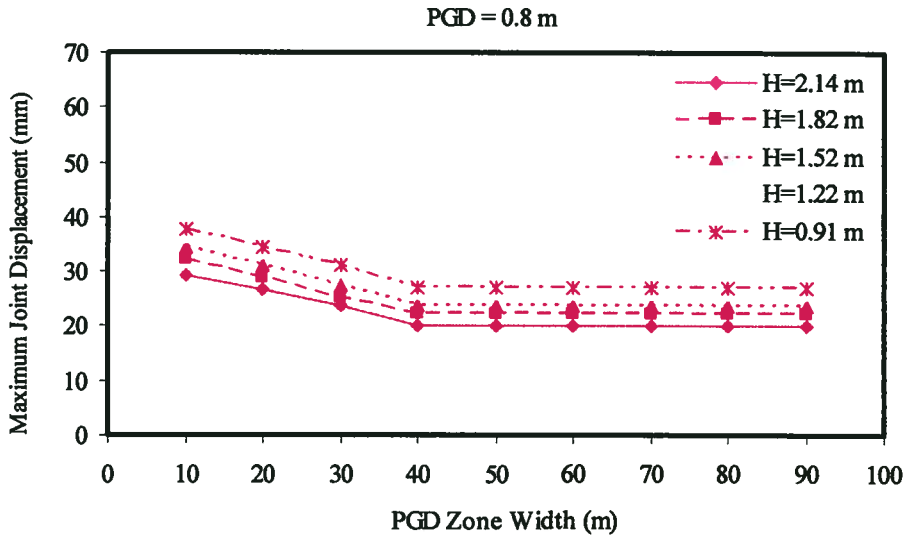


Figure 5.21 Effect of Burial Depth on the Joint Displacement of Segmented Non-Reinforced Concrete Pipe Subjected to Longitudinal PGD

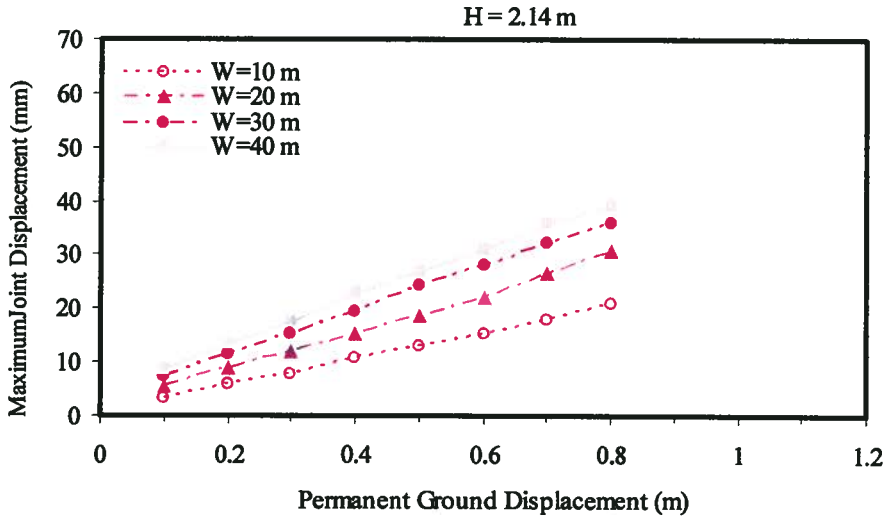


Figure 5.22 Effect of PGD Zone Width on the Joint Displacement of Segmented Vitrified Clay Pipe Subjected to Longitudinal PGD

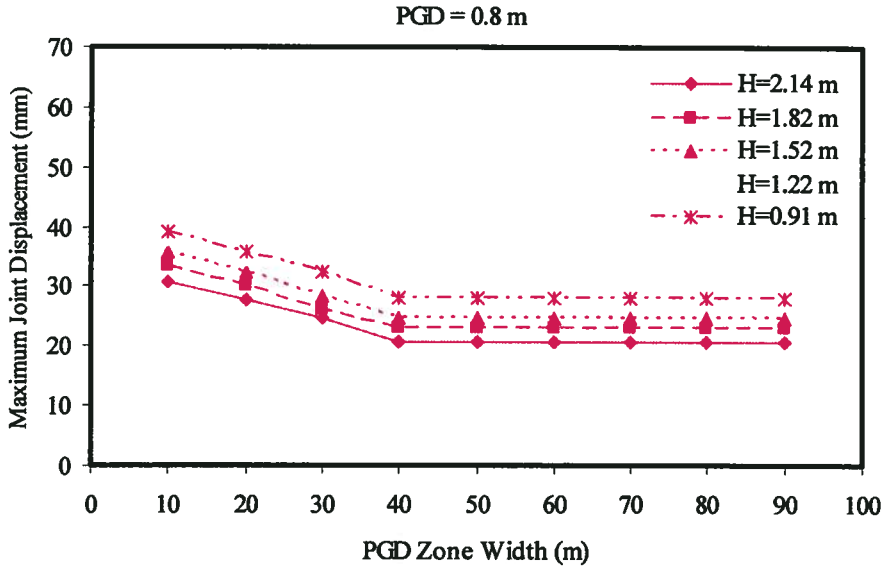


Figure 5.23 Effect of Burial Depth on the Joint Displacement of Segmented Vitrified Clay Pipe Subjected to Longitudinal PGD

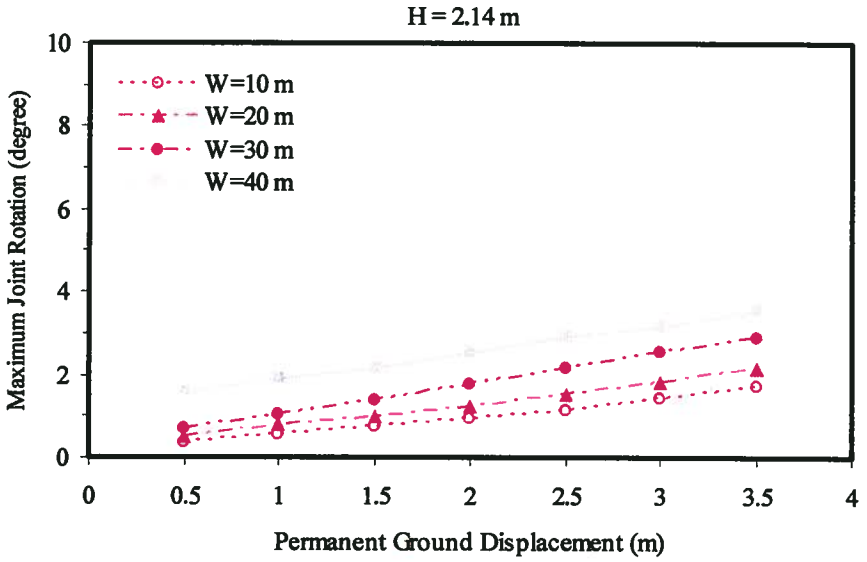


Figure 5.24 Effect of PGD Zone Width on the Joint Rotation of Segmented Reinforced Concrete Pipe Subjected to Transverse PGD

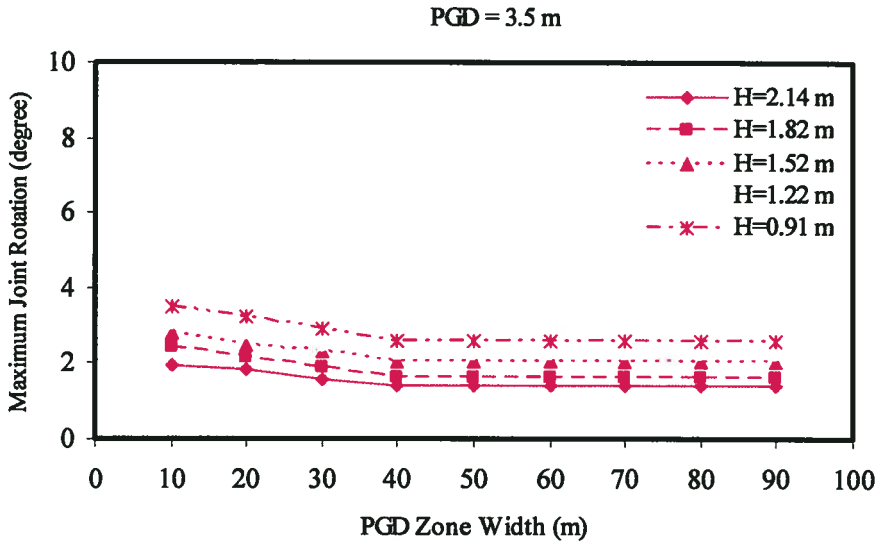


Figure 5.25 Effect of Burial Depth on the Joint Rotation of Segmented Reinforced Concrete Pipe Subjected to Transverse PGD

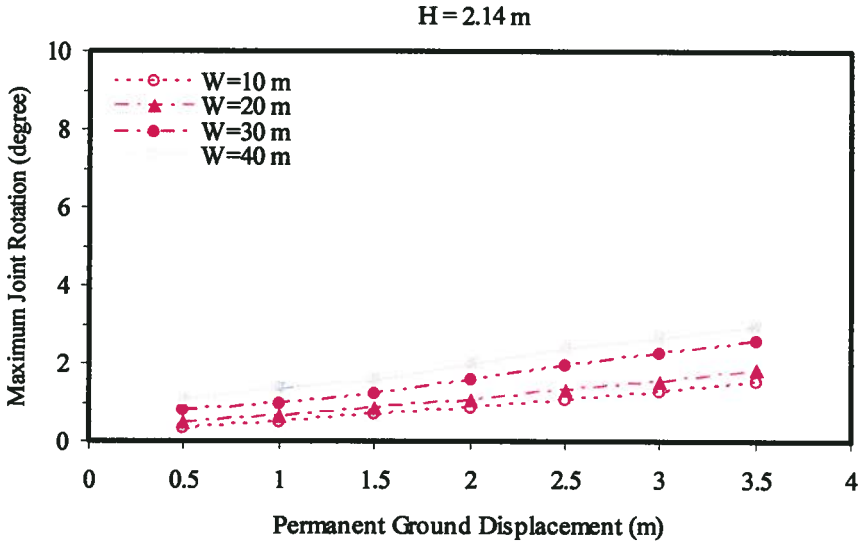


Figure 5.26 Effect of PGD Zone Width on the Joint Rotation of Segmented Non-Reinforced Concrete Pipe Subjected to Transverse PGD

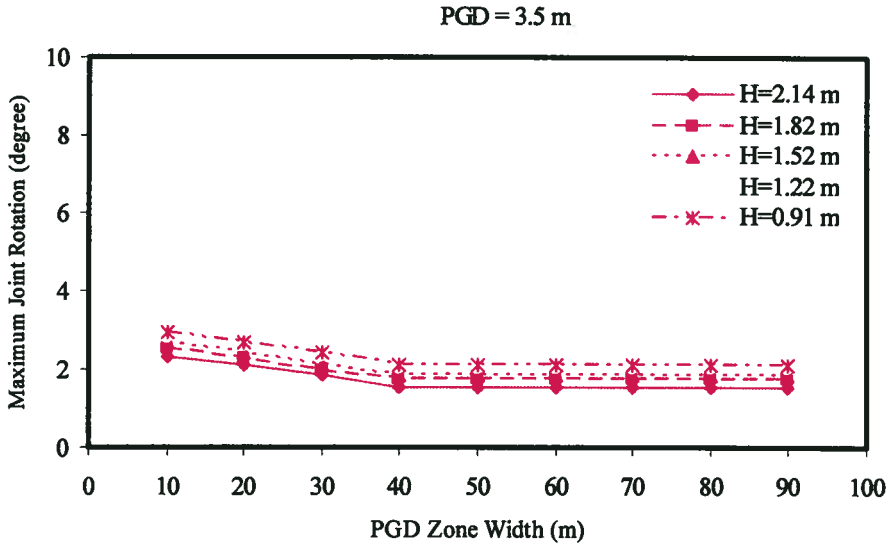


Figure 5.27 Effect of Burial Depth on the Joint Rotation of Segmented Non-Reinforced Concrete Pipe Subjected to Transverse PGD

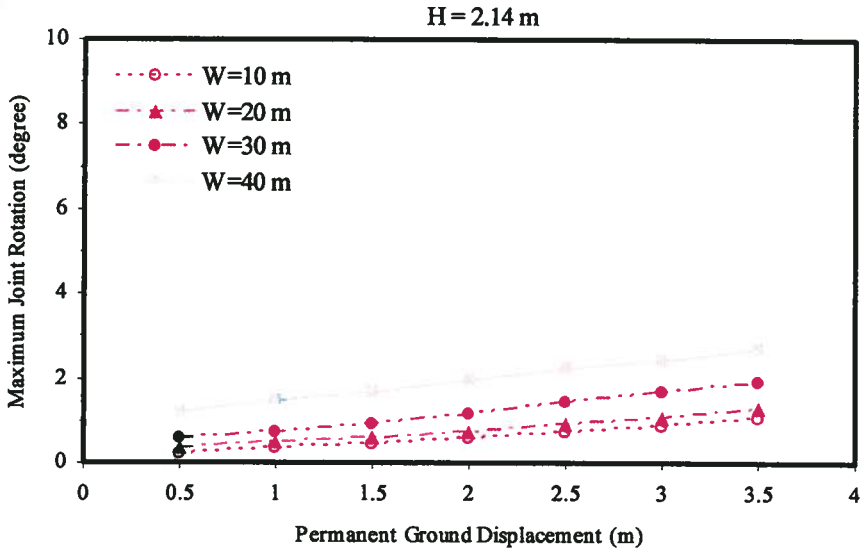


Figure 5.28 Effect of PGD Zone Width on the Joint Rotation of Segmented Vitrified Clay Pipe Subjected to Transverse PGD

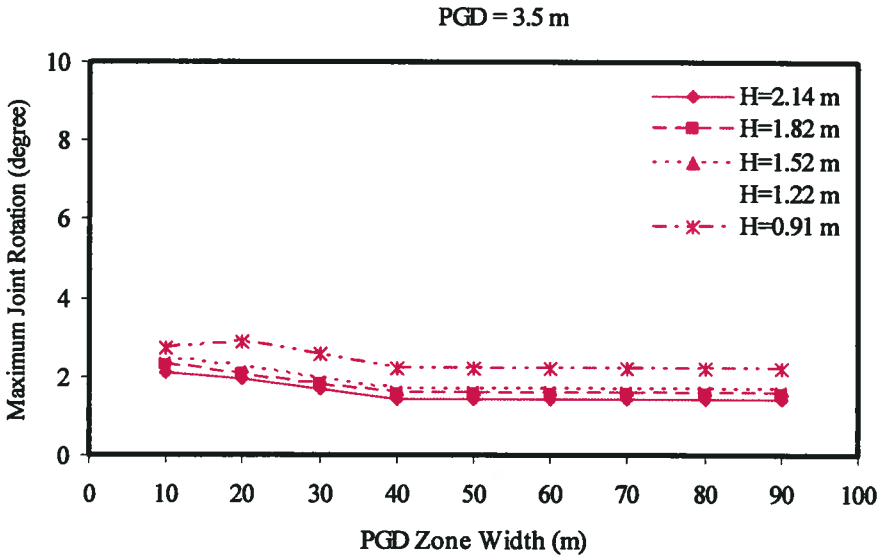


Figure 5.29 Effect of Burial Depth on the Joint Rotation of Segmented Vitrified Clay Pipe Subjected to Transverse PGD

# CHAPTER SIX

# MODELING OF REHABILITATED SEGMENTED PIPELINE UNDER SEISMIC EFFECTS

## 6.1 INTRODUCTION

Traditionally, sewers used to serve urban areas have been made from rigid materials such as concrete and vitrified clay. Over time, soil movements have tended to crack the rigid pipes where imposed strains could not be accommodated in the pipe joints, allowing infiltrations into the sewers of groundwater and of backfill materials enter the sewers and contribute to sedimentation. Deteriorated pipes require either complete expensive replacement or rehabilitation. Cured-in-place pipe CIPP is a rehabilitation technology used to provide a lining inside the deteriorated host pipe to prevent infiltration and to form a structurally sound new pipe as shown in Figure 6.1 (McAlpine, 2003). Rehabilitated buried pipelines (i.e., host pipe with liner) are often subjected to defects and/or damages from in-service (e.g., cracks), from manufacturing (e.g., out-of roundness imperfections). Other imperfections such as lack of adhesion between the encased liner and the host pipe can also strongly affect the collapse pressure of rehabilitated pipes (Tafreshi, 2004). Earthquake events can also cause damage to buried rehabilitated pipelines due to the forces and deformation imposed on them through interactions at the pipe-soil interface.

Over the past four decades, analytical solutions, experimental tests, and finite element analyses have been carried out by researchers in order to analyze the behaviours of rehabilitated pipes (see Tables 3.1 and 3.3). Despite the growing research interest outlined in the literature, the behaviours of rehabilitated pipes under seismic loads is not sufficiently understood nor adequately modeled at the present time.

The stability problem of rehabilitated segmented pipeline involves pure axial tensile or compressive stresses, bending stresses, and local delamination (i.e., debonding) between the liner and its host pipe, all of which lead to possible local buckling (see Figure 6.2). Delamination is the most frequent cause of defects and failure in laminated structures, particularly under compressive load and external pressures (Tafreshi, 2004). Like any other laminated materials, rehabilitated pipes have composite sections that suffer from liner debonding or delamination, which in turn may lead to premature failures. Delamination has an important effect on the stiffness loss of composite sections and can create a local instability that may lead to compressive failure. Such delamination may be induced in composite rehabilitated pipes due to manufacturing defects, installation consequences, transportation impacts, and/or environmental effects (e.g., host pipe cracks and groundwater leak) during the service life of the structural component (Rasheed, 1996).

The prediction of stress and strain in rehabilitated segmented pipe induced by transverse movement is important since they can lead to rupture or splitting of the fully bonded felt or to shear failure by debonding or delamination of the CIPP liner and the adhesive material (resin or epoxy) from the underlying pipe segments. Usually, delamination begins at the location of the segmented pipe joint and can lead to the CIPP liner material peeling from the pipe segment, surface. Furthermore, liner strain is affected by the method of cleaning and the surface preparation of the host pipe, as well as by the resin or epoxy type used, all of which will affect the entire cost of the rehabilitation process. This means that good cleaning and preparation of the deteriorated host pipe will allow for choosing of resin types with lower friction for the CIPP liner, which in turn will reduce the cost of the liner installation.

According to the literature available to date, there have been no previous studies addressing the effects of delamination on the structural capacity of rehabilitated pipes subjected to seismic effects. Thus, the present work is intended to address the current needs by developing a numerical model for rehabilitated joint behaviour under external loadings and/or seismic effects.

The aim of this research study is to develop finite element models for the joint structural behaviour of rehabilitated segmented pipeline under seismic loading conditions. Thus, the objective of the finite element modeling program is to investigate the delamination phenomenon at the host pipe-liner interface and to determine the axial and rotational stiffness and other characteristics that might influence the seismic behaviour of rubber gasket joints in rehabilitated segmented pipeline. These characteristics are the force-displacement as well as the moment-rotation behaviours of the joint in rehabilitated segmented pipeline. To the best knowledge of the author, no test results are available to validate and calibrate the finite element models. Therefore, the previous numerical models for joint behaviours (chapter 4) and seismic behaviours of buried segmented pipes (chapter 5) are developed and then used to study the joint behaviour as well as the delamination growth in rehabilitated buried segmented pipelines.

The present chapter begins with numerical analyses of two finite element models developed to simulate joints behaviour in rehabilitated segmented pipelines. The following sections present the application of these two numerical models in order to predict the delamination and the seismic behaviours of rehabilitated buried segmented pipelines. Finally, a parametric study is presented in section 6.4 to investigate the effects of the important parameters on the maximum pipe and liner strains for both longitudinal and transverse PGD effects.

## 6.2 PREDICTION OF AXIAL/BENDING BEHAVIOUR OF JOINTS IN REHABILITATED SEGMENTED PIPELINE

To the best knowledge of the author, no experimental data studying the structural behaviours of joints for rehabilitated concrete and vitrified clay pipes are available. However, studies do exist for the axial behaviour of rubber gasket joints in reinforced concrete cylinder pipes (see Bouabid, 1993; Bouabid and O'Rourke, 1994). Experimental work allowed the determination of the force-deformation relationship of joints in segmented pipe. As shown in chapter 4, the research of Bouabid (1993) and Bouabid and

O'Rourke (1994) was used as a benchmark to develop a finite element model that can be a tool to characterize the joint structural behaviour of concrete and vitrified clay pipes. These experimental results are compiled with materials properties of reinforced concrete pipes in order to calibrate and validate the finite element model which is investigating the axial behaviour of unrestrained joints in segmented pipes using ABAQUS.

The numerical modeling presented in this section focuses on the simulation of axial compression and bending behaviour of rehabilitated joints for the same material properties, contact conditions between the rubber gasket and the pipe segments, boundary conditions, and loading conditions used previously in chapters 4. The finite element models that are described in chapter 4 are modified by introducing a modeling of a CIPP liner inside the existing host segmented pipe (see Figures 6.1 and 6.2). Two types of CIPP liner are commonly used in the trenchless industry namely; polyester and vinylester liners. The properties of the CIPP liner materials considered in this study are given in Table 6.1 are adopted from ASTM F1216. The wall thicknesses of the CIPP liners predicted according to the standard ASTM F1216 (fully deteriorated case as described in chapter 3, section 3.2 and Table 3.1) are shown in Table 6.2. The finite element model is used to develop a simplified rheological constitutive model for the joint in order to predict the axial and rotational stiffnesses of rubber gasket joints in rehabilitated rigid pipes.

Since most of the expected non-linear behaviour will be concentrated in the joint behaviour, only the rehabilitated joint region will be investigated. The numerical model assumptions, geometry, material properties, contact interface, boundary conditions, and solution are the same (see section 4.2.3 and 4.3.3). As in chapters 4 and 5, the pipe material behaviour is assumed to be elastic. As in chapter 3, the liner material behaviour is considered to be elasto-plastic (short-term), based on the experimental tests data reported by Zhu (2000). All materials are assumed to be isotropic and homogenous throughout the wall thickness. For the axial behaviour modeling, by simplifying the pipe-liner section as a two-dimensional axisymmetric system, the pipe as well as the liner is discretized using axisymmetric solid elements. Using symmetry plane, only half of the

bell-spigot joint configuration of a rehabilitated segmented pipe is modeled. The convergence analysis shows that 13 elements must be used in the thickness of the host pipe, where a minimum of 2 layers of axisymmetric elements stacked in the wall thickness direction of the liner are needed. A typical mesh used in the analyses is shown in Figure 6.3.

For the compression/tension tests simulation, the rehabilitated pipe is assumed to be simply supported at one end while the incremental load is applied at the other end (see section 4.2.3). For bending tests modeling, both ends of the model are fixed while the joint is subjected to incremental bending loads (see section 4.3.3).

The interface between the pipe and the liner is simulated using a cohesive element (denoted as COH2D4 in ABAQUS). Cohesive elements can be used in all stress/displacement analysis types. Although they do not have any degrees of freedom other than displacement, they can be used in to bond together composite materials components to simulate mechanical failure of interfaces. Cohesive elements are useful in modeling adhesives and bonded interfaces. The connectivity of cohesive elements is like that of continuum elements, but it is composed of two faces separated by a very thin thickness (0.025 mm). The constitutive behavior of the cohesive elements is defined by a continuum-based model. The material properties of the cohesive element are assumed to be similar to the liner material (i.e., elasto-plastic). The cohesive elements model the initial loading, the initiation of delamination, and the propagation of debonding leading to eventual failure in the material. The interface between the liner and the cohesive element is modeled so that the lower surface of the cohesive element is fully bonded to the liner surface by using the SURFACE BEHAVIOUR, NO SEPARATION command. The interface between the pipe and the cohesive element is simulated using element-based contact surfaces of either full-slip or smooth interaction condition. The surfaces of the contact area for the cohesive element and the pipe are defined by the SURFACE command and the potential for contact is set up using CONTACT PAIR command. For the contact between the encased liners and the host pipe, it is useful to consider the two limit interface conditions in the contact region when the friction effect is considered. In

the development of the finite element model, it is possible to consider different contact conditions between the liner and the host pipe within a range between the perfectly smooth case and the fully bonded case by using different friction coefficients. The first condition assumes perfectly smooth contact where the liner can slip freely on the host pipe (no shear forces can be transmitted), while the second contact condition assumes a full bond between the host pipe and the liner (shear forces transmitted fully). Actually, these two conditions can be expected to give the upper and lower estimates of the ultimate pressures for a given material and geometric configuration. Two-dimensional finite element analysis has been performed to determine the stress and strain distributions across the adhesive bond thickness of the joint for rehabilitated segmented pipeline. Small-load increments are applied on the pipe-liner system till the ultimate load at which delamination onset occurs. The delamination is seen to grow along the interface surface of the liner and the host pipe at the joint region for axial/bending loadings as shown in Figure 6.4. Figure 6.5 shows the evolution of the delamination for the rehabilitated segmented pipeline under seismic effect with different contact conditions between the liner and the host pipe.

The results are illustrated in terms of an index called the delamination index and defined as the percentage between the delaminated length of the encased liner versus the total length of the host pipe. The delaminated length of the liner is estimated from the deformed shape of model as the distance between the delaminated nodes (see Figure 6.5). The applied loads to the rehabilitated segmented pipes are normalized with respect to the ultimate load. The Ultimate load is defined as the maximum load that allows delamination onset occurs. Figure 6.6a and b illustrates the delamination index with the normalized applied load for different types of loading in rehabilitated segmented pipe for full bond case. As is shown in these figures, the delamination index is an increasing function of the normalized applied force before the ultimate load; whereafter the delamination index is not significantly changed. Figures 6.4 and 6.6 also indicate that the delamination occurs at the joint zone and the average delamination indexes are 8% and 12% for the compression and tensile tests, respectively. This means that the loss in structural performance of the pipe-liner system will be kept to a minimum and that,

subsequently full-length rehabilitation may be not necessary to restore the pipeline hydraulic capacity since the delamination occurs in the joint region.

Furthermore, the bending tests of rubber gasket joints for ductile iron pipes carried out by Singhal (1984a, b) were used as a baseline to verify the finite element model developed in chapter 4 for predicting the moment-rotation response of the joints in segmented pipes. For the bending behaviour, the finite element model consists of axisymmetric elements with incompatible mode elements for both the pipe and the liner. These elements include incompatible modes for the purpose of improving the bending response (Hibbitt et al., 2005). For the bending tests simulation, the applied moments are normalized with respect to the ultimate bending moments of the rehabilitated segmented pipes. Figure 6.6c shows the predicted normalized moment vs. the delamination index obtained by the finite element models for the joints of reinforced concrete rehabilitated pipes for bending tests. As shown in this figure the delamination increases almost linearly with the applied moment up to 80% of the ultimate moment. At this point, the delamination reaches a constant maximum value. As the model reaches the maximum rotation, the bell and spigot come into contact and the behaviour of the joint becomes independent of the properties of the rubber gasket of the joint. This contact will cause the joint to fail, as a small increment in the rotation of the joint causes a large bending moment and excessive stress result. The figure also shows that for the bending loading; the average of the predicted delamination index is 20%, which means that the loss in the structural performance of the pipe-liner system will be relatively small and so subsequent full-length rehabilitation might not be necessary since the liner is peeled off through the joint region.

Figure 6.6 demonstrates that larger-diameter pipe has the smaller delamination index. This finding is due to the fact that the axial stiffness of the pipe and subsequently; the liner resistance to delaminate increase by increasing the wall thickness. Figure 6.7 shows a comparison between the predicted force-displacement relationships obtained by the finite element models for the non-rehabilitated (no liner) and the rehabilitated (with liner)

joints of reinforced concrete, non-reinforced concrete, and vitrified clay pipes for compression tests.

The comparison of the moment-rotation relationships obtained by the finite element models for the non-rehabilitated (no liner) and the rehabilitated (with liner) joints of reinforced concrete, non-reinforced concrete, and vitrified clay pipes for bending tests are shown in Figure 6.8. The simulated global behaviour of the rehabilitated segmented pipes has a similar trend to the results predicted in the previous chapter for non-rehabilitated segmented pipes. The axial/bending stiffnesses predicted for the rehabilitated segmented pipes are significantly larger than that for non-rehabilitated segmented pipes (see Tables 6.3 and 6.4). Both the elastic and the post-elastic axial/rotational stiffnesses are calculated directly by determining the slopes of the corresponding structural responses as shown in Tables 6.3 and 6.4. Numerical modeling results of the axial/bending behaviours of joints in rehabilitated segmented pipes show that the axial/rotational stiffness of the joint in non-reinforced concrete pipe is slightly larger than that in the vitrified clay pipe. However, it is found that the axial/rotational stiffness and the maximum compression load/bending moment is an increasing function of the diameter and the wall thickness of the rehabilitated pipe.

## 6.3 NUMERICAL MODELING OF SEISMIC BEHAVIOUR OF BURIED REHABILITATED SEGMENTED PIPELINE

From past events, it is recognized that permanent ground deformation PGD is the major source of failure in buried pipelines. When subjected to PGD, a segmented pipeline will deform in the axial direction and bend as it attempts to accommodate the transverse ground movement. The failure mode for pipe depends upon axial and flexural bending strains as well as upon the joint behaviour (O'Rourke, 1995). Permanent ground deformation can be divided into two components, namely longitudinal PGD (soil movement parallel to the pipe axis) and transverse PGD (soil movement perpendicular to the pipe axis). Similar to the response of continuous pipelines, the behaviour of a given buried segmented pipeline is a function of the type of PGD (e.g., longitudinal or

transverse), the amount of the peak ground movement δ, the width of the PGD zone W, and the pattern of ground movement within the zone (O'Rourke and Liu, 1999).

It is usually acknowledged that unrestrained joints permit pipe systems to absorb some transient displacements and permanent ground deformation PGD where the pipe sections act as rigid bodies and all movement occurs at the joints (Rucker and Dowding, 2000). As the rehabilitated pipe has more axial and bending joint stiffness in comparison to the non-rehabilitated pipe, the probability of failure at the joint zone of the deteriorated pipe may be reduced after rehabilitation because the stress levels in the host pipe wall will be reduced. However, the slip and debonding mechanisms are the most critical factors for rehabilitated pipe safety in seismic zones as they are closely related to the structural behaviour of the joints.

To the best knowledge of the author, neither numerical analysis nor experimental data studying the seismic behaviour of buried rehabilitated segmented pipes are available. Thus, the approach is extended and combined with the numerical model developed earlier to predict the joints behaviour of rehabilitated pipes in order to study the seismic effect on the buried rehabilitated segmented pipes. Two cases of axial and transverse PGD were considered to provide insight into the seismic behaviours of rehabilitated segmented pipeline systems. The idealized block pattern loading is used in the present study. For the transverse direction, the cosine function pattern proposed by O'Rourke (1989) was selected from among the possibilities.

The methodology for modeling segmented pipeline subjected to seismic effects is discussed in chapter 5. The geometry, material properties, and boundary conditions for the pipe and the joint used in chapters 4 and 5 were used for the numerical model of the seismic behaviour of buried rehabilitated segmented pipeline system. The material properties for the rehabilitated joint predicted in section 6.2 will be used for the numerical simulations (see Tables 6.3 and 6.4 as well as Figures 6.7 and 6.8). The rehabilitated buried pipe system was modeled using a beam element for both the liner and the host pipe, and the rehabilitated joint behaviour was represented by bi-linear springs in

the axial and transverse directions. The pipe-soil interaction was modeled using a bi-linear spring element to connect the pipe to the soil. The characteristics at the soil pipe interface were estimated using the formulas given in the TCLEE guideline (ASCE, 1984), based upon the mean soil properties given in Table 5.2 (see Appendix B). The solution will be static and the ground displacements, as reported in chapter 5, were assumed to be symmetric across the width of the PGD zone while the maximum displacements occurred at the center.

The contact between the host pipe and the liner is simulated using tube-to-tube contact element (denoted as ITT21 in ABAQUS) could model the finite sliding interaction between two pipelines or tubes where one tube lies inside the other. In this contact it is assumed that the inner tube (i.e., liner) can be considered the slave surface and the outer tube (i.e., rehabilitated pipe) is the master surface. Furthermore, this contact assumes a finite clearance between the two tubes, which has the effect that the separation distance is finite even when contact occurs. The relative motion of the two tubes or pipes is predominantly along a slide line defined by the axis of one of the tubes where the relative rotations of the pipe axis are assumed to be small and the radial clearance between the host pipe and the encased liner. This model prevents penetration between contact surfaces. In this study, the interface along the slide line is assumed to be a frictional adhesive one with a conventional Coulomb friction model. The basic concept of this model is to relate the maximum frictional (i.e., shear) stress across an interface to the contact pressure between the contacting bodies. In the basic form of the Coulomb friction model, two contacting surfaces can carry shear stresses up to a certain magnitude across their interface before they start sliding relative to one other; this state is known as sticking. The Coulomb friction model defines this critical shear stress, at which sliding of the surfaces starts as a fraction of the contact pressure. This fraction is known as the coefficient of friction.

For the contact between the encased liners and the host pipe, it is usually accepted that there are two distinct interface conditions in the contact region when the friction effect is considered. One is the fully bond case (i.e., friction coefficient = 1) and the other is the

fully slip case (i.e., friction coefficient = 0). Actually, these two conditions can be expected to be the upper and lower estimates of stress levels for a given material and geometric configuration. Three different pipe materials with five different contact conditions (i.e., different friction coefficients, namely: 0, 0.25, 0.5, 0.75, and 1) cover the range of the two cases that are considered in these analyses.

Tables 6.5, 6.6, 6.7, and 6.8 present the seismic maximum host pipe and liner strains for rehabilitated segmented pipelines subjected to longitudinal and transverse PGD, respectively. The predicted strains are normalized with respect to the ultimate strains of the liner and the host pipe (referred to as the normalized maximum strain). Ultimate strain is defined as the maximum strain that allows delamination onset occurs. Figure 6.9 shows the numerical simulation model results for rehabilitated pipeline subjected to longitudinal PGD, while Figure 6.10 illustrates the numerical simulation model results for rehabilitated pipeline subjected to transverse PGD. The results of these figures as well as the effect of the liner material, the PGD amount, and the PGD zone width are discussed in more details in the following sections.

## 6.4 PARAMETRIC STUDIES OF SEISMIC ANALYSIS OF BURIED REHABILITATED SEGMENTED PIPELINE

In practice, collapse or cracking may occur in buried pipeline networks if the systems are not designed properly. For rehabilitated pipes, the condition of the host pipe and the liner should be examined thoroughly. The present study aims to gain a good understanding of the important parameters that affect the seismic behaviours of buried rehabilitated segmented pipelines with unrestrained rubber gasketed joints. In fact, many parameters have a significant influence on the stress and strain distribution in the liner's and pipe's walls. The parameters of interest include the material of the host pipe, the material of the liner, host pipe-liner interaction condition, liner wall thickness variation, and host pipe stiffness variation.

A parametric study was conducted using the finite element model by considering three different host pipe materials with two different CIPP liner materials and five different interface friction conditions. The same boundary conditions and PGD pattern types used for the validation were assumed in the parametric study.

Both the results of the seismic behaviours of buried segmented pipelines and the numerical modeling results of the seismic behaviours of buried rehabilitated segmented pipelines show that the maximum pipe strain due to transverse affects is larger than that due to longitudinal effects (see Tables 6.5 and 6.6 for the longitudinal PGD case and Tables 6.7 and 6.8 for the transverse PGD case). Hence, transverse PGD appears more likely to cause damage to segmented pipes than does longitudinal PGD for the range of nominal diameters considered in this study.

It should be noted that modeling the complex behaviour of reinforced concrete, which is both non-homogenous and anisotropic, was simplified in the model by using elastic–perfectly plastic material. No significant cracking effects were anticipated in these typical small diameters pipes because the tensile/compressive stresses are relatively low.

### 6.4.1 EFFECT OF HOST PIPE MATERIAL

Sewers and water distribution pipes are manufactured of different materials including reinforced concrete, non-reinforced concrete and vitrified clay. Finite element analyses were performed to examine the effect on the host pipe material type of the seismic behaviour of a rehabilitation pipeline system subjected to longitudinal and transverse PGD. Results of the analyses as shown in Figures 6.9 and 6.10 for the axial and transverse PGD, respectively, indicate that as the stiffness of the host material increases, the levels of stresses and strains in the CIPP liner decrease. In both PGD cases, the similarity in the trend of the maximum pipe strain prediction had shown in these figures results from assumed material homogeneity throughout the pipe wall thickness. This indicates that the material properties do not have a great influence on the maximum strain of the encased liner. By comparing these figures, it is clear that the performance of the

reinforced concrete pipe is better than those of the other types under study (i.e., non-reinforced concrete and vitrified clay pipe). However, the stresses and strains in the CIPP liners did not significantly differ in the cases of reinforced concrete, non-reinforced concrete, and vitrified clay host pipes. This is due to the fact that delamination between the rigid rehabilitated pipe and the flexible liner occurs when there is significant micro-cracking of the liner resin (in shear or tension or both) as the ultimate load at which the delamination commences is fairly close to the estimated tensile and flexural strength of the liner resin.

### 6.4.2 EFFECT OF CONTACT CONDITION

Finite element analyses were conducted on three different host pipe materials to be rehabilitated with two different CIPP liner materials. This analysis was carried out to investigate different interface conditions between the host pipe and the inner liner. Five types of interface friction conditions were examined with friction coefficients in the range of 0 to 1, which represents the complete range of interaction from full slip case to full bond case. This analysis is recommended for the design of lined pipes since it is extremely difficult to determine the exact interaction condition in the field, which usually is somewhere between those two extreme cases (WEF, 1994). The liner-pipe system can be structurally designed either as a flexible pipe (if no strong bond exists between the liner and the host pipe), or as a rigid pipe (if a perfect bond exists between the liner and host pipe). No bonding case represents the interface slip, which is similar to the flexible pipe design condition. A full bonding exists where the interface between the host pipe and the surrounding soil is totally rough, which is similar to the case of a composite pipe condition (Chunduru, 1996). All other interface conditions would be similar to the case of a rigid pipe design condition where the degree of rigidity varies from no strength to full strength.

Results of these analyses indicate that for various friction conditions between the liner and the host pipe, liner strains increase linearly with the coefficient of friction. The higher friction coefficient will lead to high adhesion between the liner and the host pipe. This

will create more resistance for micro-cracking by increasing the friction energy which will cause larger strains. This means that increasing the friction coefficient stabilizes the delamination between the host pipe and the liner. The results are illustrated in Figure 6.9a for the longitudinal PGD case and in Figure 6.10a for the transverse PGD case, indicating that liner strains are increasing function of the coefficient of friction and independent from the pipe material. The liner strains for the full bond case are increased by an average of 20% and 46% when compared with the condition of elastic slip interface, for the longitudinal PGD case and the transverse PGD case, respectively. It is observed that for the analyzed numerical models, the maximum strains corresponding to fully smooth and full bond are not identical. Therefore, ignoring the effect of contact between the encased liner and the host pipe can lead to incorrect estimations of the maximum seismic strains.

Bakeer and Guice (1997) test results showed that even for a well processed lining system, there would be some appreciable annular space in the liner-pipe system due to various reasons such as tolerances in pipe dimension, and radial expansion in the pipeline material during installation. Therefore, it is expected that a full interaction between the host pipe and the liner does not exist in the field conditions. Thus, in practice, the condition of an elastic slip interface would be more representative than would be a rough interface condition under the most common behaviour of the soil surrounding the deformed/reformed liner system in a typical field condition.

### 6.4.3 EFFECT OF PIPE STIFFNESS

To explore the effect of the pipe stiffness on the seismic response of buried segmented pipelines reduction values for the pipe stiffness varying from 10% to 50% were used. This is done by reducing the modulus of elasticity of the host pipe material by 10% to 50% to reflect the effect of aging. As shown in Figure 6.9b for the longitudinal PGD case as well as in Figure 6.10b for the transverse PGD case, the results indicate that the 50% reduction in the pipe stiffness led to an average of 52% reduction in the pipe strain. This is due to the fact that the reduction in the pipe wall stiffness will increase the strain throughout the wall thickness. Therefore, the long-term design of an encased liner should

be accounted for the condition of a completely deteriorated host pipe with higher yield stresses and strains. This is true because the condition of a completely deteriorated host pipe is similar to the condition of an unsupported CIPP liner in a host pipe. The slight differences in the host pipe and liner strain predictions may be attributed to the different strengths of material used for the rigid pipes and the flexible liners.

### 6.4.4 EFFECT OF LINER THICKNESS

For both the longitudinal and the transverse PGD cases, the effect of the liner thickness on the seismic responses of buried rehabilitated segmented pipelines were investigated using liner thickness increment values varying between 0% to 100% of the original liner thickness.

Figure 6.9c for the longitudinal PGD case and Figure 6.10c for the transverse PGD case show the effects of liner thickness variation on the predicted strains. The results indicate that when the liner thickness is increased by 100 % (i.e., twice the original liner thickness) then the liner strain reduces by 58% and 49% in comparison with liner strain for the original thickness, for the longitudinal PGD case and the transverse PGD case, respectively. This led to the smallest joint displacements in the pipelines for the longitudinal PGD and the lowest joint rotations for the transverse PGD. This is significant as the resistance of the liner against the axial and bending loadings will protect the host pipeline from leakage or failure at relatively small permanent ground displacements.

### 6.4.5 EFFECT OF LINER MATERIAL

To study the effects of the liner material on the seismic responses of buried rehabilitated segmented pipelines, two liner material types were considered namely; (i) polyester CIPP liner, and (ii) vinylester CIPP liner. While both materials (i.e., polyester and vinylester resins) form chains of molecules that wrap themselves around the CIPP liner fiber, vinylester resin has a longer distance between cross-links and considered a hybrid form of polyester resin. This gives the vinylester superior adhesive properties than the

polyester which greatly increase the strength of the interface between the host pipe and the liner. For this reason, the polyester resin can fracture easily and is substantially weaker than the vinylester resin. Thus, the CIPP liner fibers can pull-out of the polyester resin more easily when stressed. The properties of the liner materials considered in the analyses are given in Table 6.1. Results of the analyses shown in Figures 6.11a and b for the longitudinal and transverse PGD cases indicate that vinylester CIPP liner performance is slightly better than that of the polyester CIPP liner because the strains in the CIPP liner with vinylester resin are less within an average of 5% than of the polyester resin. Therefore, it is clear that the higher adhesive rigidity of the vinylester resin will lead to lower strains in the liner. Figures 6.11a and b also show that the liner strain is reduced by an average of 50% for both the longitudinal and the transverse PGD when the liner thickness is doubled. However, this work confirms that the seismic response of both types of liner is similar as both liners will be delaminated from their host pipe.

### 6.4.6 EFFECT OF PGD AMOUNT

The effects of the PGD amounts on the seismic responses of buried rehabilitated segmented pipelines was investigated using transverse PGD amount increment values varying between 0.5 m to 3.5 m for the transverse PGD. Figure 6.12a shows the effect of PGD amount variation on the predicted delamination index. The results show that delamination index is increased by an average of 130% as the PGD amount is increased from 0.5 m to 3.5 m. This reflects the fact that the larger increment of the PGD magnitude led to the larger delamination index in the rehabilitated pipeline. This is due to the largest joint rotation for the transverse PGD. This is significant as the resistance of the liner against the bending loadings will protect the host pipeline from leakage or failure at relatively small permanent ground displacements. This figure also illustrate that the delamination index is an increasing function of the PGD width and this index is increased by an average of 30% when the PGD width is increased from 10 m to 40 m.

### 6.4.7 EFFECT OF PGD ZONE WIDTH

The effect of the PGD zone width on the seismic responses of buried rehabilitated segmented pipelines was investigated using PGD zone width increment values varying between 10 to 90 m for the transverse PGD. Figure 6.12b shows the effect of PGD zone width variation on the estimated delamination index. The results show that delamination index is reduced by an average of 68% as the PGD width is increased from 10 m to 90 m. This indicates that the larger increment of the PGD zone width led to the smaller delamination index in the rehabilitated pipeline. This is due to the lowest joint rotation for the transverse PGD for larger PGD zone width where the PGD effect is distributed on to more joints. Furthermore, this figure also reflects that the delamination index is a decreasing function of the burial depth and this index is decreased by an average of 11% when the burial depth is increased from 0.91 m to 2.14 m.

## 6.5 SUMMARY AND CONCLUSIONS

This chapter deals with the numerical modeling of delamination of rehabilitated segmented buried pipelines. Finite element analyses procedures considering friction effects in the contact boundary are proposed to predict the axial behaviour, the flexural behaviour of the unrestrained joint, and the delamination index in rehabilitated segmented pipeline under external loads or seismic effects. To study the effects of delamination on rehabilitated segmented buried pipelines, finite element analyses are developed based on previous verified numerical models for joint behaviours and seismic analyses of buried segmented pipelines. Two finite element models were developed to simulate the delamination between the encased liner and the host pipe. Further, two finite element models are developed to investigate the seismic analyses of buried rehabilitated segmented pipelines under longitudinal and transverse PGD.

A review of the numerical simulation of rehabilitated joint behaviour and the major effects of the longitudinal and transverse PGD on the seismic behaviour of buried rehabilitated segmented pipelines led to the following conclusions:

1. It is shown that the liner strains are increasing function of the coefficient of friction and independent from the pipe material. The liner strains for the full bond case are increased by an average of 20% and 46% when compared with the condition of elastic slip interface, for the longitudinal PGD case and the transverse PGD case, respectively.

2. It can be observed that the delamination index is an increasing function of the applied load. The results of the study indicate that the delamination occurs at the joint zone and the average delamination indexes are 8%, 12% and 20% for the compression, tensile and bending loading, respectively. The presence of delamination does not significantly change the ultimate load of the rehabilitated joints. However, for a large delamination index, the ultimate load is not related to the load-carrying capacity of the system and any failure will be due to the delamination growth, which in turn depends on the fracture toughness of the material. It is also shown that ignoring the effect of contact between the encased liner and the host pipe can lead to incorrect estimations of the delamination index.

3. The results demonstrate that only the joint region is delaminated. Thus, full-length rehabilitation of segmented pipeline is not required unless the hydraulic capacity of the pipe is required to be restored, which will reduce significantly the cost of the rehabilitation process. Nevertheless, to investigate the bonding capability of the rehabilitated pipe using CIPP trenchless technology, it is recommended that more experimental work for the peel test is required for better understanding for the delamination phenomenon under different types of loading.

4. Longitudinal and bending strains increase toward the joint region but drop significantly at the ends of rehabilitated segmented pipeline. For the models considered, the ultimate load of the joint of rehabilitated segmented pipeline is about 1.25 times the ultimate load of the joint of segmented pipeline without the liner. This means that the rehabilitated joint could absorb slightly these amounts of deformations, and therefore slightly increase the seismic durability of the segmented pipes renovated by the CIPP liner. The encased liner

is debonded or delaminated at the joint region, resulting in a decrease in the rigidity of the joint when the axial and flexural loads are increased. However, this work confirms that the seismic response of both types of liner is similar as both liners will be delaminated from their host pipe at the joint region. This means that the delamination process is independent of the liner material. Thus, there is an urgent need for research to develop new techniques to modify the structural behavior of the joint or to use two liners at the joint region so that the joint will have more resistance under earthquake events.

5. The results of effects of the liner thickness on the seismic responses of buried rehabilitated segmented pipelines indicate that the liner strain is a decreasing function of the liner thickness. The results indicate that when the liner thickness is increased by 100 % (i.e., twice the original liner thickness) then the liner strain reduces by 58% and 49% in comparison with liner strain for the original thickness, for the longitudinal PGD case and the transverse PGD case, respectively. On the other hand, the results of effects of the pipe stiffness show that 50% reduction in the pipe stiffness led to an average of 52% reduction in the pipe strain. However, variation in the liner wall thickness has more impact on the seismic response of buried rehabilitated segmented pipes than does the host pipe stiffness. The reason for this is most probably related to the fact that the liner stiffness is proportional to the cube of the wall thickness, and the higher stiffness will give a smaller strain.

6. It is clear that the structural performance of the reinforced concrete pipe is better than those of the non-reinforced concrete and vitrified clay pipes. However, the stresses and strains in the CIPP liners did not significantly differ in the cases of reinforced concrete, non-reinforced concrete, and clay host pipes.

7. The numerical modeling approach established in this work offers high potential for further investigation and development in conjunction with fracture mechanics concepts in order to better understand the delamination phenomenon in rehabilitated pipelines under different types of loadings. Thus, the onset and growth of other damage mechanisms such as liner fiber fracture and host pipe cracking should be taken into account in the analyses

when trying to predict the joint behaviour accurately. To fully study the effect of the fractures on the complex soil-pipe-liner system, it is important to model these fractures explicitly. Extra work is required to model the time-dependent behaviour of the polymer liner material and to evaluate its effects on the variation of the critical strains and stresses with time. Furthermore, for better understanding of the delamination phenomenon under different types of loading, it is recommended that more experimental work for the peel test (ASTM D903) is required for the rehabilitated pipe using CIPP trenchless technology.

Table 6.1 CIPP Liner Materials Properties

| Material | Modulus of Elasticity ($E$) MPa (psi) | Poisson's Ratio ($\nu$) | Flexural Strength (ASTM D790) MPa (psi) | Tensile Strength (ASTM D638) MPa (psi) |
|---|---|---|---|---|
| CIPP-Polyester Resin | 1724 (250000) | 0.30 | 31.03 (4500) | 20.68 (3000) |
| CIPP-Vinylester Resin | 2070 (300000) | 0.30 | 34.47 (5000) | 27.58 (4000) |

Table 6.2 Wall Thickness Design for CIPP Liner (ASTM F1216)

Partially Deteriorated Case (Circular Host Pipe - Ovality $q$ = 0%)

| Liner Resin Type | Liner Wall Thickness ($t$) (mm) | | | $SDR=D/t$ | | |
|---|---|---|---|---|---|---|
| | 200 mm | 250 mm | 300 mm | 200 mm | 250 mm | 300 mm |
| CIPP-Polyester | 2.219 | 2.774 | 3.329 | 91.563 | 91.563 | 91.563 |
| CIPP-Vinylester | 2.089 | 2.612 | 3.134 | 97.256 | 97.256 | 97.256 |

*hydrostatic pressure only

Table 6.3 Comparison of Axial Stiffness of Joints for Rehabilitated and Not-Rehabilitated Rigid Pipes Predicted from FE Models of Compression Tests

| Pipe Material | Pipe Condition | Joint Elastic Stiffness (N/mm) | | | Joint Post-Elastic Stiffness (N/mm) | | |
|---|---|---|---|---|---|---|---|
| | | 200 mm | 250 mm | 300 mm | 200 mm | 250 mm | 300 mm |
| Reinforced Concrete (Wall B) | No-Liner | 12461 | 12807 | 13455 | 2484 | 2567 | 2615 |
| | With Liner | 15259 | 15767 | 16874 | 3255 | 3392 | 3486 |
| Non-Reinforced Concrete (Class II) | No-Liner | 5156 | 5678 | 6313 | 751 | 832 | 840 |
| | With Liner | 6338 | 7106 | 8025 | 976 | 1095 | 1111 |
| Vitrified Clay (Class 160) | No-Liner | 5607 | 5679 | 5775 | 846 | 909 | 977 |
| | With Liner | 6810 | 7074 | 7476 | 1126 | 1231 | 1321 |

Table 6.4 Comparison of Rotational Stiffness of Joints for Rehabilitated and Not-Rehabilitated Rigid Pipes Predicted from FE Models of Bending Tests

| Pipe Material | Pipe Condition | Joint Elastic Stiffness (N-mm/deg) | | | Joint Post-Elastic Stiffness (N-mm/deg) | | |
|---|---|---|---|---|---|---|---|
| | | 200 mm | 250 mm | 300 mm | 200 mm | 250 mm | 300 mm |
| Reinforced Concrete (Wall B) | No-Liner | 141420 | 146788 | 164333 | 5544 | 7884 | 9615 |
| | With Liner | 169923 | 179295 | 204031 | 7277 | 10506 | 12900 |
| Non-Reinforced Concrete (Class II) | No-Liner | 40650 | 42565 | 46132 | 3960 | 5642 | 6893 |
| | With Liner | 48913 | 52550 | 56390 | 5190 | 7456 | 9272 |
| Vitrified Clay (Class 160) | No-Liner | 65644 | 67904 | 78185 | 2147 | 2599 | 4858 |
| | With Liner | 80096 | 83675 | 98866 | 2837 | 3523 | 6002 |

Table 6.5 Seismic Maximum Pipe Strains for Rehabilitated Segmented Pipes Due to Longitudinal PGD

| Pipe Type | Inner Diameter (mm) | Seismic Maximum Pipe Strain (x 0.00001) | | | | | | | |
|---|---|---|---|---|---|---|---|---|---|
| | | Longitudinal PGD amount δ (m) | | | | | | | |
| | | 0.1 | 0.2 | 0.3 | 0.4 | 0.5 | 0.6 | 0.7 | 0.8 |
| Reinforced Concrete (Wall B) | 200 | 0.424 | 1.346 | 1.713 | 1.995 | 2.096 | 2.383 | 2.397 | 2.403 |
| | 250 | 0.378 | 1.130 | 1.510 | 1.782 | 1.992 | 2.154 | 2.245 | 2.250 |
| | 300 | 0.320 | 0.904 | 1.310 | 1.553 | 1.808 | 1.972 | 2.058 | 2.018 |
| Non-Reinforced Concrete (Class II) | 200 | 0.780 | 1.755 | 2.600 | 3.375 | 3.818 | 4.058 | 4.249 | 4.259 |
| | 250 | 0.602 | 1.463 | 2.155 | 2.718 | 3.241 | 3.588 | 3.702 | 3.711 |
| | 300 | 0.434 | 1.123 | 1.700 | 2.150 | 2.596 | 2.828 | 2.982 | 2.990 |
| Vitrified Clay (Class 160) | 200 | 1.211 | 2.109 | 2.685 | 3.128 | 3.498 | 3.634 | 3.759 | 3.768 |
| | 250 | 1.009 | 1.829 | 2.433 | 2.793 | 3.123 | 3.322 | 3.458 | 3.466 |
| | 300 | 0.867 | 1.526 | 2.053 | 2.435 | 2.834 | 3.092 | 3.249 | 3.257 |

Table 6.6 Seismic Maximum Pipe Strains for Rehabilitated Segmented Pipes Due to Transverse PGD

| Pipe Type | Inner Diameter (mm) | Seismic Maximum Pipe Strain (x 0.001) | | | | | | |
|---|---|---|---|---|---|---|---|---|
| | | Transverse PGD amount δ (m) | | | | | | |
| | | 0.5 | 1 | 1.5 | 2 | 2.5 | 3 | 3.5 |
| Reinforced Concrete (Wall B) | 200 | 0.824 | 1.034 | 1.248 | 1.441 | 1.624 | 1.776 | 1.773 |
| | 250 | 0.710 | 0.901 | 1.073 | 1.232 | 1.416 | 1.498 | 1.496 |
| | 300 | 0.566 | 0.778 | 0.921 | 1.020 | 1.110 | 1.187 | 1.185 |
| Non-Reinforced Concrete (Class II) | 200 | 2.577 | 3.237 | 3.725 | 4.041 | 4.279 | 4.401 | 4.394 |
| | 250 | 1.619 | 2.023 | 2.316 | 2.492 | 2.690 | 2.847 | 2.842 |
| | 300 | 0.944 | 1.214 | 1.368 | 1.455 | 1.494 | 1.600 | 1.597 |
| Vitrified Clay (Class 160) | 200 | 1.897 | 2.381 | 2.873 | 3.318 | 3.739 | 4.088 | 4.081 |
| | 250 | 1.635 | 2.075 | 2.470 | 2.835 | 3.260 | 3.449 | 3.443 |
| | 300 | 1.304 | 1.791 | 2.120 | 2.350 | 2.555 | 2.733 | 2.729 |

Table 6.7 Seismic Maximum Liner Strains for Rehabilitated Segmented Pipes Due to Longitudinal PGD

| Host Pipe Type | Inner Diameter (mm) | Seismic Maximum Liner Strain (x 0.00001) | | | | | | | |
|---|---|---|---|---|---|---|---|---|---|
| | | Longitudinal PGD amount δ (m) | | | | | | | |
| | | 0.1 | 0.2 | 0.3 | 0.4 | 0.5 | 0.6 | 0.7 | 0.8 |
| Reinforced Concrete (Wall B) | 200 | 0.361 | 1.143 | 1.452 | 1.707 | 1.796 | 2.010 | 2.029 | 2.034 |
| | 250 | 0.322 | 0.960 | 1.280 | 1.525 | 1.707 | 1.817 | 1.901 | 1.904 |
| | 300 | 0.273 | 0.768 | 1.110 | 1.329 | 1.549 | 1.664 | 1.742 | 1.708 |
| Non-Reinforced Concrete (Class II) | 200 | 0.665 | 1.491 | 2.204 | 2.888 | 3.271 | 3.423 | 3.598 | 3.605 |
| | 250 | 0.513 | 1.243 | 1.827 | 2.326 | 2.777 | 3.027 | 3.134 | 3.141 |
| | 300 | 0.370 | 0.954 | 1.441 | 1.840 | 2.224 | 2.386 | 2.525 | 2.531 |
| Vitrified Clay (Class 160) | 200 | 1.032 | 1.792 | 2.276 | 2.677 | 2.997 | 3.066 | 3.183 | 3.189 |
| | 250 | 0.860 | 1.554 | 2.062 | 2.390 | 2.676 | 2.802 | 2.928 | 2.934 |
| | 300 | 0.739 | 1.296 | 1.740 | 2.084 | 2.428 | 2.608 | 2.751 | 2.757 |

Table 6.8 Seismic Maximum Liner Strains for Rehabilitated Segmented Pipes Due to Transverse PGD

| Host Pipe Type | Inner Diameter (mm) | Seismic Maximum Liner Strain (x 0.001) | | | | | | |
|---|---|---|---|---|---|---|---|---|
| | | Transverse PGD amount δ (m) | | | | | | |
| | | 0.5 | 1 | 1.5 | 2 | 2.5 | 3 | 3.5 |
| Reinforced Concrete (Wall B) | 200 | 0.678 | 0.863 | 1.022 | 1.183 | 1.328 | 1.454 | 1.456 |
| | 250 | 0.584 | 0.752 | 0.879 | 1.012 | 1.158 | 1.227 | 1.228 |
| | 300 | 0.465 | 0.650 | 0.755 | 0.838 | 0.907 | 0.972 | 0.973 |
| Non-Reinforced Concrete (Class II) | 200 | 2.119 | 2.703 | 3.052 | 3.318 | 3.498 | 3.604 | 3.608 |
| | 250 | 1.331 | 1.689 | 1.897 | 2.046 | 2.199 | 2.331 | 2.334 |
| | 300 | 0.776 | 1.014 | 1.121 | 1.195 | 1.221 | 1.310 | 1.311 |
| Vitrified Clay (Class 160) | 200 | 1.560 | 1.988 | 2.354 | 2.725 | 3.057 | 3.348 | 3.351 |
| | 250 | 1.344 | 1.733 | 2.024 | 2.328 | 2.665 | 2.824 | 2.827 |
| | 300 | 1.072 | 1.495 | 1.737 | 1.930 | 2.089 | 2.238 | 2.241 |

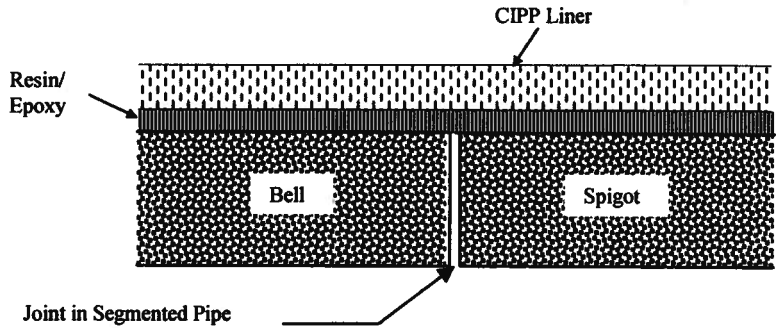


Figure 6.1 Joint Configuration of Rehabilitated Pipe (CIPP Liner).

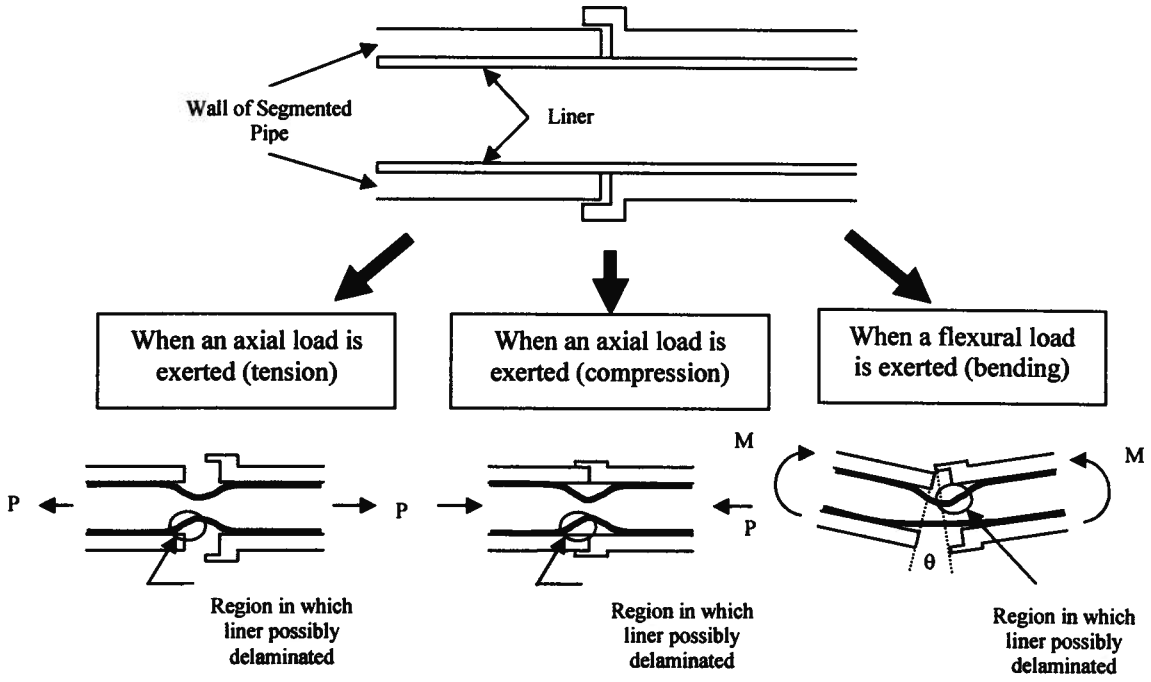


Figure 6.2 Behaviour of Rehabilitated Pipe at the Joint Region under Different Types of Loading.

(a) Full Model Mesh for Rehabilitated Segmented Pipe

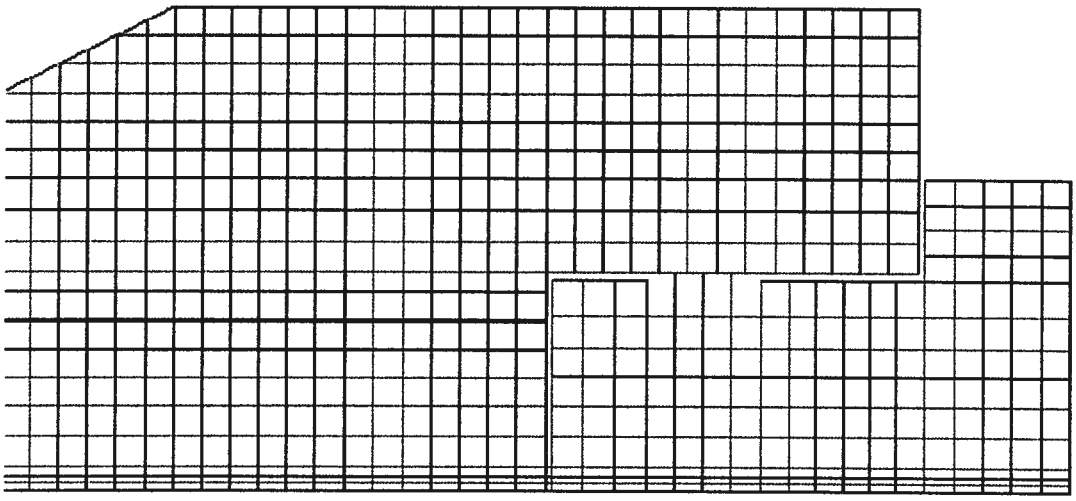


(b) Enlargement for Full Model Mesh at Inner Side of Rehabilitated Segmented Pipe

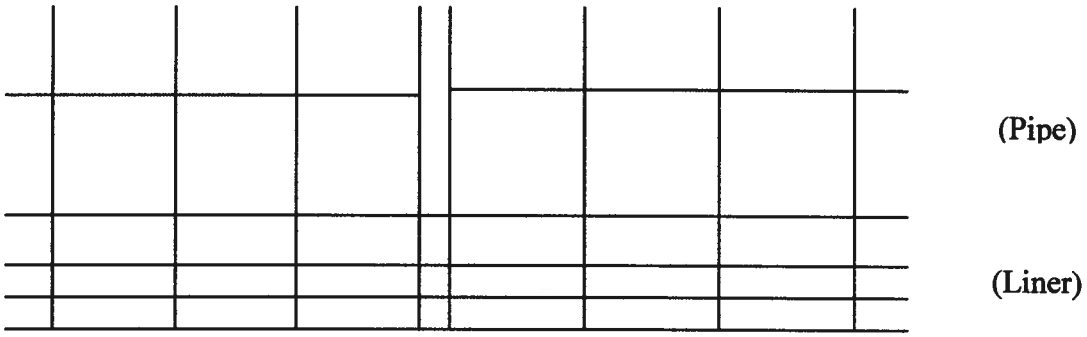


(c) Enlargement for Full Model Mesh at Host Pipe-Liner Interface

Figure 6.3 Finite Element Mesh used for Joint Modeling in Rehabilitated Segmented Pipe

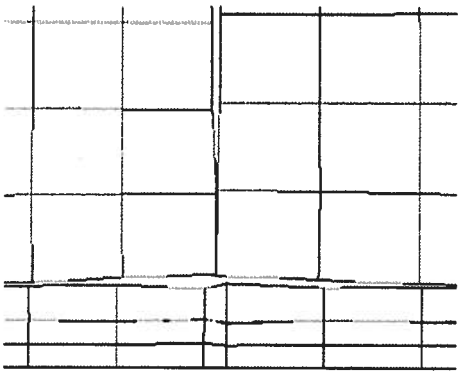


(a) Compressive Loading

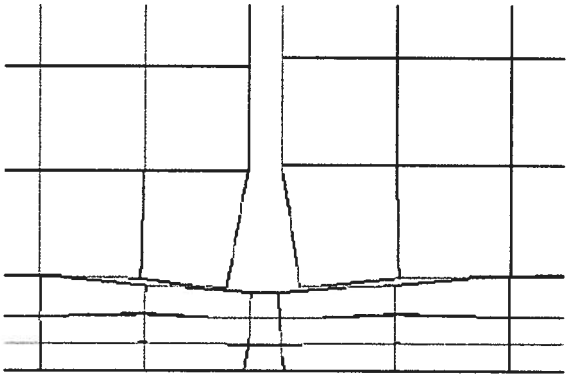


(b) Tensile Loading

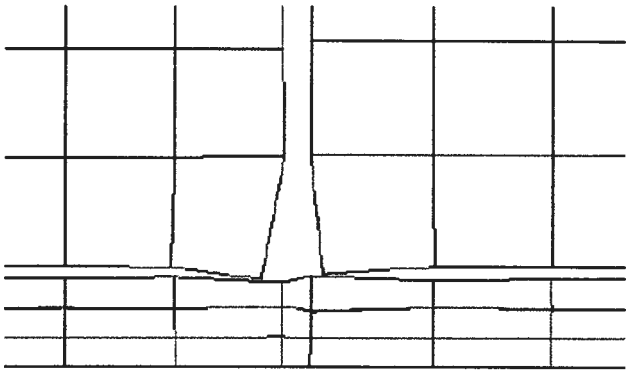


(c) Bending Loading

Figure 6.4 Delamination of CIPP Liner at the Joint for Different Types of Loading in Rehabilitated Segmented Pipe (Full Bond)

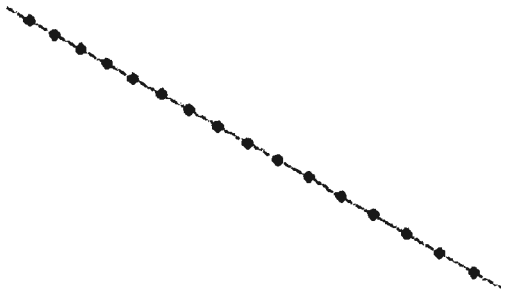

(a) Longitudinal PGD (Full Bond, friction coefficient = 1)

(b) Transverse PGD (Full Bond, friction coefficient = 1)

(c) Transverse PGD (Half Bond, friction coefficient = 0.5)

Figure 6.5 Delamination Evolution of CIPP Liner in Rehabilitated Segmented Pipeline for Different Types of Seismic Loading

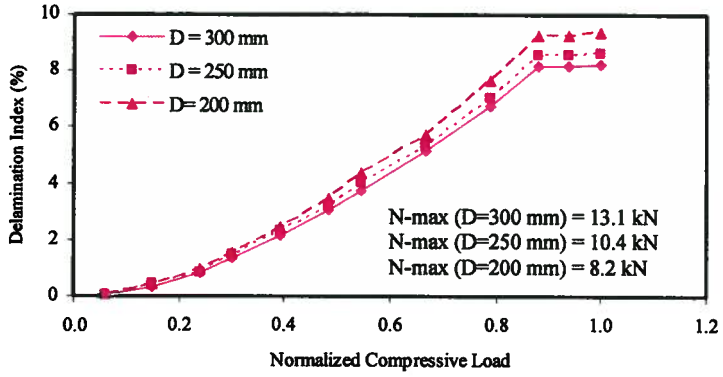


(a) Compressive Loading

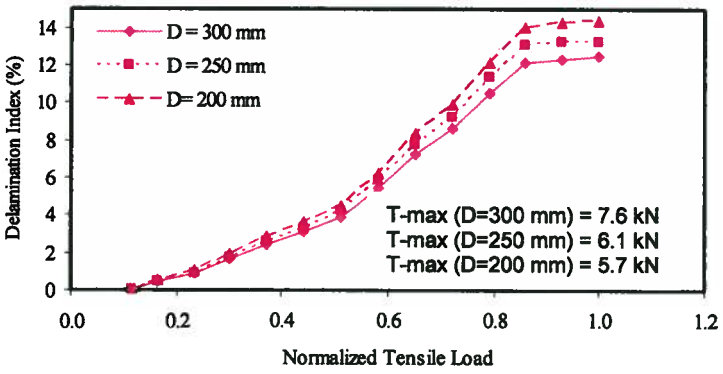


(b) Tensile Loading

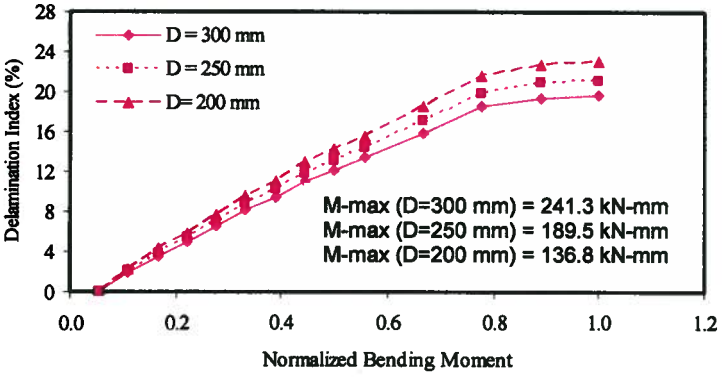


(c) Bending Loading

Figure 6.6 Delamination Index of CIPP Liner at the Joint for Different Types of Loading in Rehabilitated Segmented Pipe (Full Bond)

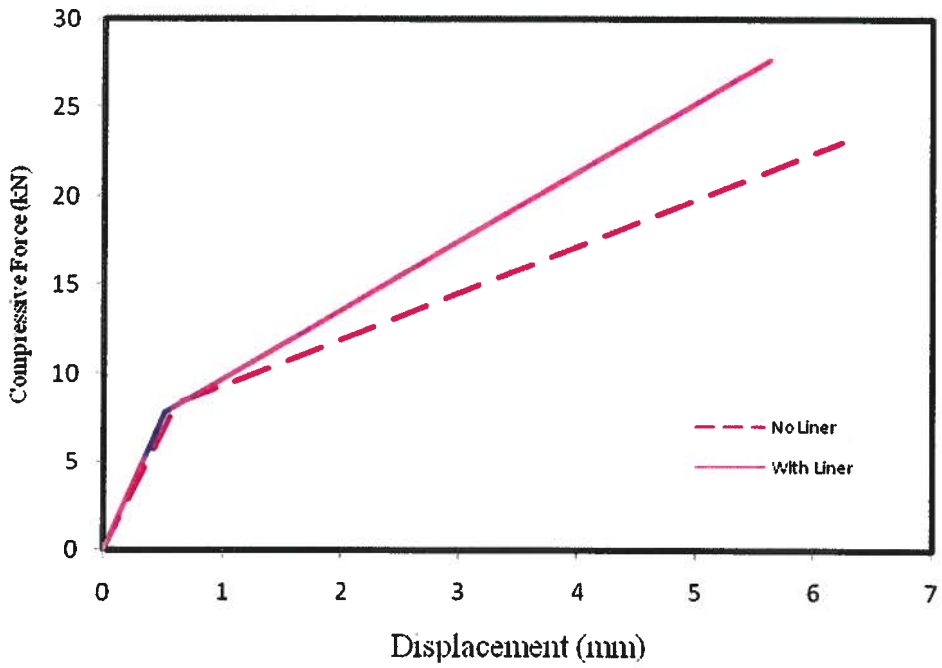


(a) Reinforced Concrete Pipes

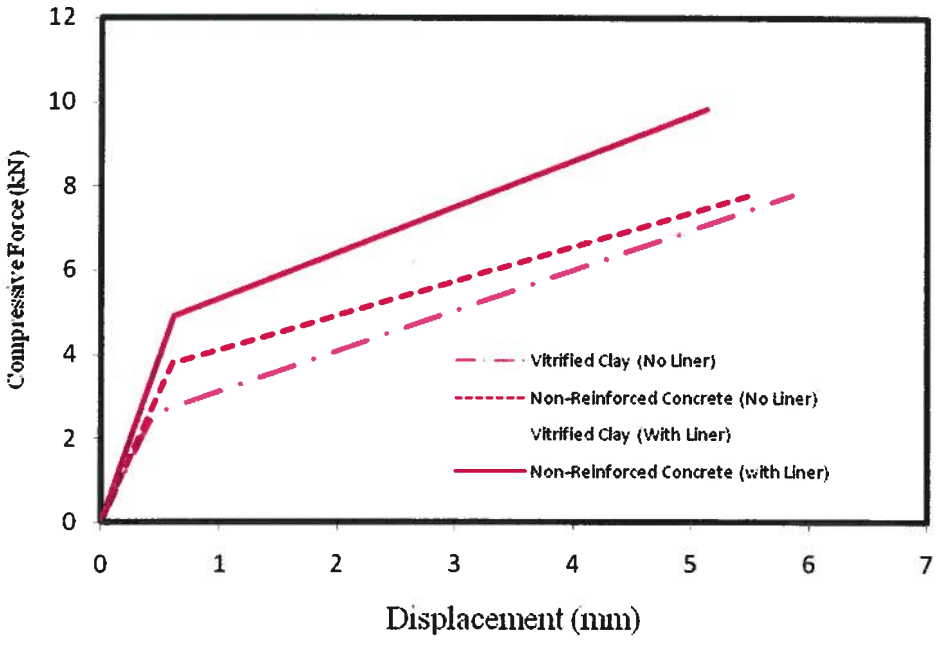


(b) Non-Reinforced Concrete and Vitrified Clay Pipes

Figure 6.7 Axial Behaviour of Joint (Compression Modeling Prediction) for Three Types of Rehabilitated Segmented Pipes

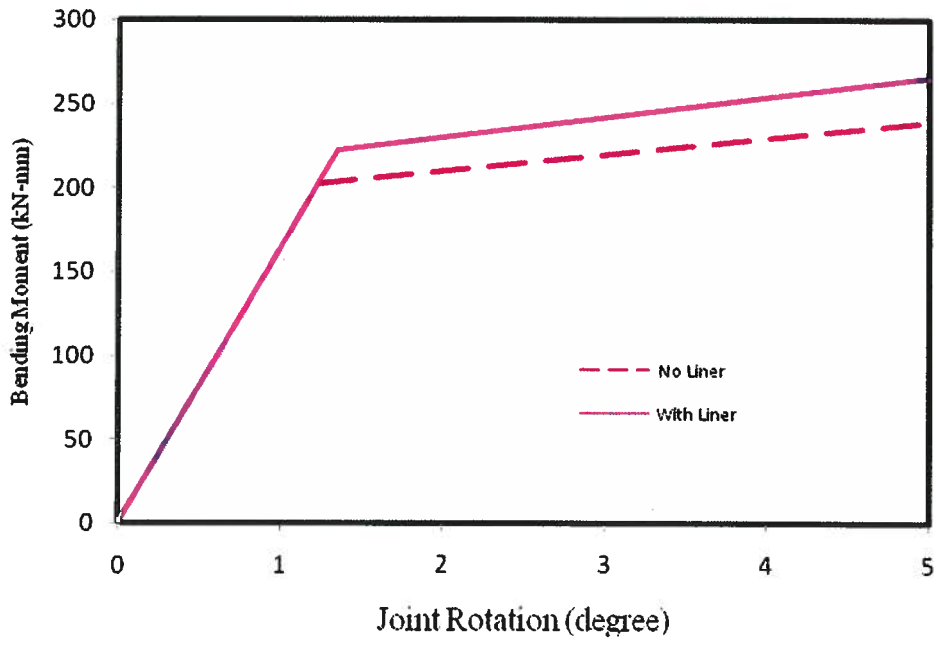


(a) Reinforced Concrete Pipes

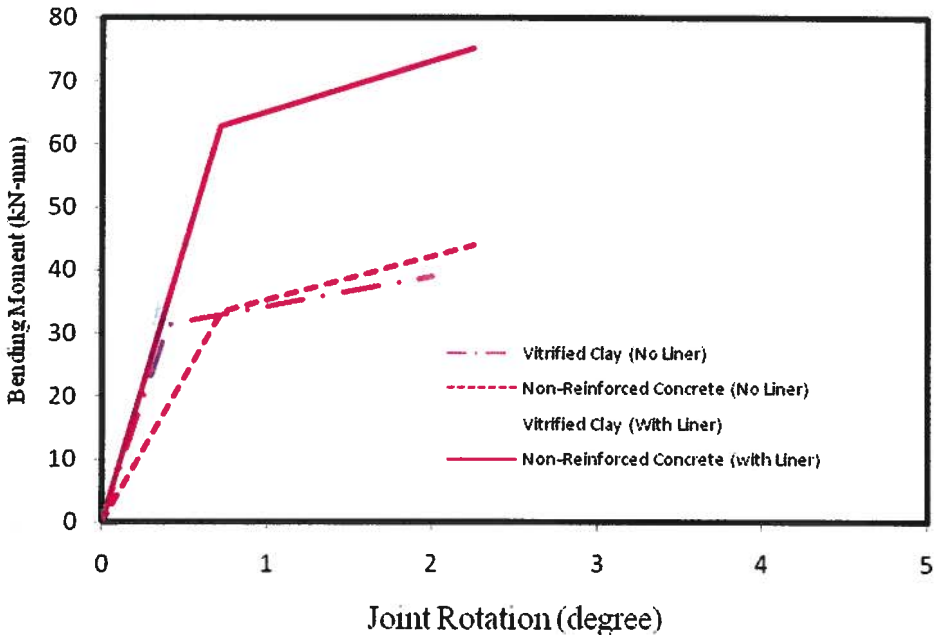


(b) Non-Reinforced Concrete and Vitrified Clay Pipes

Figure 6.8 Bending Behaviour for Joint (Bending Modeling Prediction) for Three Types of Rehabilitated Segmented Pipes

ε-max (x 0.00001) - (Reinforced concrete) = 2.03
ε-max (x 0.00001) - (Non-Reinforced concrete) = 3.6
ε-max (x 0.00001) - (Vitrified Clay) = 3.2

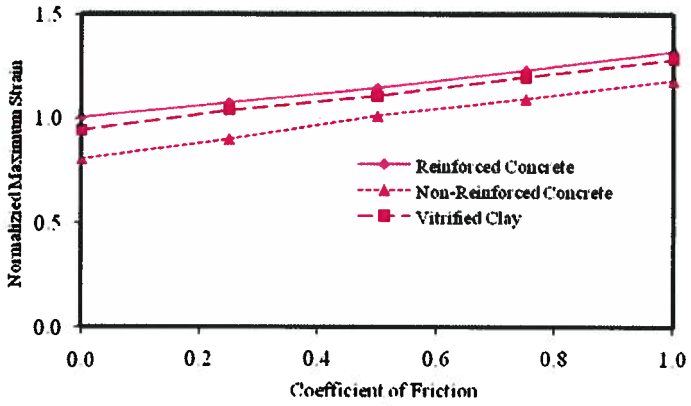


(a) Effect of Liner-Pipe Interface Condition

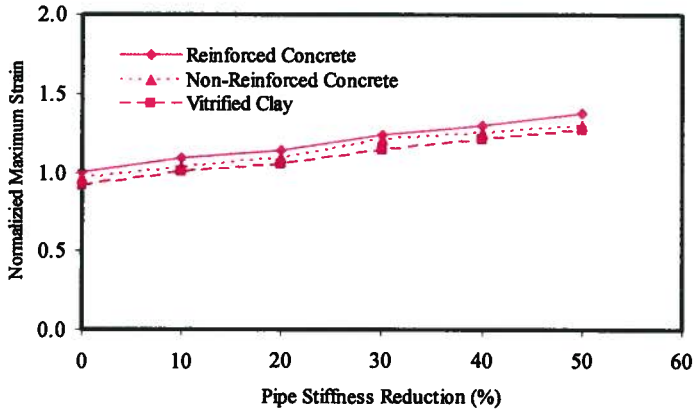


(b) Effect of Pipe Stiffness Reduction (Full Bond)

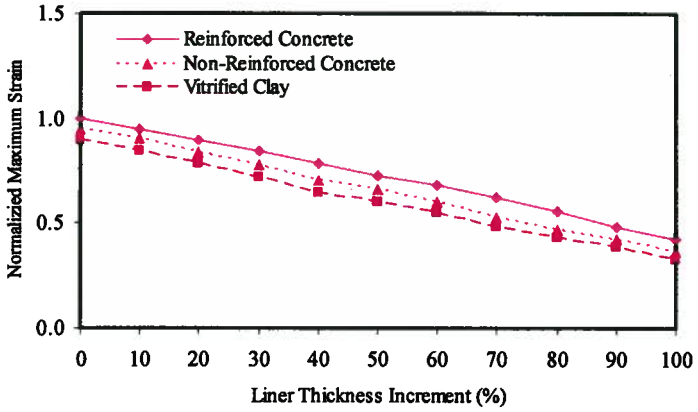


(c) Effect of Liner Thickness Increment (Full Bond)

Figure 6.9 Comparison of Normalized Maximum Liner Strain for Rehabilitated Segmented Pipe under Longitudinal PGD

ε-max (x 0.001) - (Reinforced concrete) = 1.45
ε-max (x 0.001) - (Non-Reinforced concrete) = 3.6
ε-max (x 0.001) - (Vitrified Clay) = 3.4

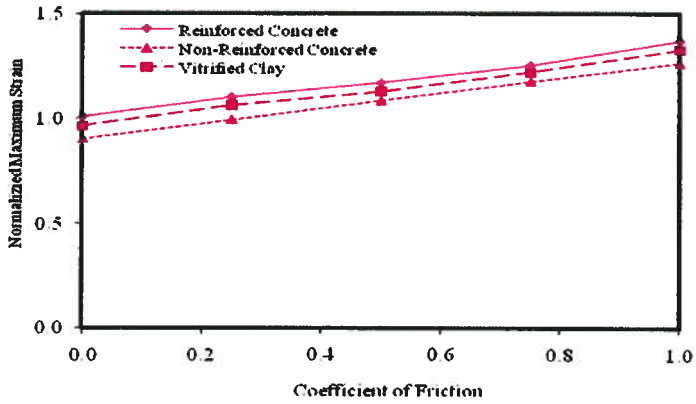


(a) Effect of Liner-Pipe Interface Condition

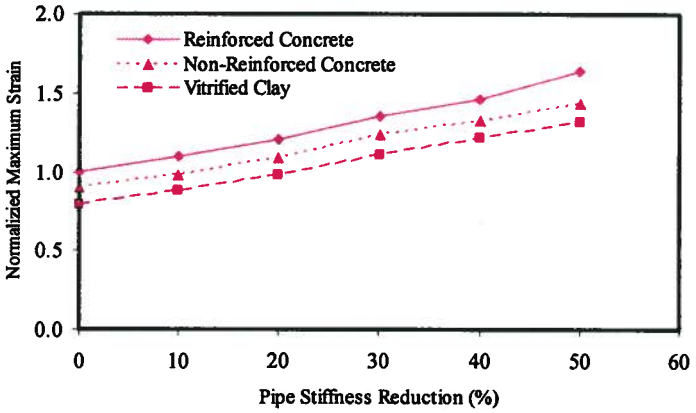


(b) Effect of Pipe Stiffness Reduction (Full Bond)

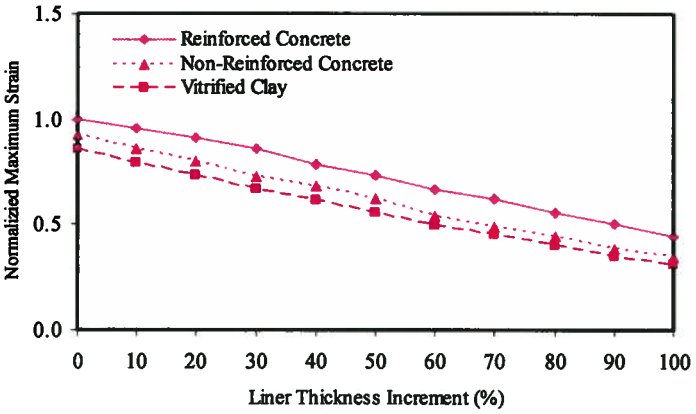


(c) Effect of Liner Thickness Increment (Full Bond)

Figure 6.10 Comparison of Normalized Maximum Liner Strain for Rehabilitated Segmented Pipe under Transverse PGD

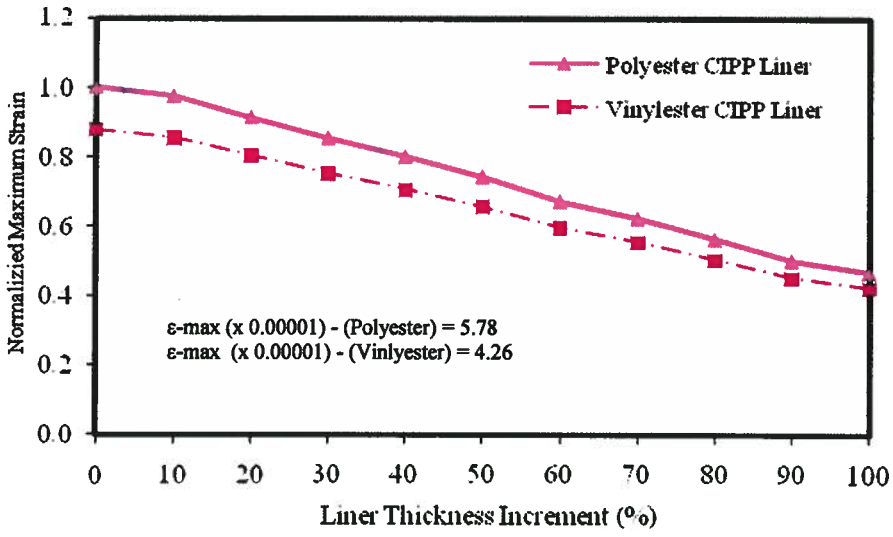


(a) Effect of Longitudinal PGD

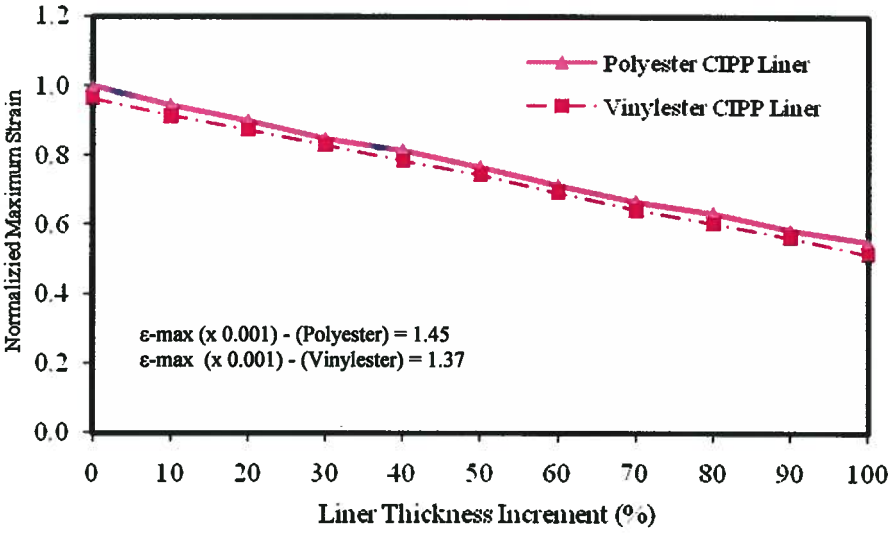


(b) Effect of Transverse PGD

Figure 6.11 Effect of Liner Material in the Response of Reinforced Concrete Pipe Strain Subjected to Seismic Effect (Full Bond)

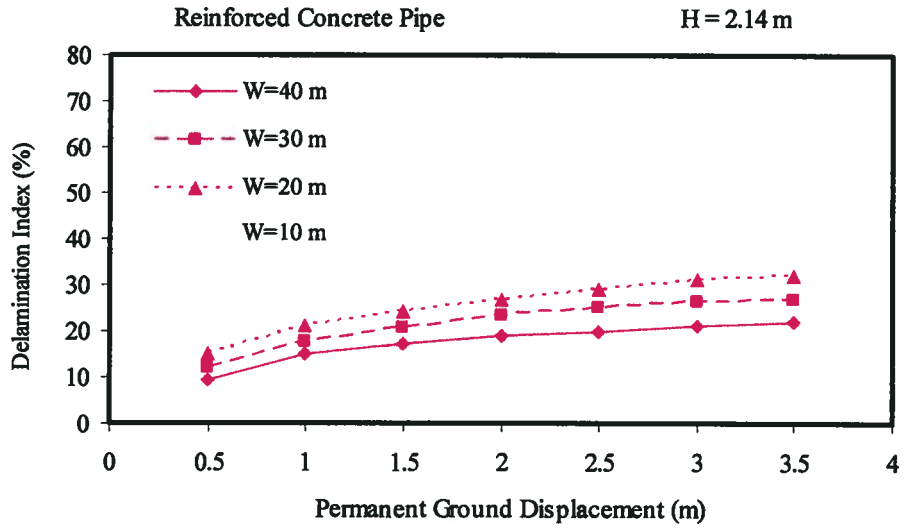


(a) Effect of PGD Amount

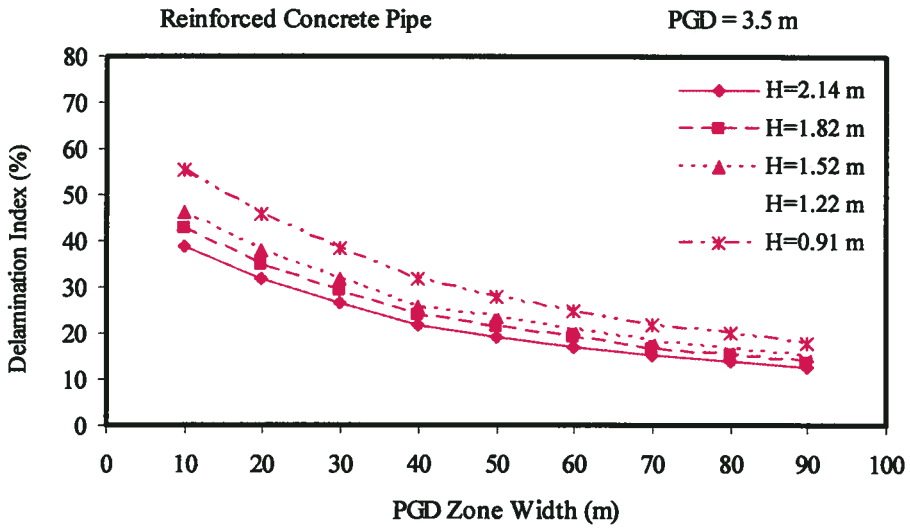


(b) Effect of PGD Zone Width

Figure 6.12 Comparison of Delamination Index for Rehabilitated Segmented Pipeline under Transverse PGD (Full Bond)

# CHAPTER SEVEN

# SUMMARY, CONCLUSIONS, AND RECOMMENDATIONS

## 7.1 SUMMARY

The current research work is focused on studying the seismic behaviours of rehabilitated buried segmented pipes using CIPP trenchless technology. A literature review relevant to this study is presented in two parts: the first addresses the performance of buried pipelines under seismic effects, and the second considers current methods of analysis and design of liners for buried pipes rehabilitation.

A review and analysis of major existing analytical and experimental models for the prediction of buckling pressure on encased liners is presented. A general formula is adopted to include each of these models. Statistical analysis of the experimental tests results was carried out using the statistical analysis software SPSS. The results of both the analysis of variance and capability analysis are reported for all the available experimental tests for the buckling of encased liners. Numerical finite element models for the analysis of buckling of liner subjected to uniform external pressure are developed for long and short-term buckling for circular and oval host pipe. The developed finite element model has been verified with Seemann tests (2000) and Zhu model (2000) where the buckling pressure errors between the finite element prediction and the short-term and long-term tests were less than 10% and 11%, respectively.

The numerical modeling of predicting the axial compression and bending behaviour of segmented pipe joints using the finite element method is presented. Both the axial and rotational capacities of the joint as they influence the overall behaviour the pipeline system are taken into account. The results of published full- scale experimental tests by others (Bouabid, 1993; Singhal, 1984a, b) of unrestrained joints for typical rigid pipes were employed to validate and calibrate the finite element models. The simulation indicates that a good agreement is achieved between the force-displacement curves of

Bouabid (1993) and the developed numerical model as the ultimate displacement error is 2.2% to 4.5%. Furthermore, the present numerical study results are in good correlation with the range of the experimental results of Singhal (1984a, b) within an ultimate joint rotation error of 3.1% to 4.9%. After gaining confidence for the developed finite element model, the analysis is generalized for typical rubber gasket unrestrained joints where experimental results currently are not available. The axial and bending stiffnesses of the rigid pipes with unrestrained joints for reinforced concrete, non-reinforced concrete, and vitrified clay pipes with diameters of 200 mm, 250 mm, and 300 mm are predicted. Despite the simplicity of the finite element models used in this work to predict the axial/rotational stiffness of the joint, their performance can be considered adequate for practical design.

The current study also develops a numerical simulation for the seismic analysis of buried segmented pipeline networks including axial and lateral permanent ground deformation. The developed numerical models used for the seismic analysis of buried segmented pipes have been verified successfully with the results of previous studies (Selventhiran, 2002; Liu and O'Rourke, 1997). The analytical and the numerical results of Selventhiran and the current work numerical model showed very close agreement, which indicates that the modeling procedures are consistent with the expected behaviour within a relative error of maximum pipe strain of an average 3.1% for the continuous pipeline and an average of 2.7% to7.9% for the segmented pipeline. The numerical models of the present study and that of Liu and O'Rourke are within approximately 4.9% to 8.7% relative error for the maximum pipe strain predictions for the continuous pipeline and 4.9% to 8.7% for the segmented pipeline; which indicate a good agreement between the numerical models. The reasonable accuracy of the developed finite element models for segmented buried unrestrained pipelines under seismic effects gives the necessary confidence that the analysis can be generalized for typical rigid segmented buried pipelines under seismic effects where experimental results and numerical analysis are not available.

The final part of this research is focused on developing a numerical modeling of the delamination of rehabilitated segmented buried pipelines. Two finite element models are

developed based on previous verified numerical models for joint behaviours and seismic analyses of buried segmented pipelines. A finite element analysis procedure considering friction effects in the contact boundary is proposed to predict the axial behaviour, the flexural behaviour of the unrestrained joint, and the delamination index of the liner in rehabilitated segmented pipeline under external loads or seismic effects. The simulated global behaviour of the rehabilitated segmented pipes has a similar trend to the results predicted for non-rehabilitated segmented pipes. The axial/bending stiffnesses predicted for the rehabilitated segmented pipes are significantly larger than that for non-rehabilitated segmented pipes. The average delamination indexes are 8%, 12% and 20% for the compression, tensile and bending loading, respectively.

The results of the simulation analyses indicate that the liner strains for the full bond case are increased by an average of 20% and 46% when compared with the condition of elastic slip interface, for the longitudinal PGD case and the transverse PGD case, respectively. Thus, the liner trains are increasing function of the coefficient of friction and independent from the pipe material. The results indicate that when the liner thickness is increased by 100 % (i.e., twice the original liner thickness) then the liner strain reduces by 58% and 49% in comparison with liner strain for the original thickness, for the longitudinal PGD case and the transverse PGD case, respectively. On the other hand, the results of effects of the pipe stiffness show that 50% reduction in the pipe stiffness led to an average of 52% reduction in the pipe strain.

## 7.2 CONCLUSIONS

A review of the results of the numerical simulations of rehabilitated pipelines under seismic effects (i.e., longitudinal and transverse PGD) can lead to the following conclusions:

1- The study of the experimental tests programs of buckling of encased liners under short-term and long-term conditions showed the consistency of each test program when taken independently. When the data set includes all available results, the

statistics of these results indicates poor consistency, suggesting a lack of uniform protocol conducting the buckling tests on liners. Moreover, it is worthwhile to mention that neither the analytical models nor the experimental tests took into account that encased liner in real conditions is subjected to non-uniform groundwater pressure.

2- The comparison between the analytical models and the existing tests showed that no one model has clear superiority over the others. This is related to the fact that all the analytical models use the same methodology and assumptions, with some improvements and modifications, and therefore they inherit the same characteristics. However, the Glock's equation seems to be the closest analytical formula for predicting the critical buckling pressure on encased liners measured by the Aggarwal and Cooper (1984) experimental tests. The comparison between encased liner models show that the ASTM F1216 standard which is currently used for design is too conservative and will overestimate the liner thickness and thus the cost of the rehabilitation will increase.

3- The short-term and long-term buckling of encased liners models proposed in this study can effectively predict the liner buckling resistance for a given pressure when based on appropriate liner configurations and material properties. The liners buckling models proposed in this work were purposely made simple, and their performance is superior to that of any of the analytical models. Thus, the numerical simulation of buckling of liners is an alternative that addresses the main problems in an effective way. Despite the simplicity of the finite element model the results appear to be slightly on the conservative side, but most importantly they are consistent from one test to another. Finite element models have the advantage of being extendable to include ovality, gap, and geometric non-linearity effects, and they capture the buckling phenomena successfully. The numerical solutions are conservative relative to the experimental test results.

4- The parametric study of the axial and rotational behaviours of typical rigid pipes,

unrestrained joints shows that the axial/rotational stiffness and the ultimate load/bending moment are an increasing function of the pipe diameter, as well as of the pipe wall thickness. Both developed simulation models for the axial and rotational behaviour of the joint are adequate tools for predicting the unrestrained joints behaviours for working conditions and for ultimate failure predictions, as well as for the seismic analysis of buried segmented pipelines networks whenever experimental data is not available.

5- The applications of the developed finite element models for seismic behaviour of buried segmented pipeline generalize the work of the Selventhiran (2002) and the Liu and O'Rourke (1997) models. The numerical simulation for the seismic behaviour of buried segmented pipes under axial and transverse PGD showed that pipe strain is an increasing function of the burial depth and the PGD zone width. Parametric study results under transverse PGD loading show smaller joint rotation when compared with the results of the longitudinal PGD loading. Thus, it has been shown that in general, longitudinal PGD causes more damages (e.g., joint separation) than does transverse PGD. The damage increases with increasing PGD width and magnitude.

6- Failure analysis indicates that all types of rigid pipes under longitudinal PGD loading will become damaged when the PGD amount exceeds 0.3 m. On the other hand, all types of rigid pipes under study subjected to transverse PGD loading will become damaged when the PGD amount exceeds 2.5 m. Thus, there is an urgent need after an earthquake event, to check the status of the pipeline at the joint zone.

7- Two finite element models were developed to simulate the delamination between the encased liner and the host pipe. It can be observed that delamination occurs at the joint zone and the delamination index is an increasing function of the applied load. It is also shown that ignoring the effect of contact between the encased liner and the host pipe can lead to incorrect estimations of the delamination index. The

simulation results for the rehabilitated pipes showed that only the joint region is delaminated. Thus, to restore the hydraulic capacity of the segmented pipeline a full-length rehabilitation is not required if the damage is partial and it is within the joints region, which will reduce significantly the cost of the rehabilitation process.

8- Another important conclusion of these analyses is that the encased liner is debonded or delaminated at the joint region, resulting in a decrease in the rigidity of the joint when the axial and flexural loads are increased. Two finite element models are developed to investigate the seismic analyses of buried rehabilitated segmented pipelines under longitudinal and transverse PGD. The results of these analyses show that the longitudinal and bending strains increase toward the joint region but drop significantly at the ends of rehabilitated segmented pipeline.

9- The variation in the liner wall thickness has more impact on the seismic response of buried rehabilitated segmented pipes than does the host pipe stiffness. The reason for this is most probably related to the fact that the liner stiffness is proportional to the cube of the wall thickness, and the higher stiffness will give a smaller strain.

## 7.3 RECOMMENDATIONS

Several recommendations for improvement of the seismic performance of buried rehabilitated pipelines are listed hereunder:

1. It is recommended that further controlled, robust, and statistically significant buckling tests, that account for the initial gap, ovality, longitudinal imperfections, end effect, groundwater pressure non-uniformity, and creep behaviour of liner material; must be carried out in a highly controlled environment in order to improve the confidence in the finite element solution, to minimize the scattering and variability observed in this study, and to validate any new analytical model properly.

2- There is an urgent need for research to address the longitudinal discontinuity at unrestrained gasket rubber joints. The reason for this urgency is the lack of an acceptable design guideline to deal with the dimensions, tolerances, properties, and capacities of such joints. Currently, the design of unrestrained rubber gasketed joints is left up to the pipe manufactures. However, the methodology presented in this work to predict the axial/rotational stiffness of the joint is the first step toward understanding the structural behaviours and the design of the joint in segmented pipelines.

3- There is an urgent need for research to develop new techniques to modify the structural behavior of the joint or to use two liners at the joint region so that the joint will have more resistance to seismic effect.

4- The Finite element models use assumptions to simplify the different simulation parameters such as the material properties and the real interactions between the buried segmented pipeline components and the seismic environment. Thus, full-scale experimental tests are required to understand the actual behaviours of buried segmented pipelines. Then, numerical models could be employed to reproduce each of these tests. As a result, a reliable and accurate physical model as well as a rigorous engineering mechanics analysis could be achievable. However, to account for the effect of possible cracking of concrete, it is recommended to use the smeared cracking approach, which employs a plasticity-based constitutive law that simulates the tension-stiffening behaviour of the concrete elements in the finite element modeling.

5- The numerical modeling approach established in this work offers high potential for further investigation and development in conjunction with fracture mechanics concepts to understand the delamination phenomenon in rehabilitated pipeline under different types of loadings. Thus, the onset and growth of other damage mechanisms such as liner fiber fracture and host pipe cracking should be taken

into account in the analyses when trying to accurately predict joint behaviour. To fully study the effect of fractures on the complex soil-pipe-liner system, it is important to model these fractures explicitly. Extra work is required to model the time-dependent behaviour of the polymer liner material and to evaluate its effects on the variation of the critical strains and stresses with time.

6- To investigate the bonding capability of the rehabilitated pipe using CIPP trenchless technology, it is recommended that more experimental work for the peel test (ASTM D903) is required for better understanding of the delamination phenomenon under different types of loading.

7- The phenomenon of progressive failure in rehabilitated segmented buried pipelines under seismic effects is yet to be fully understood. As a result, reliable strategies for designing encased liners for desired increased life and strength in seismic-prone areas are imperative.

## REFERENCES

**ACPA**, (2000). "Concrete Pipe Design Manual", American Concrete Pipe Association, TX, USA.

**Aggarwal**, S. C. and Cooper, M. J. (1984). "External Pressure Testing of Insituform Lining", Internal Report, Coventry (Lanchester) Polytechnic, Coventry, UK.

**Ahmad**, S. and McAlpine, G. (1994). "Structural Characteristics of the Danby Pipe Renovation System", Proceedings of 3rd Materials Engineering Conference, Materials Engineering Division/ASCE, INFRASTRUCTURE: New Materials and Methods of Repair, November 13-16, San Diego, California, USA.

**ALA** (2001a). "Seismic Fragility Formulations for Water Systems", Part 1 and 2, American Lifelines Alliance, Washington D.C., USA.

**ALA** (2001b). "Guidelines for the Design of Buried Steel Pipe", American Lifelines Alliance, Washington D.C., USA.

**ALA** (2002). "Seismic Design and Retrofit of Piping System", American Lifelines Alliance, Washington D.C., USA.

**Allouche**, E. and Ariaratnam, S. (2002). "State-of-The-Art-Review of No-Dig Technologies for New Installations", ASCE Pipelines 2002 beneath Our Feet: Challenges and Solutions, Proceedings of the Pipeline Division Conference, August 4-7, Cleveland, Ohio, USA.

**Ariman**, T., Hamada, M., Singhal, A. C., Haroun, M. A., and Cakmak, A. S. (1987). "Recent Advances in Lifeline Earthquake Engineering, Developments in Geotechnical Engineering", Vol. (49), Elsevier Science Publishers B.V., New York, USA.

**Ariman**, T. and Lee, B. J. (1991). "Tension/Bending Behaviour of Buried Pipelines under Large Ground Deformations in Active Faults", Proceedings of the 3rd U. S. Conference on Lifeline Earthquake Engineering, Michael A. Cassaro (Editor), American Society of Civil Engineers, Reston, VA, USA , pp. 226 - 233.

**ASCE** (1983). "Seismic Response of Buried Pipelines and Structural Components", Committee of the ASCE Structural Division on Seismic Analysis of Nuclear Structures and Materials, American Society of Civil Engineers, Reston, VA, USA, pp. 1 - 56.

**ASCE** (1984). "Guidelines for the Seismic Design of Oil and Gas Pipeline Systems", The ASCE Technical Council on Lifeline Earthquake Engineering, American Society of Civil Engineers, Reston, VA, USA.

**ASCE** (1999). "Guidelines for the Seismic Evaluation and Upgrade of Water Transmission Facilities", The ASCE Technical Council on Lifeline Earthquake Engineering - Monograph No. (15), American Society of Civil Engineers, Reston, VA, USA.

**ASTM** C1208M-(2000). "Standard Specification for Vitrified Clay Pipe and Joints for Use in Microtunneling, Sliplining, Pipe Bursting, and Tunnels", American Society for Testing and Materials, West Conshohocken, PA, USA.

**ASTM** C14-(2005). "Standard Specification for Concrete Sewer, Storm Drain, and Culvert Pipe", American Society for Testing and Materials, West Conshohocken, PA, USA.

**ASTM** C700-(2005). "Standard Specification for Vitrified Clay Pipe, Extra Strength, Standard Strength, and Perforated", American Society for Testing and Materials, West Conshohocken, PA, USA.

**ASTM** C443-(2005). "Standard Specification for Joints for Concrete Pipe and Manholes, Using Rubber Gaskets", American Society for Testing and Materials, West Conshohocken, PA, USA.

**ASTM** C425-(2005). "Standard Specification for Compression Joints for Vitrified Clay Pipe and Fittings", American Society for Testing and Materials, West Conshohocken, PA, USA.

**ASTM** D638-(2008). "Standard Test Method for Tensile Properties of Plastics", American Society for Testing and Materials, West Conshohocken, PA, USA.

**ASTM** D790-(2007). "Standard Test Methods for Flexural Properties of Un-reinforced and Reinforced Plastics and Electrical Insulating Materials", American Society for Testing and Materials, West Conshohocken, PA, USA.

**ASTM** D903-(2004). "Standard Test Method for Peel or Stripping Strength of Adhesive Bonds", American Society for Testing and Materials, West Conshohocken, PA, USA.

**ASTM** F1741-(1996). "Standard Practice for Machine Spiral Wound Poly Vinyl Chloride (PVC) Liner Pipe for Rehabilitation of Existing Sewers and Conduits", American Society for Testing and Materials, West Conshohocken, PA, USA.

**ASTM** F1743-(1996). "Standard Practice for Rehabilitation of Existing Pipelines and Conduits by Pulled-in-Place Installation of Cured-in-Place Thermosetting Resin Pipe (CIPP)", American Society for Testing and Materials, West Conshohocken, PA, USA.

**ASTM** F1216-(1993). "Standard Practice for Rehabilitation of Existing Pipelines and Conduits by the Inversion and Curing of a Resin-Impregnated Tube", American Society for Testing and Materials, West Conshohocken, PA, USA.

**ASTM** F2019-(2000). "Standard Practice for Rehabilitation of Existing Pipelines and Conduits by the Pulled-in-Place Installation of Glass Reinforced Plastic (GRP) Cured-in-Place Thermosetting Resin Pipe (CIPP)", American Society for Testing and Materials, West Conshohocken, PA, USA.

**ASTM** F1962-(1999). "Standard Guide for Use of Maxi-Horizontal Directional Drilling for Placement of Polyethylene Pipe or Conduit under Obstacles, Including River Crossings", American Society for Testing and Materials, West Conshohocken, PA, USA.

**AWWA**-C950-(1988). "Standard for Fiberglass Pressure Pipe", American Water Works Association, Denver, CO, USA.

**Ayala**, G. and O'Rourke, M. (1989). "Effects of the 1985 Michoacan Earthquake on Water Systems and Other Buried Lifelines in Mexico", Technical Report NCEER-89-009, Multidisciplinary Center for Earthquake Engineering Research, Buffalo, NY, USA.

**Bakeer**, R. M., and Barber, M. E., Perchon, S. E., Taylor, S. E., and Chunduru, S. (1999). "Buckling of HDPE Liners under External Uniform Pressure", Journal of Materials in Civil Engineering, American Society of Civil Engineers, Vol. (11), No. (4), pp. 353 - 361.

**Bakeer**, R. M., and Barber, M. E., Perchon, S. E., and Taylor, S. E. (2001). "Long-Term Buckling Performance of HDPE Liners", Journal of Materials in Civil Engineering, American Society of Civil Engineers, Vol. (13), No. (3), pp. 176 - 184.

**Bakeer**, R. M., and L. K. Guice (1997). "Tests for Evaluating Fluid Migration in the Annular Space of Lined Piping Systems", Tulane University, New Orleans, LA, and Louisiana Tech. University, Ruston, LA, USA.

**Ballantyne,** D. B., Berg, E., Kennedy, J., Reneau, R. and Wu, D. (1990). "Earthquake Loss Estimation Modeling of the Seattle Water System", Technical Report, Kennedy/Jenks/Chilton, Federal Way, WA, USA.

**Bardet,** J. P., Mace N., and Tobita T., (2000). "Liquefaction-Induced Ground Deformation and Failure", Pacific Earthquake Engineering Research Center, Report PEER 2000/08, Arlington, VA, USA.

**Bartlett**, S. F. and Youd, T. L. (1995). "Empirical Prediction of Liquefaction Induced Lateral Spread", Journal of Geotechnical Engineering, American Society of Civil Engineers, Vol. (121), No. (4), pp. 316 - 329.

**Boot**, J. C. (1998). "Elastic Buckling of Cylindrical Pipe Linings with Small Imperfections Subject to External Pressure", J. of Trenchless Technology Research, Elsevier Science Publishers B.V., New York, Vol. (12), No. (1-2), pp. 3 - 15.

**Boot**, J. C. and Gumbel, J. E. (1998). "Discussion by Boot and Gumbel on Structural Analysis of Sewers Lining", J. of Trenchless Technology Research, Elsevier Science Publishers B. V., New York, Vol. (12), No. (1-2), pp. 49 - 52.

**Boot**, J. C. and Javadi, A. A. (1998). "The Structural Behaviour of Cured-in-Place Pipe",
Proceedings of the Plastic Pipes Conference, September, Göteborg, Sweden.

**Boot**, J. C. and Javadi, A. A. (1998). "Experimental Determination of Buckling Capacities of Cured-in-Place Pipe Linings", Proceedings of the 11$^{th}$ International Conference on Experimental Mechanics, Oxford, UK.

**Boot**, J. C., Guan, Z. W., and Toropova, I. (1996). "Structural Performance of Thin-Walled Polyethylene Pipe Linings for the Renovation of Water Mains", Trenchless Technology Research, Elsevier Science Publishers B.V., New York, Vol. (11), No. (1), pp. 37 - 51.

**Bouabid**, J. (1993). "Behaviour of Rubber Gasketed Concrete Pipe Joints during Earthquakes", Ph. D. Thesis, Rensselaer Polytechnic Institute, Troy, New York, USA.

**Bouabid**, J. and O'Rourke, M. (1994). "Seismic Vulnerability of Concrete Pipelines", Proceedings of the 5th US National Conference on Earthquake Engineering, Chicago, IL, July, Vol. (IV), pp. 789 - 798.

**Bucciarelli**, L. L. and Pian, T. H. (1964). "Effect of Initial Imperfection on the Instability of a Ring Confined in an Imperfect Rigid Boundary", J. Applied Mech. Trans, American Society of Mechanical Engineers, New York, pp. 979 - 989.

**Cheney**, J. A. (1971). "Pressure Buckling of Ring Encased in Cavity", Journal of Engineering Mechanics, American Society of Civil Engineers, pp. 333 - 343.

**Chicurel**, R. (1968). "Shrink Buckling of Thin Circular Rings", Journal of Applied Mechanics, American Society of Mechanical Engineers, New York, pp. 608 - 610.

**Chung**, M. P., (1984). "Seismic Analysis of Buried Pipelines Networks", Ph. D. Dissertation, University of Arizona, Tempe, AZ, USA.

**Chung**, R., (Editor) (1996). "The January 17, 1995 Hyogoken-Nanbu (Kobe) Earthquake; Performance of Structures, Lifelines, and Fire Protection Systems", Special Publication (901), National Institute of Standards and Technology, July, Gaithersburg, MD, USA.

**Chunduru**, S. (1996). "Material Performance and Numerical Modeling of HDPE Deformed/Reformed Liners", Ph. D. Dissertation, Tulane University, New Orleans, LA, USA.

**Dakoulas**, P., Yegian, M., and Holtz, B. (1998). "Geotechnical Earthquake Engineering and Soil Dynamics III", Volume (II), Geotechnical Special Publication No. (75), Proceedings of a Specialty Conference, Aug. 3-6, Seattle, WA, USA.

**Davis**, C. A. (2000). "Study of Near-Source Earthquake Effects on Flexible Buried Pipes", Ph. D. Dissertation, University of South California, Los Angeles, CA, USA.

**Davis**, C. A. and Bardet, J. P. (2000). "Response of Buried Corrugated Metal Pipes to Earthquakes", American Society of Civil Engineers, Journal of Geotechnical and Geoenvironmental Engineering, Vol. (126), No.(1), January, pp. 28 - 39.

**Eguchi**, R. T. (1983). "Seismic Vulnerability Models for Underground Pipes", Proceedings, Earthquake Behaviour and Safety of Oil and Gas Storage Facilities, Buried Pipelines and Equipment, PVP-77, American Society of Mechanical Engineers, New York, pp. 368 - 373.

**Eguchi**, R. T. (1991). "Seismic Hazard Input for Lifeline Systems", J. Structural Safety, Elsevier Science Publishers B.V., New York, Vol. (10), pp. 193 - 198.

**Eidinger**, J. (2001). "Seismic Fragility Formulations for Water Systems", G & E Report 47.01.01, Revision (1), July, G & E Engineering Systems Inc., Oakland, CA, USA.

**Eisenberger**, M. and Yankelevisky, D. Z. (1985). "Exact Stiffness Matrix for Beams on Elastic Foundation", Journal of Computers & Structures, Elsevier Science Publishers, Oxford, Vol. (21), No. (6), pp. 1355 - 1359.

**Eisenberger**, M. and Bielak, J. (1992). "Finite Beams on Infinite Two Parameters Elastic Foundation", Journal of Computers & Structures, Elsevier Science Publishers, Oxford, Vol. (42), No. (4), pp. 661 - 664.

**Elhmadi**, K. and O'Rourke, M. (1989). "Seismic Wave Effects on Straight Jointed Buried Pipelines", Technical Report NCEER-89-0022, National Center for Earthquake Engineering Research, State University of New York at Buffalo, NY, USA.

**Elhmadi**, K. and O'Rourke, M. (1990). "Seismic Damage to Segmented Buried Pipelines", Earthquake Engineering & Structural Dynamics, Wiley Inter Science, John Wiley and Sons Ltd.., May, Vol. (19), No. (4), pp. 529 - 539.

**El-Bayoumy**, L. (1972). "Buckling of a Circular Elastic Ring Confined to a Uniformly Contraction Circular Boundary", American Society of Mechanical Engineers, J. Applied Mechanics, Vol. (94), pp. 758 - 766.

**El-Sawy**, K. (1996). "Non-linear Analysis of Liners for Rigid Pipe Rehabilitation", Ph. D. Dissertation, University of Western Ontario, London, ON, Canada.

**El-Sawy**, K. (2001). "Inelastic Stability of Tightly Fitted Cylindrical Liners Subjected to External Uniform Pressure", J. Thin-Walled Structures, Elsevier Science Publishers B.V., New York, Vol. (39), No. (9), pp. 731 – 744.

**El-Sawy**, K. (2002). "Inelastic Stability of Loosely Fitted Cylindrical Liners", J. Structural Engineering, American Society of Civil Engineers, July, Vol. (128), No. (7), pp. 934 –941.

**El-Sawy**, K., and I. D. Moore (1995). "Stability Analysis of Thick Imperfect Liners within a Rigid Circular Cavity", Tech. Rep. GEOT-16-95, Geotechnical Research. Center, University of Western Ontario, London, ON, Canada.

**El-Sawy**, K., and Moore, I. D. (1996). "A Two-level Iterative FEM Technique for Rigorous Solution of Non-linear Interaction Problems under Large Deformations", Journal of Computers & Structures, Elsevier Science Publishers, Oxford, Vol. (61), No. (1), pp. 43 - 54.

**El-Sawy**, K. and Moore, I. (1997). "Parametric Study for Buckling of Liners: Effect of Liner Geometry and Imperfection", Proceeding of the ASCE Conference on Trenchless Pipeline Projects-Practical Applications, June 8-11, Boston, Massachusetts, USA, pp. 416 - 423.

**El-Sawy**, K. and Moore, I. (1998). "Stability of Loosely Fitted Liners Used to Rehabilitate Rigid Pipes", J. of Structural Engineering, American Society of Civil Engineers, November, Vol. (124), No. (11), pp. 1350 – 1357.

**Falter**, B. (1996). "Structural Analysis of Sewer Linings", J. of Trenchless Technology Research , Elsevier Science Publishers B.V., New York, Vol.(11), No.(2), pp. 27 - 41.

**Flores-Berrones**, R. and O'Rourke, M. (1992). "Seismic Effects on Underground Pipelines due to Permanent Longitudinal Ground Deformations", Proceedings of the 4th Japan-U.S. Workshop on Earthquake Resistant Design of Lifelines Facilities and Countermeasures for Soil Liquefaction, Honolulu, Hawaii, Technical Report NCEER-92-0019, National Center for Earthquake Engineering Research, State University of New York at Buffalo, NY, pp. 465 - 480.

**Fuchida**, K., Wang, L., Akiyoshi. T. (1994). "Parametric Analysis of Buried Pipelines Subjected to Liquefied Ground Movements", 5th U.S. National Conference on Earthquake Engineering Proceedings, Earthquake Engineering Research Institute, Oakland, CA, Vol. (IV), pp. 959 - 968.

**Glock**, D. (1977). "Post-Critical Behaviour of a Rigidly Encased Circular Pipe Subject to External Water Pressure and Temperature Rise", Der Stahlbau, Vol. (46), No. (7), pp. 212 - 217.

**Guice**, L. K., and Li, J. Y. (1994). "Buckling Models and Influencing Factors for Pipe Rehabilitation Design", Proceedings of the North American No-Dig 1994, Dallas, Texas, April, (invited).

**Guice**, L. K. and Norris, C. (1993). "Long-Term Hydrostatic Pressure Testing of Liner Materials", Proceedings of Trenchless Technology, An Advanced Technical Seminar, Vicksburg, MS, USA.

**Guice**, L. K., Straughan, T., Norris, C. R., and Bennett, R. D. (1994). "Long-Term Structural Behaviour of Pipeline Rehabilitation Systems", TTC Technical Report (302), Louisiana Tech. University, Ruston, LA, USA.

**Gumbel**, J. E. (1993). "Rehabilitation of Sewers by Structural Lining", Asian Trenchless Technology, Dubai, UAE.

**Gumbel**, J. E. (1998). "Structural Design of Pipe Linings 1998 - Review of Principles, Practice and Current Developments Worldwide", Proceedings of the 4th ASTT Conference, Brisbane, Australia.

**Gumbel**, J. E. (2001). "New Approach to Design of Circular Liner Pipe to Resist External Hydrostatic Pressure", ASCE Pipeline Division Conference, San Diego, CA, USA.

**Gumbel**, J. E., Heavens, J. W, and Boot, J. C. (1995). "Design and Selection Criteria for Plastics Lining Systems for the Renovation of Pressure Pipelines", 1st International Conference on Coatings and Linings for the Water and Wastewater Industry, Prague, Czech.

**Hall**, E. and Newmark, N. (1977). "Seismic Design Criteria for Pipelines and Facilities", Current State of Knowledge of Lifeline Earthquake Engineering, American Society of Civil Engineers, pp. 18 - 34.

**Hall**, W. J. and O'Rourke, M. (1991). "Seismic Behaviour and Vulnerability of Pipelines", Lifeline Earthquake Engineering, Michael A. Cassaro (Editor), American Society of Civil Engineers, pp. 761 - 773.

**Hall**, D. E. and Zhu, M. (2001). "Creep Induced Contact and Stress Evolution in Thin-Walled Pipe Liners", J. of Thin-Walled Structures, Elsevier Science Publishers B.V., New York, Vol. (39), No. (11), pp. 939 - 959.

**Hamada**, M. (1991). "Estimation of Earthquake Damage to Lifeline Systems in Japan", Proceedings of the 3rd Japan-U.S. Workshop on Earthquake Resistant Design of Lifelines Facilities and Countermeasures for Soil Liquefaction, San Francisco, CA, Technical Report NCEER-91-0001, National Center for Earthquake Engineering Research, State University of New York at Buffalo, NY, pp. 5 - 22.

**Hamada**, M., Isoyama, R., and Wakamatsu, K. (1996). "Liquefaction Induced Ground Displacement and Its Related Damage to Lifeline Facilities", Soils and Foundations - Special Issue on Geotechnical Aspects of the January 17, 1995 Hyogoken-Nambu Earthquake, J. of Soils and Foundations, Japanese Geotechnical Society, Tokyo, pp. 81 - 97.

**Hamada**, M., and T. D. O'Rourke, (Editors) (1992). "Case Studies of Liquefaction and Lifeline Performance during Past Earthquakes", Report No. NCEER-92-0001, National Center for Earthquake Engineering Research, State University of New York, Buffalo, NY, USA.

**Hamada**, M., Yasuda, S., Isoyama, R., and Emoto, K. (1986). "Study on Liquefaction Induced Permanent Ground Deformations", Association for the Development of Earthquake Prediction, Japan, Tokyo, 87p.

**Hartley**, J. D. and Duncan, J. M. (1987). "E' and Its Variation with Depth", J. of Transportation Engineering, American Society of Civil Engineers, Vol. (113), No. (5), pp. 538 - 553.

**Hibbitt**, Karlsson, and Sorensen Inc. (2005). "ABAQUS/Standard User's Manual", Version (6.5), Pawtucket, RI, USA.

**Hindy**, A. and Novak, M. (1980). "Pipeline Response to Random Ground Motion", Journal of Engineering Mechanics, American Society of Civil Engineers, Vol. (106), No. (EM2), April, pp. 339 - 359.

**Iwamatu**, J. et al. (1998). "Damage to Buried Water Distribution Pipelines and Ground Deformations from the 1995 Hyogoken-Nanbu Earthquake", Proceeding of Workshop for Anti-Seismic Measures on Water Supply, International Water Services Association (IWSA), Tokyo, Japan.

**Iwamoto**, T., Wakai, N., and Yamaji, T. (1984). "Observation of Dynamic Behaviour of Buried Ductile Iron Pipelines during Earthquakes", 8th World Conference on Earthquake Engineering, San Francisco, CA, Vol. (VII), pp. 231 - 238.

**Iwamoto**, T., Yamamura, Y., and Hojo, S. (1985). "Observations and Analysis at the Bend and Tee Portions of Buried Ductile Iron Pipelines during Earthquakes", Seismic Performance of Pipelines and Storage Tanks, PVP–98-4, American Society of Mechanical Engineers, New York, pp. 69 - 79.

**Jeyapalan**, J. (1998). "Pipeline Market - 20 Billion Dollars for 1998 Would You Like Some of This Work? Proceedings of the Pipeline Division Conference", Proceedings of the 1998 Pipeline Division Conference, Aug 23-27, San Diego, CA, pp. 763 - 781.

**Jeyapalan**, J. (2001). "Unified Design Method for Most No-Dig Rehabilitation Liners", Proceedings of the ASCE International Conference on Pipeline: Advances in Pipeline Engineering and Construction, July 15-18, San Diego, CA, USA.

**Jeyapalan**, J. K., and Jeyapalan, M. (1995). "Advances in Underground Pipeline Engineering", Proceedings of the 2nd International Conference, Sponsored by ASCE Technical Council on Lifeline Earthquake Engineering, Bellevue, Washington, June 25-28, USA.

**Jeyapalan**, J. K., and Watkins, R. (2004). "Modulus of Soil Reaction (E′) Values for Pipeline Design", Journal of Transportation Engineering, American Society of Civil Engineers, Vol. (130), No. (1), Jan/Feb, pp. 43 - 48.

**Katayama**, T., Kubo, K., and Sato, N. (1975). "Earthquake Damage to Water and Gas Distribution System", Proceedings of US National Conference on Earthquake Engineering, pp. 396 - 405.

**Kennedy**, R. P., Chow, A. W., and Williamson, R. A. (1977). "Fault Movement Effects on Buried Oil Pipeline", Journal of the Transportation Engineering, American Society of Civil Engineers, Vol. (103), No. (TES), May, pp. 617 - 633.

**Kitaura**, M., Miyajima, M., and Namatame, N. (1998). "Damage to Water Supply Pipelines during the 1995 Hyogoken Nambu Earthquake and its Seismic Response Analysis", The 3rd China-Japan-US Trilateral Symposium on Lifeline Earthquake Engineering, Kunming City, China, pp. 81-88.

**Kobayashi**, T., Nakane, H., Suzuki, N., and Ishikawa, M. (1989). "Parametric Study on Flexibility of Buried Pipeline Subject to Large Ground Displacement", Proceedings of the 2nd U.S.-Japan Workshop on Liquefaction, Large Ground Deformation and Their Effects on Lifelines, Technical Report NCEER-89003, Buffalo, NY, pp. 348 - 362.

**Kyriakides, S.**, and Babock, C.D. (1983). "Buckle Propagation Phenomenon in Pipelines Collapse, The Buckling of Structures in Theory and Practice", Proceedings of the IUTAM Symposium on Collapse, London, Aug., (Edited by J.M.T. Thompson and G. W. Hunt), Cambridge University Press, pp.75 - 91.

**Kyriakides**, S., and Youn, S. K. (1984). "On the Collapse of Circular Confined Rings under External Pressure", International J. of Solids and Structures, Vol. (20), No. (7), pp. 699 - 713.

**Levy**, M. (1884). "Memoir on a New Integrable Case of the Problem of Elasticity and One of Its Applications", J. Mathematical Pure et Application (Liouville), Series (3), Vol. (10), pp. 5 - 42.

**Li**, F., and Kyriakides, S. (1991). "On the Response and Stability of Two Concentric Contacting Rings under External Pressure," J. Solids & Structures, Elsevier Science Publishers B.V., NY, Vol. (27), No. (1), pp. 1 - 14.

**Lim Y. M.**, Kim, M. K. Kim, T. W. and Jang, J. W. (2001). "The Behaviour Analysis of Buried Pipeline Considering Longitudinal Permanent Ground Deformation", Proceedings of ASCE Pipeline 2001, San Diego, CA., USA.

**Liu**, Xuejie (1996). "Response of Buried Continuous Pipelines Subject to Earthquake Effects", Ph. D. Dissertation, Rensselaer Polytechnic Institute, Troy, New York, USA.

**Liu**, Xuejie, and O'Rourke M. J. (1997). "Behaviour of Continuous Pipeline Subject to Transverse PGD", J. of Earthquake Engineering & Structural Dynamics, Wiley Inter Science, John Wiley and Sons Ltd., Vol. (26), pp. 989 - 1003.

**Liu**, W., Lee, K. M., and Zhang, S.D. (1994). "Modeling of a Large Underground Excavation in China", Centrifuge 1994, Proceedings of the International Conference on

Geotechnical Centrifuge Modeling, Edited by Leung, Lee and Tan, Balkema, Rotterdam, Netherlands, pp. 675 - 680.

**Lo**, K. H., and Zhang, J. Q., (1994). "Collapse Resistance Modeling of Encased Pipes", Buried Plastic Pipe Technology, Vol. (2), ASTM STP (1222), Dave Eckstein (Editor), American Society for Testing and Materials, West Conshohocken, PA, USA, pp. 97 - 110.

**Lo**, Bogdanoff, Goldberg and Crawford (1962). "A Buckling Problem of a Circular Ring", Proceedings of the 4th U.S. National Congress of Applied Mechanics, American Society of Mechanical Engineers, pp. 691 - 695.

**Lueke**, J. (2003). "Trenchless Technology: A New Paradigm in Construction", Trenchless Technology Lecture Series, ENF 231, NASTT Chapter of University of Calgary, BC, Canada.

**Lund**, L. (2003). "Pipeline Seismic Mitigation Using Trenchless Technology", Proceedings of the 6th U.S. Conference and Workshop on Lifeline Earthquake Engineering: Advancing Mitigation Technologies and Disaster Response for Lifeline Systems, August 10-13, Long Beach, CA, USA, pp. 736 - 743.

**Luscher**, U. (1966). "Buckling of Soil Surrounded Tubes", J, of Soil Mechanics and Foundation Division, American Society of Civil Engineers, Vol. (92), No. (SM6), November.

**McAlpine**, G. (1996). "Statistical Analysis and Implications or Test Data from Long-Term Structural Behaviour of Pipeline Rehabilitation Systems", Proceedings of the Water Environment Federation 69th Annual Conference & Exposition, Dallas, TX, USA.

**McAlpine**, G. (2003). "Rehabilitation of Fully Deteriorated Rigid Pipes by Flexible and Rigid Liners", Proceedings of the ASCE International Conference on Pipeline

Engineering and Construction: New Pipeline Technologies, Security, and Safety, July 3-16, Baltimore, Maryland, USA, pp. 363 - 372.

**Meis**, R. D. (2003). "Behaviour of Underground Piping Joints Due to Static and Dynamic Loading", Ph. D. Dissertation, University of Nevada, Reno, USA.

**Missacatte**, D., (2000). "Finite Element Calculations of Stresses and Deformations in Buried Flexible Pipes", M. Sc. Thesis, University of Ottawa, Ottawa, ON, Canada.

**Miyajima**, M. and Kitaura, M. (1989). "Effects of Liquefaction-Induced Ground Movement on Pipeline", Proceedings of the 2nd U.S.-Japan Workshop on Liquefaction, Large Ground Deformation and Their Effects on Lifelines, Technical Report NCEER-89-0032, Buffalo, NY, pp. 386 - 400.

**Moore**, I. D., and El-Sawy, K. (1996). "Buckling Strength of Polymer Liners Used in Sewer Rehabilitation", Transportation Research Record, No. (1541), Transportation Research Board, Washington D. C., USA, pp. 127 - 132.

**Moore**, I. D. (1998). "Tests for Pipe Liner Stability: What We Can and Cannot Learn", Proceedings of the North America No-Dig '98 Conference, Albuquerque, New Mexico, pp. 444 - 457.

**Moser**, A. P. (2001). "Buried Pipe Design", 2nd edition, McGraw-Hill, New York, USA, 544p.

**Newmark**, N. M. (1965). "Effects of Earthquakes on Dams and Embankments", Geotechnique, Vol. (15), No. (2), pp. 139 - 160.

**Newmark**, N. M. (1967). "Problems in Wave Propagation in Soil and Rocks", Proceedings of International Symposium on Wave Propagation and Dynamic Properties of Earth Materials, Albuquerke, New Mexico, pp. 7 - 26.

**Newmark**, N. M., and Hall, W. J. (1975). "Pipeline Design to Resist Large Fault Displacement", Proceedings of the 1st US Conference on Earthquake Engineering, Ann Arbor, MI, pp. 416 - 425.

**Omara**, A. M. (1997). "Analysis of Cured-In-Place Pipes (CIPP) installed in Circular and Oval Deteriorated Host Pipes", Ph. D. Dissertation, Dept. of Civil Engineering, Louisiana Tech. University, Ruston, LA, USA.

**Omara**, A. M., and Akl, F. A. (1998). "Trenchless Construction Methods", Journal of Infrastructure Systems, American Society of Civil Engineers, Vol. (4), No.(1), March, pp. 5 - 18.

**O'Rourke**, M. J. (1989). "Approximate Analysis Procedures for Permanent Ground Deformation Effects on Buried Pipelines", Proceedings of the 2nd US-Japan Workshop on Liquefaction, Large Ground Deformation and Their Effect on Lifelines, Technical Report NCEER-89-0032, National Center for Earthquake Engineering Research, State University of New York at Buffalo, NY, pp. 336 - 347.

**O'Rourke**, M. J. (1995). "Lifeline Earthquake Engineering", Proceedings of the Fourth US Conference, San Francisco, CA, USA, Aug. 10-12, Sponsored by the Technical Council on Lifeline Earthquake Engineering, ASCE, Monograph No. (6).

**O'Rourke,** M. and Ballantyne, D. (1992). "Observations on Water System and Pipeline Performance in the Limon Area of Costa Rico Due to the April 22, 1991 Earthquake", Technical Report NCEER-92-0017, Multidisciplinary Center for Earthquake Engineering Research, Buffalo, NY, USA.

**O'Rourke**, M. and Bloom, M. C. and Dobry, R. (1982). "Apparent Propagation Velocity of Body Waves", J. of Earthquake Engineering & Structural Dynamics, Wiley Inter Science, John Wiley and Sons Ltd.., Vol. (10), 1982, pp. 283 - 294.

**O'Rourke,** M., Castro, G. and Hossain, I. (1984). "Horizontal Soil Strain Due to Seismic Waves", Journal of Geotechnical Engineering, American Society of Civil Engineers, September, Vol. (110), No. (9), pp. 1173 - 1187.

**O'Rourke**, M. and Elhmadi, K. E. (1988). "Analysis of Continuous Buried Pipelines for Seismic Wave Effects", J. of Earthquake Engineering & Structural Dynamics, Wiley Inter Science, John Wiley and Sons Ltd., Vol. (16), pp. 917 - 929.

**O'Rourke**, M. and Liu, X. (1999)."Response of Buried Pipelines Subject to Earthquake Effects", Monograph Publications, Multidisciplinary Center for Earthquake Engineering Research, State University of New York at Buffalo, USA.

**O'Rourke**, M. and Liu, X. (1998). "Seismic Loading and Behaviour of Buried Pipelines", American Society of Mechanical Engineers, Proceedings of the 1998 ASME/JSME Joint Pressure Vessels and Piping Conference, Jul 26-30, San Diego, CA, USA, pp. 513 - 519.

**O'Rourke**, M., Liu, X. and Flores-Berrones, R. (1995). "Steel Pipe Wrinkling due to Longitudinal Permanent Ground Deformation", Journal of Transportation Engineering, ASCE, September/October, Vol. (121), No. (5), pp. 443 - 451.

**O'Rourke**, M. and Nordberg, C. (1991). "Analysis Procedures for Buried Pipes Subjected to Longitudinal and Transverse Permanent Ground Deformation", Proceedings of the 3rd Japan-U.S. Workshop on Earthquake Resistant Design of Lifelines Facilities and Countermeasures for Soil Liquefaction, San Francisco, CA, December 1990, Technical Report NCEER-91-0001, National Center for Earthquake Engineering Research, State University of New York at Buffalo, NY, pp. 439 - 453.

**O'Rourke**, M. and Nordberg, C. (1992). "Behaviour of Buried Pipes Subjected to Permanent Ground Deformation", Proceedings of the 10th World Conference on Earthquake Engineering, Madrid, Spain, July 19-24, Vol. (9), pp. 5411 - 5416.

**O'Rourke**, M., and O'Rourke, T. D. (1995). "Pipeline Response to Permanent Ground Deformation: A Benchmark Case", Proceedings of the 4th US Conference on Lifeline Earthquake Engineering, TCLEE, ASCE, San Francisco, CA, August, pp. 288 - 295.

**O'Rourke**, M., Stewart, H. E., Gowdy, T. E., and Pease, J. W. (1991). "Lifelines and Geotechnical Aspects of the 1989 Loma Prieta Earthquake", Proceedings of the 2nd International Conference on Recent Advances in Earthquake Engineering and Soil Dynamics, St. Louis, MO, pp. 1601 - 1612.

**O'Rourke**, T. (1988). "Critical Aspects of Soil-Pipeline Interaction for Large Deformation", Proceedings of the 1st US-Japan Workshop on Liquefaction, Large Ground Deformation, and Their Effect on Lifelines, pp. 118 - 126.

**O'Rourke**, T. (1992). "Earthquake Countermeasures for Lifelines in the Central and Eastern United States", TCLEE Monograph No. (5), D.B. Ballantyne (Editor), ASCE, USA, pp. 168 - 191.

**O'Rourke**, T. (1996). "Lessons Learned for Lifelines Engineering from Major Urban Earthquakes", Proceedings of the 11th World Conference on Earthquake Engineering, Pergamon, Elsevier Science Ltd., Oxford, England, Paper No. (2172).

**O'Rourke**, T. (1998). "Overview of Geotechnical and Lifeline Earthquake Engineering", Geotechnical Special Publication, Vol. (2), 1998, Proceedings of the 1998 Conference on Geotechnical Earthquake Engineering and Soil Dynamics III, Part 2, Aug 3-6, Seattle, WA, USA, pp. 1392 - 1426.

**O'Rourke**, T. ,Gowdy, T. E., Stewart, H. E., and Pease, J. W. (1991). "Lifelines Performance and Ground Deformation in the Marina District during the 1989 Loma Prieta Earthquake", Proceedings of the 3rd Japan-U.S. Workshop on Earthquake Resistant Design of Lifelines Facilities and Countermeasures for Soil Liquefaction, San Francisco, California, Technical Report NCEER-91-0001, Multidisciplinary Center for Earthquake Engineering Research, State University of New York at Buffalo, USA.

**O'Rourke**, T., Grigoriu, M. D. and Khater, M. M. (1985). "A state of the Art Review: Seismic Response of Buried Pipelines", Decade of Progress in Pressure Vessel Technology, (Editor: C. Sundararajan), American Society for Mechanical Engineers, USA.

**O'Rourke**, T., Jeon, S. S. (1999). "Factors Affecting the Earthquake Damage of Water Distribution Systems", Technical Council on Lifeline Earthquake Engineering Monograph (16), Proceedings of the 1999 5th U.S. Conference on Lifeline Earthquake Engineering: Optimizing Post-Earthquake Lifeline System Reliability, Aug 12-14, Seattle, WA, USA, pp. 379 - 388.

**O'Rourke**, T. and Jeon, S. S. (2000). "Seismic Zonation for Lifelines and Utilities", 6th International Conference on Seismic Zonation, Earthquake Engineering Research Institute, Oakland, CA, USA.

**O'Rourke**, T. and Lane, P. A. (1989). "Liquefaction Hazards and Their Effects on Pipelines", National Center for Earthquake Engineering Research, Technical Report NCEER 89-0007, Buffalo, NY, USA.

**O'Rourke**, T. and Palmer, M. (1996). "Earthquake Performance of Gas Transmission Pipelines", Earthquake Spectra: The Professional Journal of the Earthquake Engineering Research Institute, Vol. (12), No. (3), August, pp. 493 - 527.

**O'Rourke**, T. and Pease, J. W. (1992). "Large Ground Deformations and Their Effects on Lifelines; 1989 Loma Prieta Earthquake", United States Case Studies of Liquefaction and Lifeline Performance during Past Earthquakes, Technical Report NCEER-92-0002, Multidisciplinary Center for Earthquake Engineering Research, State University of New York at Buffalo, USA.

**O'Rourke**, T., Roth, B. L. and M. Hamada (1992). "Large Ground Deformations and Their Effects on Lifeline Facilities: 1971 San Fernando Earthquake", Report No. NCEER-92-0002, National Center for Earthquake Engineering Research, State University of New York, Buffalo, NY, USA, pp. 3.1 - 3.85.

**O'Rourke**, T. and Tawfik, M. S. (1983). "Effects of Lateral Spreading on Buried Pipelines During the 1971 San Fernando Earthquake", Earthquake Behaviour and Safety of Oil and Gas Storage Facilities, Buried Pipelines and Equipment, PVP-77, American Society for Mechanical Engineers, New York, June, pp. 124 - 132.

**O'Rourke**, T., S. Toprak, and Y. Sano (1998). "Factors Affecting Water Supply Damage Caused by the Northridge Earthquake", Proceedings of the 6$^{th}$ U.S. National Conference on Earthquake Engineering, Seattle, WA, USA, pp. 1 - 12.

**O'Rourke**, T. and Trautmann, C. (1981). "Earthquake Ground Rupture Effects on Jointed Pipe", Proceedings of the 2nd Specialty Conference of the Technical Council on Lifeline Earthquake Engineering, American Society for Civil Engineers, August, USA, pp. 65 - 80.

**Paulin**, M. J. (1998). "An Investigation into Pipelines Subjected to Lateral Soil Loading", Ph. D. Dissertation, Memorial University of Newfoundland, St. John's, Newfoundland, Canada.

**Pian**, T. H. I. and Bucciarelli, L. L. Jr. (1967). "Constrained Circular Ring under Distributed Loading", Int. J. Solids and Structure, Vol. (3), pp. 715 - 730.

**Pradhan**, S. K. (2002). "Dynamic Soil-Structure Interaction Using Distributed State Concept and Artificial Neutral Networks for Parameter Evaluation", Ph. D. Dissertation, University of Arizona, Tempe, AZ, USA.

**Ramberg**, W. and Osgood, W. (1943). "Description of Stress-Strain Curves by Three Parameters", Technical Note No. (902), National Advisory Committee for Aeronautica, 28p.

**Rasheed**, H. A. (1996). "Behaviour and Strength of Composite Tubes Considering Delamination and Other Defects", Ph. D. Dissertation, University of Texas at Austin, Austin, TX, USA.

**Reddy**, K. P. (1993). "Lifeline Structures under Earthquake Excitations", M. SC. Thesis, Florida Atlantic University, Boca Raton, FL, USA.

**Rucker**, M. and Dowding, C. (2000). "Segmented (Buried Utilities) Pipeline Damage Rates from Dynamic Loadings", Proceedings of EM2000, 14th Engineering Mechanics Conference of the American Society of Civil Engineers, May 21-24, Austin, TX, USA.

**Sato**, Tadanobu, Yagi, Izabro, and Sakuragi, Hiroyuki (1997). "Earthquake Damage to Buried Water Supply Pipes and Their Renovation by Hose Lining Technology", Proceedings of the 7th US-Japan Workshop on Earthquake Disaster Prevention for Lifeline Systems, November 4-7, Seattle, WA, pp 39 - 53.

**Schafer**, B. W. and McGrath, T. J. (2003). "Buried Corrugated Thermoplastic Pipe: Simulation and Design", J. of Transportation Research Record, Vol. (1849), pp. 135 - 143.

**Schiff**, Anshel J. and Tang, Alex K. (2000). "CHI-CHI, Taiwan, Earthquake of September 21, 1999", Lifelines Performance, Technical Council on Lifeline Earthquake

Engineering, Monograph No. (18), July, American Society of Civil Engineers, Reston, VA., USA.

**Schrock**, B. J. (Editor) (1994). "Existing Sewer Evaluation and Rehabilitation", ASCE Manual and Report on Engineering Practice, No. (62): Water Environment Federation Manual of Practice, FD-6, Alexandria, VA, USA.

**Schrock**, J. and Gumbel, J. (1997). "Pipeline Renewal-1997", Proceeding of the Conference and Exhibition of Trenchless Technology, North America No-Dig '97 Conference, April 18-21, Seattle, WA, USA.

**Schrock**, J. (2003). "Pipeline System Renewal Technologies", Proceeding of International Conference on Pipeline Engineering and Construction, ASCE, Mohammed Najafi (Editor), July 13-16, Baltimore, Maryland, USA, pp. 341 - 351.

**Seemann**, R. K. (2000). "Short-Term Buckling Tests for Pipe Liners Installed in Ovalized Host Pipes", M. Sc. Thesis, Louisiana Tech. University, Ruston, LA, USA.

**Seemann**, R. K., Hall, D. E. and Straughan, W. T. (2001). "Buckling Experiments for CIPP Liners Installed in Ovalized Host Pipes", TTC Research Report, Louisiana Tech. University, Ruston, LA, USA.

**Selventhiran**, K. (2002). "Non-linear Analysis of Buried Restrained and Unrestrained Segmental Pipelines Subjected to Permanent Ground Deformation", M. SC. Thesis, University of Nevada, Reno, USA.

**Serpente**, R. F. (1994). "Understanding the Modes of Failure for Sewers", in Urban Drainage Rehabilitation Programs and Techniques, Edited by William A. Macaitis, ASCE.

**Shaoping**, S. (1994). "A Review of Buried Lifeline Earthquake Engineering in China", Proceedings of 2nd China-Japan-US Trilateral Symposium on Lifeline Earthquake Engineering, Edited by Hou, Z., Takada, S., and Wang, L. R. L., April, Xi'an, China, pp. 17 - 42.

**Singhall**, A. (1984a). "Non-linear Behaviour of Ductile Iron Pipeline Joints", J. of Technical Topics in Civil Engineering, ASCE, Vol. (110 ), No. (1), pp. 29 - 47.

**Singhall**, A. (1984b). "Non-linear Behaviour of Ductile Iron Pipeline Joints", J. of Transportation Engineering, ASCE, Vol. (110 ), No. (2), pp. 235 - 250.

**Singhall**, A. and Benavides, J. C. (1983). "Non-linear Behaviour of Ductile Iron Pipeline Joints", J. of American Water Works Association, AWWA, Research and Technology, November, pp. 572 - 578.

**Singhall**, A. C. and Meng, Chain-Lee (1983). "Junction Stresses in Buried Jointed Pipelines", ASCE, Journal of Transportation Engineering, Vol. (109), No. (3), May, pp. 450 - 461.

**Straughan**, W. T., Guice, L. K., and Mal-Duraipandian, C. (1995). "Long-Term Structural Behaviour of Pipeline Rehabilitation Systems", ASCE, Journal of Infrastructure Systems, Vol. (1), No. (4), December, pp. 214 - 220.

**Straughan**, W. T., Tantirungrojchai, N. Guice, L. K. and Lin, Y. (1998). "Creep Test of Cured-in-Place Pipe Material under Tension, Compression and Bending", Journal of Testing and Evaluation, Vol. (26), No. (6), pp. 594 - 601.

**Straughan**, T. et al. (1998a). " Preliminary Short-Term Buckling Tests Results", Internal Report, Trench Technology Center (TTC), Louisiana Tech. University, Ruston, LA, USA.

**Straughan**, T. et al. (1998b). "Long-Term Buckling Tests Data", Internal Report, Trench Technology Center (TTC), Louisiana Tech University, Ruston, LA, USA.

**Sun**, Lixun, (2001). "Centrifuge Modeling and Finite Element Analysis of Pipeline Buried in Liquefiable Soil", Ph. D. Dissertation, Columbia University, New York, NY, USA.

**Sun**, S. and Shien, L. (1983). "Analysis of Seismic Damage to Buried Pipelines in Tangshan Earthquake", Earthquake Behaviour and Safety of Oil and Gas Storage Facilities, Buried Pipelines and Equipment, PVP-77, ASME, New York, June, pp. 365 - 367.

**Suzuki**, N., Arata, O. and Suzuki, I. (1988). "Lifelines Subject to Liquefaction-Induced Permanent Ground Displacement", Proceedings of the 1st Japan-U.S. Workshop on Liquefaction, Large Ground Deformation and Their Effects on Lifelines, November, pp. 237 - 252.

**Suzuki**, N., and Masuda, N. (1991). "Idealization of Permanent Ground Movement and Strain Estimation of Buried Pipes", Proceedings of the 3rd Japan-U.S. Workshop on Earthquake Resistant Design of Lifelines Facilities and Countermeasures for Soil Liquefaction, February, pp. 455 - 469.

**Tafreshi**, A. (2004), "Delamination Buckling and Post-Buckling in Composite Cylindrical Shells under External Pressure", Journal of Thin-Walled Structures, Vol. (42), pp. 1379 - 1404.

**Takada**, S. (1984). "Model Analysis and Experimental Study on Mechanical Behaviour of Buried Ductile Iron Pipelines Subjected to Large Ground Deformations", Proceedings of the 8th World Conference Earthquake Engineering, San Francisco, California, Vol. (VII), pp. 255 - 262.

**Takada**, S., Higashi, S., and Tanaka, T., (1998). "Investigation and Dynamic Analysis on the Performance of Sewage FRPM Pipelines during the Great Hanshin-Awaji Earthquake", The 3rd China-Japan-US Trilateral Symposium on Lifeline Earthquake Engineering, Kunming City, China, pp.173 - 180.

**Takada**, S., and Abdel-Aziz, M. (1998). "A Proposal for Improving the Current Seismic Design Method for the Transverse Direction of Shield Tunnels", The 3rd China-Japan-US Trilateral Symposium on Lifeline Earthquake Engineering, Kunming City, China, pp. 275 - 282.

**Takada**, S., and Tanabe, K. (1988). "Estimation of Earthquake Induced Settlements for Lifeline Engineering", Proceedings of the 9th World Conference Earthquake Engineering, August, Vol. (VII), pp. 109 - 114.

**Tawahata**, I., Tokida, K., Tamari, Y. Matsumoto, H. and Yamada, K. (1990). "Prediction of Permanent Lateral Displacement of Liquefied Ground by Means of Variation Principle", Proceedings of the 3rd U.S.-Japan Workshop on Liquefaction, Large Ground Deformation and Their Effects on Lifelines, December, Technical Report NCEER-91-0001, Buffalo, NY, pp. 348 - 362.

**Tawfik**, M. S. and O'Rourke, T. D. (1985). "Load-Carrying Capacity of Welded Slip Joints", Journal of Pressure Vessel Technology, ASME, New York February, Vol. (107), pp. 37 - 43.

**Thépot**, O. (2000). "A New Design Method for Non-Circular Sewer Linings", J. Trenchless Technology Research, Vol. (15), No. (1), pp. 25 - 41.
Thépot, O. (2004). "International Comparison of Methods for the Design of Sewer Lining", Erschienen in 3R International 8-9/2004.

**Timoshenko**, S. P. and Gere, J. M. (1961). "Theory of Elastic Stability", 2nd Edition, McGraw-Hill, New York, USA.

**Tohda**, J., Yoshimura, H., and Li, L. (1996). "Characteristic Features of Damage to the Public Sewerage Systems in the Hanshin Area", Soils and Foundations - Special Issue on Geotechnical Aspects of the January 17, 1995 Hyogoken-Nambu Earthquake, Japanese Geotechnical Society, Tokyo, Japan, pp. 335 - 347.

**Toprak**, S. (1998). "Earthquake Effects on Buried Lifeline Systems", Ph. D. Dissertation, Dept. of Civil Engineering, Cornell University, Ithaca, NY, USA.

**Toprak**, S., O'Rourke, T., and Tutuncu, I. (1999). "GIS Characterization of Spatially Distributed Lifeline Damage", Technical Council on Lifeline Earthquake Engineering Monograph No. (16), Proceedings of the 5th U.S. Conference on Lifeline Earthquake Engineering: Optimizing Post-Earthquake Lifeline System Reliability, August, Seattle, WA, USA, pp. 110 - 119.

**Trautmann**, C. E. and O'Rourke, T. D. (1983). "Load-Displacement Characteristics of a Buried Pipe Affected by Permanent Earthquake Ground Movements", Proceedings of the 4$^{th}$ National Congress on Pressure Vessel and Piping Technology, ASME, New York, PVP-77, January, pp. 254 - 262.

**Trifunac**, M. and Todorovska, M. (1997). "Northridge-California Earthquake of 1994: Density of Pipe Breaks and Surface Strains", Soil Dynamics and Earthquake Engineering, Vol. (16), pp. 193 - 207.

**Tucker**, M. (1995). "Ductile Iron Pipe in Earthquake/Seismic Activity", Proceedings of the 2nd International Conference: Advances in Underground Pipeline Engineering, June 25-28, Bellevue, WA, pp. 359 - 369.

**Varnes**, D. J. (1978). "Slope Movement Types and Processes, Landslides Analysis and Control", Special Report (176), Transportation Research Board, National Academy of Sciences, Washington D. C., pp. 11 - 33.

**Wang**, L. R. L. (1979). "Some Aspects of Seismic Resistant Design of Buried Pipelines", Lifelines Earthquake Engineering-Buried Pipelines, Seismic Risk and Instrumentation, PVP-34, ASME, New York, pp. 117 - 131.

**Wang**, L. R. L. (1990). "Performance of Water Pipeline Systems from 1987 Whittier Narrows, California Earthquake", Proceedings of the 4th US National Conference on Earthquake Engineering, May, Vol. (1), pp. 965 - 974.

**Wang**, S. (2002). "A New Long-Term Design Model for Rehabilitation Pipe Liners", Ph. D. Dissertation, Louisiana Tech. University, College of Engineering and Science, Ruston, LA, USA.

**Wang**, L. and Cheng, K. (1979). "Seismic Response Behaviour of Buried Pipelines", Journal of Pressure Vessel Technology, February, Vol. (II), pp. 21 - 30.

**Wang**, L. and Li, H. (1994). "Experimental Study on the Damping and Resistant Characteristics of Conventional Pipe Joints", Proceedings of the 5th US National Conference on Earthquake Engineering, Earthquake Engineering Research Institute, Oakland, California, Vol. (II), pp. 837 - 846.

**Watkins**, R. K. and Shupe, O. K. (1988). "Tests Prove Insituform Adds Significant Structural Strength", Utah State University, Buried Structures Laboratory, Civil and Environmental Engineering, Unpublished Report to Insituform of North America Inc., Cary, NC, USA.

**Watkins**, R. K. (1993). "Strength of Buried Broken Rigid Pipes with Danby Liners", Utah State University, Buried Structures Laboratory, Civil and Environmental Engineering, Unpublished Report to Danby of North America Inc., Cary, NC, USA.

**Watkins**, R. K. and Anderson, L. R. (2000). "Structural Mechanics of Buried Pipes", 1st Edition, CRC Press, Boca Raton, FL, USA.

WEF Manual of Practice FD-6, (1994). "Existing Sewer Evaluation and Rehabilitation", ASCE Manual and Report on Engineering Practice No. (62), NY, USA.

**Welch**, A. J. (1989), "Creep Buckling of Infinitely Long Constrained Cylinders under Hydrostatic Loading", Ph. D. Dissertation, University of Bradford, Bradford, UK.

**Wells**, D. L. and Coppersmith, K. J. (1994). "New Empirical Relationships among Magnitude", Rupture Length, Rupture Width, Rupture Area, and Surface Displacement, Bulletin of the Seismological Society of America, Vol. (84), No. (4), August, pp. 974 - 1002.

**White**, H. L. and Layer, J. P. (1960). "The Corrugated Metal Conduit as a Compression Ring", Proceedings of Highway Research Board, Washington D. C., Vol. (39), pp. 369 - 397.

**WRc** (1994). "Sewerage Rehabilitation Manual-(SRM)", Water Research Center, Swindon, Wiltshire, UK.

**Yeh**, G. (1974). "Seismic Analysis of Slender Buried Beams", Bulletin of the Seismological Society of America, October, Vol. (64), No. (5), pp. 1551 - 1562.

**Zhang**, C., and Moore, I. D. (1997a). "Non-Linear Mechanical Response of High Density Polyethylene: Part I - Experimental Investigation and Model Evaluation", J. Polymer Eng. and Science, Vol. (37), No. (2), pp. 404 - 413.

**Zhang**, C., and Moore, I. D. (1997b). "Non-Linear Mechanical Response of High Density Polyethylene: Part II - Uniaxial Constitutive Modeling", J. Polymer Eng. and Science, Vol. (37), No. (2), pp. 414 - 420.

**Zhang**, S. D., and Zhang, H. D. (1994). "Stability of Deep Excavations in Soft Clay", Centrifuge 1994, Proceedings of the International Conference on Geotechnical Centrifuge Modeling, Edited by Leung, Lee and Tan, Balkema, Rotterdam, Netherlands, pp. 643 - 647.

**Zhao**, Q. (1999). "Finite Element Simulation of Creep Buckling of CIPP Liners under External Pressure", Ph.D. Dissertation, Department of Computation Analysis and Modeling, Louisiana Tech. University, Ruston, LA, USA.

**Zhao**, J. Q., and Rajani, B. (2002). "Construction and Rehabilitation Costs for Buried Pipe with a Focus on Trenchless Technologies", National Research Council Canada, Institute for Research in Construction, Research Report No. (101), Ottawa, Canada.

**Zhao**, J. Q. and Daigle, L. (2001). "Structural Performance of Sliplined Watermain", Canadian Journal of Civil Engineering, Vol. (28), pp. 969 - 978.

**Zhao**, J. Q., Daigle, L. and Desnoyers, R. (1999). "Gloucester Street Watermain Rehabilitation Research Aspect", National Research Council Canada, Institute for Research in Construction, NRCC-43687, Ottawa, Canada.

**Zhao**, W. (2003). "Finite Element Analysis and Statistical Modeling of Pipeline Rehabilitation Liners with Material Imperfections", Ph.D. Dissertation, College of Engineering and Science, Louisiana Tech. University, Ruston, LA, USA.

**Zhou**, Z. and Murray, D. W. (1993). "Behaviour of Buried Pipelines Subjected to Imposed Deformations", Proceedings of the 12$^{th}$ Offshore Mechanics and Arctic Engineering Conference, ASME, Glasgow, Scotland, Vol. (V), pp. 115 - 122.

**Zhu**, M. (2000). "Computational Investigation of Stress, Contact Conditions, and Buckling of Thin-Walled Pipe Liners", Ph.D. Dissertation, Department of Civil Engineering, Louisiana Tech. University, Ruston, LA, USA.

# APPENDICES

## APPENDIX A
## Pipes and Liners Data

### A.1 Pipes Types and Dimensions

**Pipe Type: Vitrified Clay – Class 160**

| Nominal Size Inches (mm) | Inner Diameter Inches (mm) | Wall Thickness Inches (mm) | Outer Diameter Inches (mm) | Outer Radius Inches (mm) |
|---|---|---|---|---|
| 8 (200) | 8 (203.2) | 0.98 (24.9) | 9.96 (253.0) | 4.98 (126.5) |
| 10 (250) | 10 (254.0) | 1.02 (25.9) | 12.04 (305.8) | 6.02 (152.9) |
| 12 (300) | 12 (304.8) | 1.12 (28.4) | 14.24 (361.7) | 7.12 (180.9) |

**Pipe Type: Non-Reinforced Concrete – Class II**

| Nominal Size Inches (mm) | Inner Diameter Inches (mm) | Wall Thickness Inches (mm) | Outer Diameter Inches (mm) | Outer Radius Inches (mm) |
|---|---|---|---|---|
| 8 (200) | 8 (203.2) | 0.875 (22.2) | 9.75 (247.7) | 4.875 (123.8) |
| 10 (250) | 10 (254.0) | 1.000 (25.4) | 12.00 (304.8) | 6.000 (152.4) |
| 12 (300) | 12 (304.8) | 1.375 (34.9) | 14.75 (374.7) | 7.375 (187.3) |

**Pipe Type: Reinforced Concrete – Wall B**

| Nominal Size Inches (mm) | Inner Diameter Inches (mm) | Wall Thickness Inches (mm) | Outer Diameter Inches (mm) | Outer Radius Inches (mm) |
|---|---|---|---|---|
| 8 (200) | 8 (203.2) | 2 (50.8) | 12 (304.8) | 6 (152.4) |
| 10 (250) | 10 (254.0) | 2 (50.8) | 14 (355.6) | 7 (177.8) |
| 12 (300) | 12 (304.8) | 2 (50.8) | 16 (406.4) | 8 (203.2) |

**Pipe Type: Reinforced Concrete (Equivalent-Composite Section) (Short –Term)**

| Nominal Size Inches (mm) | Inner Diameter Inches (mm) | Wall Thickness Inches (mm) | Outer Diameter Inches (mm) | Outer Radius Inches (mm) |
|---|---|---|---|---|
| 8 (200) | 8 (203.2) | 2.0173 (51.24) | 12.035 (305.7) | 6.0173 (152.9) |
| 10 (250) | 10 (254.0) | 2.0173 (51.24) | 14.035 (356.5) | 7.0173 (178.3) |
| 12 (300) | 12 (304.8) | 2.0173 (51.24) | 16.035 (407.3) | 8.0173 (203.6) |

## A.2 CIPP Liner Design - ASTM F1216-Partially Deteriorated Gravity Pipe Case

### Calculations Sample

The current ASTM F1216-2007 for partially deteriorated gravity pipe condition may be used to determine the thickness required for the CIPP liner:

$$P = \frac{2KE}{1-\upsilon^2}\frac{1}{(SDR-1)^3}\frac{C}{N}$$

where:

$P$ = groundwater load (MPa)

$K$ = enhancement factor

(minimum of 7 is recommended where there is a full support of the existing pipe)

$E$ = long-term modulus of elasticity for CIPP liner (MPa)

(typically assumed to be 50% of the short-term modulus of elasticity for CIPP liner)

$\sigma$ = long-term flexural strength for CIPP liner (MPa)

(typically assumed to be 50% of the short-term flexural strength for CIPP liner)

$\upsilon$ = Poisson's ratio for CIPP (average of 0.3)

$SDR$ = Standard Dimension Ratio of CIPP liner

$$SDR = \frac{D_o}{t}$$

$D_o$ = mean outer diameter of CIPP liner (mm)

$t$ = CIPP liner thickness (mm)

$q$ = percentage ovality of original pipe (%)

$$q = \frac{MeanInsideDiameter - MinimumInsideDiameter}{MeanInsideDiameter} x100$$

$C$ = ovality reduction factor

$$C = \left(\frac{\left[1-\frac{q}{100}\right]}{\left[1+\frac{q}{100}\right]^2}\right)^3$$

$N$ = factor of safety (typically a value of 2)

The CIPP liner thickness is determined by using the ASTM F1216-2007 for partially deteriorated gravity pipe condition previously defined, the equation can be solved for CIPP liner thickness and rearranged into the following form:

$$t = \frac{D_o}{\left[\frac{2KEC}{P(1-\nu^2)N}\right]^{1/3} + 1}$$

Note 1:

If there is no groundwater above the pipe invert (i.e., $P = 0$), the ASTM F1216 can not be used to calculate the CIPP liner thickness. In this case, the CIPP liner should typically have a maximum SDR of 100, dependent upon design condition. Therefore, the CIPP liner maximum thickness will be:

$$t = \frac{D_o}{SDR} = \frac{D_o}{100}$$

Note 2:

If the original pipe is oval (i.e., $q > 0$), the stress due to bending may govern. Thus, the CIPP liner thickness should be checked to ensure that the bending stress does not exceed the long-term flexural strength of the CIPP liner. Then the CIPP liner should have a minimum thickness calculated by the following formula:

$$1.5\frac{q}{100}\left(1+\frac{q}{100}\right)SDR^2 - 0.5\left(1+\frac{q}{100}\right)SDR = \frac{\sigma}{PN}$$

**CIPP liner design (circular host pipe case)**

Input Data:

Safety factor $N = 2$

Enhancement factor $K = 7$

Short-term flexural modulus of elasticity of CIPP liner (polyester) $E = 1724$ MPa

Short-term flexural strength of CIPP liner (polyester) $\sigma = 31.03$ MPa

Poisson's ratio of CIPP liner $\nu = 0.30$

Mean outer diameter of CIPP liner $D_o = 203.2$ mm

Mean inside diameter of the pipe $D_i = 203.2$ mm

Minimum inside diameter of the pipe $D_{im} = 203.2$ mm

Height of soil on top of pipe $H = 2.140$ m

Ground water height above the top of the pipe $H_w = 0.91$ m

Output Data:

Ovality of host pipe $q = 0\%$

Ovality reduction factor $C = 1.0$

Ground water load (hydrostatic pressure) $P_w = 9.81 * H_w = 8.927$ kPa

CIPP liner thickness $t = 2.219$ mm

Standard Dimension Ratio of CIPP liner $SDR = 91.563$

**CIPP liner design (oval host pipe case)**

Using the same input data for the circular host pipe case, except:

Minimum inside diameter of the pipe $D_{im}$ = 193.05 mm

Output Data:

Ovality of host pipe $q$ = 5%

Ovality reduction factor $C$ = 0.640

Ground water load (hydrostatic pressure) $P_w = 9.81 * H_w$ = 8.927 kPa

CIPP liner thickness $t$ = 2.571 mm

Standard Dimension Ratio of CIPP liner $SDR$ = 79.048

Check for allowable long-term bending stress:

Long-term flexural strength of CIPP liner σ = 0.5*31.03 = 15.515 MPa

$$\sigma_{bending} = PN\left[1.5\frac{q}{100}\left(1+\frac{q}{100}\right)SDR^2 - 0.5\left(1+\frac{q}{100}\right)SDR\right]$$

$\sigma_{bending}$ = 8.036 MPa < 15.515 MPa

Since the long-term bending stress is less than the long-term flexural strength of CIPP liner, the initial design is OK.

# APPENDIX B

## SOIL SPRING STIFFNESS CALCULATIONS
## TCLEE Guideline (ASCE, 1984)

### B.1 CALCULATIONS SAMPLE FOR SOIL SPRING STIFFNESSES

**Example:**

Calculation of Ultimate Soil Resistance to the Movement of Buried Pipeline

**Problem Statement:**

A pipeline has been constructed to carry natural gas at an operating pressure of 75 $kg/cm^2$. The pipe is of API X-52 Grade steel with 0.6 m outer diameter and 0.0064 m wall thickness and buried at a soil cover of 1.2 m. The subsurface soil in which the pipe runs through is of medium sandy soil with coefficient of cohesion = 0.3 $kg/cm^2$, $\varphi = 32°$ and effective unit weight of 18 $kN/m^3$.

Calculate the ultimate resistance of soil for pipe movement in:

(a) axial (b) transverse, and (c) vertical direction.

**Given Data:**

**Pipe data:**

Pipe diameter = D = 0.6 m

Pipe wall thickness = $t$ = 0.0064 m

Pressure in the pipeline = 75 $kg/cm^2$

Pipe Grade = API X-52

**Soil data:**

Clear soil cover over the pipeline = H =1.2 m

Soil type: Medium sandy soil

Coefficient of cohesion = C = 0.3 $kg/cm^2$

Angle of friction = $\varphi = 32°$

Effective unit weight of soil = $\gamma^- = 18000\ N/m^3$

**Calculations:**

(a) Axial soil force:

The maximum axial soil force transmitted to the pipe per unit length:

$t_u = \pi DC\alpha + 0.5\pi D\gamma^{-} H(1+k_o)\tan(k\varphi)$

Where:

C = 0.3 kg/cm$^2$ = 30 kPa

k = 0.7, for smooth steel pipe (Table C-1)

α = adhesion factor

$$\alpha = 0.608 - 0.123c - \frac{0.274}{c^2+1} + \frac{0.695}{c^3+1} \qquad \text{in which c is in (kPa/100)}$$

$$= 0.608 - 0.123(0.30) - \frac{0.274}{(0.30)^2+1} + \frac{0.695}{(0.30)^3+1}$$

$$= 0.9964$$

Interface angle of friction between soil and pipe = $\delta' = k\varphi = 0.7(32°) = 22.4°$

Coefficient of soil pressure at rest = $k_o = 1 - \sin 32° = 0.47$ (Table C-2)

Hence,

$t_u = (\pi)(0.6)(0.9964)(30000) + 0.5(\pi)(0.6)(1.2)(18000)(1+0.47)(\tan 22.4^{o})$

= 68680 N/m = 68.7 kN/m

Considering the soil as medium sandy (loose), the yield displacement of soil at $t_u$:

$x_u$ = 5 mm = 0.005 m (Table C-3)

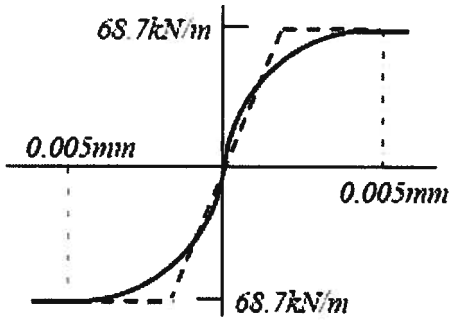

(b) Pipe movement in transverse (lateral) direction:

The maximum transverse soil force that is transmitted to the pipe per unit length:

$P_u = N_{ch} CD + N_{qh} \bar{\gamma} HD$

Where

$N_{ch}$ = Horizontal bearing capacity factor for clay (0 for C=0)

$$N_{ch} = a + bx + \frac{c}{(x+1)^2} + \frac{d}{(x+1)^3} \leq 9$$

For

$$x = \frac{H}{D} = \frac{1.2}{0.6} = 2$$

From Table C-4

a = 6.752, b = 0.065, c = -11.063, and d = 7.119

So,

$$N_{ch} = a + bx + \frac{c}{(x+1)^2} + \frac{d}{(x+1)^3} \leq 9$$

$$N_{ch} = 6.752 + 0.065(2) + \frac{-11.063}{(2+1)^2} + \frac{7.119}{(2+1)^3} = 5.916 \leq 9$$

$N_{qh}$ = Horizontal bearing capacity factor for sandy soil (0 for φ=0)

$N_{qh} = a + bx + cx^2 + dx^3 + ex^4$

For

$x = \frac{H}{D} = \frac{1.2}{0.6} = 2$ and φ=32°, from Table C-4

a = 5.4654, b = 1.548, c = -0.1118 , d = 5.6254 x $10^{-3}$, and e = -1.2227 x $10^{-4}$

So,

$N_{qh} = 5.4654 + 1.548(2) - (0.1118(2^2)) + (5.6254(10^{-3})(2^3)) - (1.2227\ (10^{-4})(2^4))$

$= 8.1572$

Hence,

$P_u = N_{ch} CD + N_{qh} \bar{\gamma} HD$

$P_u = (5.916(30000)(0.6)) + (8.1572(18000)(1.2)(0.6)) = 212205$ N/m = 212.2 kN/m

The yield displacement of soil at $P_u$:

$$y_u = 0.04\left(H + \frac{D}{2}\right) = 0.04\left(1.2 + \frac{0.6}{2}\right) = 0.06 \text{ m}$$

(b) Pipe movements in vertical direction

Vertical uplift:

The maximum uplift resistance force of the soil upon unit length of the pipeline:

$Q_u = N_{cv}\, CD + N_{qv}\, \gamma^- HD$

Where

$N_{cv}$ = Vertical uplift factor for clay

$$N_{cv} = 2\left(\frac{H}{D}\right) \le 10$$

$$N_{cv} = 2\left(\frac{1.2}{0.6}\right) = 4 \le 10$$

$N_{qv}$ = Vertical uplift factor for sand

$$N_{qv} = \left(\frac{\varphi H}{44D}\right) \le N_q$$

$$N_{qv} = \left(\frac{32(1.2)}{44(0.6)}\right) = 1.454 \le N_q$$

From Figure C-1, for ($\varphi$=32°):

$N_c$=36 , $N_q$=23, $N_\gamma$=27

Hence

$Q_u = N_{cv}\, CD + N_{qv}\, \gamma^- HD$

$Q_u$ = 4 (30000)(0.6) + 1.454 (180000 )(1.2 )( 0.6)

= 90843.8 N/m

The yield displacement of soil at $Q_u$:

$z_u = 0.15H = 0.15(1.2)$

$z_u$ = 0.18 m

Vertical bearing:

The maximum bearing resistant force of the soil upon unit length of the pipeline:

$$Q_d = N_c\, CD + N_q\, \gamma^- + N_\gamma\, \gamma^- \left(\frac{D^2}{2}\right)$$

Hence,

$$Q_d = 36\,(30000)(0.6) + 23\,(18000)(1.2)(0.6) + 27\,(18000)\left(\frac{0.6^2}{2}\right) = 1033560 \text{ N/m}$$

The yield displacement of soil at $Q_d = 0.125\,D = 0.125\,(0.6) = 0.075$ m

Soil spring stiffness (Maximum Resistance Force & Displacement) can be summarized as follow:

| Direction of pipe movement | | Notations | Maximum Resistance Force (N/m) | Displacement (m) |
|---|---|---|---|---|
| Axial | | $t_u$ | 68680 | 0.005 |
| Transverse | | $P_u$ | 212205 | 0.06 |
| Vertical | Uplift | $Q_u$ | 90844 | 0.18 |
| | Bearing | $Q_u$ | 1033560 | 0.075 |

Table B.1.1 Friction Factor (k) for Various External Coating (ALA, 2001)

| Pipe Coating | k |
|---|---|
| Concrete | 1.0 |
| Coal Tar | 0.9 |
| Rough Steel | 0.8 |
| Smooth Steel | 0.7 |
| Fusion Bonded Epoxy | 0.6 |
| Polyethylene | 0.6 |

Table B.1.2 Lateral Pressure Coefficient at Rest ($k_o$) for Different Soils (ALA, 2001)

| Type of Soil | $k_o$ |
|---|---|
| Loose Soil | 0.5-0.6 |
| Dense Soil | 0.3-0.5 |
| Clay (drained) | 0.5-0.6 |
| Clay (undrained) | 0.8-1.1 |
| Over-consolidated Soil | 1.0-1.3 |

Table B.1.3 Axial Soil Spring Displacement ($x_u$) for Different Soils (ALA, 2001)

| Type of Soil | $x_u$ (mm) |
|---|---|
| Loose Sand | 5 |
| Dense Sand | 3 |
| Stiff Clay | 8 |
| Soft Clay | 10 |

Table B.1.4 Bearing Capacity Factors for Different Soil Friction Angles (ALA, 2001)

| Factor | φ | x | a | b | c | d | e |
|---|---|---|---|---|---|---|---|
| $N_{ch}$ | 0° | H/D | 6.752 | 0.065 | -11.063 | 7.119 | |
| $N_{qh}$ | 20° | H/D | 2.399 | 0.439 | -0.03 | 1.059x10-3 | -1.754x10-5 |
| $N_{qh}$ | 25° | H/D | 3.332 | 0.839 | -0.09 | 5.606x10-3 | -1.319x10-4 |
| $N_{qh}$ | 30° | H/D | 4.565 | 1.234 | -0.089 | 4.275x10-3 | -9.159x10-5 |
| $N_{qh}$ | 35° | H/D | 6.816 | 2.019 | -0.146 | 7.651x10-3 | -1.683x10-4 |
| $N_{qh}$ | 40° | H/D | 10.959 | 1.783 | 0.045 | -5.425x10-3 | -1.153x10-4 |
| $N_{qh}$ | 45° | H/D | 17.658 | 3.309 | 0.048 | -6.443x10-3 | -1.299x10-4 |

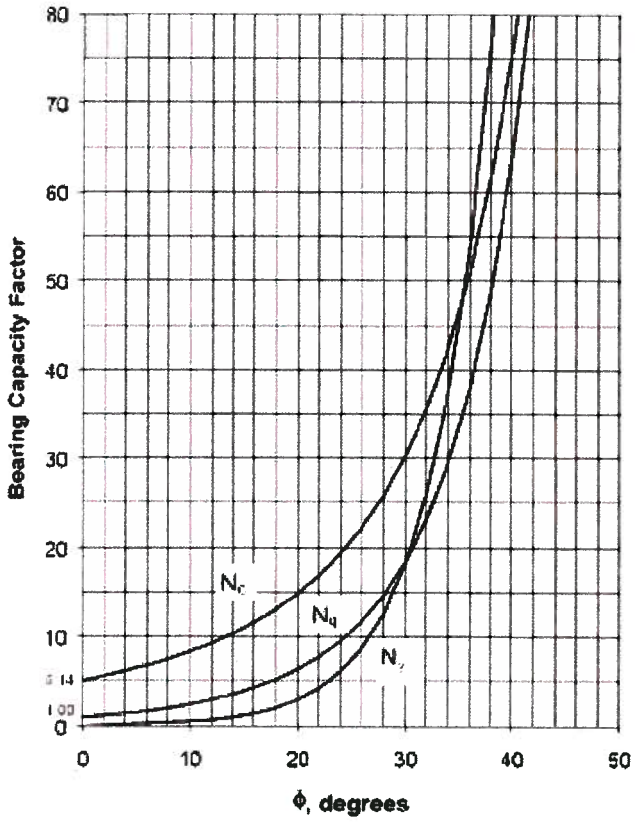


Figure B.1 Bearing Capacity Factors of Different Soil Friction Values (ALA, 2001)

Table B.2 Soil Springs Stiffnesses Calculations (Reinforced Concrete Pipe)

**H = 3 ft (0.91 m)**

| Soil Spring Properties | Pipe Diameter (mm) | | |
|---|---|---|---|
| | **200** | **250** | **300** |
| Axial maximum resistance force ($t_u$) (N/m) | 8988 | 10359 | 11726 |
| Yield displacement ($x_u$) (mm) | 5 | 5 | 5 |
| Horizontal maximum resistance force ($P_u$) (N/m) | 65195 | 71769 | 78203 |
| Yield displacement ($y_u$) (mm) | 0.8 | 0.8 | 0.8 |
| Vertical maximum resistance force ($Q_u$) (N/m) | 12420 | 12420 | 12420 |
| Yield displacement ($z_u$) (mm) | 136.5 | 136.5 | 136.5 |

**H = 4 ft (1.22 m)**

| Soil Spring Properties | Pipe Diameter (mm) | | |
|---|---|---|---|
| | **200** | **250** | **300** |
| Axial maximum resistance force ($t_u$) (N/m) | 12050 | 13887 | 15721 |
| Yield displacement ($x_u$) (mm) | 5 | 5 | 5 |
| Horizontal maximum resistance force ($P_u$) (N/m) | 96678 | 106011 | 115063 |
| Yield displacement ($y_u$) (mm) | 1.1 | 1 | 1 |
| Vertical maximum resistance force ($Q_u$) (N/m) | 22323 | 22323 | 22323 |
| Yield displacement ($z_u$) (mm) | 183 | 183 | 183 |

**H = 5 ft (1.52 m)**

| Soil Spring Properties | Pipe Diameter (mm) | | |
|---|---|---|---|
| | **200** | **250** | **300** |
| Axial maximum resistance force ($t_u$) (N/m) | 15013 | 17302 | 19586 |
| Yield displacement ($x_u$) (mm) | 5 | 5 | 5 |
| Horizontal maximum resistance force ($P_u$) (N/m) | 130440 | 142747 | 154598 |
| Yield displacement ($y_u$) (mm) | 1.3 | 1.3 | 1.3 |
| Vertical maximum resistance force ($Q_u$) (N/m) | 34652 | 34652 | 34652 |
| Yield displacement ($z_u$) (mm) | 228 | 228 | 228 |

**H = 6 ft (1.82 m)**

| Soil Spring Properties | Pipe Diameter (mm) | | |
|---|---|---|---|
| | **200** | **250** | **300** |
| Axial maximum resistance force ($t_u$) (N/m) | 17977 | 20717 | 23452 |
| Yield displacement ($x_u$) (mm) | 5 | 5 | 5 |
| Horizontal maximum resistance force ($P_u$) (N/m) | 166988 | 182551 | 197460 |
| Yield displacement ($y_u$) (mm) | 1.5 | 1.5 | 1.6 |
| Vertical maximum resistance force ($Q_u$) (N/m) | 49680 | 49680 | 49680 |
| Yield displacement ($z_u$) (mm) | 273 | 273 | 273 |

Table B.2 Soil Springs Stiffness Calculations (Reinforced Concrete Pipe) (cont.)

**H = 7 ft (2.14 m)**

| Soil Spring Properties | Pipe Diameter (mm) | | |
|---|---|---|---|
| | **200** | **250** | **300** |
| Axial maximum resistance force ($t_u$) (N/m) | 21137 | 24360 | 27575 |
| Yield displacement ($x_u$) (mm) | 5 | 5 | 5 |
| Horizontal maximum resistance force ($P_u$) (N/m) | 208680 | 227989 | 246425 |
| Yield displacement ($y_u$) (mm) | 1.8 | 1.8 | 1.8 |
| Vertical maximum resistance force ($Q_u$) (N/m) | 68686 | 68686 | 68686 |
| Yield displacement ($z_u$) (mm) | 321 | 321 | 321 |

Table B.3 Soil Springs Stiffness Calculations (Non-Reinforced Concrete Pipe)

**H = 3 ft (0.91 m)**

| Soil Spring Properties | Pipe Diameter (mm) | | |
|---|---|---|---|
| | **200** | **250** | **300** |
| Axial maximum resistance force ($t_u$) (N/m) | 6665 | 8205 | 10062 |
| Yield displacement ($x_u$) (mm) | 5 | 5 | 5 |
| Horizontal maximum resistance force ($P_u$) (N/m) | 53586 | 61359 | 70360 |
| Yield displacement ($y_u$) (mm) | 0.8 | 0.8 | 0.8 |
| Vertical maximum resistance force ($Q_u$) (N/m) | 12420 | 12420 | 12420 |
| Yield displacement ($z_u$) (mm) | 136.5 | 136.5 | 136.5 |

**H = 4 ft (1.22 m)**

| Soil Spring Properties | Pipe Diameter (mm) | | |
|---|---|---|---|
| | **200** | **250** | **300** |
| Axial maximum resistance force ($t_u$) (N/m) | 8936 | 11000 | 13490 |
| Yield displacement ($x_u$) (mm) | 5 | 5 | 5 |
| Horizontal maximum resistance force ($P_u$) (N/m) | 79941 | 91187 | 104019 |
| Yield displacement ($y_u$) (mm) | 1 | 1 | 1.1 |
| Vertical maximum resistance force ($Q_u$) (N/m) | 22323 | 22323 | 22323 |
| Yield displacement ($z_u$) (mm) | 183 | 183 | 183 |

**H = 5 ft (1.52 m)**

| Soil Spring Properties | Pipe Diameter (mm) | | |
|---|---|---|---|
| | **200** | **250** | **300** |
| Axial maximum resistance force ($t_u$) (N/m) | 11133 | 13705 | 16808 |
| Yield displacement ($x_u$) (mm) | 5 | 5 | 5 |
| Horizontal maximum resistance force ($P_u$) (N/m) | 108140 | 123156 | 140128 |
| Yield displacement ($y_u$) (mm) | 1.3 | 1.3 | 1.3 |
| Vertical maximum resistance force ($Q_u$) (N/m) | 34652 | 34652 | 34652 |
| Yield displacement ($z_u$) (mm) | 228 | 228 | 228 |

**H = 6 ft (1.82 m)**

| Soil Spring Properties | Pipe Diameter (mm) | | |
|---|---|---|---|
| | **200** | **250** | **300** |
| Axial maximum resistance force ($t_u$) (N/m) | 13330 | 18348 | 20125 |
| Yield displacement ($x_u$) (mm) | 5 | 5 | 5 |
| Horizontal maximum resistance force ($P_u$) (N/m) | 138628 | 169141 | 179246 |
| Yield displacement ($y_u$) (mm) | 1.5 | 1.5 | 1.5 |
| Vertical maximum resistance force ($Q_u$) (N/m) | 49680 | 49680 | 49680 |
| Yield displacement ($z_u$) (mm) | 273 | 273 | 273 |

Table B.3 Soil Springs Stiffness Calculations (Non-Reinforced Concrete Pipe) (cont.)

**H = 7 ft (2.14 m)**

| Soil Spring Properties | Pipe Diameter (mm) | | |
|---|---|---|---|
| | **200** | **250** | **300** |
| Axial maximum resistance force ($t_u$) (N/m) | 15674 | 19295 | 23663 |
| Yield displacement ($x_u$) (mm) | 5 | 5 | 5 |
| Horizontal maximum resistance force ($P_u$) (N/m) | 173441 | 197189 | 223893 |
| Yield displacement ($y_u$) (mm) | 1.7 | 1.7 | 1.8 |
| Vertical maximum resistance force ($Q_u$) (N/m) | 68686 | 68686 | 68686 |
| Yield displacement ($z_u$) (mm) | 321 | 321 | 321 |

Table B.4 Soil Springs Stiffness Calculations (Vitrified Clay Pipe)

**H = 3 ft (0.91 m)**

| Soil Spring Properties | Pipe Diameter (mm) | | |
|---|---|---|---|
| | **200** | **250** | **300** |
| Axial maximum resistance force ($t_u$) (N/m) | 6811 | 8232 | 9737 |
| Yield displacement ($x_u$) (mm) | 5 | 5 | 5 |
| Horizontal maximum resistance force ($P_u$) (N/m) | 54336 | 61495 | 68804 |
| Yield displacement ($y_u$) (mm) | 0.8 | 0.8 | 0.8 |
| Vertical maximum resistance force ($Q_u$) (N/m) | 12420 | 12420 | 12420 |
| Yield displacement ($z_u$) (mm) | 136.5 | 136.5 | 136.5 |

**H = 4 ft (1.22 m)**

| Soil Spring Properties | Pipe Diameter (mm) | | |
|---|---|---|---|
| | **200** | **250** | **300** |
| Axial maximum resistance force ($t_u$) (N/m) | 9131 | 11037 | 13054 |
| Yield displacement ($x_u$) (mm) | 5 | 5 | 5 |
| Horizontal maximum resistance force ($P_u$) (N/m) | 81034 | 91382 | 101813 |
| Yield displacement ($y_u$) (mm) | 1 | 1 | 1.1 |
| Vertical maximum resistance force ($Q_u$) (N/m) | 22323 | 22323 | 22323 |
| Yield displacement ($z_u$) (mm) | 183 | 183 | 183 |

**H = 5 ft (1.52 m)**

| Soil Spring Properties | Pipe Diameter (mm) | | |
|---|---|---|---|
| | **200** | **250** | **300** |
| Axial maximum resistance force ($t_u$) (N/m) | 11376 | 13751 | 16263 |
| Yield displacement ($x_u$) (mm) | 5 | 5 | 5 |
| Horizontal maximum resistance force ($P_u$) (N/m) | 109604 | 123415 | 137223 |
| Yield displacement ($y_u$) (mm) | 1.3 | 1.3 | 1.3 |
| Vertical maximum resistance force ($Q_u$) (N/m) | 34652 | 34652 | 34652 |
| Yield displacement ($z_u$) (mm) | 228 | 228 | 228 |

**H = 6 ft (1.82 m)**

| Soil Spring Properties | Pipe Diameter (mm) | | |
|---|---|---|---|
| | **200** | **250** | **300** |
| Axial maximum resistance force ($t_u$) (N/m) | 13621 | 16465 | 19473 |
| Yield displacement ($x_u$) (mm) | 5 | 5 | 5 |
| Horizontal maximum resistance force ($P_u$) (N/m) | 140493 | 158070 | 175575 |
| Yield displacement ($y_u$) (mm) | 1.5 | 1.5 | 1.5 |
| Vertical maximum resistance force ($Q_u$) (N/m) | 49680 | 49680 | 49680 |
| Yield displacement ($z_u$) (mm) | 273 | 273 | 273 |

Table B.4 Soil Springs Stiffness Calculations (Vitrified Clay Pipe) (cont.)

**H = 7 ft (2.14 m)**

| Soil Spring Properties | Pipe Diameter (mm) | | |
|---|---|---|---|
| | **200** | **250** | **300** |
| Axial maximum resistance force ($t_u$) (N/m) | 16016 | 19360 | 22897 |
| Yield displacement ($x_u$) (mm) | 5 | 5 | 5 |
| Horizontal maximum resistance force ($P_u$) (N/m) | 175756 | 197598 | 219341 |
| Yield displacement ($y_u$) (mm) | 1.7 | 1.7 | 1.8 |
| Vertical maximum resistance force ($Q_u$) (N/m) | 68686 | 68686 | 68686 |
| Yield displacement ($z_u$) (mm) | 321 | 321 | 321 |

## PUBLICATIONS

1- Jasem, S., Ghrib, F., and Tayebi, K. (2008a). "Seismic Analysis of Buried Segmented Pipelines", J. (in press)

2- Jasem, S., Ghrib, F., Tayebi, K., and Hearn, N. (2008b). "Modeling of Axial and Bending Behavior of Unrestrained Joints in Segmented Pipelines", J. (in press)

3- Jasem, S., Ghrib, F., Tayebi, K., and Hearn, N. (2008c). "Liners Buckling Models for Pipeline Rehabilitation- A Comparative Study", J. (in press)

4- Jasem, S., Ghrib, F., Tayebi, K., and Hearn, N. (2008d). "Modeling of Rehabilitated Segmented Pipeline under Seismic Effects", J. (in press)

5- Ghrib, F., Jasem, S., and Tayebi, K. (2008e). "Modeling of Buried Segmented Pipelines Subjected to Permanent Ground Displacement", Presented in the Canadian Society of Civil Engineering Annual Conference, Quebec, June 10-13, 2008.

## VITA AUCTORIS

| | |
|---|---|
| NAME | Sami Mirri Kadhim Jasem |
| PLACE OF BIRTH | Shamiyah, Diwaniyah, Iraq |
| YEAR OF BIRTH | 1958 |
| EDUCATION | University of Baghdad, Baghdad, Iraq<br>1975 - 1979 B.Sc. |
| | University of Baghdad, Baghdad, Iraq<br>1981 - 1983 M. Sc. |
| | University of Windsor, Windsor, Ontario<br>2003 - 2008 Ph. D. Candidate |
| AFFILIATION | Ontario Professional Engineers (PEO)<br>Ontario, Canada |
| | Association of Professional Engineers & Geoscientists of Saskatchewan (APEGS), Saskatchewan, Canada |
| | Association of Professional Engineers & Geoscientists of British Columbia (APEGBC), British Columbia, Canada |
| | Iraqi Engineers Union (IEU)<br>Baghdad, Iraq |